

**THE BIOELECTRIC CONTROL OF  
METASTATIC PROCESSES DURING  
MORPHOGENESIS IN *XENOPUS LAEVIS***

A dissertation  
submitted by

Maria Lobikin

In partial fulfillment of the requirements  
for the degree of

Doctor of Philosophy

in

Biology

TUFTS UNIVERSITY  
Graduate School of Arts and Sciences

May, 2015

Advisor: Michael Levin, Ph.D.

## Abstract

Understanding the mechanisms by which cellular communication and large-scale pattern formation is coordinated in the developing embryo is of high priority to developmental biology, regenerative medicine, and oncology. Proper patterning of body axes during morphogenesis is important to the overall physiology of the organism, and involves bioelectric processes in addition to chemical signaling and genetic networks. We first examined the effects of mutations in the cytoskeletal protein tubulin in the very early steps of left-right patterning of frog embryos – a process known to involve bioelectric signaling downstream of cytoskeletal transport. Our functional data demonstrate a remarkable molecular conservation of mechanisms controlling laterality among widely divergent phyla, and reveal the first few cleavages as the stage at which symmetry breaking is initiated in the frog embryo. We then addressed bioelectric signaling in later development, looking at the consequences of changing resting potential *in vivo*, by specifically targeting chloride flux. Depolarization of the sparse, yet widely distributed cell population expressing the glycine-gated chloride (GlyCl) channel non-cell-autonomously induces the neoplastic-like conversion of melanocytes, characterized overproliferation, inappropriate migration, and a change in overall melanocyte morphology. These drastic changes in cell behavior occur via a serotonin-transporter-dependent increase of extracellular serotonin. In addition to the metastatic phenotype induced in melanocytes, we demonstrate disruptions to blood vessel and muscle patterning, the latter also occurring in a serotonin-transporter-dependent manner. Taking advantage of a hypersensitive GlyCl mutant we demonstrate that the depolarization of very few instructor cells (cells capable of producing a metastatic

phenotype in melanocytes) is sufficient to induce embryo-wide hyperpigmentation. Using the same hypersensitive mutant under the control of tissue-specific promoters, we show that instructor cells resident in muscle are more effective in triggering the metastatic conversion of ectodermal melanocytes than those of the nervous system. Surprisingly, the depolarization of muscle cells results in the appearance of cells expressing muscle markers in neural regions, revealing new details on the bioelectric reprogramming of cell behavior. Finally, we show that the neoplastic conversion of melanocytes is mediated by cAMP, CREB, and the transcription factors Sox10 and Slug as well as the MSH-secreting melanotrope cells of the pituitary and formulate a comprehensive computational model explaining the quantitative penetrance data for this all-or-none phenotype within each treated population. These data reveal the upstream and downstream mechanisms by which  $V_{mem}$  can function as an important biophysical regulator of cell behavior, with implications for evolutionary biology, cancer therapeutics, and development.

## **Acknowledgements**

The research described in this dissertation would not have been possible without the help and support of very many people.

First and foremost, I would like to thank my wonderful advisor, Dr. Michael Levin, for everything that he has done for me over the past six years. Thank you for your unwavering support and guidance; it was exactly what I needed to be successful in my own research endeavors. Thank you for your wonderfully odd stories, and crazy ideas that have led to such interesting lines of research. I am so grateful to have worked with someone who is so unique, genuine, and intelligent.

I would also like to thank my other committee members: Drs. Kelly McLaughlin, Susan Ernst, and Barry Trimmer for their support along the way. Thank you for the lively conversations, valuable suggestions, and creative perspectives and for making me feel more like a peer than a student during my committee meetings. I would also like to thank Dr. Tobias Schatton for graciously agreeing to sit on my defense as an outside examiner.

To the members of the Levin Lab, past and present, thank you all for making the lab so fun and stimulating! You each have had a unique and important contribution to my work/life and I am so grateful for it. I would especially like to thank Dr. Laura Vandenberg for taking the time to mentor me and be my go-to person when I first started in the lab; I am a better scientist because of your help and encouragement.

I am also deeply grateful to the entire Biology Department at Tufts. Thank you all for being such a welcoming and supportive group. Special thanks to the administrative staff; Bill, Eileen, Liz, Karen, Mike, Tony and Michael for keeping

everything running so smoothly.

Finally, I have to thank my wonderful family and friends for everything over the last six years; their love and support has kept me going and made this all possible. To my wonderful group of girlfriends, our brunches and birthday dinners and cape weekends were much necessary escapes and venues to vent; I am so thankful to have you all in my life. To Travis, thank you for taking it upon yourself to be my personal stress and anxiety relief coach; our sailing trips were all such wonderful reprieves.

Lastly, to my parents, who have been instrumental in my achievements; fostering my creativity and teaching me that anything is possible with enough effort. I dedicate this thesis to you.

## Table of Contents

<b>Abstract .....</b>	<b>ii</b>
<b>Acknowledgements .....</b>	<b>iv</b>
<b>List of Figures.....</b>	<b>ix</b>
<b>List of Tables .....</b>	<b>xii</b>
<b>List of Abbreviations .....</b>	<b>xiii</b>
<b>Summary of Chapters.....</b>	<b>xv</b>
<b>Chapter 1: Endogenous bioelectric cues as morphogenetic signals <i>in vivo</i> .....</b>	<b>2</b>
<b>Abstract .....</b>	<b>3</b>
<b>Introduction: Bioelectricity and the history of ‘animal spirits’ .....</b>	<b>4</b>
<b>The role of endogenous electric fields and voltage gradients in morphogenesis .....</b>	<b>7</b>
<b>Endogenous electric fields &amp; ionic flow in the detection &amp; treatment of cancer ..</b>	<b>16</b>
<b>Conclusion .....</b>	<b>19</b>
<b>Acknowledgments .....</b>	<b>21</b>
<b>Chapter 2: Early, nonciliary role for microtubule proteins in left-right patterning is conserved across kingdoms.....</b>	<b>22</b>
<b>Abstract .....</b>	<b>23</b>
<b>Introduction.....</b>	<b>24</b>
<b>Results .....</b>	<b>25</b>
<b>Discussion.....</b>	<b>38</b>
<b>Materials and methods.....</b>	<b>42</b>
<b>Acknowledgments .....</b>	<b>43</b>
<b>Supporting information.....</b>	<b>43</b>

<b>Chapter 3: Transmembrane potential of GlyCl-expressing instructor cells induces a neoplastic-like conversion of melanocytes via serotonergic pathway .....</b>	<b>61</b>
<b>Summary .....</b>	<b>62</b>
<b>Introduction.....</b>	<b>63</b>
<b>Results .....</b>	<b>67</b>
<b>Discussion.....</b>	<b>93</b>
<b>Translational impact .....</b>	<b>105</b>
<b>Methods .....</b>	<b>107</b>
<b>Acknowledgements .....</b>	<b>113</b>
<b>Competing interests.....</b>	<b>113</b>
<b>Supplementary material .....</b>	<b>113</b>
<b>Chapter 4: Resting potential, oncogene-induced tumorigenesis, and metastasis: the bioelectric basis of cancer <i>in vivo</i> .....</b>	<b>117</b>
<b>Abstract .....</b>	<b>118</b>
<b>Introduction.....</b>	<b>119</b>
<b>Materials and methods .....</b>	<b>130</b>
<b>Results .....</b>	<b>132</b>
<b>Discussion.....</b>	<b>154</b>
<b>Acknowledgements .....</b>	<b>160</b>
<b>Supplementary material .....</b>	<b>161</b>
<b>Chapter 5: Selective depolarization of transmembrane potential alters muscle patterning and muscle cell localization in embryonic <i>Xenopus laevis</i>.....</b>	<b>165</b>
<b>Abstract .....</b>	<b>166</b>
<b>Introduction.....</b>	<b>167</b>
<b>Results .....</b>	<b>169</b>

Discussion .....	183
Acknowledgements .....	188
Materials & methods .....	189
Supplementary material .....	192
<b>Chapter 6: Serotonergic reculation of metastatic potential in melanocytes: a bioelectric network explain all-or-none stochastic hyperpigmentation .....</b>	<b>194</b>
Abstract .....	195
Introduction.....	196
Results .....	198
Acknowledgments .....	233
Supplemental Material .....	241
<b>Chapter 7: Conclusions and future prospects .....</b>	<b>251</b>
Conclusion .....	252
Future Directions .....	255
Biomedical Implications .....	257
<b>Appendix 1: Effect of introducing hyperpolarizing potassium channels into melanoma cell lines .....</b>	<b>260</b>
Introduction.....	261
Material and Methods .....	262
Lentivirus production .....	262
Results .....	264
Conclusion .....	268
<b>References .....</b>	<b>270</b>

## List of Figures

Figure 1.1. Sources of bioelectric signals at multiple levels of organization. ....	8
Figure 1.2. Mechanisms for converting membrane voltage change into transcriptional events. ....	12
Figure 1.3. A mind-map of the field of bioelectricity. ....	20
Figure 2.1. Tubulin mutations affect LR asymmetry before the first cleavage event. ....	27
Figure 2.2. Tubulin mutations perturb sidedness of asymmetric gene expression in <i>Xenopus</i> . ....	31
Figure 2.3. Tubulin mutations affect early microtubule-dependent motor protein transport. ....	32
Figure 2.4. Tubulin mutations alter biased Cofilin-1 expression. ....	35
Figure 2.5. Mutant tubulin disrupts LR asymmetry in <i>C. elegans</i> embryos and cultured HL-60 cells. ....	37
Supplemental Figure 2.1. $\alpha$ -Tubulin and the $\gamma$ -tubulin associated protein complex, Tubgcp2, are highly conserved among organisms. ....	47
Supplemental Figure 2.2. Early mRNA injection gives rise to proteins by the first cleavage. ....	48
Supplemental Figure 2.3. Injection into one of two early blastomeres allows targeting of the left or right side of embryo. ....	49
Supplemental Figure 2.4. Heterotaxia rates in tdTomato:Cofilin-a1 coinjections. ....	50
Supplemental Figure 2.5. A model for tubulin's role in LR asymmetry in <i>Xenopus</i> . ....	51
Figure 3.1. Ivermectin exposure induces hyperpigmentation. ....	69
Figure 3.2. Ivermectin induces invasiveness in melanocytes. ....	73
Figure 3.3. Early ivermectin exposure induces an increase in pigment cell proliferation. ....	76
Figure 3.4. Expression of GlyCI- $\alpha$ mRNA and protein. ....	81
Figure 3.5. Hyperpigmentation is due to depolarization. ....	86

Figure 3.6. Serotonergic controls of melanocyte behavior and their relationship to GlyCl-expressing cells. ....	90
Figure 3.7. Human melanocytes exhibit arborization when the membrane is depolarized. ....	92
Figure 3.8. A model of melanocyte control by transmembrane potential of cells in the neural crest's environment. ....	97
Supplemental Figure 3.1. Depolarization by ivermectin exposure. ....	114
Supplemental Figure 3.2. Glycine exposure induces hyperpigmentation. ....	116
Figure 4.1. Depolarization of instructor cells induces a metastatic phenotype in melanocytes. ....	126
Figure 4.2 GlyCl-mediated depolarization induces abnormal vascular structure <i>in vivo</i> . ....	135
Figure 4.3. Hyperpigmentation requires the depolarization of only a small number of instructor cells. ....	139
Figure 4.4. A model of melanocyte control by serotonergic signaling downstream of voltage change. ....	145
Figure 4.5. Exposure to carcinogen 4NQO induces hyperpigmentation, embryo-wide depolarization, and tumor-like structures. ....	147
Figure 4.6. Overexpression of <i>Gli1</i> results in ITLSs with unique Na <sup>+</sup> signature	149
Figure 4.7. Oncogene-induced ITLSs can be suppressed by prior injection of hyperpolarizing channel mRNA ....	151
Figure 4.8. Pharmacological targeting of endogenous Cl <sup>-</sup> channels suppresses <i>Xrel3</i> ITLSs. ....	153
Supplemental Figure 4.1. A network model of serotonergic signaling downstream of voltage. ....	161
Figure 5.1. Depolarization of instructor cells results in abnormal muscle structure independent of immobilization. ....	172
Figure 5.2. Driving GlyR-A288G expression in neural tissue is sufficient to induce hyperpigmentation. ....	174
Figure 5.3. Driving GlyR-A288G expression in muscle tissue is sufficient to induce hyperpigmentation. ....	176
Figure 5.4. Expressing GlyR-A288G and selectively depolarizing muscle-specific cells results in abnormal localization. ....	178

Figure 5.5. Mislocalized Car promoter-driven GFP+ cells in neural tube are not completely neural. ....	182
Supplemental Figure 5.1. Injection of depolarizing TPC3 channel induces embryo-wide hyperpigmentation. ....	192
Supplemental Figure 5.2. Tadpoles with mislocalized muscle cells in neural regions can learn associated stimulus avoidance in an automated assay. ....	193
Figure 6.1. Cyclic AMP (cAMP) and cAMP response mediating protein (CREB) are involved in mediating instructor cell signaling. ....	200
Figure 6.2. The pituitary gland is necessary for ivermectin-mediated hyperpigmentation. ....	205
Figure 6.3. Both concentrated and sparse, widely distributed depolarization results in upregulation of Sox10. ....	209
Figure 6.4. Ivermectin-induced depolarization results in upregulation of neoplasm-related, and cancer-related genes at early and late stages, respectively. ....	212
Figure 6.5 Automatically discovered dynamic stochastic network. ....	218
Figure 6.6. Dynamic model performance with training experiments and novel predictions. ....	221
Figure 6.7. Phase space of the dynamic model with stochastic developmental trajectories and pharmacological treatment bifurcations. ....	223
Supplemental Figure 6.1. Serotonin and $\alpha$ MSH signaling mediating instructor cell depolarization are part of a single pathway. ....	241
Supplemental Figure 6.2 Methodology to reverse-engineer dynamic signaling networks. ....	242
Supplemental Figure 6.3. Pathway model for melanocyte control downstream of serotonin signaling. ....	243
Figure A1.1 Hyperpolarizing ion channel expression A-375 cells affects soft agar colony formation. ....	266
Figure A1.2 Expression of Kv1.5 and Kir2.1 enhances the motility of melanoma cells. ....	267
Figure A1.3 The xenograft mouse model. ....	269

## List of Tables

Table 1.1. Known transduction mechanisms by which ion flows impact morphogenesis. ....	15
Supplemental Table 2.1. Protein localization bias is abolished by tubulin mutants for certain proteins. ....	53
Supplemental Table 2.2. Heterotaxia in embryos injected at various early cleavage stages. ....	54
Supplemental Table 2.3. Left-biased proteins in four-cell <i>X. laevis</i> embryos ....	55
Supplemental Table 2.4. Right-biased proteins in four-cell <i>X.laevis</i> embryos ....	57
Supplemental Table 2.5. Fluorescent signal localization for tdTomato:cofilin-1a injections .....	60
Table 3.1. Proliferation rates in melanocytes .....	78
Table 3.2. Using Cl <sup>-</sup> levels to modulate voltage-dependent hyperpigmentation. ....	85
Table 3.3. Rescue of hyperpigmentation phenotype reveals serotonergic involvement.....	89
Table 4.1. Known ion translocators as oncogenes. ....	122
Table 4.2. Hyperpigmentation involves VMAT function. ....	141
Table 4.3. Blocking multiple 5-HT receptors induces hyperpigmentation, but inhibits depolarization-induced hyperpigmentation. ....	141
Table 4.4. Rescue of hyperpigmentation reveals involvement of 5-HT receptors 1, 2, and 5. ....	143
Supplemental Table 6.1. Cancer-related genes shown to be differentially expressed in stage 45 <i>Xenopus</i> tadpole embryos following depolarizing ivermectin treatment .....	245
Supplemental Table 6.2. Reference genes & primers for qPCR .....	247
Supplemental Table 6.3. Enriched gene ontology categories affected in late embryos. ....	247
Table 7.1 Summary of ion channels expressed in melanoma. ....	256

## List of Abbreviations

4NQO	Carcinogen 4-Nitroquinoline 1-oxide
5-HT	5-hydroxytryptamine (serotonin)
AC	Adenylyl cyclase
ANOVA	Analysis of variance
cAMP	Cyclic adenosine monophosphate
CarPr	Cardiac actin promoter
CC2-DMPE	N-(6-chloro-7-hydroxy-2-oxo-2H-1-benzopyran-3-carboxamidoacetyl)-dimyristoylphosphatidyl ethanolamine
CIC	Chloride channel
CREB	cAMP response element-binding protein
DC	Direct current
DiBAC <sub>4</sub> (3)	Bis-(1,3-dibutylbarbituric acid)trimethine Oxonol
DMSO	Dimethyl sulfoxide
DN	Dominant negative
EAG	Ether-a-go-go
EF	Electric Field
GFP	Green fluorescent protein
Gli1	Glioma-associated oncogene family zinc finger 1
GlyCl	Glycine gated chloride channel
GlyR	Glycine-gated chloride channel
GRP	Gastrocoel roof plate
H3B-P	Phosphorylated histone 3B
HDAC	Histone deacetylase
hERG	Human ether-a-go-go-related gene
ITLS	Induced tumor-like structure
IVM	Ivermectin
KCNE1	Potassium voltage-gated channel, Isk-related family, member 1
KCNK9	Potassium channel, subfamily K, member 9
KCNQ1	Potassium voltage-gated channel, KQT-like subfamily, member 1
KHC	Kinesin heavy chain
Kir	Inward-rectifying potassium channel
KRAS	Kirsten rat sarcoma viral oncogene homolog
Kv	Voltage-gated potassium channel
LD	Left-dorsal
LR	Left-right
minK	KCNE1, Potassium voltage-gated channel, Isk-related family, member 1
MITF	Microphthalmia-associated transcription factor
MMP	Matric metalloproteinase
MMR	Marc's Modified Ringer's Solution

MSH	Melanocyte stimulating hormone
MTOC	Microtubule organizing center
NaV	Voltage-gated sodium channel
NBT	Neural beta tubulin
NF-kB	Nuclear factor kappa-light chain enhancer of activated B cells
NT	Neural tube
PBS	Phosphate buffered saline
PBST	Phosphate buffered saline + 0.1% Tween-20
PKA	Phosphokinase A
POMC	Pro-opiomelanocortin
PTEN	Phosphatase and tensin homolog
RV	Right-ventral
SERT	Serotonin transporter
SIK	Salt-inducible Kinase
TEP	Transepithelial potential
TGF $\beta$	transforming growth factor beta
TNFR	Tumor necrosis factor receptor
TPC3	Two-pore channel 3
TRP1	Tyrodinase-related protein 1
V-ATPase	Vacuolar-type H <sup>+</sup> -ATPase
VGCC	Voltage-gated calcium channel
VMAT	Vesicular monoamine transporter
V <sub>mem</sub>	Transmembrane potential
Xnr-1	Xenopus nodal-related 1
Xrel1	Xenopus v-rel avian reticuloendotheliosis viral oncogene homolog 1
$\beta$ -gal	Beta-galactosidase

## Summary of Chapters

**Chapter 1:** Published as a chapter in Fields of Cells (2014), this chapter provides an in depth review of how bioelectrical properties function to coordinate large-scale pattern formation, and outlines the importance of these signals to embryonic development, organ regeneration and cancer suppression. This chapter briefly outlines the history of bioelectricity, before discussing modern data that demonstrate how bioelectrical properties are key determinants of cell migration, differentiation and proliferation. It provides an overview of studies from our lab and others' of known transduction mechanisms by which ion flows impact morphogenesis. It also introduces the paradigm of cancer as a disease of geometry: a disruption in the ability to maintain target morphology. Chapter 1 serves as an introduction to the data presented in Chapters 3-6.

**Chapter 2:** Published in Proceedings of the National Academy of Sciences (2012), this chapter describes the highly conserved role of the cytoskeletal protein, tubulin, in left-right (LR) asymmetric morphogenesis. The proper establishment of body axes during embryogenesis is necessary to set up the large-scale patterning events that follow, including those mediated by bioelectrical signaling. Moreover, the bioelectric gradients that drive asymmetry are known to be dependent on cytoskeleton-mediated intracellular transport. This study addresses a major controversy in the field of LR asymmetry: the degree of conservation of initiating mechanisms and the timing of the origin of laterality. Mutations homologous to those shown to affect symmetry in plants were made in *Xenopus laevis*  $\alpha$  tubulin and a  $\gamma$  tubulin-associated protein. We show that injection of these mutated tubulin proteins into very early embryos (but not

embryos after the 2<sup>nd</sup> cell cleavage) randomizes the left-right axis, controlling the left-right pathway upstream of the first asymmetrically localized marker, *Nodal* and affecting the consistent differential distribution of maternal proteins to either the left or right blastomere at the first cell division (as characterized by our proteomic approach). Remarkably, the same mutations affecting plant coiling, and organ placement of the vertebrate *X.laevis* also affect the asymmetric neural patterning in *C.elegans*, as well as chirality of human cells in culture. Collectively, these data implicate cytoskeletal tubulin as a fundamental, conserved initiator of chirality, instrumental to the proper establishment of many different body plans, and thus overall morphogenesis during development.

**Chapter 3:** Published in *Disease Models and Mechanisms* (2011), this chapter lays the groundwork for understanding the bioelectric and serotonergic control of melanocyte behavior. To determine how changes in  $V_{mem}$  regulate cell behavior *in vivo*, we took advantage of an endogenous cell population expressing the GlyCl channel. We show that depolarization of GlyCl-expressing cells results in a neoplastic-like conversion of melanocytes; they overproliferate, become highly arborized, and invade ectopic regions such as the neural tube lumen. We show that this effect is specific to  $V_{mem}$  (not dependent on the GlyCl channel or chloride ions), and is non-cell-autonomous. Moreover, we showed that these changes in the steady-state  $V_{mem}$  in GlyCl-expressing cells are transduced into changes in melanocyte behavior through the control of serotonin transport. Taken together, these data reveal a new role for ion flow and serotonergic signaling in melanocyte regulation, and reveal a new cell population, termed 'instructor cells', that can signal other populations and drastically change their behavior at a

considerable distance.

**Chapter 4:** Extending chapter 3's work focused on how bioelectric signals can induce a neoplastic phenotype in *X.laevis* melanocytes, this chapter reviews molecular data on the role of bioelectric cues in cancer and presents new findings on the biophysical properties of a microenvironment contribute to cancer *in vivo*. First, I show that in addition to the metastatic phenotype induced in melanocytes, GlyCl-expressing instructor cell depolarization also results in disruptions in blood vessel patterning in developing tadpoles. Using a mutant GlyCl channel, I demonstrate that the depolarization of very few instructor cells is sufficient to induce embryo-wide hyperpigmentation, and implicate the function of VMAT and serotonin receptors 1, 2 and 5 in transducing the change in  $V_{mem}$  to changes in melanocyte behavior. Together with Daniel Lobo, I present a model of antagonistic signaling by serotonin receptors that explains the unusual all-or-none nature of this effect. Additionally, Brook Chernet presents data on the bioelectrical properties of tumor-like structures induced by known oncogenes. Tumors induced by oncogenes show abnormally high sodium levels, suggesting sodium as a non-invasive diagnostic modality. Importantly, oncogene-induced tumorigenesis can be significantly reduced by forced prior expression of hyperpolarized ion channels. Together, these data extend our understanding of the role of  $V_{mem}$  in the metastatic conversion of cell behavior and tumor formation. This work is published in *Physical Biology* (2012).

**Chapter 5:** Extending chapter 4's findings describing aberrant vasculogenesis in addition to changes in instructor cell depolarization, we investigated whether

additional phenotypes affecting non-pigmented cells may have gone undetected. We found that depolarization resulted in dystrophic-like development of skeletal muscle in a serotonin-dependent manner. Continuing previous work describing the small amount of instructor cells sufficient to induce embryo-wide changes in melanocyte behavior, we sought to determine whether specific cell populations were responsible for the effects observed. Using a hypersensitive GlyCl-channel under the control of tissue-specific promoters we demonstrate that instructor cells resident within muscle are more effective at triggering the metastatic conversion of melanocytes than those of a neural origin. Surprisingly, we found that depolarization of muscle cells results in the appearance of cells expressing muscle markers within the neural tube, which impacts, but does not abolish, the ability of these tadpoles to perform in an associative conditioning assay. Collectively, these data reveal new details on the long-range reprogramming of cell behavior by alteration of  $V_{\text{mem}}$  of specific embryonic subpopulations. This work has been accepted by the International Journal of Developmental Biology, and is currently in press.

**Chapter 6:** Extending chapter 3 and 4's work on the serotonin-dependent mechanism by which depolarization of instructor cell's  $V_{\text{mem}}$  leads to changes in melanocyte behavior, we sought to better understand the downstream signaling mechanisms mediating these transforming effects. We found that this process is coordinated by cAMP, CREB, and the transcription factors Sox10 and Slug, which have been previously implicated with various cancers, including melanoma. Furthermore, we show that the signal transduction involves the MSH-secreting melanotrope cells of the pituitary and using a novel computational

method, we develop a model for the molecular pathway linking the bioelectrical properties in a melanocyte's microenvironment to the genetic and cellular changes induced in this metastatic phenotype. Together, these data fill in important gaps in our understanding of the molecular steps by which voltage change in specific cell populations can drastically affect the behavior of other cell types and demonstrate a proof-of-principle computational method for understanding stochastic and bi-stable decision-making by cells during development and cancer. This work has been submitted to Science Signaling and is currently in review.



**The bioelectric control of  
metastatic processes during  
morphogenesis in *Xenopus  
laevis***

# Chapter 1

## Introduction

### **Endogenous bioelectric cues as morphogenetic signals *in vivo***

Maria Lobikin and Michael Levin, PhD

Fields of the Cell, 2014: 283-302  
ISBN: 978-81-308-0544-3  
Editors: Daniel Fels and Michal Cifra

## **Abstract**

Complex pattern formation requires mechanisms to coordinate individual cell behavior towards the anatomical needs of the host organism. Alongside the well-studied biochemical and genetic signals functions an important and powerful system of bioelectrical communication. All cells, not just excitable nerve and muscle, utilize ion channels and pumps to drive standing gradients of ion content and transmembrane resting potential. In this chapter, we discuss the data that show that these bioelectrical properties are key determinants of cell migration, differentiation, and proliferation. We also highlight the evidence for spatio-temporal gradients of transmembrane voltage potential as an instructive cue that encodes positional information and organ identity, and thus regulates the creation and maintenance of large-scale shape. In a variety of model systems, it is now clear that bioelectric prepatterns function during embryonic development, organ regeneration, and cancer suppression. Moreover, genetic and pharmacological modulation of the prepatterns resident in physiological networks is a powerful modality for controlling growth and form. Recent data have revealed the mechanisms by which voltage gradients are transduced into downstream transcriptional cascades. Thus, mastery of the endogenous bioelectrical signaling pathways will have transformative implications for developmental biology, regenerative medicine, and synthetic bioengineering.

## **Introduction: Bioelectricity and the history of ‘animal spirits’**

Understanding the mechanisms by which cell-to-cell communication and large-scale pattern formation are coordinated in the developing embryo is of high priority to developmental biology, regenerative medicine, and oncology.

Alongside well-characterized biochemical modes of cellular communication that regulate cellular behavior during pattern formation there exists an important and powerful signaling system that is only now beginning to be understood and integrated with canonical biochemical and genetic pathways [1]. This system of information exchange functions through bioelectrical mechanisms.

### ***What is endogenous bioelectricity?***

Bioelectricity, in general, refers to signals carried by voltage gradients, ion flows and electric fields that all cells receive and generate. Bioelectricity is most well known in the context of neuronal excitation in which rapid changes in transmembrane potential ( $V_{mem}$ ) give rise to rapid action potentials. However, long-term, steady state ion fluxes, electric fields, and pH gradients are present in *all* cells and across epithelial sheets. At the cellular level, transmembrane potentials result from the presence of ion channels and pumps within cell membranes that function to segregate ions in differing concentrations internally and externally. This segregation of charges gives rise to transmembrane voltage potentials, usually on the order of -50 mV. It is becoming increasingly clear that these bioelectric parameters serve functional roles in signaling pathways that control cell proliferation, differentiation and migration. Thusly, understanding how these mechanisms function is of high priority to developmental biology, regenerative medicine and cancer research. In complement to other work on electromagnetic radiation and other

biophysical properties of cells, this chapter focuses on the endogenous patterning roles and signaling mechanisms of spatially-distributed and slowly-varying (resting) transmembrane potentials in living tissues.

### ***A brief history***

The study of bioelectricity began long ago. Original experiments date back to the 17<sup>th</sup> century to experiments done by the Dutch biologist and microscopist Jan Swammerdan who believed that muscle contraction was caused by the flow of 'animal spirits' [2]. Swammerdan placed frog muscle into glass vessels and observed that physically irritating nerves with scissors or another instrument caused the muscles to contract. However, it wasn't until the 18<sup>th</sup> century that evidence of 'animal electricity' was procured by the Italian physicist and physician, Luigi Galvani [3]. In his famous experiments in the late 1700's, Galvani observed that extracted frog muscles would twitch when exposed to currents produced during lightning storms. Galvani believed that the activation of these muscle movements was generated by electrical fluid carried to the muscles by nerves. This phenomenon was termed 'Galvanism', and is credited with being the underpinnings to the modern study of electrophysiology [4]. Galvani fought most of his life to persuade skeptical colleagues that 'animal electricity' was a reality and it wasn't until some 75 years later that modern experimental electrophysiology was launched by Emil du Bois-Reymond's *Researches on Animal Electricity* [5].

Further experimentation conducted in the 19<sup>th</sup> century implicated electrical potentials in the process of wound healing. In 1831, Matteucci demonstrated the existence of action potentials in nerve and muscle cells for the first time by measuring injury potentials at cut ends using a galvanometer [3]. Injury

potentials are now known to be a steady state, long-lasting direct current (DC) voltage gradient induced within the extracellular and intracellular spaces by current flowing into and around an injured nerve. Emil du-Bois Reymond built upon the initial observations of Matteucci by measuring current flowing out of a cut on his finger. This flow of current is due to the short-circuiting of the transepithelial potential (TEP) difference that occurs at a skin lesion (the TEP drives charged ions through the wound because the gap in the epithelium forms a low-resistance path for current flow). Human skin, as well as that of guinea pigs and amphibians, maintains a TEP across epithelial layers. When the skin is cut, a large, steady electric field (EF) arises immediately and persists for hours at the wound edge, as current pours out the lesion from underneath the wounded epithelium. This injury current is known to be essential for the regeneration of new limbs, where currents between 10 and 100  $\mu\text{A}/\text{cm}^2$  create a steady voltage drop of roughly 60 mV/mm within the first 125  $\mu\text{m}$  of extracellular space [3, 6].

Transcellular currents are also known to drive development and morphology. Elmer Lund carried out extensive research on electrical potentials between in the 1920s and 30s, arguing that electrical patterns are intimately related to the morphogenetic processes and vector properties of cell and tissue functions [7, 8]. The modern reformulation of these ideas is largely due to the work of Lionel Jaffe and his colleagues (done some 30 years later), demonstrating that electrical properties of individual cells, epithelial sheets, neural structures and limbs were necessary for growth and proper pattern and polarity establishment [9, 10].

### ***Bioelectricity in the molecular age***

Several key aspects demarcate modern studies of bioelectricity from its foundations. First is an increased appreciation of spatial distribution of resting potentials. While classical works focused on electric fields and ion fluxes (mostly due to epithelia) [11-16], we now know that the spatial organization of plasma membrane voltage levels across tissues and organs carries vital patterning information that drives anatomy [17]. Secondly, techniques are now available for the molecular characterization of the mechanisms that both produce and respond to these gradients [18]. Together with traditional techniques such as physiological measurements and applied fields, endogenous gradients can now be manipulated with tight spatio-temporal specificity at the molecular level, via the genetic modulation of well-characterized channels and pump proteins [19]. Thus, in addition to functional data on the electric properties themselves, the source and downstream effectors of changes in  $V_{\text{mem}}$  can now be dissected in great detail; for the first time, the patterning information encoded within dynamic bioelectrical networks are being integrated with well-known biochemical cascades and gene-regulatory networks. The results of these efforts reveal that embryonic patterning, regenerative repair and the suppression of cancerous disorganization all require continuous signal exchange between cells, tissues and organ systems [20, 21].

### **The role of endogenous electric fields and voltage gradients in morphogenesis**

The sources of endogenous bioelectric signals are shown in Figure 1.1. Modern experimental techniques to probe animal electricity have come a long way since Galvani first made dead frog muscle twitch by applying an electric

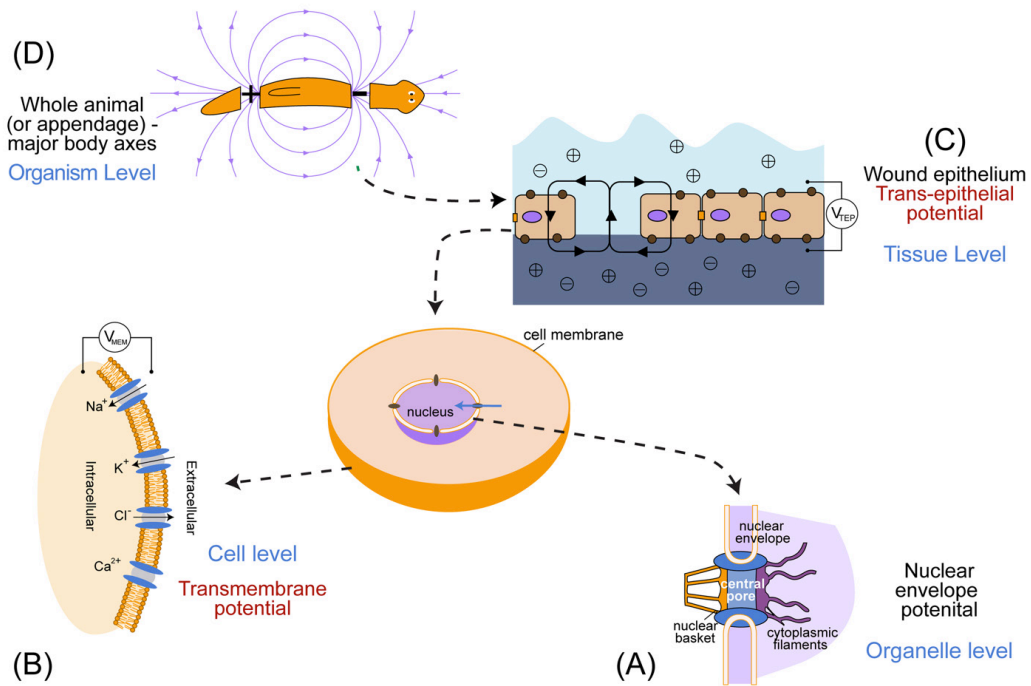


**Figure 1.1. Sources of bioelectric signals at multiple levels of organization.** Endogenous bioelectric signals comprise a set of biophysical properties that include voltage gradients, electric fields, and individual ion flows. *In vivo*, these originate at multiple levels of organization. (A) Organelle membranes generate voltage gradients, such as the nuclear envelope potential (largely unexplored) and the well-understood mitochondrial potentials. In recent years, the roles of resting potential across the plasma membrane of the cell (B) has become known as an important determinant of cell fate; spatial gradients of such voltage values over cell fields are now known as regulators of pattern formation in embryogenesis and regeneration. Decades ago it was recognized that the trans-epithelial electric field resulting from the parallel activities of polarized cell layers (C) was an important factor for guidance of migratory cell types during development and wound healing. Finally, at the level of entire appendages or even whole organisms (D), large-scale potential differences presage and control anatomical polarity and organ identity.

current to a nerve. Using standard techniques of molecular genetics, we can now target the expression patterns of ion channels and transporters for rational modulation. The use of knockout, RNAi, or morpholinos (antisense oligonucleotides to target specific mRNA sequences) allows gene-specific loss-of-function experiments. Pharmacological blockade, while not as specific as molecular approaches, offers the benefits of temporal control of inhibition, as well as the ability to target whole groups of ion channels or pumps at once – an important feature given that multiple ion translocators of the same family are often co-expressed and can compensate for each other, thus masking important phenotypes in gene-targeting experiments [22].

In the past decade, much work has begun to identify the endogenous ion conductances that are responsible for important patterning events, and the mechanisms by which cells can translate these signals into known gene regulatory networks [21]. Conversely, exogenous ion channels or pumps can be introduced into cells and thus allow predictable changes in transmembrane potential to reveal gain-of-function phenotypes. These techniques have now been used in numerous model species to show that endogenous bioelectric gradients are among the most important sources of morphogenetic information *in vivo* [6, 17, 19, 23, 24].

### ***V<sub>mem</sub> as a regulator of cell behavior***

Morphogenesis broadly defined is the dynamic process by which the geometry and topology of complex biological structures is established. This occurs during embryogenesis, but is also important during remodeling and regeneration during adulthood. The establishment and maintenance of shape on many scales (cells, tissues, organs, and entire bodyplans) is regulated by a

number of epigenetic factors controlling gene expression. Cells with different membrane and cytoplasm properties, but with identical DNA complements must consistently form and maintain various embryonic and adult structures. It has long been known that voltage gradients can mediate some of the necessary long-range communication through endogenous electric fields [9, 10, 25]. More recent work has shown that targeted perturbation of transmembrane voltage results in specific, coherent changes of large-scale patterning. Remarkably, modulation of resting potential does not in itself impair embryonic viability, and it is often possible to dissociate subtle patterning functions of bioelectric states from basic housekeeping physiology of cells. Thus,  $V_{\text{mem}}$  levels in key groups of cells have been implicated in controlling the head-to-tail [26] and left-right [27] body axis polarity, the patterning of craniofacial structures [28], the induction of eye development [24], and the initiation of *Xenopus* tail regeneration [29, 30].

One example of how  $V_{\text{mem}}$  values regulate the behavior of key cell populations *in vivo* is demonstrated by the discovery of a set of cells in the frog embryo that can confer a neoplastic-like phenotype upon stem cell derivatives, resulting in an embryo-wide 'hyperpigmentation' phenotype [31]. The expression of the glycine-gated chloride channel (GlyCl) demarcates a widely, yet sparsely distributed cell population that can be specifically targeted by exposing embryos to the potent GlyCl channel agonist, ivermectin [32]. Then, controlling the extracellular concentrations of chloride in accordance to the Goldman equation, the membrane potential of GlyCl-expressing cells can be specifically modulated to known levels (and monitored with voltage-reporting fluorescent dyes). When depolarized, these GlyCl-expressing cells instruct, over a significant

distance (mediated by regulation of serotonin signaling), the neural crest cell-derived melanocytes to undergo a neoplastic-like conversion acquiring three major properties commonly associated with metastasis: they hyperproliferate, become highly invasive, and undergo a change in shape, as well as up-regulating genes associated with neoplasia – SLUG and Sox10 [33]. Crucially, this metastasis-like phenotype can be reproduced by misexpressing mRNAs encoding sodium, potassium, or proton transporters, and can be rescued by the simple manipulation of extracellular ion content or through misexpression of opposing (hyperpolarizing) channels that drive the bioelectric state of the instructing cells back to normal. Together these data demonstrate that the control of instructor cell-derived signaling is driven by voltage *per se*, not necessary any one specific channel protein or type of ion.

***How is  $V_{mem}$  change transduced into specific cellular responses?***

Several known mechanisms (Figure 1.2) convert long-term changes in  $V_{mem}$  levels into second-messenger cascades that ultimately drive transcriptional responses [34]. Voltage-driven conformational changes of molecules such as integrins [35, 36] and phosphatases [37, 38], as well as voltage-regulated movement of signaling molecules through calcium channels [39], gap junctions [40, 41], and neurotransmitter transporters [42], can all play a role in linking biophysical events to changes in gene transcription. These processes then feed into several known genetic mechanisms, often involving changes in expression or function of genes such as PTEN, Integrin, SLUG/Sox10, Notch, SIK, and NF- $\kappa$ B. This, in turn, leads to changes in cell cycle, position, orientation and differentiation. It is now known that the nuclear membrane also possesses its own complement of ion transporters [43-46]; although the function of the

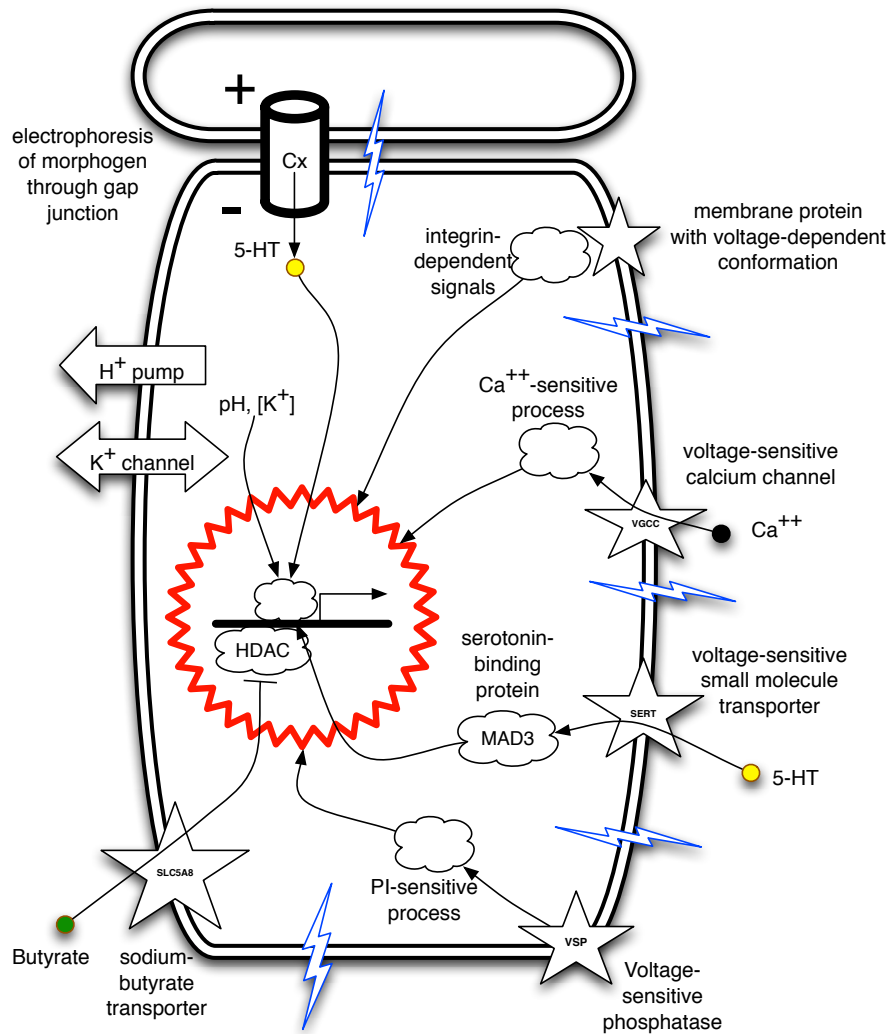


**Figure 1.2. Mechanisms for converting membrane voltage change into transcriptional events.**

Multiple mechanisms exist within cells to transduce changes in  $V_{mem}$  (a biophysical event) into genetic responses. Transcriptional cascades are initiated by second messenger systems that are voltage-regulated, including the movement of small molecules such as serotonin (5HT) through gap junctions via electrophoresis (voltage gradient between two connected cells) or through voltage-powered transporters such as the serotonin transporter SERT. Other molecules, such as integrin receptors and voltage-sensitive phosphatases can convert changes in  $V_{mem}$  into powerful integrin- and PTEN-dependent downstream signaling. Additional small molecules include Calcium, mediated by voltage-gated calcium channels, and butyrate/sodium transporters (such as SLC5A8) that allow voltage to control the import of key epigenetic regulators such as butyrate. Legend: star indicates membrane protein. Cloud indicates a process (chain of signaling steps). Lightning bolt indicates local change in transmembrane potential. Cylinder indicates a gap junction pore to neighboring cell. Colored circles represent small signaling molecules.

nuclear envelope potential has not been explored in developmental patterning, it is possible that the current picture of bioelectric signaling needs to be expanded beyond cell surface events. Thus,  $V_{\text{mem}}$  changes and ion flows can function as one link in the continuous interplay between genetic networks (which establish patterns of ion channel and pump expression) and the biophysical events that redistribute signaling molecules and control cell behavior within the long-range signaling pathways that occur during development and regeneration.

### ***Techniques for identifying voltage transduction mechanism***

How can the particular transduction mechanism mediating any bioelectric effect be identified in a specific assay? One example is provided by the identification of the ‘instructor cells’ that, when depolarized, cause a hyperpigmentation phenotype in *Xenopus laevis*. In this case, as well as other similar examples *in vivo*, the mechanism by which long-term depolarization is transduced into transcriptional and cell behavior changes was identified through a suppression drug screen. In such a loss-of-function approach, each possible signal transduction candidate is probed by inhibiting it to determine whether this suppresses a given effect of  $V_{\text{mem}}$  change [19, 47]. In the case of melanocytes, inhibitors of  $\text{Ca}^{2+}$  influx, of serotonin transporter (SERT) function, or of gap junctional connectivity were used together with the depolarizing ivermectin treatments. Only exposure to the specific inhibitor of the serotonin transporter (fluoxetine) blocked ivermectin-induced hyperpigmentation in all of the treated embryos, suggesting that SERT is required for the transduction of this bioelectrical signal [31]. Consistently with this model, embryos treated directly with extracellular serotonin also resulted in consistent hyperpigmentation. Similar screens have resulted in the identification of the various transduction mechanisms in various morphological events (summarized in

Table 1)

***Bioelectric signals for coordination of non-local morphogenesis***

Large-scale pattern formation requires the orchestration of numerous cell-level processes. Bioelectric gradients are an ideal mechanism for implementing such coordination because they function across a range of size scales [1, 22, 48] and control basic cell behaviors such as cell cycle progression [48, 49] and differentiation [50, 51], in a wide range of cell types, including human mesenchymal stem cells [52], embryonic stem cells [53], and mature somatic cells [54, 55]. Many studies have also examined the effects of  $V_{\text{mem}}$  on cell migration and orientation, and significant progress has been made on dissecting the molecular mechanisms driving these processes in the context of wound healing [3, 6, 18, 56] and whole-body embryogenesis [16, 57].

Given the abilities of voltage gradients to exert influence both cell-autonomously and over long distances, what kind of patterning information can bioelectric signals mediate? Transmembrane potential can specify tissue identity at the level of cell groups [17] as evidenced by recent findings showing that the artificial manipulation of  $V_{\text{mem}}$  (hyperpolarization to a specific level) in developing *Xenopus* embryos can turn cell groups far from the anterior neuroectoderm to an eye fate [24].  $V_{\text{mem}}$  changes can also control large-scale axial polarity, such as the head-tail polarity of regenerating planarian fragments [26, 58, 59], and the left-right patterning of the early frog embryo [42, 60]. In the latter series of studies, a pharmacological screen first implicated several ion transporters in establishment of correct laterality [61]; serotonergic mechanisms mediating the effect were later found using a suppression screen [41, 62]. Transmembrane voltage patterns across tissues can also provide positional

**Table 1.1. Known transduction mechanisms by which ion flows impact morphogenesis.**

<b>Developmental role</b>	<b>Key biophysical event</b>	<b>Transduction mechanism</b>	<b>Reference</b>
Tail regeneration in <i>Xenopus</i> : 1° step	Voltage change (repolarization)	Guidance of neural growth	[29]
Tail regeneration in <i>Xenopus</i> : 2° step	Intracellular sodium content	SIK2 (salt-inducible kinase)	[63]
Proliferation of progenitor cells	Voltage change	Ca <sup>++</sup> flux through voltage-gated calcium channels	[64]
Neoplastic conversion of melanocytes in <i>Xenopus</i> tadpoles	Voltage change (depolarization)	Serotonin movement through SERT	[31, 33]
Polarity determination in planarian regeneration	Voltage change	Ca <sup>++</sup> flux through voltage-gated calcium channels	[26]
Left-right patterning in <i>Xenopus</i> embryos	Voltage change	Serotonin movement through gap junctions	[41, 61, 62, 65]
Trachea size control in <i>Drosophila</i>	Ion-independent function	Planar polarity, septate junction structure	[66]

information to guide migratory cells in vertebrate neurulation [16] or specify the spatial patterns of gene expression during craniofacial morphogenesis [28] – a kind of subtle prepattern that underlies the biochemical and genetic prepatterns that drive anatomy. In addition to providing large-scale anatomical identity and controlling the geometry of gene expression, bioelectric gradients can act as master regulators, triggering highly-orchestrated, self-limiting downstream patterning cascades such as regeneration of an entire appendage. For example, regeneration of the tadpole tail can be induced by very simple signals consisting of modulations of proton or sodium ion movement in the blastema during non-regenerative stages [29, 30].

Given this epigenetic control of cellular processes, it should come as no surprise that bioelectric properties are essential to many developmental processes that require the proliferation, differentiation, migration and orientation of a vast number of cells. These same signals that are necessary in the regeneration and remodeling of complex tissues also participate in the continuous battle of multicellular organisms to avoid the runaway growth of cancer.

### **Endogenous electric fields & ionic flow in the detection & treatment of cancer**

The same signaling mechanisms required for stem cell specification and lineage restriction during embryonic pattern formation also play fundamental roles in adult tissue regeneration and cancer. Indeed, cancer can be described as a lack of morphostasis, or a disruption in the ability to maintain target morphology [67-69].

### ***The molecular physiology of cancer***

Many of the same signaling pathways (i.e. TGF $\beta$ , Wnt, Notch, etc.) regulate self-renewal in both stem cell and cancerous cell types [70-73]. While the unique bioelectrical properties of tumor tissue have long been recognized [74-77], it is only in recent years that ion channels and bioelectric communication have emerged as important players in cancer-related processes. Many ion channels have been found to be involved in cancer-related cellular behaviors such as proliferation, apoptosis, migration and angiogenesis [31, 33, 78-82]. In fact, ion channels are involved in each of the six traditional hallmarks of cancer: 1) self-sufficiency in growth signals, 2) insensitivity to antigrowth signals, 3) evasion of programmed cell death (apoptosis), 4) limitless replicative potential, 5) sustained angiogenesis, and 6) tissue invasion & metastasis[83, 84].

The bioelectric profiles of different cell types demonstrate the link between membrane voltage and proliferative potential. The resting  $V_{\text{mem}}$ 's of various cell types vary widely (generally -10 mV to -90 mV) with plastic, embryonic, stem and tumor cells being relatively depolarized, whereas quiescent, terminally differentiated cells are relatively hyperpolarized [48, 49]. Membrane potentials are involved in the control of mitosis rate, as the modulation of  $V_{\text{mem}}$  has been shown to be required for both the G<sub>1</sub>/S and G<sub>2</sub>/M phase transitions [22, 85]. Mitotic arrest can be achieved by hyperpolarizing Chinese hamster ovary cells to -75 mV, and reversed by depolarizing to -10 mV [86]. Depolarization is also responsible for the hyper-proliferation of melanocytes in *Xenopus* embryos [31, 33].  $V_{\text{mem}}$  thus provides a convenient target for the modulation of proliferative potential.

A number of ion channels have also been implicated in enhanced cell

migration, motility and invasion; all crucial components of tumor metastases. For example, voltage-gated sodium channels have been detected in biopsies of metastatic breast, prostate and cervical cancers as well as in metastatic cancer-derived cell lines [87-90]. Potassium and chloride channels have also been implicated in the dynamic changes in cell shape and volume required for the capacity to move and invade extracellular spaces in glioma cells [84, 91]. A number of these studies indicate that highly metastatic cancers express embryonic isoforms of voltage gated sodium channels, further supporting the notion that cancer is a recapitulation of a developmental state. More recently, two studies revealed that depolarized membrane voltage is both a physiological signature by which nascent tumors can be non-invasively detected using fluorescent reporter dyes, and a functional parameter that can be used to control tumorigenesis: artificial hyperpolarization of oncogene-expressing cells by a range of ion channel types significantly reduces the formation of tumors in an amphibian model [92, 93].

***Cancer: rogue genetics or loss of tissue organization?***

In fact, developmental systems are a convenient model for the studies of cancer biology, providing access to a number of stem cell populations that are present throughout embryogenesis, many of which have been implicated with neoplasms. Perturbations in embryonic systems that can induce neoplastic-like phenotypes thus allow significant insights into the signaling mechanisms that may give rise to the creation of cancerous stem cells. Stem cells can be regarded as the center of the regeneration-development-cancer triad [94] and the backbone of the cancer stem cell hypothesis [95]. Melanomas, for example, are tumors of pigmented cells known as melanocytes. Recent

studies have highlighted that melanoma cells seem to revert to a more stem cell-like phenotype as they become more aggressive, showing decreased expression of the microphthalmia-associated transcription factor (MITF) and tyrosinase-related protein 1 (TRP1) [96, 97]. This de-differentiation might make highly aggressive tumors more difficult to identify in routine histopathology amplifying the need for different classification standards.

There is currently significant debate as to whether stem cell dysregulation and genetic mutation [98, 99], or epigenetic signals from the microenvironment [100-103] are the better perspective from which to understand cancer. Importantly however, bioelectric mechanisms have now been shown as central players in both types of events [104]. Regardless of which view turns out to be the more accurate, continued advances in the understanding of regulation of stem and somatic cells by voltage gradients, and the interplay between biophysical and genetic regulators, are likely to have significant implications for the cancer problem.

## **Conclusion**

Endogenous membrane voltage are one key component of the rich set of electromagnetic events taking place in living tissues; their spatio-temporal distribution represents important, yet still under appreciated, sources of instructive information in the control of morphogenesis. Recent work, making use of modern experimental techniques, has allowed scientists to probe the connections between these biophysical signals and the molecular-genetic downstream pathways that control cell behavior and thus large-scale patterning. However, we are only beginning to scratch the surface, and much development

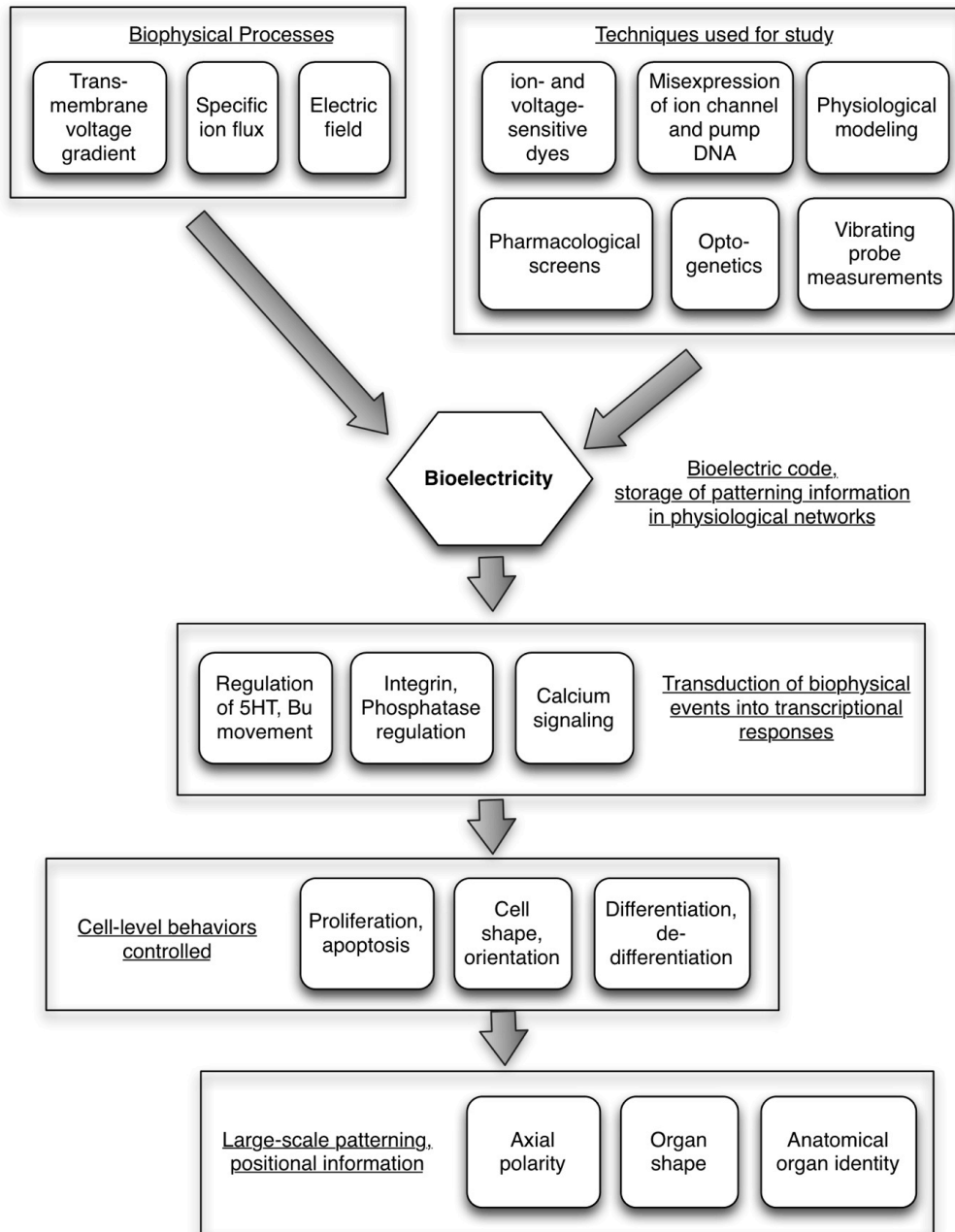


**Figure 1.3. A mind-map of the field of bioelectricity.**

of technology and conceptual apparatus must take place before a full understanding of self-generated order and information storage in physiological networks can be gained. This includes development of theoretical formalisms for modeling information storage in real-time physiological (not genetic) networks, comprehensive (quantitative) physiomic profiling of morphogenetic model systems *in vivo*, and the application of tools such as optogenetics to allow the experimental re-writing of bioelectric patterns in living tissues. Bioelectricity (Figure 1.3) still represents a novel area of research in the life sciences, and improvement in the ability to control bioelectrical information is sure to be transformative for regenerative medicine, bioengineering, and synthetic biology.

### **Acknowledgments**

We thank the members of the Levin lab and the bioelectricity community for many useful discussions. M.L. is grateful for support of the NIH (awards AR061988, AR055993, EY018168), the G. Harold and Leila Y. Mathers Charitable Foundation, and the Telemedicine and Advanced Technology Research Center (TATRC) at the U.S. Army Medical Research and Materiel Command (USAMRMC) through award W81XWH-10-2-0058.

## Chapter 2

### **Early, nonciliary role for microtubule proteins in left–right patterning is conserved across kingdoms**

Maria Lobikin, Gang Wang, Jingsong Xu, Yi-Wen Hsieh, Chiou-Fen Chuang, Joan M. Lemire, and Michael Levin

Proceedings of the National Academy of Sciences 109(31),  
12586-91 (2012)

**Data contributions:** I contributed data to figures 2.1, 2.2, 2.3, 2.4 and supplemental figures S2.1, S2.2, S2.3, S2.4, S2.5 and Supplemental Tables S2.1-S2.5. Gang Wang, Jingsong Xu, Yi-Wen Hsieh and Chiou-Fen Chuang contributed data to figure 2.5

## **Abstract**

Many types of embryos' bodyplans exhibit consistently oriented laterality of the heart, viscera, and brain. Errors of left–right patterning present an important class of human birth defects, and considerable controversy exists about the nature and evolutionary conservation of the molecular mechanisms that allow embryos to reliably orient the left–right axis. Here we show that the same mutations in the cytoskeletal protein tubulin that alter asymmetry in plants also affect very early steps of left–right patterning in nematode and frog embryos, as well as chirality of human cells in culture. In the frog embryo, tubulin  $\alpha$  and tubulin  $\gamma$ -associated proteins are required for the differential distribution of maternal proteins to the left or right blastomere at the first cell division. Our data reveal a remarkable molecular conservation of mechanisms initiating left–right asymmetry. The origin of laterality is cytoplasmic, ancient, and highly conserved across kingdoms, a fundamental feature of the cytoskeleton that underlies chirality in cells and multicellular organisms.

## Introduction

Consistent laterality is a fascinating aspect of embryonic development and has considerable implications for the physiology and behavior of the organism. Although vertebrates are generally bilaterally symmetric externally, most internal organs, such as the heart, viscera, and brain display asymmetric structure and/or unilateral positioning with respect to the left–right (LR) axis. A common defect in LR patterning is the loss of concordance among the sidedness of individual organs known as heterotaxia. In human beings, abnormalities in the proper development of laterality occur in more than 1 in 8,000 live births and often have significant medical consequences [105]. Organ asymmetry is highly conserved among species; however, considerable controversy exists about the early steps of LR patterning among phyla [106-108] and the physical mechanisms that can break symmetry [109].

One model predicts that cilia-driven extracellular fluid flow during gastrulation is the origin of LR asymmetry [110]. Because numerous species initiate asymmetry before (or without) the presence of cilia [111, 112], this model implies that asymmetry generation must be poorly conserved, with numerous distinct mechanisms used throughout phyla. However, “ciliary” proteins, such as left–right dynein, known to be important for LR patterning, also have intracellular roles compatible with cilia-independent functions in laterality [113-116]. In contrast to the nodal flow model, we have suggested that asymmetry is instead an ancient, well-conserved property of individual cells arising from the chirality of cytoskeletal structures that is subsequently amplified by physiological mechanisms [108, 116, 117]. Thus, we sought the most evolutionarily distant model systems, and ones that are known not to rely on cilia for LR patterning, to test the hypothesis of fundamental molecular conservation of asymmetry

mechanisms.

Recent findings in *Arabidopsis thaliana* have shown that mutations in  $\alpha$ -tubulin and in a  $\gamma$ -tubulin-associated protein (Tubgcp2) play an important role in the symmetry properties of the plant's axial organs [118-120]. Wild-type *A. thaliana* axial organs do not twist during normal elongation, and its flowers are radially symmetrical. This symmetry can be broken by mutations in tubulin and tubulin-associated protein complexes. The tubulin mutations *spiral1*, *spiral2*, and *spiral3* produce right-handed helical growth mutants. *Lefty* (*lefty1* and *lefty2*) mutants were found to be suppressor mutants of *spiral1*, and when outcrossed displayed a prominent left-handed helical growth [118, 120]. Both  $\alpha$ -tubulin and  $\gamma$ -tubulin complexes are ubiquitous in eukaryotes and are involved in the formation and nucleation of microtubules. Here, we characterize the laterality phenotypes induced by the same mutations in a vertebrate (the frog *Xenopus laevis*), the nematode *Caenorhabditis elegans*, and mammalian cells, supporting a fundamental role for tubulin in the cilia-independent generation of LR asymmetry.

## Results

To determine if the same tubulin proteins implicated in *Arabidopsis* asymmetry also control large-scale asymmetry of both vertebrate and plant systems, homologous mutations were made in *X. laevis*  $\alpha$  tubulin and  $\gamma$  tubulin-associated protein Tubgcp2 (Figure S2.1). These mutations function as dominant negatives when assembled into the cytoskeleton together with native subunits [118, 121]. Synthetic mRNAs encoding mutant tubulins were injected into *Xenopus* embryo blastomeres (at various early stages) using standard methods [122]. At stage 45, embryos were analyzed for position (situs) of the heart, stomach, and gallbladder

(Figure 2.1 A–C), the definitive readout of LR patterning. All treatments were titrated to avoid nonspecific defects (resulting in embryos with perfectly normal dorsoanterior development, clear left- or right-sided organs with normal morphology, correct size and relative proportions, and wild-type behavior), ruling out general toxicity as a cause of LR phenotypes.

Embryos injected immediately after fertilization with mRNA encoding the dominant negative mutant  $\alpha$ -tubulin (tub4a) displayed significant levels of heterotaxia (independently randomized sidedness of the three scored organs, Figures 2.1D and E), revealing a common genetic underpinning of regulation of asymmetry between plant and vertebrate systems. Injections of wild-type tub4a mRNA had no effect. Co-injections of both mutants' mRNAs together did not significantly increase the incidence of heterotaxia, suggesting that these impact the same pathway (are not additive). We next introduced the mutant mRNAs at different time points during development, to determine when the tubulins functioned in LR patterning and test the possibility that the relevant tubulin structures are in the cilia at the gastrocoel roof plate (GRP).

Synthetic mRNAs injected immediately after fertilization are already translated by the two-cell stage (Figure S2.2 and [123]); studies of GRP cilia routinely inject at the four-cell stage to target reagents to this structure [124]. If tubulins were to function in LR asymmetry at any time after the first few cleavages (e.g., in the GRP during neurulation), injections at the two- or four-cell stages would show the same randomizing effects on asymmetry as do injections at one-cell stage. In contrast, injections of mutant tub4a mRNA into both blastomeres of the two-cell embryo (or later) had no effect on asymmetry. The mutant tubulin's introduction into very early embryos randomizes LR patterning when present during the earliest events of cleavage-stage development, but

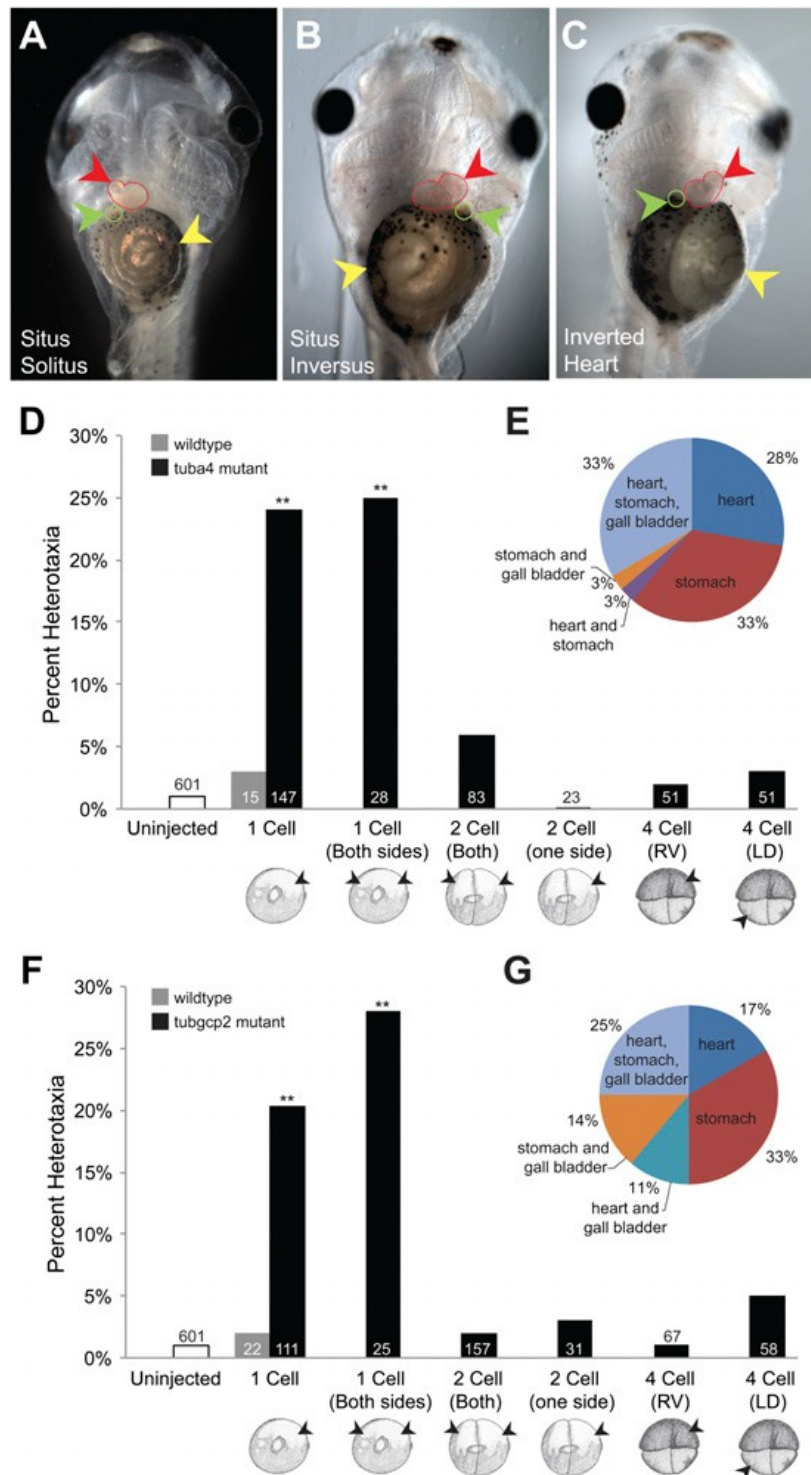


**Figure 2.1. Tubulin mutations affect LR asymmetry before the first cleavage event.**

(A–C) Organ situs of stage 45 embryos scored by observation. (A) A wild-type embryo, ventral view, showing the normal arrangement of the stomach (yellow arrowhead), heart apex (red arrowhead), and gall bladder (green arrowhead). (B) A heterotaxic embryo (ventral view) showing reversal of all three organs, i.e.,

situs inversus, induced by misexpression of the tubulin mutant. (C) A heterotaxic embryo (ventral view) showing reversal of the heart. (D) Statistical comparison of heterotaxia levels scored at stage 45 in embryos injected with mutated  $\alpha$ -tubulin mRNA at various early cleavage stages. (E) Types of heterotaxia observed from embryos injected with mutated  $\alpha$ -tubulin mRNA at the one-cell stage. (F) Statistical comparison of heterotaxia levels in embryos injected with mutated Tubgcp2 mRNA at various early cleavage stages. (G) Types of heterotaxia observed from embryos injected with mutated Tubgcp2 mRNA at the one-cell stage. \*\*P < <0.01, Welch's t test, sample sizes as noted in Table S2. For both constructs, it is only the presence before two-cell stage that allows these reagents to randomize laterality.

cannot affect the LR axis when introduced as early as the two-cell stage, ruling out involvement in LR patterning steps occurring after the first cleavages.

The *Xenopus* fate map facilitates targeting to the right or left halves of the embryo (Figure S2.3), allowing us to test spatial requirements for tubulin mutant-induced randomization with respect to the ciliated organ. Targeted injections were made in four-cell stage embryos, in the left-dorsal (LD) blastomere, which is known to be an early precursor of the GRP and the only side required for nodal flow [124], or the right-ventral (RV) cell, whose descendants do not contribute to the GRP [125]. Neither injection made at the four-cell stage produced significant levels of heterotaxia (Figure 2.1D), a result incompatible with mutant  $\alpha$ -tubulin affecting asymmetry via impact upon cilia-related events at the node. The same results were obtained using injections of mRNA encoding mutated  $\gamma$ -tubulin associated protein (*tubgcp2*) mRNA (Figure 2.1F and G). For both constructs, a single injection or two injections 180° apart at the one-cell stage randomized laterality, but injections of both or a single blastomere at the two-cell stage or later did not, ruling out the possibility that effects at the one-cell stage are due to an imbalance of injected mRNA on one side but not the other. These data reveal that the same functions of tubulin that alter asymmetry in a plant species are also involved in LR patterning in frog embryos, and that this function takes place at or just before the first cleavage.

To determine whether the tubulin-regulated events function in the same pathway as known early LR mechanisms and control downstream asymmetric transcription, we asked whether the expression of tubulin mutants perturbed the normally left-sided expression of the earliest known asymmetric gene in *Xenopus*: the TGF- $\beta$  signaling factor Nodal (*Xnr-1*) [126]. *Xnr-1* is normally expressed only on the left side of the embryo at approximately stage 22 [127].

Embryos injected with mutated tubulin mRNAs at the one-cell stage were fixed at stage 22 and processed for *in situ* hybridization with an *Xnr-1* probe. A significant percentage (64.7% for tub4a and 32.5% for tubgcp2) of mutant-injected embryos displayed incorrect *Xnr-1* expression (Figure 2.2), showing that these tubulin mutations affect LR asymmetry upstream of Nodal expression.

One model is that mutant tubulins perturb the normal rightward bias in the intracellular transport provided by the cytoskeleton in cleavage-stage frog embryos [123, 128]. These oriented cytoskeletal tracks allow cytoplasmic motors, such as kinesins and dyneins, to localize specific protein cargo to the left or right sides. We previously showed that the cytoskeleton during the one-cell stage confers rightward bias to kinesin heavy chain (KHC) motors and their cargo [61, 65, 129]. We asked whether this aspect of the normal *Xenopus* cytoskeleton might be perturbed following the misexpression of our mutant proteins. Embryos were injected at the one-cell stage with mRNA encoding KHC fused to a  $\beta$ -gal reporter protein, and sectioned at the four-cell stage to quantify the distribution of  $\beta$ -gal (blue) signal on the left vs. right sides; this assay [130] provides a readout of the cytoskeletal orientation via localization of the microtubule-dependent motor protein KHC (Figure 2.3A). Embryos receiving  $\beta$ -gal alone (which cannot localize by intracellular transport) most often exhibited bilateral signal. As previously described,  $\beta$ -gal:KHC fusions were preferentially localized on the right; crucially, the localization of  $\beta$ -gal:KHC signal in embryos also injected with the tubgcp2 mutant became disrupted, and exhibited approximately equal number of right, left, and bilateral localizations for the KHC motor and its cargo (Figure 2.3B and C). The difference in localization of microtubule-dependent motor protein cargo between these three conditions was statistically significant ( $P < 0.01$ ,  $\chi^2$ ), confirming that the introduction of the tubgcp2 mutant alters a known

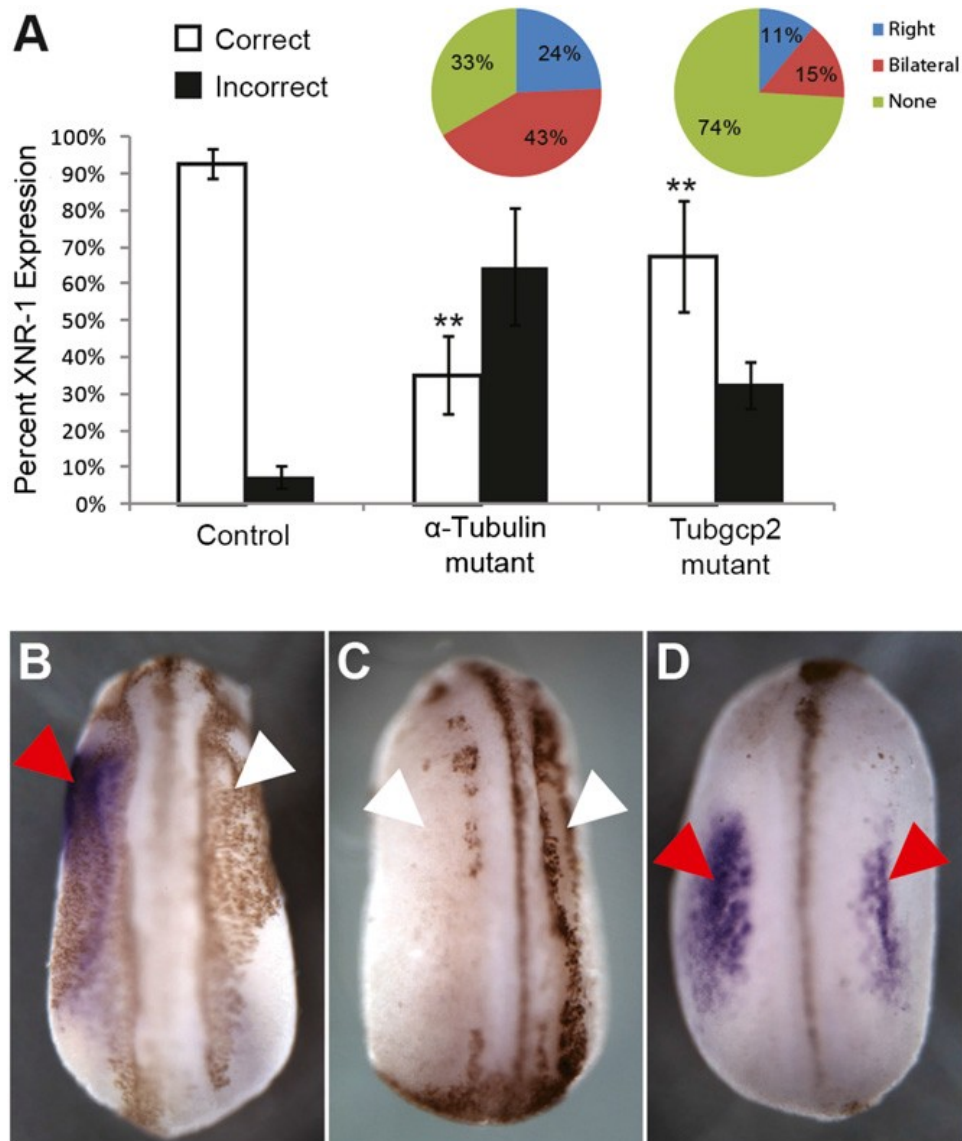


**Figure 2.2. Tubulin mutations perturb sidedness of asymmetric gene expression in *Xenopus*.**

Embryos injected with either tub4a mutant or Tubgcp2 mutant were processed for *in situ* hybridization at stage 22 with an *Xnr-1* probe. (A) Both tubulin mutants deviated significantly (denoted with double asterisks) from control embryos (Tub4a: 64.7% incorrect expression,  $n = 51$ ,  $P < <0.01$  Welch's t test; Tubgcp2: 32.5% incorrect expression,  $n = 83$ ; control: 7.33% incorrect expression,  $n = 150$ ,  $P < <0.01$  Welch's t test). (B–D) *Xnr-1* expression pattern (purple stain) characterized in tubulin mutant mRNA-injected embryos. (B) Left expression indicated by one red arrow and one white arrow. (C) Absence of expression as indicated by two white arrows. (D) Bilateral expression as indicated by two red arrows.

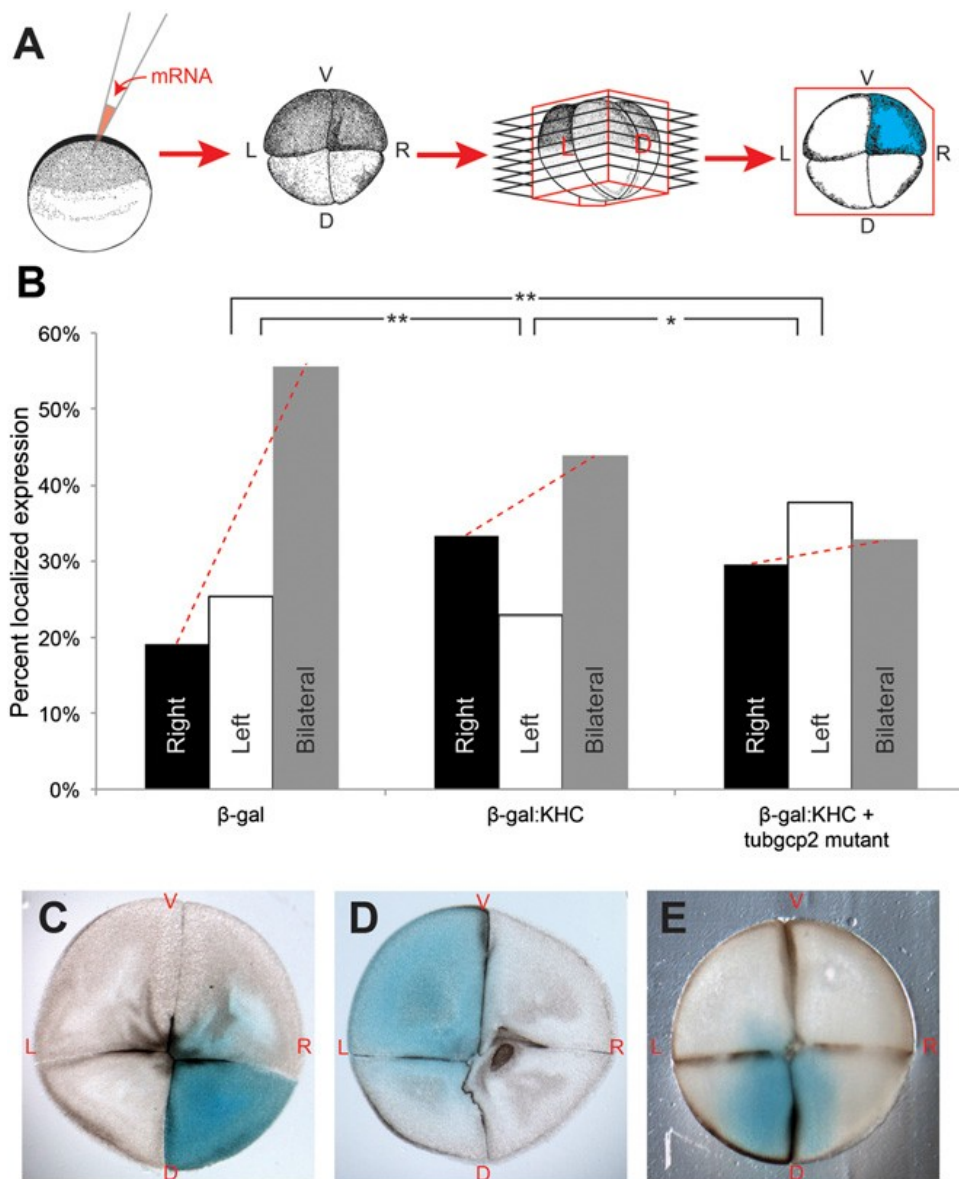


**Figure 2.3. Tubulin mutations affect early microtubule-dependent motor protein transport.**

(A) Embryos were injected into the very top of the animal pole shortly after fertilization with either a control  $\beta$ -gal mRNA, mRNA encoding the  $\beta$ -gal:KHC motor protein fusion construct or a mixture of  $\beta$ -gal: KHC and mutated tubgcp2. At the four-cell stage, embryos were fixed and processed for  $\beta$ -gal staining then embedded with consistent LR orientation, sectioned and scored for localization of the blue stain in the blastomeres as described (19). (B) Control embryos, injected with  $\beta$ -gal mRNA, displayed little LR bias (19% right, 25% left, 56% bilateral), whereas embryos that had been injected with  $\beta$ -gal:KHC displayed a significant rightward bias in  $\beta$ -gal localization (33% right, 23% left, 44% bilateral). Coinjections of tubgcp2 with the  $\beta$ -gal:KHC reversed this rightward bias (30% right, 38% left, 33% bilateral). \* $P < 0.05$ , \*\* $P < 0.01$ ,  $\chi^2$  test. (C–E) Typical  $\beta$ -gal expression patterns observed in sectioned four-cell embryos.

aspect of early microtubule function. Interestingly,  $\beta$ -gal signal was almost never detected in embryos when the *tuba4* mutant was coinjected with the  $\beta$ -gal:KHC (109 out of 110 embryos); although this remains to be investigated in future studies, it is conceivable that some new aspect of cytoskeletal organization can also trigger protein degradation machinery for molecular motors' cargo.

Having shown an alteration in cytoskeletal organization and a mislocalization of previously described asymmetric transport, we next sought a comprehensive (unbiased) analysis of asymmetric maternal components in the early embryo, and wanted to determine which of these were dependent on tubulin (thus identifying also those asymmetric *Xenopus* proteins for which no immunohistochemistry-suitable antibody is available). We performed a quantitative proteomics profiling of the left and right sides of four-cell embryos. Control embryos, and those injected at the one-cell stage with either the *tub4a* or *tubgcp2* mutant, were fixed in methanol at the four-cell stage, oriented, and split along the LR axis (first cleavage plane) with a blade. The left and right sides were pooled (n = 50), and samples were analyzed via liquid chromatography-mass spectrometry. Proteins showing a significant ( $P < 0.05$ , ANOVA) (more than 3 $\times$  difference in either direction) left- or right-sided bias in control embryos were selected. The analysis confirmed asymmetric localization of ion transporters (Tables S3 and S4) and the higher frequency of right-biased targets, which has been noted in previous work [61, 65, 123]. The presence of mutated tubulin significantly affected the endogenous bias in localization of some proteins, either reversing or completely abolishing it (Tables S2.3 and S2.4). As expected, this included cytoskeletal and transport-related proteins such as dynactin, cofilin-1, and a nonmuscle myosin (Table S2.1).

Cofilin-1, an actin depolymerization and filament severing protein [131],

was chosen for further investigation because of the known importance of actin in early cytoskeletal organization, Cofilin's role in directing the intracellular trafficking of ion transporter cargo [132], and recent data showing cofilin is asymmetrically transcribed in the two-cell mouse embryo [133]. Fertilized eggs injected with either tdTomato:Cofilin-1a alone, or in conjunction with a tubulin mutant, were allowed to develop and analyzed for tdTomato localization (Figure 2.4) at stage 45, where the embryo's transparency allowed clear detection of which side's progenitor cells had inherited the tagged cofilin. Whereas injections of tdTomato alone showed no significant bias in localization, tdTomato:Cofilin-1a injections revealed a significant ( $P \ll 0.01$ , paired t test) leftward bias in the fluorescent signal (Left localized: Right localized ratio, L:R, of 1.35), confirming that cofilin protein is indeed localized asymmetrically during the first cleavages. Coinjections of either tubulin mutant together with the tdTomato:cofilin-1a significantly ( $P < 0.05$ ) altered the normal left-ward bias of cofilin localization, and lead to subsequent randomization of organ situs (Figure S2.4 and Table S2.5). Coinjection with the tuba4 mutant resulted in a 0.91 L:R bias, thus abolishing cofilin's leftward bias, whereas the tubgcp2 mutant resulted in a 0.69 L:R ratio, reversing the bias (Figure 2.4 C and D). Scoring organ situs in tdTomato:cofilin-injected embryos revealed a weak but significant (8%) incidence of heterotaxia, consistent with some impairment of the interaction of cofilin with the LR localization machinery due to the addition of a large tdTomato structure (thus likely artificially lowering the bias in localization we observed). Thus, tubulin mutations are perturbing the normal consistent LR bias of a range of maternal proteins at the four-cell stage, consistent with models in which cytoskeletal organization drives positioning of LR-relevant cargo during the first cleavages.

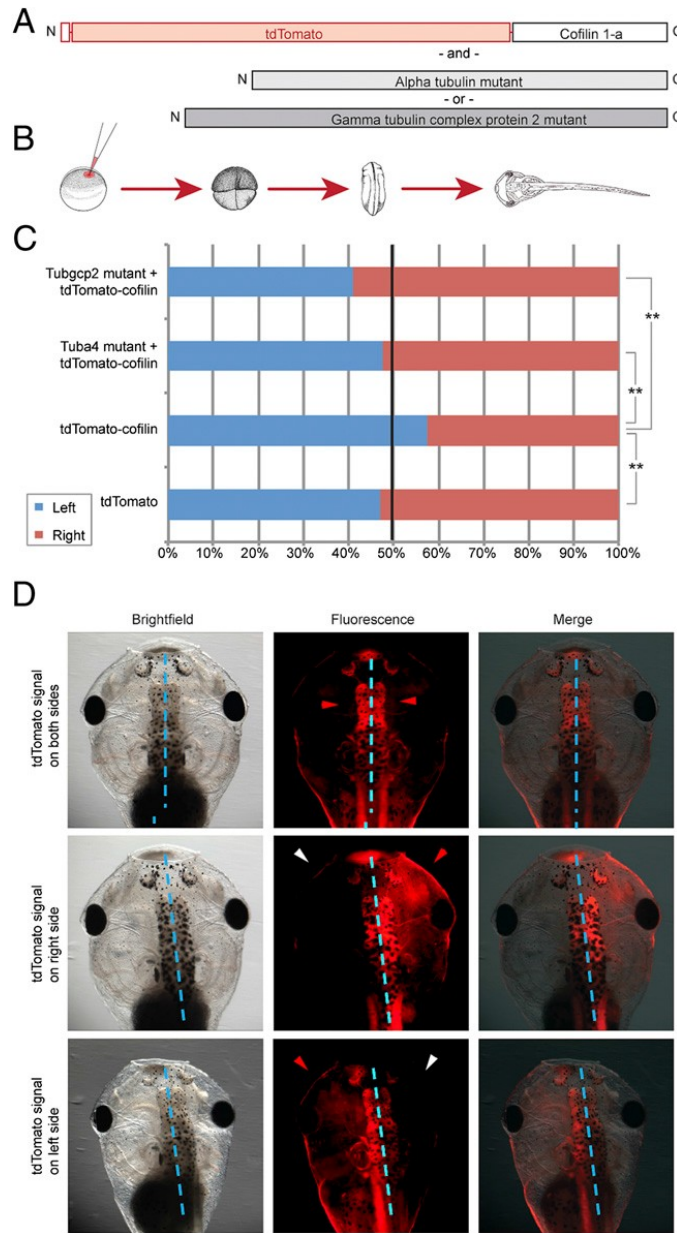


**Figure 2.4. Tubulin mutations alter biased Cofilin-1 expression.**

(A) tdTomato: Cofilin-1a fusion mRNA was injected into *Xenopus* embryos either alongside tub4a mutant mRNA, tubgcp2 mutant mRNA or on its own. (B) Injections were made shortly after fertilization; embryos were reared to stage 45 before scoring for tdTomato fluorescent signal. (C) Control embryos, injected with solely the tdTomato fluorescent marker displayed virtually no bias for signal localization (left localized:right localized ratio, L:R = 0.89, n = 117), whereas tdTomato:Cofilin-1a injected embryos displayed a leftward bias (L:R ratio = 1.35, n = 192). Embryos that had been coinjected with the tdTomato: Cofilin-1a and a tubulin mutant (either tub4a or tubgcp2) resulted in reversals in this bias (0.91 L:R ratio in tub4a mutant, n = 127; L:R ratio = 0.69 in tubgcp2 mutant, n = 208). Blue dashed line indicates embryo midplane. (D) tdTomato expression patterns observed in stage 45 *Xenopus* embryos. \*P < 0.05; \*\*P < 0.01.

Having observed the remarkable conservation of asymmetry roles for tubulin proteins between frog and *Arabidopsis*, we tested the same mutations in two additional model systems: the nematode *C. elegans*, and human HL-60 cells, thereby covering an extremely broad range of asymmetry types and bodyplans.

The two “AWC” olfactory neurons of *C. elegans* are morphologically symmetric, but display asymmetric expression of chemosensory receptors along the LR axis. Wild-type animals generate one AWC<sup>ON</sup> cell, which expresses the reporter gene *str-2p::GFP*, and one AWC<sup>OFF</sup> cell, which does not (Figure 2.5 A–C) [134]. Specific disruption of microtubules in AWC by nocodazole and benomyl generates two AWC<sup>ON</sup> neurons, suggesting that microtubules are required for LR AWC neuronal asymmetry [135]. *C. elegans* TBA-9  $\alpha$ -tubulin shares 75% identical amino acids with *A. thaliana* TUA6  $\alpha$ -tubulin. We mutated the conserved aspartic acid (256th) and glutamic acid (259th) residues in TBA-9 to alanine and expressed the TBA-9<sup>D256A/E259A</sup> mutant protein in AWC under the control of the *odr-3* promoter. Like nocodazole treatment, expression of TBA-9<sup>D256A/E259A</sup> caused a two-AWC<sup>ON</sup> phenotype at a frequency significantly higher than that caused by expression of wild-type TBA-9 when injected at the same concentration (Figure 2.5C). Both *odr-3p::tba-9* and *odr-3p::tba-9<sup>D256A/E259A</sup>* transgenes also caused a weak two-AWCOFF phenotype. Thus, two conserved residues in the GTPase-activating domain of  $\alpha$ -tubulins regulate microtubule dynamics required for precise LR patterning of *C. elegans*. An important recent finding is the observation that mammalian cells in culture, having neither node-like structure nor cilia-derived fluid flow, establish and maintain consistent LR asymmetries with respect to axes defined by internal polarity markers [136, 137]. Neutrophil-like HL-60 cells in culture extend pseudopodia to the left of an axis drawn between the nucleus and centrosome [137]. To test whether this asymmetry

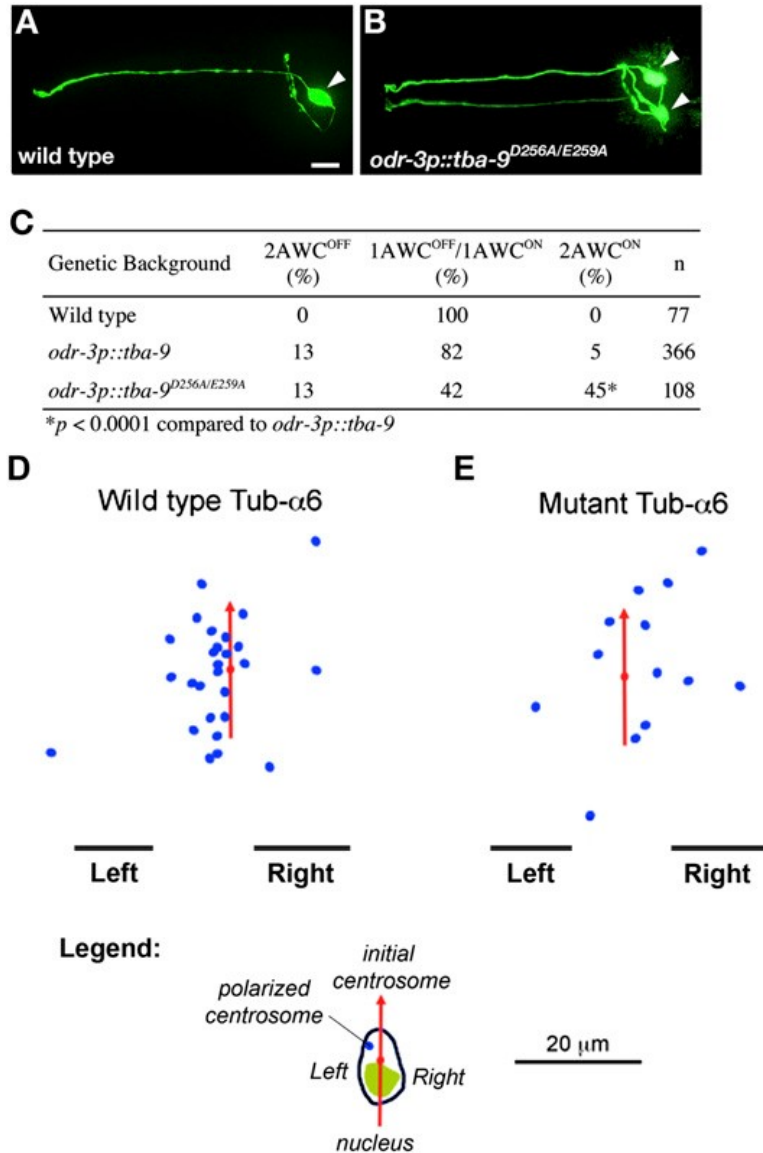


**Figure 2.5. Mutant tubulin disrupts LR asymmetry in *C. elegans* embryos and cultured HL-60 cells.**

(A) Wild-type *C. elegans* generate one AWC<sup>ON</sup> olfactory neuron cell, which expresses the reporter gene *str-2p::GFP*, and one AWC<sup>OFF</sup> cell, which does not (32). (B) *C. elegans* bearing mutations in aspartic acid (256th) and glutamic acid (259th) residues in  $\alpha$ -tubulin exhibit a 2 AWC<sup>ON</sup> phenotype at a frequency significantly higher than that caused by expression of wild-type TBA-9. These frequencies are quantified in C. Differentiated HL-60 cells were transiently co-transfected with GFP-Arrestin-3 (as marker of MTOC) and wild type tub-a6 (D) or mutant tub-a6 (E), and then exposed to uniform fMLP (100 nM), which induced polarization. The red arrow is drawn through the center of the nucleus, pointing to the centrosome, at 0 s as described (35). Final centrosome positions are indicated by the blue dots, relative to all red arrows co-aligned. Whereas wild-type tub-a6 does not affect the leftward bias, mutant tub-a6 abolishes it ( $\chi^2$  test,  $P < 0.01$ ). (Scale bar, 20  $\mu$ m.)

likewise depended on functional tubulin proteins, we transfected differentiated HL-60 cells with GFP-Arrestin-3 (a marker of the microtubule organizing center) and one of the tubulin constructs: wild-type tub-a6 (Figure 2.5D), or mutant tub-a6 (Figure 2.5E). Whereas wild-type tub-a6 (at expression levels achievable by transfection) did not affect the leftward bias, mutant tub-a6 abolished it. Thus, the same tubulin mutations that specifically randomize asymmetry in plant, vertebrate, and nematode systems likewise do so in mammalian cells.

## Discussion

The ciliary flow paradigm is forced to postulate highly divergent origins of asymmetry, because numerous invertebrate phyla establish consistent LR asymmetry without cilia or a node. Moreover, neither the pig nor the chick use cilia in their LR patterning pathway [112, 138]; zebrafish [139-141] and mouse [142] mutants exhibit normal asymmetry despite ciliary defects, and even mouse embryos already have LR-nonequivalent blastomeres by the third cleavage [143]. We tested a model of much earlier asymmetry-determining processes that would exhibit a more satisfying evolutionary conservation across a wide range of phyla.

Our data show that the presence of well characterized mutant forms of either  $\alpha$ - or  $\gamma$ - tubulin subunits in frog embryos specifically randomizes the LR axis (Figure 2.1), controlling the LR pathway upstream of the well conserved asymmetric expression of Nodal (Figure 2.2). Although the levels of heterotaxia were clearly significantly different from controls, they were below the ~87% theoretical maximum (for three fully randomized organs) because of the need to titer mutant tubulin mRNA to low levels to avoid possibility of confounding pure asymmetry phenotypes with general toxicity. Despite the crucial housekeeping

roles of tubulin, we were able to find a level of expression of mutants that allowed dissection of their LR patterning roles independent of any toxicity or generalized teratology.

Varying the time of injection allowed us to place strict bounds on the timing of the activity of these proteins in the LR pathway. Strikingly, whereas one-cell injections (whether made on one or both sides of the prospective midline) randomized asymmetry, injections at the two- or four-cell stage were already too late to do so (Figure 2.1D and F), suggesting that the function of tubulin in asymmetry occur no later than approximately the four- or eight- cell stage (because two-cell injections produce protein by then). Most crucially, injections of both cells at the two-cell stage do not affect asymmetry, ruling out interference with cilia-driven events at the GRP as the mechanism by which these mutants randomize the LR axis. Because the GRP is strongly affected by reagents injected at four-cell stage [124], our results show that expressing mutant tubulin in GRP cells makes no difference to asymmetry; the key factor that determines whether or not the LR axis will be randomized is whether tubulin mutant mRNA was injected before the two-cell stage and thus was available for translation during the earliest stages of development. The need to function during the first few cleavages (Figure 2.1) is incompatible with explanations involving cilia or nodal flow. Instead, the data are consistent with models in which the early cytoskeleton is nucleated by a chiral structure [144] that orients itself with respect to the other two axes, and thus biases the intracellular transport of key determinants along the LR axis [116, 145]. One such mod[146]el is shown in Figure S2.5.

As in snail embryos [147], early cytoskeletal dynamics are transduced into changes of asymmetric gene expression in vertebrate embryos. We

previously showed that orientation of the cytoskeleton at the first few cleavages is crucial for the correct asymmetric localization of several maternal proteins whose activity is in turn transduced into asymmetric transcription [61, 123]; by the second cell cleavage, the cytoskeleton already exhibits a directionality that results in accumulation of kinesin-associated cargo (or marker molecules) to the right side [123]. Others showed that a preexisting consistent chirality of the cytoskeleton exists in the egg cortex [148]. Despite the reduced levels of mRNA needed for double injections ( $\beta$ -gal:KHC + tubgcp2 mutant), introduction of the mutant tubulin significantly affected the ability of the native cytoskeleton to direct normal localization of motor protein cargo (Figure 2.3). We hypothesize that the presence of these mutant tubulin proteins alter subtle aspects of the intracellular cytoskeleton that are required to properly localize laterality-relevant cargo molecules across the LR axis.

To get the first unbiased glimpse of such asymmetries existing very soon after establishment of the midline, we performed a proteomic analysis comparing the left and right blastomeres' contents. This analysis revealed proteins with significant LR bias at the four-cell stage (Tables S2.3 and S2.4). Although the functions of these asymmetrically localized proteins remain to be probed by future studies, these data confirm the existence of consistent molecular asymmetries at very early stages (long before gastrulation) [61, 129, 146, 149] and exhibit a relative enrichment of right-sided proteins as found in our previous screens.

Although the large yolky cells of the early frog embryos are not conducive to the high-resolution imaging of cytoskeletal structure needed to identify subtle changes in chirality, the proteomic data reveal the consequences of tubulin mutation for the asymmetric distribution of early embryonic components, despite

the unavailability of antibodies. Analysis of protein distribution after microinjection of the two mutant cytoskeletal protein mRNAs showed (Table S2.1) that a number of important signaling proteins become mislocalized. Thus, we propose that the role of tubulins during early development is to serve as components of the chiral cytoskeleton by means of which asymmetric components sort to the left and right sides during the first cleavages, and as an important component of other intracellular localization events taking place at the two- to eight-cell stages. We selected cofilin, and labeled it with a fused fluorescent protein. Although this had somewhat of a destabilizing effect on asymmetry (Figure S2.4, suggesting a possible functional role for cofilin), we were able to observe a statistically significant bias in its native localization (Figure 2.4C and D) and showed that this native LR bias is abolished when tubulin mutants are introduced in the one-cell embryo.

Our data support previous models in which cytoskeletal chirality is amplified via differences in intracellular transport of key cargo during very early stages [128, 145, 150, 151]. Although the details are somewhat different, that same scheme is used by snail and *C. elegans* [135] embryos, and the same initial asymmetry is also compatible with a number of subsequent amplification mechanisms including asymmetric chromatid segregation [113] and planar cell polarity [108]. Perhaps the most remarkable aspect of these data is the widespread evolutionary conservation (even across the independent origin of multicellularity in plants and animals) of the role of these tubulin proteins in asymmetry, extending to plant coiling [119], *C. elegans* asymmetric neural patterning (Figure 2.5A–C), pseudopodial asymmetries in human cells in culture (Figure 2.5D and E), and organ placement of the vertebrate *X. laevis* (Figure 2.1). These findings are consistent with the nonciliary roles for tubulin in frog

asymmetry, as neither nematodes nor plants nor HL-60 cells use cilia in their asymmetry pathways. We have previously stressed the evolutionary conservation of several asymmetry-amplifying mechanisms across multiple diverse taxa [111, 116, 117, 152]. The above results implicate a single protein as an ancient, fundamental element with a highly conserved role as the initiator of chirality, upon which very different bodyplans can establish consistent downstream asymmetries of form and function.

### **Materials and methods**

For frogs, plasmids containing *X. laevis* tuba4 and Tubgcp2 (Xgrip110) and cofilin cDNA were purchased from Open Biosystems (clone IDs: 7010865, 5078639, and 5571290, respectively). The coding regions of these cDNAs were amplified by PCR and inserted into pCS2+ expression vectors using the In-Fusion Advantage PCR Cloning kit (Clontech). Tuba4 pCS2 and TubGCP2 pCS2 plasmids were linearized with Acc65I for SP6 transcription. Tuba4-mut (Ala180 replaced with Phe) and tubgcp2-mut (Gly453 replaced with Arg) were generated using the QuikChange II Site-directed Mutagenesis kit (Stratagene).

For nematodes, full-length *tba-9* cDNA (1368 bp) was obtained with RT-PCR of total mRNA from mixed stage worms and was subcloned to make *odr-3p::tba-9::SL2::TagRFP*. *odr-3p::tba-9<sup>D256A/E259A</sup>::SL2::TagRFP* was generated by site-directed mutagenesis (Stratagene QuikChange kit). *odr-3p::tba-9::SL2::TagRFP* (50 ng/μL) and *odr-3p::tba-9<sup>D256A/E259A</sup>::SL2::TagRFP* (50 ng/μL) were injected as described [153]. The coinjection marker *ofm-1p::DsRed* was injected at 30 ng/μL. Please see SI Materials and Methods for additional methods details. All experiments were conducted according to approved protocols (Institutional Animal Care and Use Committee, No. M2008-08).

## Acknowledgments

We thank Claire Stevenson for assistance with molecular biology; Punita Koustubhan and Amber Currier for *Xenopus* husbandry; Erol Gulcicek, Christopher Colangelo, and Thomas Abbott for assistance with interpretation of proteomic data; and Laura Vandenberg and the other members of the M. Levin laboratory for useful discussions. M. Levin acknowledges funding support from National Institutes of Health (NIH) Grant R01-GM077425 and American Heart Association Established Investigator Grant 0740088N; J.X. acknowledges funding support from NIH Grant HL095716; Y.-W.H. was supported by an NIH Training Grant of Organogenesis; and C.-F.C. was supported by a Whitehall Foundation Research Award and an Alfred P. Sloan Research Fellowship.

## Supporting information

### ***SI Materials and Methods***

**Animal Husbandry.** *Xenopus* embryos were collected and maintained according to standard protocols [122] in 0.1× Modified Marc's Ringers (MMR), pH 7.8 with 0.1% Gentamicin, and staged according to [154]. Wild-type strains of *C. elegans* were variety Bristol, strain N2. Strains were maintained by standard methods [155]. Integrated transgenes and transgenes maintained as extra chromosomal arrays included: *kyls140 [str-2p::GFP, lin-15(+)] I (33)*, *vyEx1089, 1090 [odr-3p::tba-9::SL2::TagRFP; ofm-1p::DsRed]*, and *vyEx1091, 1092, 1093 [odr-3p::tba-9<sup>D256A/E259A</sup>::SL2::TagRFP; ofm-1p::DsRed]*.

**Microinjection.** Capped, synthetic mRNAs were dissolved in water and injected into embryos in 3% Ficoll using standard methods [122]. mRNA injections were made into the locations indicated using borosilicate glass needles calibrated to bubble pressures of 50–70 kPa in water, delivering 100 ms pulses. After 30 min, embryos were washed in 0.75× MMR for 30 min and cultured in 0.1× MMR until desired stages.

**Laterality Assays.** *Xenopus* embryos were analyzed for position (situs) of three organs; the heart, stomach and gallbladder [156]. Heterotaxic embryos were defined as having a reversal in one or more organs. Only embryos with normal dorsoanterior development and clear left- or right-sided organs were scored. Percent heterotaxia was calculated as the number of heterotaxic divided by the number of total scorable embryos (error bars indicate variability from eggs of individual females). A  $\chi^2$  test (with Pearson correction for increased stringency) was used to compare absolute counts of heterotaxic embryos.

**In Situ Hybridization.** Whole mount *in situ* hybridization was performed using standard protocol [157]. *In situ* hybridization probes against *Xnr-1* (the *Xenopus* nodal) mRNAs [127] were generated *in vitro* from linearized template using DIG labeling mix (Roche). Embryos injected with mutated tubulins were examined for *Xnr-1* localization. A  $\chi^2$  test was used to compare absolute counts of embryos with correct versus incorrect *Xnr-1* expression.

**Quantitative Proteomics.** Snap-frozen *Xenopus* embryos (n = 30-50) in MeOH whose color and morphology at four-cell stage clearly indicated the dorso-ventral axis were divided in half along the first cleavage plane. Left and right sides were

pooled and placed in 20 µl per embryo of lysis buffer. The resulting digested peptides were cleaned and desalted with C18 stage tips for direct LC-MS/MS analysis.

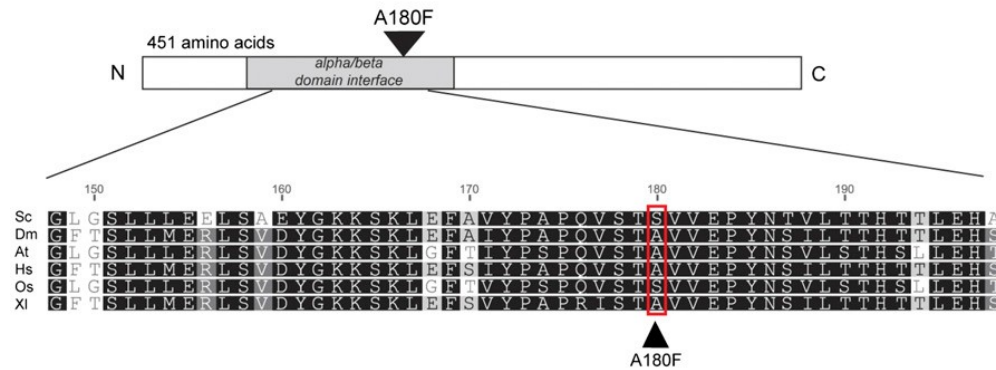
### **NanoUPLC-MS/MS: Protein Identification and Label-Free Quantitation**

**(LFQ).** To test the protein extraction protocol, the left and right sides of 50 pooled control embryos were first subjected to a pilot protein ID analysis via ultrahigh-pressure liquid chromatography-mass spectrometry using Waters nanoACQUITY with AB Sciex 5600 Triple ToF mass spectrometer. To ascertain the quantitative protein differences between the two halves, the left and right pooled samples from 30 embryos were then subjected to LFQ on a Thermo Fischer Scientific LTQ Orbitrap XL mass spectrometer containing the same Waters nAcquity system. All of the left- and right-side samples were randomized, and 0.2 µg of each of the enzymatically digested peptides was injected in three technical replicates with blank injected runs in between to minimize carry over. For the LFQ experiments, the LTQ Orbitrap is equipped with a Waters nano-Acquity UPLC system. The mass spectrometer acquired one survey run in the Orbitrap mode at 60,000 resolving power (400–2,000 m/z) and three consecutive data-dependent MS/MS runs in LTQ operating in CID mode. The raw data files were searched against a *Xenopus* database using Mascot search algorithm. In LFQ experiments, the Mascot database search is integrated into the Non Linear Progenesis Software ([www.nonlinear.com](http://www.nonlinear.com)), which performs feature extraction (peptide m/z peaks), chromatographic and spectral alignment, data filtering, and statistical analysis. Proteins showing a significant ( $P < 0.05$ , ANOVA and more than threefold difference in either direction) left- or right-sided bias in control embryos were selected as significant.

**Human Cell Culture, Transfection, and Microscopic Analysis.** Culture of HL-60 cells and transfections were performed as described [158]. For transient transfection, cells (on day 6 after addition of DMSO) were washed once in RPMI medium 1640-Hepes and resuspended in the same medium to a final concentration of  $10^8 \text{ mL}^{-1}$ . DNA was then added to the cells (50  $\mu\text{g}$  of GFP-arrestin-3 plasmid), and the cell-DNA mixture was incubated for 10 min at room temperature, transferred to electroporation cuvettes, and subjected to an electroporation pulse on ice at 310 V and low resistance. Transfected cells were allowed to recover for 10 min at room temperature and then transferred to 20 mL of complete medium. Subsequent migration assays were performed 4 h after transfection. Live cells were allowed to adhere to fibronectin-covered coverslips, and subjected to stimulation with a uniform concentration of fMLP (100 nM), and were imaged as described [158].

## Supplementary figures and tables

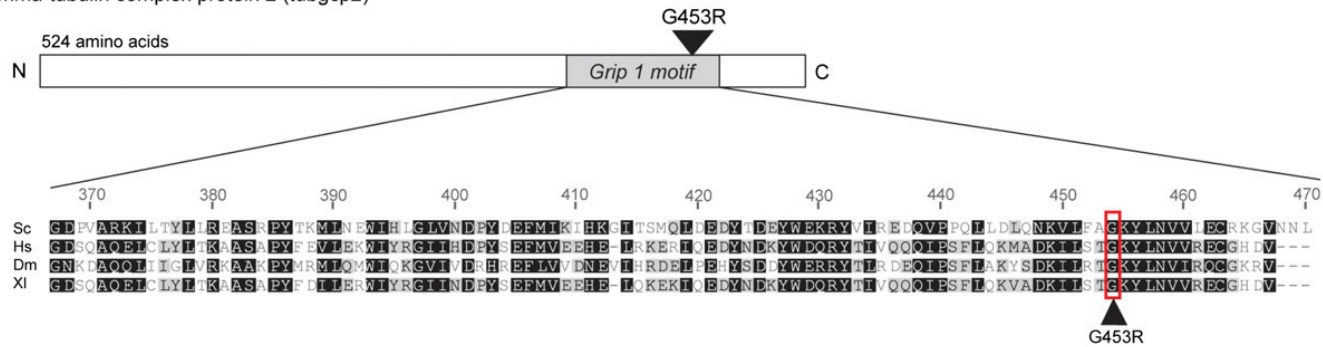
### A alpha-tubulin (tuba4)



### Legend:

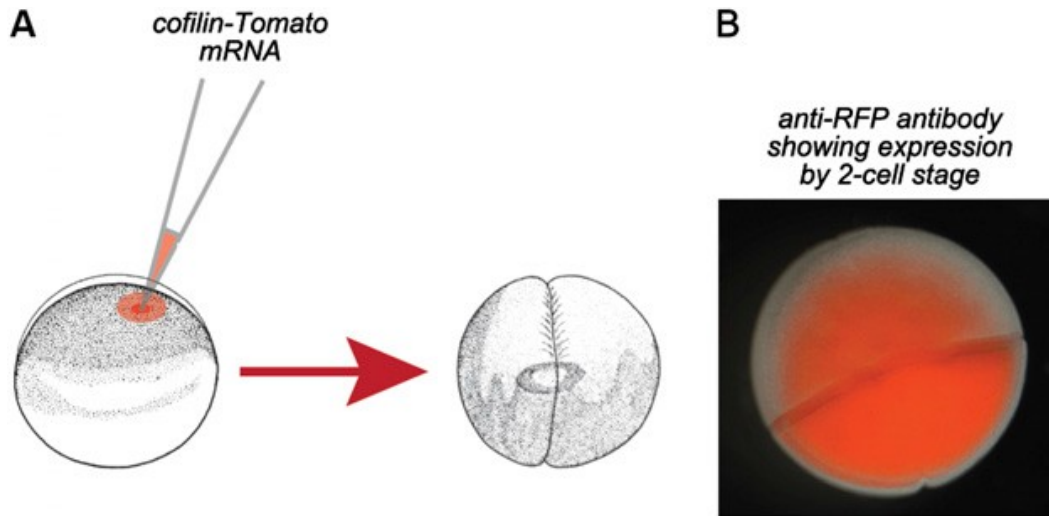
Sc Saccharomyces cerevisiae	Hs Homo sapiens
Dm Drosophila melanogaster	Os Oryza sativa
At Arabidopsis thaliana	XI Xenopus laevis

### B gamma-tubulin complex protein 2 (tubgcp2)



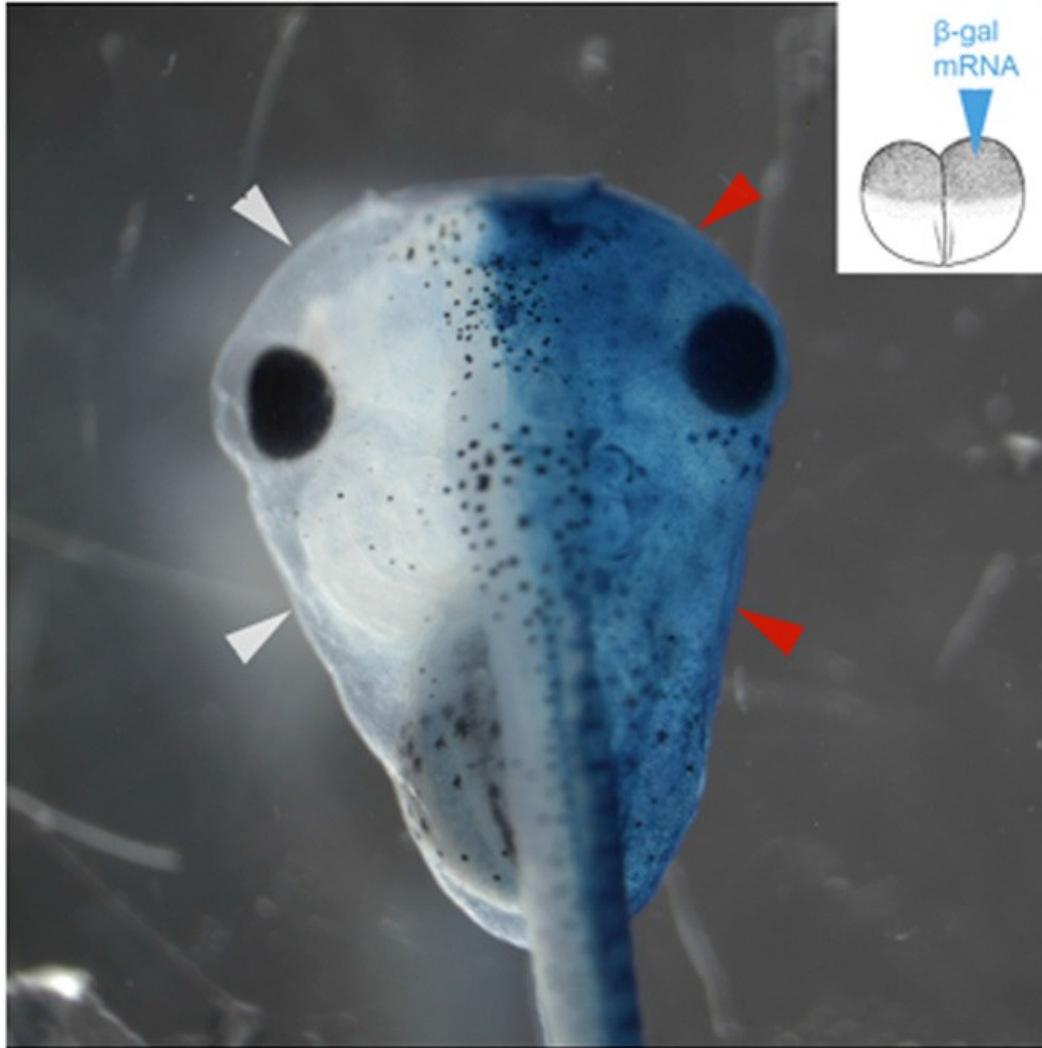
## Supplemental Figure 2.1. $\alpha$ -Tubulin and the $\gamma$ -tubulin associated protein complex, Tubgcp2, are highly conserved among organisms.

(A) Amino acid sequence alignment of the alpha/beta domain interface in various alpha tubulin orthologs. The conserved Ala180 (indicated with an arrowhead) was substituted with Phe in *Xenopus laevis*  $\alpha$ -Tubulin mutants, as in the lefty2 *Arabidopsis* mutants. (B) Amino acid sequence alignment of the Grip motif 1 in various GCP2 orthologs (known as Tubgcp2 in *Xenopus*). The conserved Gly453 was substituted with Arg in Tubgcp2 mutants, as in spr3 *Arabidopsis* mutants.



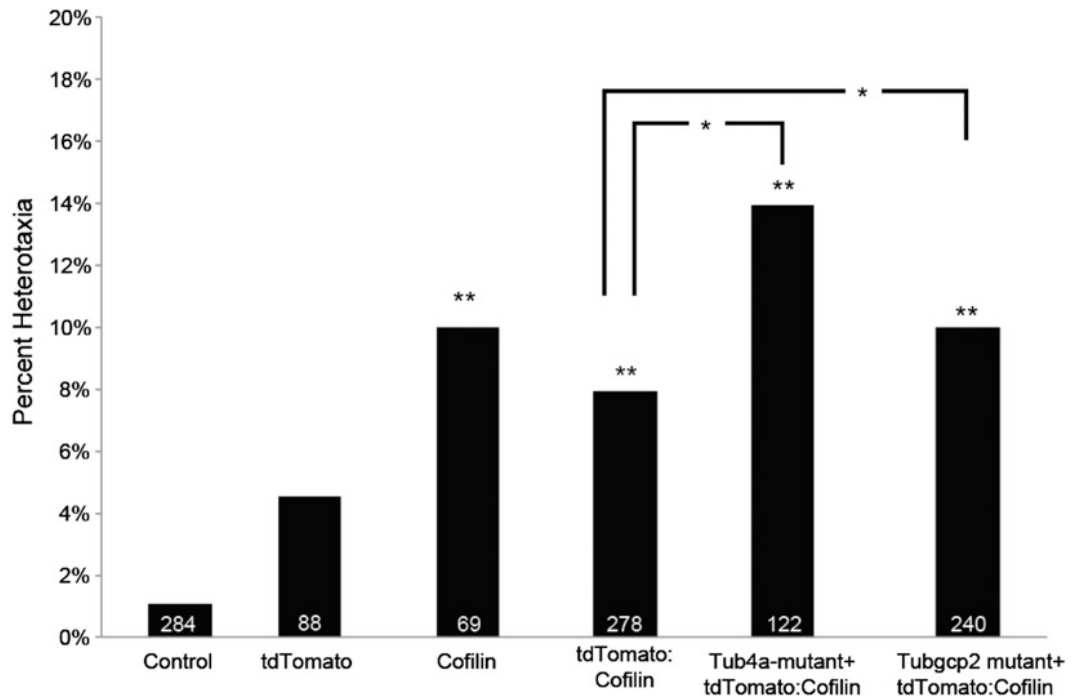
**Supplemental Figure 2.2. Early mRNA injection gives rise to proteins by the first cleavage.**

(A) Injections of mRNA encoding tdTomato:cofilin fluorescent protein fusions were performed shortly after fertilization into one side of the egg (off-center). Embryos were allowed to develop to the late two-cell stage. (B) Embryos were processed for immunohistochemistry with an anti-RFP antibody (Rockland 600–401-379) showing expression of cofilin protein is already strong by the two-cell stage, consistent with our ability to exert functional changes at the two-cell by injections made soon after fertilization.



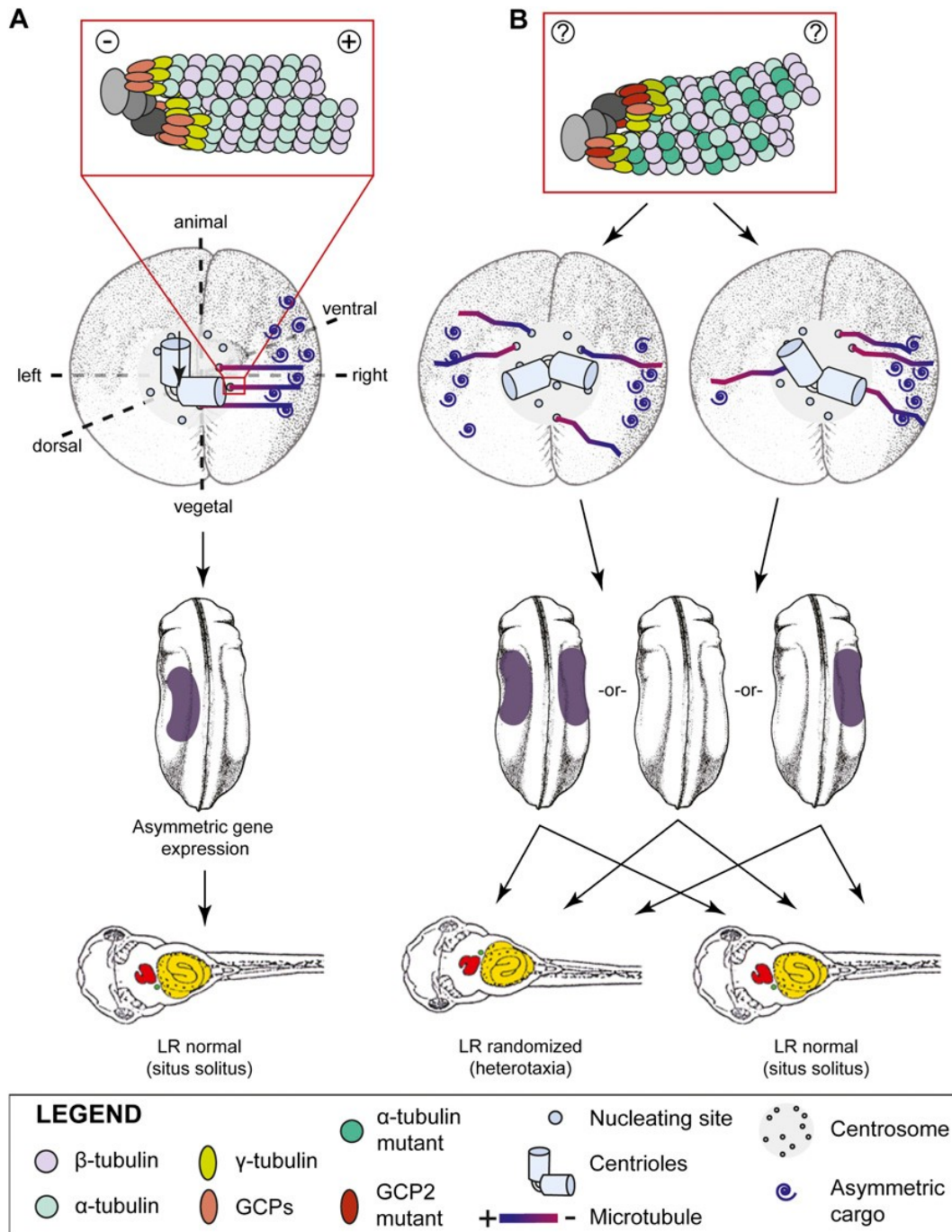
**Supplemental Figure 2.3. Injection into one of two early blastomeres allows targeting of the left or right side of embryo.**

Embryos were injected in one blastomere of the two-cell frog embryo with mRNA encoding the enzyme  $\beta$ -galactosidase. At stage 45, the embryos were developed using a chromogenic reaction, illustrating that mRNA injected in this manner targets cells on one side of the embryo. The first cleavage plane is indeed usually aligned with the prospective LR midline of the embryo; as in numerous studies, where one blastomere injection at the two-cell stage allows the other side to serve as an unaffected contralateral control, this confirms our ability to target early injections of cofilin to one side or the other.



**Supplemental Figure 2.4. Heterotaxia rates in tdTomato:Cofilin-a1 coinjections.**

Embryos injected with cofilin constructs were scored for positioning of the heart, gut, and gall bladder at stage 45. All of the cofilin constructs, but not the controls (injected with the fluorescent protein tdTomato alone) exhibited low but significant levels of heterotaxia. N's are given in the figure; Student's t test was used for significance calculations; \*P < 0.05, \*\*P < 0.01.



**Supplemental Figure 2.5. A model for tubulin's role in LR asymmetry in *Xenopus*.**

(A) In unperturbed embryos, the right-biased cytoskeleton [123, 129] is likely to derive from the orientation of the microtubule organizing center (centriole) with respect to the dorso-ventral and animal-vegetal axis, as proposed originally for a chiral "F-molecule" [145]. Correct function of both  $\alpha$ -tubulin (determining the structure of the microtubules along the animal-vegetal axis, and those involved in the dorso-ventral axis induction at cortical rotation shortly after fertilization) and  $\gamma$ -tubulin (mediating anchoring of LR-oriented microtubules to the MTOC) results in

the proper linkage of the MTOC to the two axes, allowing intracellular transport of LR determinant cargo molecules [116] to the right side, which ultimately results in correct organ situs. (B) Mutations in the GTPase-activating domain of tubulin suppress correct microtubule dynamics and promote polymerization [159]. Thus, the previously described (1) subtle right-ventral bending of the cytoskeleton would be altered when mutated  $\alpha$ -tubulin and  $\gamma$ -tubulin subunits were introduced at the early one-cell stage. In the absence of rightward intracellular transport of maternal proteins important for subsequent LR patterning steps, the downstream steps are randomized, resulting in a mixture of wild-type and heterotaxic embryos.

**Supplemental Table 2.1. Protein localization bias is abolished by tubulin mutants for certain proteins.**

Protein	Bias in Control Embryos Ratio (L:R)	Bias in $\alpha$ Tubulin mutant embryos Ratio (L:R)	Significance	Bias in Tubgcp2 mutant embryos Ratio (L:R)	Significance
Interferon-related developmental regulator 2	5.6	<b>1.2</b>	**	<b>0.78</b>	**
Nucleolin (LOC397919 protein)	4.1	<b>1.1</b>	**	<b>0.95</b>	**
Nucleolin	2.9	<b>0.87</b>	***	<b>0.98</b>	***
Protein kinase C-binding protein NELL1	2.1	<b>0.92</b>	*	<b>0.80</b>	**
Rab-like protein 3	1.9	<b>1.1</b>	**	<b>0.85</b>	**
Thioredoxin domain containing protein	1.9	<b>1.1</b>	*	<b>1.0</b>	
Ribose-5-phosphate isomerase-like	1.9	<b>0.92</b>	*	<b>1.0</b>	*
DnaJ homolog subfamily C member 9-like	1.7	<b>1.2</b>	**	<b>0.89</b>	***
Cystatin-B	1.7	<b>1.3</b>	***	<b>1.0</b>	***
Eukaryotic initiation factor 4A-III-B	1.7	<b>0.82</b>	***	<b>1.0</b>	***
Dynactin subunit 2-A	1.6	<b>1.1</b>	*	<b>0.89</b>	**
Frizzled-1	1.6	<b>1.1</b>	*	<b>0.76</b>	*
Cofilin-1-B	1.5	<b>1.2</b>	*	<b>1.1</b>	**
Cofilin-1-A	1.4	<b>1.1</b>		<b>1.1</b>	
Ionotropic glutamate receptor	0.58	<b>0.88</b>	*	<b>1.3</b>	*
Nonmuscle myosin II heavy chain A	0.57	<b>1.3</b>	***	<b>1.1</b>	*
Nascent polypeptide-associated complex subunit alpha	0.53	<b>1.2</b>	*	<b>1.2</b>	**
Transcription factor BTF3 homolog 4	0.43	<b>1.0</b>	**	<b>0.90</b>	**
Electron transfer flavoprotein subunit beta-like	0.39	<b>1.1</b>	*	<b>0.73</b>	**
u6 snRNA-specific terminal uridylyltransferase 1	0.06	<b>1.7</b>	**	<b>0.76</b>	**
40S ribosomal protein S13 $\pm$	0.05	<b>1.0</b>	*	<b>1.2</b>	*

Ratios were calculated for the relative abundances of each protein in the left vs. right halves of the embryo (using only those with ANOVA P values < 0.05). P values calculated between control ratios and those resulting from mutant tubulin injections. \*\*\*P < 0.001, \*\*P < 0.01, \*P < 0.05

**Supplemental Table 2.2. Heterotaxia in embryos injected at various early cleavage stages.**

Treatment	Timing of injections	<i>n</i>	% heterotaxia	P-value compared to controls
Non Injected	-	601	1%	-
Alpha Tubulin	1-Cell	147	24%	P<<0.01
	1-Cell (two sides)	28	25%	P<<0.01
	2-Cell (both)	83	6%	P>0.01
	2-Cell (one side)	23	0%	P>0.1
	4-Cell (RV)	51	2%	P>0.1
Tubgcp2	4-Cell (LD)	51	3%	P>0.1
	1-Cell	111	20%	P<<0.01
	1-Cell (two sides)	25	28%	P<<0.01
	2-Cell (both)	157	2%	P>0.1
	2-Cell (one side)	31	3%	P>0.1
	4-Cell (RV)	67	1%	P>0.1
	4-Cell (LD)	58	5%	P>0.1

**Supplemental Table 2.3. Left-biased proteins in four-cell *X. laevis* embryos**

<b>Protein Name</b>	<b>Accession Number</b>	<b>Ratio (L:R)</b>	<b>Description</b>	<b>Effect of <math>\alpha</math>Tubulin mutant</b>	<b>Effect of Tubgcp2 mutant</b>
Sodium-and chloride-dependent glycine transporter 2	NP_001104197	7.9	Membrane protein that recaptures glycine	Unaffected	Unaffected
NADH dehydrogenase (ubiquinone) 1, alpha/beta subcomplex	NP_001089802	7.4	Catalyzes the transfer of electrons from NADH to coenzyme Q	Reversed	Abolished
Aldehyde dehydrogenase 6 family, member A1	NP_001089889	6.6	Enzyme that plays a role in the valine and pyrimidine catabolic pathways	Unaffected	Reversed
Interferon-related developmental regulator 2	NP_001090241	5.6	Transcriptional co-activator/repressor during embryonic development and tissue regeneration	Abolished	Abolished
Chromatin licensing and DNA replication factor 1	AAH72771	5.5	Key DNA licensing factor	Unaffected	Abolished
NADH dehydrogenase (ubiquinone) Fe-S protein 4	NP_001087349	5.2	Catalyzes the transfer of electrons from NADH to coenzyme Q	Unaffected	Unaffected
Nucleolin	NP_001081557	4.1	Nucleolar phosphoprotein involved in the synthesis and maturation of ribosomes	Abolished	Abolished
High mobility group box 2	NP_001079387	3.8	Involved in binding DNA, and may be involved in protein-protein interactions	Unaffected	Unaffected
XTimeless1	BAE45344	3.7	Essential protein that regulates circadian rhythms	Unaffected	Unaffected
Ribosomal protein L13a	NP_001080130	3.7	Ribosomal protein that is a component of the 60S subunit	Reversed	Reversed
Myosin, heavy chain 6, cardiac muscle, alpha	NP_001085070	3.3	Component of cardiac muscle motor protein	Unaffected	Abolished

Hyaluronan binding protein 4	NP_001084805	3.3	May be involved in nuclear functions	Unaffected	Abolished
Ribosomal protein S29	NP_001165201	3.1	Ribosomal protein that is a component of the 40S subunit	Unaffected	Abolished
bolA homolog 2	NP_001085971	3.1	Homolog of the morpho-protein BolA from E.coli	Reversed	Reversed
LSM3 homolog, U6 small nuclear RNA associated	NP_001091408	3.0	Sm protein that forms a complex to bind RNA	Reversed	Reversed

Embryo halves of control and mutant tubulin-injected embryos were analyzed via liquid-chromatography/mass spectrometry. Ratios were calculated for each of the left conditions relative to the right conditions using average normalized abundances with ANOVA P values <0.05. \*Entries beginning with NP are from the NCBI Reference Sequence database and all others are from the GenBank database.

**Supplemental Table 2.4. Right-biased proteins in four-cell *X.laevis* embryos**

Protein Name	Accession Number	Ratio (L:R)	Description	Effect of $\alpha$ Tubulin mutant	Effect of Tubgcp2 mutant
Perilipin 2	NP_001081960	0.33	Lipid droplet protein in oocytes	Unaffected	Unaffected
Elongation factor 1-alpha	NP_001080911	0.33	Responsible for the enzymatic delivery of aminoacyl tRNAs to the ribosome	Unaffected	Unaffected
Ribosomal protein S17	NP_001085933	0.29	Ribosomal protein that is a component of the 40S subunit	Reversed	Unaffected
40S ribosomal protein S14	NP_001080235	0.27	Ribosomal protein that is a component of the 40S subunit	Unaffected	Unaffected
Golgin A2	NP_001087616	0.27	Involved in the stacking of Golgi cisternae and in vesicular transport	Unaffected	Unaffected
Glucosamine-6-phosphate deaminase 1	NP_001083469	0.27	Enzyme involved in carbohydrate metabolism	Unaffected	Unaffected
Tumor protein D52-like 2	NP_001087127	0.27	Cytoplasmic protein frequently overexpressed in breast and other cancers	Abolished	Unaffected
Proliferation-associated protein 2G4	AAH44287	0.26	RNA-binding protein that is involved in growth regulation	Unaffected	Abolished
Myosin binding protein C, cardiac	NP_001082167	0.26	Cardiac isoform of a myosin-associated protein found in the cross-bridge-bearing zone of A bands in striated muscle	Unaffected	Unaffected
Heat shock 60kDa protein 1 (chaperonin)	NP_001083970	0.25	Essential for the folding and assembly of newly imported proteins in the mitochondria	Reversed	Abolished
Protein DPCD	NP_001092165	0.25	May play a role in the formation or function of ciliated cells	Unaffected	Unaffected
Proteasome (prosome, macropain) 26S subunit, ATPase, 6	NP_001090469	0.25	Part of a multicatalytic proteinase complex	Unaffected	Abolished

60S ribosomal protein L22	NP_001081541	0.25	Epstein-Barr virus small RNA associated protein	Unaffected	Unaffected
ATPase, H <sup>+</sup> transporting, lysosomal 31kDa, V1 subunit E1	NP_001079767	0.23	component of vacuolar ATPase (V-ATPase)	Unaffected	Unaffected
Ribosomal protein L12	NP_001080122	0.20	Binds directly to 26S ribosomal RNA	Unaffected	Unaffected
Ribosomal protein S7	NP_001084502	0.19	Ribosomal protein that is a component of the 40S subunit	Unaffected	Unaffected
Small nuclear ribonucleoprotein polypeptide E	NP_001085570	0.19	Interacts with an ATP-dependent RNA helicase	Unaffected	Unaffected
Coiled-coil domain containing 25	NP_001084524	0.17	Predicted to localize to the nucleus and is upregulated in metaphase II oocytes	Unaffected	Unaffected
CAP, adenylate cyclase-associated protein 1	NP_001082639	0.17	Regulates filament dynamics, implicated in a number of complex developmental and morphological processes	Unaffected	Unaffected
ATP synthase, H <sup>+</sup> transporting, mitochondrial F1 complex	AAH78592	0.17	Subunit of mitochondrial ATP synthase	Abolished	Unaffected
Ribosomal protein S19	NP_001080796	0.16	Ribosomal protein that is a component of the 40S subunit	Unaffected	Unaffected
Histone H2A.x	NP_001086099	0.16	Histone H2A protein	Reversed	Unaffected
Tumor protein D52	NP_001086339	0.15	Cytoplasmic protein frequently overexpressed in breast and other cancers	Abolished	Unaffected
Ribosomal protein S18	NP_001084747	0.13	Ribosomal protein that is a component of the 40S subunit	Unaffected	Unaffected
Proteasome 26S ATPase subunit 1 variant	BAD96388	0.12	Regulatory subunit of the 26S proteasome which is involved in the ATP-dependent degradation of ubiquitinated proteins	Unaffected	Unaffected
Ribosomal protein S10	NP_001080728	0.12	Ribosomal protein that is a component of the 40S subunit	Unaffected	Unaffected

Hydroxyacyl-CoA dehydrogenase	NP_001080900	0.092	Oxidoreductase involved in fatty acid metabolic processes	Reversed	Unaffected
Basic transcription factor 3	NP_001088356	0.076	Transcription factor and modulator of apoptosis	Abolished	Abolished
Terminal uridylyl transferase 1	AAH82663	0.058	Uridylyltransferase that acts as a suppressor of microRNA (miRNA) biogenesis	Reversed	Abolished
Ribosomal protein S13	NP_001080351	0.051	Ribosomal protein that is a component of the 30S subunit	Abolished	Abolished
26S protease regulatory subunit 8	NP_001081635	0.012	Ribosomal protein that is a component of the 26S subunit	Unaffected	Reversed
Proteasome (prosome, macropain) subunit, alpha type, 3	NP_001080243	0.005	Part of a multicatalytic proteinase complex	Unaffected	Unaffected
Microtubule associated serine/threonine kinase-like	ZP_04753594	0.001	Kinase that plays a key role in M phase by acting as a regulator of mitosis entry and maintenance	Unaffected	Abolished
Prohibitin	NP_001079486	0.00	Involved in mitochondrial function and morphology as well as transcriptional modulation	Reversed	Unaffected
Eukaryotic translation initiation factor 2, subunit 2 beta	NP_001090288	0.00	Eukaryotic initiation factor required in the initiation of translation	Unaffected	Unaffected

Embryo halves of control and mutant tubulin-injected embryos were analyzed via liquid-chromatography/mass spectrometry. Ratios were calculated for each of the left conditions relative to the right conditions using average normalized abundances with ANOVA P values <0.05. \*Entries beginning with NP are from the NCBI Reference Sequence database and all others are from the GenBank database

**Supplemental Table 2.5. Fluorescent signal localization for tdTomato:cofilin-1a injections**

Treatment	Fluorescent signal localization	<i>N</i>	Total <i>N</i>	P-value compared to tdTomato	P-value compared to tdTomato:cofilin
tdTomato	Left	32	117	-	P<<0.001
	Right	36			
	Both	48			
tdTomato:cofilin	Left	66	192	P<<0.0001	-
	Right	49			
	Both	77			
Tuba4 + tdTomato:cofilin	Left	39	127	P>0.05	P<<0.001
	Right	43			
	Both	45			
Tubgcp2 + tdTomato:cofilin	Left	50	208	P<<0.001	P<0.001
	Right	72			
	Both	86			

## Chapter 3

### **Transmembrane potential of GlyCl-expressing instructor cells induces a neoplastic-like conversion of melanocytes via a serotonergic pathway**

Douglas Blackiston, Dany S. Adams, Joan M. Lemire,  
Maria Lobikin and Michael Levin

Disease Models & Mechanisms 4(1), 67-85 (2011)

**Data contributions:** I contributed data to figure 3.3 and table 3.1. Doug Blackiston contributed data to figures 3.1-3.8, tables 2-3 and supplementary figures 1-3. Dany S. Adams contributed data to figure 3.7.

## Summary

Understanding the mechanisms that coordinate stem cell behavior within the host is a high priority for developmental biology, regenerative medicine and oncology. Endogenous ion currents and voltage gradients function alongside biochemical cues during pattern formation and tumor suppression, but it is not known whether bioelectrical signals are involved in the control of stem cell progeny *in vivo*. We studied *Xenopus laevis* neural crest, an embryonic stem cell population that gives rise to many cell types, including melanocytes, and contributes to the morphogenesis of the face, heart and other complex structures. To investigate how depolarization of transmembrane potential of cells in the neural crest's environment influences its function *in vivo*, we manipulated the activity of the native glycine receptor chloride channel (GlyCl). Molecular-genetic depolarization of a sparse, widely distributed set of GlyCl-expressing cells non-cell-autonomously induces a neoplastic-like phenotype in melanocytes: they overproliferate, acquire an arborized cell shape and migrate inappropriately, colonizing numerous tissues in a metalloprotease-dependent fashion. A similar effect was observed in human melanocytes in culture. Depolarization of GlyCl-expressing cells induces these drastic changes in melanocyte behavior via a serotonin-transporter-dependent increase of extracellular serotonin (5-HT). These data reveal GlyCl as a molecular marker of a sparse and heretofore unknown cell population with the ability to specifically instruct neural crest derivatives, suggest transmembrane potential as a tractable signaling modality by which somatic cells can control stem cell behavior at considerable distance, identify a new biophysical aspect of the environment that confers a neoplastic-like phenotype upon stem cell progeny, reveal a pre-neural role for serotonin and

its transporter, and suggest a novel strategy for manipulating stem cell behavior.

## **Introduction**

It is now clear that misregulation of stem cell fate and division is an important component of neoplasia [160]. Some tumors (at least in the case of blood, breast, skin, brain and colon cancer) might originate from malignant transformation of stem cells [72, 161-163]. Moreover, because cancer development fundamentally involves the loss of morphogenetic order [67, 164, 165] it is not surprising that the same signaling pathways (TGF $\beta$ , Wnt, Notch, etc.) seem to regulate self-renewal in embryonic patterning, stem cells and cancer cells [71-73, 166, 167]. Developmental systems serve as convenient models for studies of cancer because they allow access to a number of stem cell populations throughout embryogenesis and benefit from well-documented regulatory networks that underlie differentiation and patterning. Perturbations that induce neoplasia-like phenotypes during embryogenesis allow great insight into the signals leading to the creation of cancer stem cells and many such links have already been established [168-171].

Thus, stem cells are at the center of the regeneration-development-cancer triad [94]. The construction of replacement tissues or organs through stem cell therapy or *in vitro* bioengineering is a fundamental hope of regenerative medicine. Although much effort is directed towards coaxing stem cells to differentiate into specific cell types, the next frontier will involve learning to harness individual cellular dynamics to achieve complex multicellular morphogenesis. Building replacement organs or whole appendages to address birth defects, tumors, degenerative disease, injury and infectious morbidity will require not merely the presence of the right cell types, but also their integration

into three-dimensional highly complex structures of appropriate physiological and mechanical function [172]. This in turn will require a detailed understanding of the role of the cellular environment of the host in regulating the behavior of stem and cancer cells alike [103, 173].

The neural crest, a crucial population of embryonic stem cells that contributes to many structures during development [174], differentiates into a variety of cell types, including smooth muscle cells, peripheral neurons and glia, and craniofacial cartilage and bone, as well as endocrine and pigment cells. The biology of neural crest regulation is also of significant biomedical relevance because neurocristopathies form an important class of birth defects [175-177]. These cells are an ideal context in which to explore the common mechanisms regulating stem cells and neoplastic processes [178-180], especially with respect to pigment cell derivatives [94, 181]. These cells not only reveal dynamics of migration control [182, 183], but are also an important subject for understanding melanoma [184, 185] and in learning to control biological assembly *in vitro* for tissue engineering [186].

One of the most interesting areas of inquiry involves epigenetic controls of tumor progression and stem cell function [187-193]. It is becoming clear that the microenvironment is a key player that mediates epigenetic signaling mechanisms [100, 103, 194, 195]. Importantly, it is now known that cell behaviors are controlled not only by secreted chemical factors, traction forces and extracellular matrix, but also by bioelectrical events. Ionic controls of differentiation, proliferation and migration have been investigated for decades [8, 15, 196-198], with solid functional data demonstrating instructive roles in growth control, limb regeneration and anterior-posterior polarity. More recently, the

investigation of bioelectric signals has been accelerated by the availability of high-resolution molecular-genetic tools allowing the functional dissection of the endogenous roles of ion flows, voltage gradients and electric fields, and their linkage to canonical genetic and biochemical networks [18, 29, 47, 199-201]. Indeed, voltage- and current-mediated signals are now known to carry morphogenetic information, including signals regulating embryonic left-right patterning, wound healing and neuromuscular appendage regeneration [3, 6, 21, 34], as well as controlling cell-level behaviors such as cell migration and proliferation [22, 48, 202, 203].

It is known that transmembrane voltage is a powerful determinant of proliferative potential in somatic cells [22, 49, 55, 204]; moreover, genomic analyses and microarray screens have now revealed a number of ion channels to be key players in neoplasia [89, 205, 206]. Recent studies have shown that stem cells exhibit unique electrophysiological profiles [207-211]. Likewise, ionic currents and channels have been found to play important roles during myoblast, cardiomyocyte, mesenchymal and neural stem cell differentiation [50, 52, 207, 211-213].

However, much of this work was done *in vitro*, which does not reveal the complex interactions that are required to integrate stem cell function into complex morphogenetic programs. Thus, the ability of endogenous electrical signals to act as a functional biophysical control mechanism in stem cell biology *in vivo* is very poorly understood. Recently, in the *Xenopus laevis* embryonic system, we showed that misexpression of a regulatory subunit of the KCNQ1 potassium channel was able to induce hyperproliferation of melanocytes and a hyperpigmented phenotype that did not involve increases of pigment content per

cell or the conversion of other cell types into melanocytes [33]. This work revealed an entirely novel control of melanocyte behavior and led to several new questions. First, because misexpression of channel mRNA must be performed at cleavage stages, the timing of the melanocyte-instructive event could not be functionally characterized. Second, for the purposes of using bioelectrical controls of cell behavior for regenerative medicine or oncology, it is essential to develop techniques that do not rely on the introduction of transgenes because of the numerous problems attendant with gene therapy in human patients [214, 215]. Third, it is not known which cells, in what anatomical region, must be depolarized for the melanocytes to acquire the metastatic phenotype. Finally, it is not known what cells in the embryo endogenously have the ability to signal to neural crest descendants when their membrane voltage potential ( $V_{\text{mem}}$ ) is modulated, nor whether the KCNE1-induced signaling could be exerted by proteins other than the KCNE1-KCNQ1 potassium channel complex.

Therefore, we developed a strategy capitalizing on the ability to control the native glycine receptor chloride channel (GlyCl), and thereby control the steady-state transmembrane potential of GlyCl- expressing embryonic cells. Molecular-genetic or pharmacological depolarization of GlyCl-expressing cells confers a neoplasia- like phenotype on melanocytes: they overproliferate, become arborized and inappropriately colonize numerous tissues in a metalloprotease-dependent fashion. A similar effect is observed in cultured human melanocytes. The effect is specific to  $V_{\text{mem}}$  (not dependent on GlyCl per se or even chloride flux), is not cell- autonomous and is mediated by voltage control of serotonin [5- hydroxytryptamine (5-HT)] transport. These data (1) identify GlyCl as a unique marker of cells that can control melanocyte behavior

non-cell-autonomously, (2) reveal a novel mechanism by which bioelectrical properties of the microenvironment mediate the stem-cell–cancer-cell transition and (3) suggest a new class of strategies for manipulating embryonic stem cell behavior without the need for gene therapy.

## Results

### ***Exposure to chloride channel opener specifically induces hyperpigmentation***

To investigate the role of bioelectric signals during embryogenesis and develop a strategy that could ultimately be used in biomedical settings, we first developed a method for modulating transmembrane potential in select groups of cells *in vivo*. Chloride channels are a convenient target because, once opened, Cl<sup>-</sup> ions can be made to exit or enter the cell when the extracellular level of chloride ([Cl<sup>-</sup>]<sub>ex</sub>) in the medium is artificially varied [216]: levels of [Cl<sup>-</sup>]<sub>ex</sub> that are lower than that of intracellular chloride will lead to the exit of negative ions and thus depolarize the cells. Conversely, a high chloride medium will cause hyperpolarization by allowing negative ions to enter cells down their concentration gradient. To open chloride channels, we utilized ivermectin – a drug commonly used as an antiparasitic agent owing to the paralyzing effect it has on muscle cells in nematodes [32]. This compound is well-characterized, specifically opening GlyCl, and is already approved for use in human patients and veterinary medicine [217].

Untreated wild-type *Xenopus* embryos develop characteristic pigment patterns after a fraction of neural crest derivatives become determined as melanocytes during late neurulation and somite stages [218, 219] and begin to produce melanin during tailbud stages. The majority of melanocytes occupy a medial position in the head and trunk of young tadpoles (Figure 3.1A,A').

*Xenopus* developing in 0.1X Modified Marc's Ringers (MMR) medium,  $[Cl^-]=10$  mM (lower than internal  $Cl^-$  concentration ( $[Cl^-]_{int}$ ), which is 40-60 mM), were exposed to 1  $\mu$ M ivermectin, which, under these conditions, is a depolarizing agent affecting cells that express GlyCl (supplementary material Figure S3.1). Treatment throughout development from early neurulation paralyzed older tadpoles, as expected from the depolarization effect. Strikingly, it also resulted in extensive hyperpigmentation. Melanocytes in treated individuals often migrated to regions normally devoid of pigment cells, such as the lateral eye field (Figure 3.1B, red arrows) and the dorsal and ventral fins (Figure 3.1B",B""), and filled the core of the tail (Figure 3.1B'). This phenotype occurred in 98% of treated larvae (Figure 3.1C; supplementary material Movies 1 and 2); importantly, however, development was otherwise normal. Embryos showed no differences in growth rate or morphogenesis compared with wild type, and had a normal dorsoanterior index in addition to proper patterning of the body axis and organs. Other neural-crest-derived organs such as the branchial arches were apparently normal, arguing against significant deviation of neural crest streams from other targets. We conclude that pharmacological opening of chloride channels in embryos specifically results in hyperpigmentation

***Ivermectin-induced hyperpigmentation involves inappropriate migration, ectopic colonization and cell shape change***

To determine whether the hyperpigmentation was due to migration of melanocytes to inappropriate locations, and whether this process, like metastasis, depends on metalloproteases (MMPs), we treated embryos with a combination of ivermectin and the well-characterized MMP inhibitor NSC-84093,

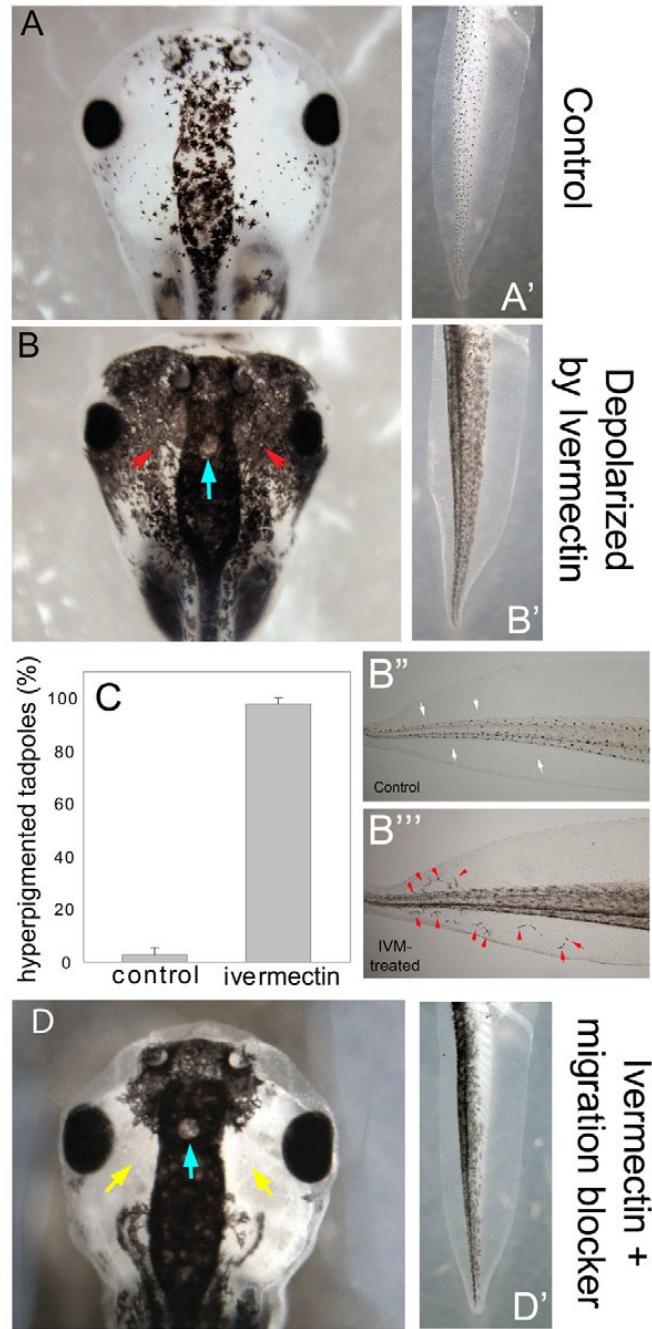


**Figure 3.1. Ivermectin exposure induces hyperpigmentation.**

(A) Control embryos display a medially concentrated pigment pattern with the lateral eye field being largely devoid of melanocytes. (A') The tail normally has a distributed population of round melanocytes over its core. (B) Embryos exposed to the chloride channel activator ivermectin while developing in the normal 10 mM Cl<sup>-</sup> medium acquire a hyperpigmented phenotype by stage 42 despite otherwise normal development; ectopic melanocytes are present (periorbital region indicated by red arrows; compare to similar region in panel A), and (B') are more numerous and spread out in the tail. Ectopic melanocytes are also

found in the dorsal and ventral fins (compare B''' to control tails in B''). White arrows indicate fin region normally devoid of melanocytes; red arrowheads indicate ectopic melanocytes. (C) The ivermectin-induced phenotype was highly penetrant, with 98% of treated embryos developing hyperpigmentation (error bars indicate one standard deviation, n=189 for controls, n=174 for ivermectin-exposed). (D) When migration was blocked by the MMP inhibitor NSC-84093 in ivermectin-exposed embryos, colonization of ectopic locations by melanocytes was prevented (yellow arrows) but the abnormal arborization remained. The effect was also observed in the tail (D'), with the ventral area remaining uncolonized. Blue arrow indicates the location of an area that remains free of ectopic melanocytes, even in heavily hyperpigmented tadpoles, possibly overlying the pineal gland.

which blocks melanocyte movement in frog embryos [220, 221]. The resulting embryos (Figure 3.1D,D') exhibited hyperpigmentation in regions normally inhabited by melanocytes (above the neural tube) but revealed an absence of ectopic melanocytes in periocular locations (Figure 3.1D, yellow arrows). We conclude that ectopic melanocytes colonize inappropriate embryonic regions via MMP-dependent cell migration processes. Interestingly, the melanocytes did not colonize the area above the pineal gland (Figure 3.1B,D, blue arrow), suggesting that they might still be responsive to specific restrictive signals that can demarcate quite sharp boundaries between permitted and restricted regions. We attempted to recapitulate this effect and restrict the metastatic melanocytes from other regions by inducing foci of high melatonin, but this was unsuccessful, suggesting that the repulsive effect of the pineal is not due exclusively to melatonin (data not shown).

One important component of the phenotype was a notable increase in cell arborization (Figure 3.1A' vs Figure 3.1B' and Figure 3.2; see supplementary material Figure S3.1F and its legend for evidence that pigment pattern is a reliable indicator of overall shape in melanocytes). The arborization remained despite MMP inhibition (Figure 3.1D,D'), suggesting that the hyperpigmentation is due not only to melanocytes being present in ectopic locations, but also to a separate process involving shape change. This was clearly apparent in sections of hyperpigmented tadpoles, which revealed extensive tissue occupation by ectopic melanocytes. In sections, wild-type animals typically have sparse pigmentation along the lateral epidermis and around the neural tube (Figure 3.2A,B), exhibiting only a small number of round melanocytes. Ivermectin-exposed hyperpigmented embryos instead possess dramatic melanocyte

coverage around the majority of the epidermis and the neural tube (Figure 3.2C,D), which includes the change of cells from a rounded morphology to a spread-out highly arborized shape with long processes.

We next investigated whether the effect was reversible. Embryos removed from ivermectin-containing medium at stage 43 (after melanocytes had migrated) and analyzed 2 days later also showed an increase in melanocyte number compared with controls but did not maintain the abnormal arborization (Figure 3.2E-H). We conclude that the arborized phenotype is reversible; however, the ectopic melanocytes remain once they colonize the region.

The migratory properties of these ectopic melanocytes were extensive. They colonized not only the lumen of the neural tube, but also penetrated the dense neural tissues (Figure 3.2I). They also sent very long projections from the edges of the somite into the neural tube (Figure 3.2J). We conclude that depolarization via chloride channel opener induces aberrant targeting and a high degree of migration while radically changing the normal morphology of melanocytes – a phenotype that is reminiscent of metastasis.

### ***Early ivermectin exposure results in an increased number of melanocytes***

We next investigated whether the hyperpigmentation effect involves increased numbers of melanocytes, in addition to ectopic migration and shape change. Exposed embryos were anesthetized and photographed; we then counted the number of melanocytes within a standard region defined by the eyes (Figure 3.3A,B), and compared each treatment to age-matched control siblings. Embryos exposed to 1  $\mu$ M ivermectin from stages 12-24 (gastrulation through to the completion of neurulation), washed three times and cultured in plain 0.1X MMR,

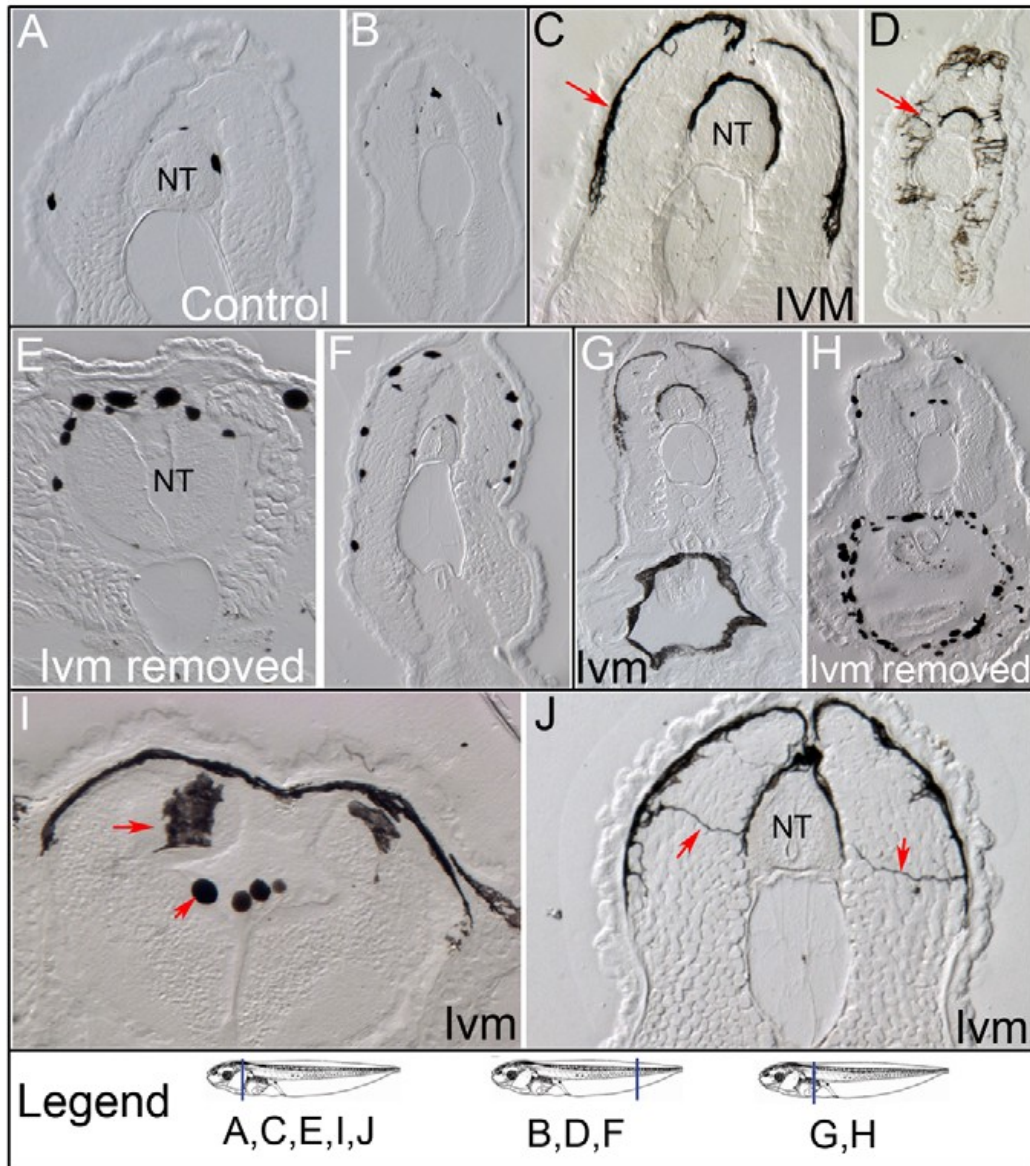


**Figure 3.2. Ivermectin induces invasiveness in melanocytes.**

Compared to control embryos (A,B), those exposed to ivermectin (IVM) throughout development (C,D) show significantly more melanocyte coverage of the neural tube (NT ) and epidermis (red arrows). Ivermectin-treated embryos removed from ivermectin at stage 43 (E,F) still show increased pigment cell number compared with controls, but the cells lose their arborized phenotypes. In addition, ivermectin induces melanocyte colonization of the gut (G,H) and the interior of the neural tube (I), and invasiveness of projections throughout the mesoderm between the epidermis and neural tube (J), indicated by red arrows. Schematics of *Xenopus laevis* embryo stages were retrieved from Xenbase, University of Calgary, Alberta T2N 1N4, Canada; <http://www.xenbase.org/>; August 2010.

show a 1.5-fold increase in melanocyte number compared with controls (Figure 3.3C; ANOVA Tukey post-hoc,  $P < 0.05$ ). These results were not confined to the eye field: melanocyte counts in the tip of the tail also showed a significant 1.5-fold increase when exposed to ivermectin throughout development (Student's t-test,  $t = 6.069$ ,  $P \leq 0.001$ ). Importantly, we detected no increase in total melanin content above that explained by the increase in cell number (absorption at 414 nm: control = 0.0534, ivermectin-treated = 0.0656,  $n = 5$  embryos per treatment, repeated five times, 1.2-fold difference); because the increase in melanocyte number (1.5-fold) is bigger than the increase in melanin content, each melanocyte is actually less pigmented in ivermectin-exposed tadpoles, ruling out higher pigment synthesis as a contributing factor to the hyperpigmented appearance.

Excess melanocytes can arise from increases in proliferation, change of cell fate of additional cells into melanocytes, or perhaps even failure of apoptosis. Quantification of cells positive for caspase-3 staining [222] in sections showed no significant difference between control and ivermectin-treated embryos (11.3 vs 10.2 apoptotic cells in the notochord of control vs ivermectin-treated embryos, respectively,  $n = 11$ ,  $P = 0.6$ ), ruling out prevention of programmed cell death as a likely reason that higher numbers of melanocytes are observed. We next investigated whether additional cells were being recruited towards a melanocyte fate by expression analysis of *Trp2* (also known as *Dct*), a definitive marker of mature melanocytes [223]. Embryos treated with ivermectin from stage 11 that were examined for expression of *Trp2* at stage 28 (prior to the migration of pre-melanocytes away from the neural crest) showed no ectopic signal (Figure 3.3D,E), indicating that regions that later exhibit abnormal numbers of

melanocytes do not do so because of any recruitment of additional cells towards this lineage. Counting melanocytes in sections, to rule out excess recruitment towards melanocyte lineage within the crest itself (which would be difficult to detect in whole-mount) revealed that control embryos have the same number of melanocytes in the dorsal neural tube as do ivermectin-treated embryos (n=10 embryos, P=0.33) (Figure 3.3F,G). Given the lack of evidence for recruitment of additional cells into melanocytes at the time when a subset of neural crest cells are assigned a pigment cell fate, we suggest that ivermectin treatment during early stages results in excess melanocytes in later embryos via increased proliferation of mature melanocytes.

To confirm the effect on proliferation of melanocytes, we characterized cell proliferation using an antibody to phosphorylated histone 3B (H3B-P) – a standard marker of cells in the G2-M transition of the cell cycle, useful for identifying mitotic cells in *Xenopus* [224, 225]. Embryos were stained for the melanocyte marker *Trp2* using *in situ* hybridization to identify melanocytes and then sectioned and processed for immunohistochemistry with anti-H3B-P antibody. Overlays of the bright-field (Figure 3.3H,H') and fluorescent (Figure 3.3I,I') signals allowed counting of all melanocytes that were actively dividing (cells positive for both markers). The data are summarized in Table 3.1, and show that, although embryos exposed at stage 16 and analyzed at stage 28 have the same number of mitotic melanocytes as controls, ivermectin-exposed embryos analyzed at stage 35 have a 2.8-fold increase in the number of melanocytes in mitosis over controls. These data confirm the induction of mitosis in mature melanocytes by ivermectin exposure.

Interestingly, embryos whose ivermectin exposure did not begin until

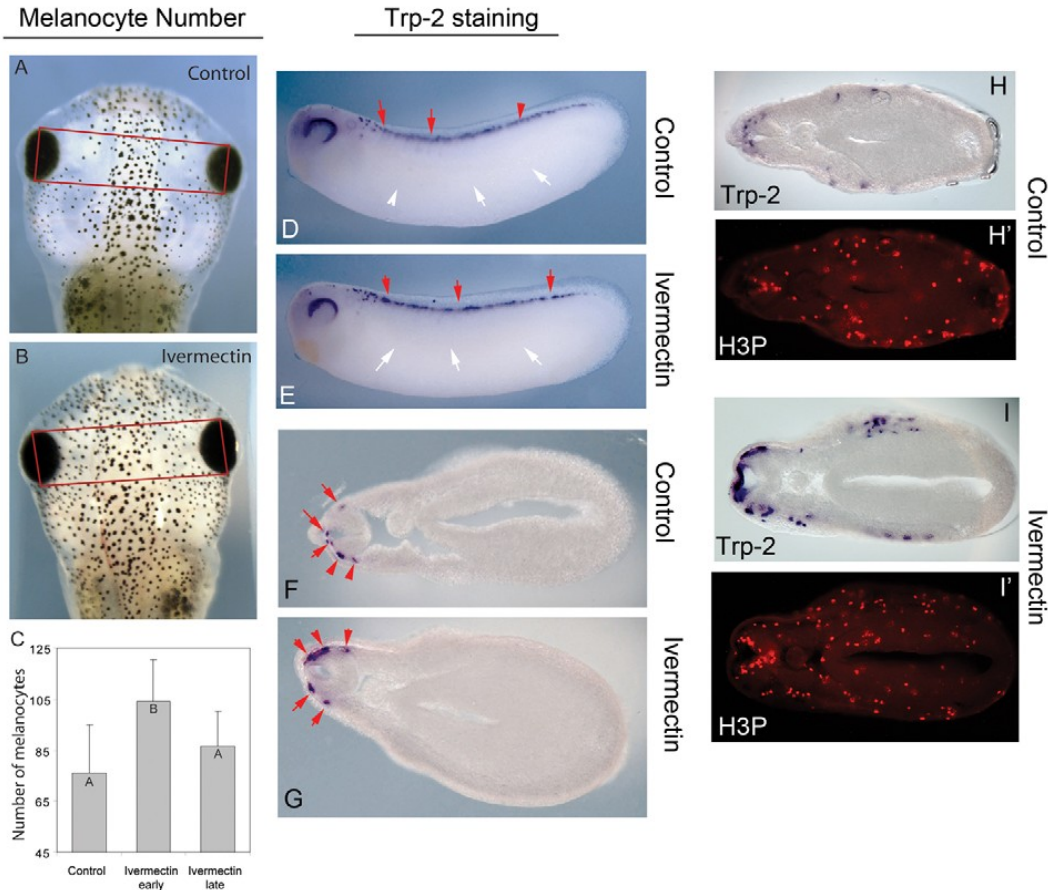


**Figure 3.3. Early ivermectin exposure induces an increase in pigment cell proliferation.**

Embryos exposed to ivermectin from stages 10-24 (early) or 28-46 (late) both show darkening due to expansion of melanocytes. To determine whether there was also a corresponding increase in melanocyte number, photographs were taken of controls (A) and ivermectin-exposed (B) embryos after tricaine anesthetization, which contracts the pigment cells. The number of melanocytes in the eye field (red boxes) were then counted. Early exposed embryos showed a 1.5-fold increase in melanocyte number relative to controls (C), whereas no detectable difference was observed between late exposed embryos and controls. Error bars indicate one standard deviation; n=24 embryos for each treatment. Control embryos processed in *in situ* hybridization for the melanocyte marker *Trp2* at stage 28 show the normal pattern of expression prior to the migration of melanocytes away from the dorsal neural tube (D). Ivermectin-treated embryos show precisely the same pattern (E) and exhibit no evidence of ectopic locations being converted into a melanocyte fate by the ivermectin treatment. Sectioning reveals that control (F) and ivermectin-treated (G) embryos have the same number of melanocytes at the neural tube, also ruling out local shifts of neural crest cells into the melanocyte lineage as the explanation for later hyperpigmentation. Red arrows indicate positive signal (melanocytes indicated by *Trp2* expression), whereas white arrows indicate lack of signal. (H-I') To directly analyze proliferation in melanocytes, embryos were stained for the

melanocyte marker *Trp2* using *in situ* hybridization to identify pigment cells, and were then sectioned and processed for immunohistochemistry with anti-H3B-P antibody. (H) *Trp2* section in control embryos; (H') corresponding signal of H3B-P stain in the same section. (I) *Trp2* section in ivermectin-exposed embryos; (I') corresponding signal of H3B-P stain in the same section. Overlays of the bright-field and fluorescent signals from the same section allowed quantification of the number of melanocytes that were in mitosis. At stage 28, there was no difference ( $P>0.2$ ,  $n=6$ ) between controls and ivermectin-treated embryos. By stage 35, there was a significant increase in the number of mitotic melanocytes in the ivermectin- treated embryos ( $P<0.009$ ,  $n=6$ ).

**Table 3.1. Proliferation rates in melanocytes**

Sample	Trp2	Number of cells positive for		%Trp2 + H3B
		H3B-P	Both	
Stage 35 controls				
1	16	94	3	18.75
2	9	48	1	11.11
3	3	38	0	0.00
4	19	64	0	0.00
5	7	41	1	14.29
			Average	8.83
			S.d.	8.5
Stage 35 ivermectin-exposed				
1	23	102	5	21.74
2	14	115	3	21.43
3	28	102	10	35.71
4	18	63	4	22.22
			Average	25.28
			S.d.	6.97
Stage 28 controls				
1	7	33	0	0.00
2	10	45	2	20.00
3	5	28	4	80.00
4	4	27	2	50.00
			Average	37.50
			S.d.	35.00
Stage 28 ivermectin-exposed				
1	4	33	0	0.00
2	8	35	4	50.00
3	6	32	2	33.33
4	10	30	0	0.00
5	2	27	1	50.00
6	10	28	2	20.00
7	4	28	1	25.00
8	5	30	2	40.00
			Average	27.29
			S.d.	19.92

Embryos were stained with the melanocyte marker Trp2 using *in situ* hybridization to identify pigment cells and then sectioned and processed for immunohistochemistry with anti-H3B-P antibody to identify mitotic cells. Overlays of the images from the same section allowed identification of cells positive for both markers (mitotic melanocytes). Student's t-test analysis of the raw data indicates that, although the difference between controls and ivermectin-exposed embryos (8.83% to 25.28%, respectively) at stage 35 is significant ( $P=0.008$ ), the difference between controls and ivermectin-exposed embryos at stage 28 is not ( $P=0.233$ ).

stage 28 (lasting tailbud through tadpole), after a subset of the neural crest has been determined into melanocytes [226], did not show a significant increase in melanocytes at stage 46 compared with control animals (Figure 3.3C). These results demonstrate that, whereas early-exposed neural crest cells respond to ivermectin by increasing proliferation of committed melanocytes, exposure to ivermectin late in development induces a shape change and aberrant migration in pigment cells but not an increase in proliferation of the melanocytes

***The hyperpigmentation induced by ivermectin is mediated by GlyCl***

Having characterized the basic properties of the phenotype, we then investigated the detailed mechanism of action. First, to confirm that the hyperpigmentation effect in *Xenopus* embryos is indeed mediated by GlyCl, and not some off-target property of ivermectin, we exposed embryos to the endogenous ligand of GlyCl, glycine. This control has an additional advantage in that glycine binds to GlyCl at a site different than that used by ivermectin [217]. Treatment with 0.13 mM glycine induced the same hyperpigmented phenotype as ivermectin (supplementary material Figure S3.2), indicating that the modulation of pigment cell number, shape and location by ivermectin is indeed mediated by its effects on GlyCl in *Xenopus*. The same result was obtained by misexpression of a constitutively open mutant GlyCl channel [227], or by raising endogenous glycine levels by inhibiting the glycine transporter (data not shown).

To identify the embryonic source of the signals induced by ivermectin, we investigated which cells expressed the ivermectin target GlyCl (a ligand-gated chloride channel consisting of a primary  $\alpha$  subunit, sufficient for conductance, and a regulator  $\beta$  subunit) (Lynch, 2009). *In situ* hybridization with an antisense probe for *GlyCl- $\alpha$ 1* [homologous to the mammalian glycine receptor subunit  $\alpha$ -3

gene (*GLRA3*) revealed expression in early embryos (Figure 3.4A,B) across the neural plate region in a classic horseshoe like pattern indicative of neural crest [182]. By stage 30, expression was restricted within the anterior central nervous system (Figure 3.4C). Sectioning revealed an enriched region in the ventral marginal zone of the neural tube (Figure 3.4E, red arrows, compare to sense probe control in Figure 3.4D). Higher resolution analysis revealed a punctate stain indicative of a sparse, broadly-distributed cell population (Figure 3.4F, red arrows), but no expression in the dorsal neural tube, where melanocyte precursors are located at this stage (Figure 3.4G). We conclude that the ivermectin target GlyCl is expressed in embryos, first in a neural-crest-associated pattern and later in a sparse punctate pattern throughout the embryo that is specifically absent from the neural crest cells themselves.

Having determined that the melanocytes themselves are not the cells expressing GlyCl (and thus are not directly depolarized by ivermectin or glycine), we further tested the apparent cell-non-autonomy of this effect. One cell of embryos at the 32-cell stage was microinjected with mRNA encoding the depolarizing channel subunit KCNE1 [33] plus mRNA encoding  $\beta$ -galactosidase as a lineage tracer. These embryos were then treated with the MMP-blocking compound NSC-84093, which prevents melanocytes from migrating (Figure 3.1D). Embryos in which KCNE1 was injected in a blastomere giving rise to only posterior tissues (Figure 3.4H, blue arrow) still exhibited hyperpigmentation (Figure 3.4H, white arrowhead). Indeed, analysis of lineage label in sections (Figure 3.4I,I') showed that targeting depolarizing reagents to posterior cells on one side induces the appearance of ectopic, highly dendritic, melanocytes in the head and on the opposite side. Because the migration blocker rules out cell

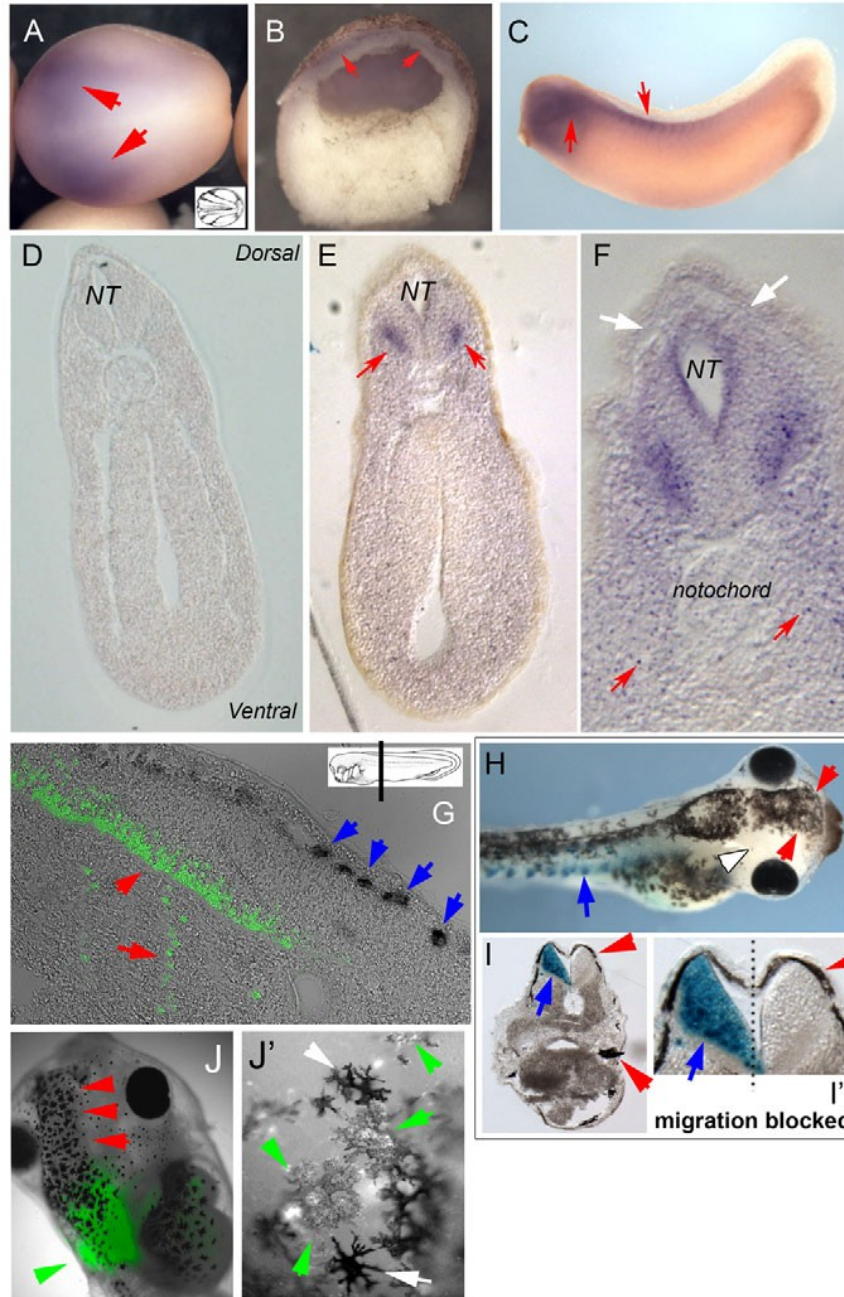


**Figure 3.4. Expression of GlyCI- $\alpha$  mRNA and protein.**

*In situ* hybridization was performed on *Xenopus* embryos with an antisense probe to GlyCI- $\alpha$ . Expression (red arrows) was first detected during neurulation in the developing neural plate (A; panel B shows a thick section in profile because expression was too weak to be clearly visible in thin sections). Expression became restricted during somite stages (C) with foci of staining observed in the ventral marginal zone of the neural tube (NT) (E). Sections also revealed punctate signal in the lateral mesoderm (F, red arrows), which was not observed in the no-primary control (D), and an absence of signal in the dorsal neural tube, where many melanocytes are located (F, white arrows). In

panels A-F, red arrows indicate expression of *GlyCl* mRNA, whereas white arrows indicate lack of expression in the dorsal neural tube from which melanocytes originate. Immunohistochemistry (with an antibody to GlyCl; green signal and red arrowheads) and *in situ* hybridization (with a probe to the melanocyte marker *Trp2*, blue arrows) on the same section of stage-31 embryos (G) revealed that the cells expressing GlyCl are at some distance from melanocytes (melanocytes do not themselves express the ivermectin target protein). (H) As an additional test of long-range signaling, embryos were injected with KCNE1+  $\beta$ -gal mRNA at the 16-cell stage in blastomeres, which resulted in depolarizing potassium channel subunit expression in posterior ventral tissues (blue arrow indicates  $\beta$  galactosidase lineage label). Red arrowheads in panels H,I indicate hyperpigmentation (aberrant melanocytes) in the region; white arrowhead in H indicates absence of  $\beta$ -gal signal from anterior regions. They were continuously treated with NSC-84093 to prevent melanocyte migration from distant regions of the embryo. Sectioning (I,I') revealed that hyperpigmentation occurred in the head and on the contralateral side, demonstrating that the metastasis-inducing signal is able to cross considerable distance along the anterior-posterior axis (from somites over the gut into the space anterior to the eyes) and across the embryonic midline (red arrowhead in I') even when melanocytes local to the KCNE1 depolarization are prevented from moving. Insets in A and G taken from Nieuwkoop and Faber [154]; schematic inset in G shows plane of sections for panels D-G. (J) A small section of neural plate from a ubiquitous GFP-transgenic donor treated with ivermectin (green arrowheads) was transplanted into an untreated host at stage 18, resulting in a hyperpigmentation phenotype (red arrowheads). (J') Similar transplant performed from an ivermectin-treated donor results in GFP-labeled melanocytes (lighter in color owing to overlap of fluorescence and black pigment; green arrowheads) shows that these melanocytes take up ectopic positions next to native melanocytes (white arrowheads) and acquire the same highly arborized shape.

motility as an explanation for the appearance of ectopic melanocytes in the head, we conclude that depolarized cells can exert their inductive effect at long range, not only crossing the midline to affect the contralateral side but signaling at least as far as the length of the head along the anterior-posterior axis. The same conclusion is confirmed by transplantation experiments: small domains of cells from an ivermectin-depolarized donor transplanted into an untreated embryo induce host melanocytes to arborize and migrate inappropriately (Figure 3.4J), whereas melanocytes from an ivermectin-depolarized donor migrate to ectopic locations in the host and acquire the same highly dendritic shape (Figure 3.4J').

### ***Hyperpigmentation is mediated by $V_{mem}$ change***

To determine whether the alteration of melanocyte behavior was due to GlyCl-dependent changes in transmembrane potential or some other effect of alterations in GlyCl function, we took three approaches: reversing the direction of  $Cl^-$  ion flow, depolarization by a GlyCl-independent method and rescue of phenotype by microinjection of a hyperpolarizing channel mRNA.

The intracellular concentration of chloride in frog embryos can be as high as 60 mM, whereas the extracellular concentration in normal 0.1X MMR medium is 10 mM [228]. To cause hyperpolarization by influx of extracellular chloride into cells via ivermectin-opened GlyCl channels (supplementary material Figure S3.1E), we raised the concentration of chloride in the extracellular MMR to 30 mM, 60 mM or 90 mM and examined the resulting phenotype following ivermectin exposure. Elemental analysis comparing control embryos with those reared in ivermectin plus 60 mM chloride showed a 40% increase in chloride by dry weight (0.130% and 0.185%, respectively), demonstrating that external chloride was indeed being taken up by embryonic cells when chloride channels

were forced open in high-Cl<sup>-</sup> medium.

Raising extracellular chloride levels to 30 mM did not inhibit hyperpigmentation, whereas 60 mM suppressed and 90 mM completely inhibited the phenotype (Table 3.2). The chloride levels tested had no observable effects on tadpole development beyond inhibiting the hyperpigmenting effects of ivermectin, and these data are precisely the outcome predicted by the Goldman-Katz equation of membrane potential: when the extracellular chloride concentration becomes equal to the intracellular, opening the GlyCl channel with ivermectin no longer depolarizes (no Cl<sup>-</sup> ions will leave cells), abolishing the hyperpigmentation phenotype.

If hyperpigmentation is truly a result of membrane depolarization, then cellular voltage modulators that function independently of chloride channels should result in the same phenotype. We therefore tested the effect of disrupting the H<sup>+</sup>-V-ATPase hyperpolarizing pump, which we previously showed plays an important role in several voltage-regulated events in *Xenopus* development [29, 65] and controls cellular  $V_{mem}$  through movement of H<sup>+</sup>, not Cl<sup>-</sup>, ions. Injection of low levels of mRNA encoding a well-characterized dominant-negative mutant of Ductin (the 16-kDa proteolipid subunit c of the hyperpolarizing V-ATPase pump complex) into one-cell embryos resulted in broad, long-lasting (tracked by fused YFP; data not shown) expression, which induced hyperpigmentation in 11.5% of embryos, significantly higher than background hyperpigmentation observed in controls (binomial calculation; n=189 for controls, n=192 for DN-Ductin, P≤0.001) (Figure 3.5A-C). Moreover, dn-xDuct-injected hyperpigmented embryos had 2.1-fold more melanocytes than control animals at stage 46 (Student's t-test, t=7.37, n=11 per treatment, P≤0.001; Figure 3.5D).

**Table 3.2. Using Cl<sup>-</sup> levels to modulate voltage-dependent hyperpigmentation.**

	10 mM Cl <sup>-</sup>	30 mM Cl <sup>-</sup>	60 mM Cl <sup>-</sup>	90 mM Cl <sup>-</sup>
Normal pigmentation	0	1	18	32
Hyperpigmented	25	23	5	0
% hyperpigmented	100	95.8	21.7	0
n	25	24	23	32

The number of embryos with each pigmentation phenotype is shown. Embryos were exposed to the chloride channel activator ivermectin (1 μM) from stage 10 through stage 46 in 0.1 MMR containing varying levels of chloride. With the two lowest levels, 10 mM and 30 mM, at which depolarization occurs by exit of chloride ions down their concentration gradient, exposure to ivermectin resulted in strong hyperpigmentation, with nearly all of the exposed embryos developing hyperpigmentation. Exposure to 60 mM chloride, a concentration at which the loss of negative charges from cells is largely diminished, resulted in partial inhibition of hyperpigmentation, and 90 mM, which hyperpolarizes membranes owing to the influx of Cl<sup>-</sup>, led to complete inhibition. Embryos raised in the various chloride treatments in the absence of ivermectin showed no abnormal development at the conclusion of the experiment.

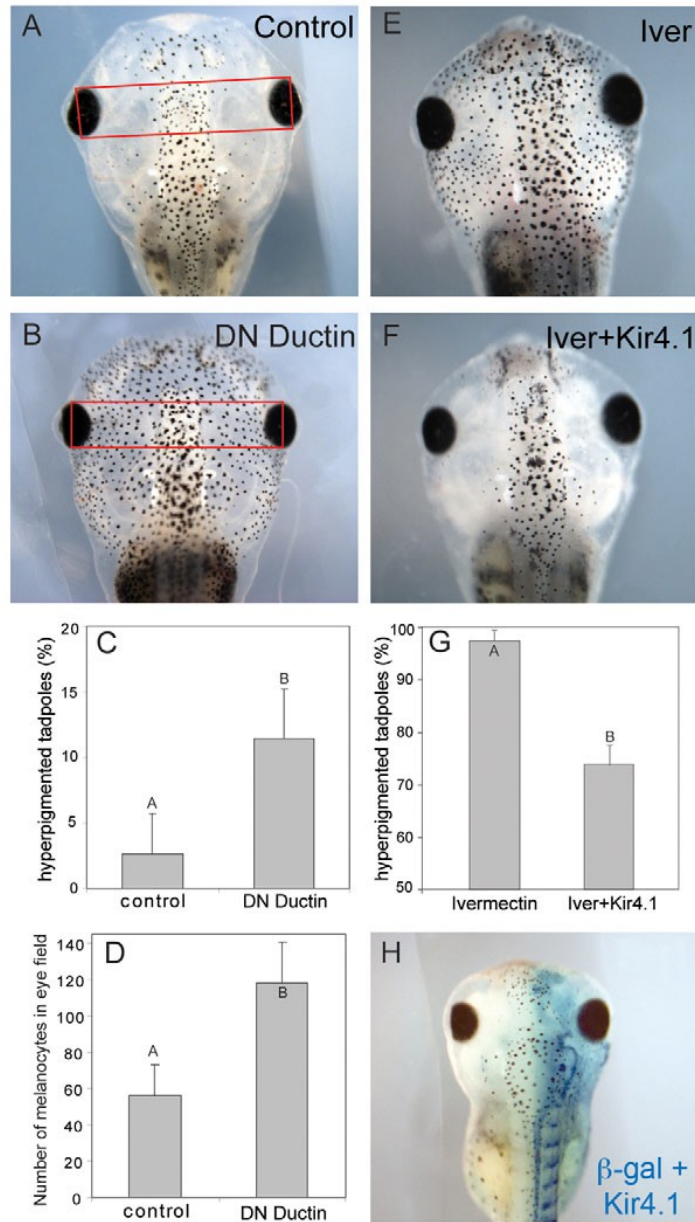


**Figure 3.5. Hyperpigmentation is due to depolarization.**

Microinjection of a dominant-negative form of ductin (dn-xDuct) at the one-cell stage inhibits the hyperpolarizing H<sup>+</sup>-V-ATPase and results in hyperpigmentation (A,B). Injections result in hyperpigmented tadpoles in 11.5% of embryos (C), significantly higher than background levels observed in control embryos.

Hyperpigmented embryos arising from dn-xDuct injections were photographed and the number of melanocytes in the eye field counted; there was a 2.1-fold increase in number of melanocytes compared with age-matched controls (D). By contrast, overexpression of the hyperpolarizing potassium channel Kir4.1 (E,F) inhibits ivermectin-induced hyperpigmentation in 25% of injected embryos (G). Kir4.1-mediated inhibition was non-cell-autonomous, because one of two cell injections, resulting in hyperpolarizing channel activity on just one side of the embryo, inhibited hyperpigmentation on both the left and right side of the embryos (H).

Finally, to confirm that misregulation of melanocyte behavior is induced by depolarization, we performed a rescue experiment. We injected Kir4.1 [123], a hyperpolarizing potassium channel [229, 230], into one- or two-cell embryos before placing them into ivermectin. Ivermectin alone induced hyperpigmentation in 97.6% of embryos (n=73), whereas only 73.4% of embryos injected with Kir4.1 were hyperpigmented (n=74), a 25% reduction (Figure 3.5E-G). The effect was not cell-autonomous, because Kir4.1 injections into only half of the embryo (one blastomere at the two-cell stage) inhibited hyperpigmentation on both sides of the embryo (Figure 3.5H). Together, these data demonstrate that hyperproliferation is induced by depolarization – not by chloride per se or by channel-independent functions of ivermectin or of GlyCl. These results also demonstrate that control of extracellular chloride, together with ivermectin, is a simple and effective technique for rational modulation of transmembrane potential *in vivo*.

### ***Ivermectin-induced changes in $V_{mem}$ are transduced by serotonin***

How do cells sense long-term depolarization [231] and convert this biophysical signal to changes in transcription and cell behavior? We tested three transduction mechanisms that can function downstream of depolarization: influx of  $Ca^{2+}$  through voltage-gated calcium channels (VGCC) [232-234], control of levels of serotonin by electrical modulation of serotonin transporter function [41, 62, 65] and electrophoretic transport of signaling molecules through gap junctions [40, 60, 156, 235, 236]. Our strategy was to apply inhibitors of each of these pathways together with ivermectin, to determine which mechanism is required for depolarization to be effectively transduced into changes of melanocyte behavior.

Treatment with potent VGCC blockers (0.1 mM cadmium chloride, 0.1 mM verapamil) or with the gap junction blocker lindane (1.7 mM) did not result in any reduction in ivermectin-induced hyperpigmentation (Table 3.3). However, exposure to a specific inhibitor of the serotonin transporter (10 mM fluoxetine) blocked ivermectin-induced hyperpigmentation in all of the treated embryos, without any apparent effects on overall patterning or embryo health.

To determine whether ivermectin-induced depolarization and the function of the serotonin transporter SERT were taking place in the same cells, we performed immunohistochemistry for both receptors on sections of stage 32 *Xenopus* embryos. SERT protein expression significantly overlapped with that of glycine receptors in cells of the ventral neural tube, suggesting that cells sensitive to ivermectin also respond to fluoxetine (Figure 6A-C).

Fluoxetine increases the availability of extracellular serotonin by blocking its internalization. To ensure that the hyperpigmentation was indeed due to serotonergic signaling and not some other role of SERT or an off-target effect of fluoxetine, we treated embryos with excess extracellular serotonin. This resulted in a consistent and powerful hyperpigmentation (Fig. 6D,E). Taken together, the data strongly suggest that function of the serotonin transporter SERT is required for the transduction of  $V_{mem}$  changes into cell behavior changes observed during hyperpigmentation.

### ***Human epidermal melanocytes respond to changes in membrane potential***

Although simple *in vitro* culture cannot demonstrate the non-cell-autonomous effects observed in the embryo, we investigated whether human epidermal melanocytes showed any phenotypes as a result of membrane depolarization. Ivermectin could not be used to depolarize the membrane because the required

**Table 3.3. Rescue of hyperpigmentation phenotype reveals serotonergic involvement**

	<b>Control</b>	<b>Ivermectin</b>	<b>Ivermectin + cadmium chloride</b>	<b>Ivermectin + verapamil</b>	<b>Ivermectin + fluoxetine</b>	<b>Ivermectin + lindane</b>
Normally-pigmented tadpoles	57	3	1	0	38	0
Hyperpigmented tadpoles	0	61	47	52	0	48
% hyperpigmented	0	95.3	97.9	100	0	100
n	57	64	48	52	38	48

Embryos were exposed to 10  $\mu$ M ivermectin from stage 10 through 46 (from gastrulation to organogenesis). Concurrently, they were exposed to one of four drugs; the calcium channel inhibitors cadmium chloride and verapamil, the selective serotonin reuptake inhibitor fluoxetine, and the gap junction inhibitor lindane. Ivermectin alone resulted in a strong incidence of hyperpigmentation, a phenotype that was absent from control embryos. Exposure to cadmium chloride, verapamil or lindane in the presence of ivermectin did not inhibit hyperpigmentation. However, exposure to fluoxetine completely inhibited ivermectin-induced hyperpigmentation. All drugs were used at doses that did not result in any developmental defects.

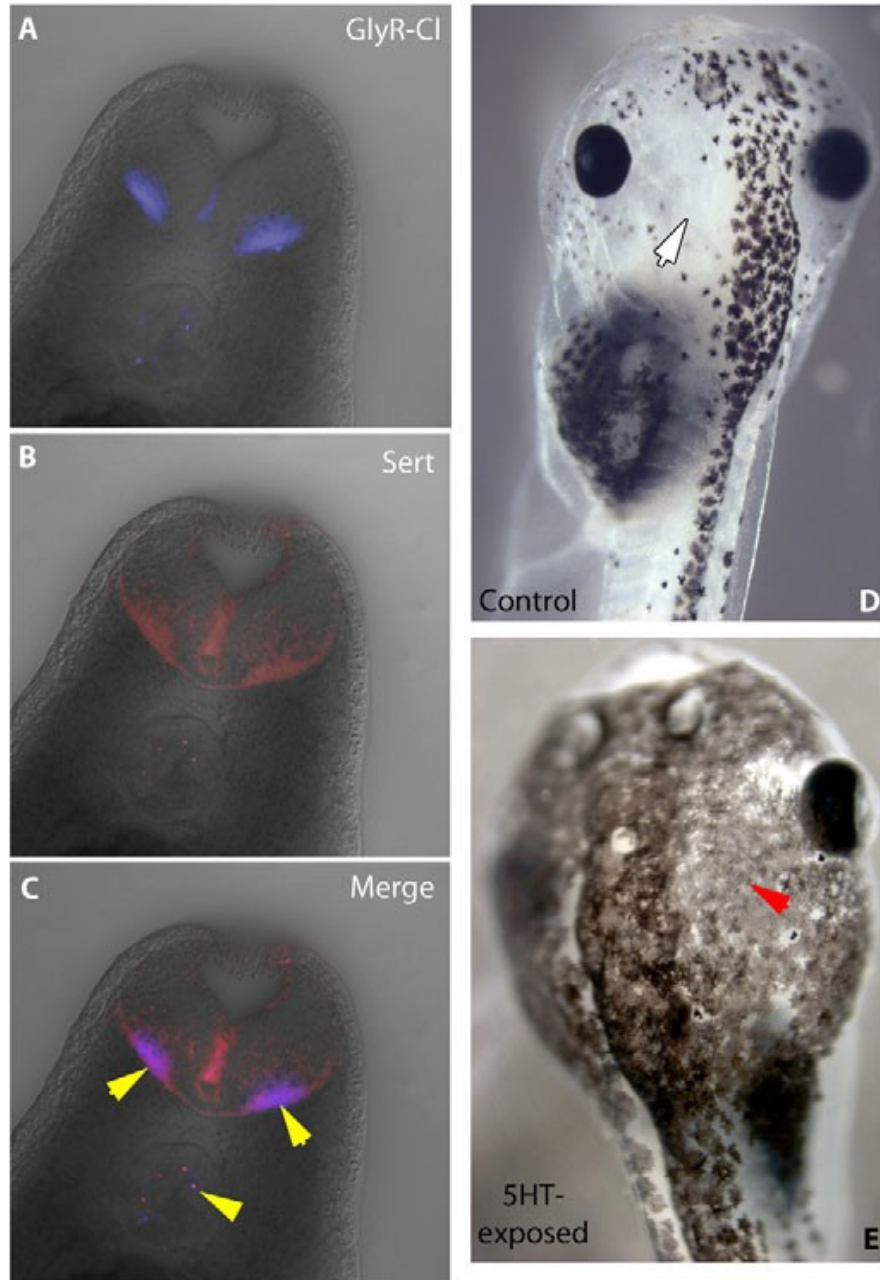


**Figure 3.6. Serotonergic controls of melanocyte behavior and their relationship to GlyCI-expressing cells.**

(A) Sections of a stage 32 embryo processed by immunohistochemistry with an anti-GlyCI antibody and visualized with a fluorescent secondary antibody (Alexa Fluor 647). (B) The same section processed by immunohistochemistry with an anti-SERT antibody and visualized with Alexa Fluor 546. (C) Merge of A and B showing colocalization of GlyCI and SERT. Yellow arrowheads indicate areas of overlapping expression (cells containing both GlyCI and SERT). Unlike controls (D), embryos treated with external serotonin acquire the hyperpigmentation phenotype (E), consistent with SERT mediating the effect of depolarized GlyCI-expressing cells on melanocytes. White arrow indicates a region normally devoid of melanocytes; red arrowhead indicates ectopic melanocytes.

culture medium of this cell line has a very high chloride content. Instead, we raised extracellular  $K^+$  levels by addition of potassium gluconate, which also depolarizes cells (reduces the ability of  $K^+$  ions to exit cells through potassium channels). This also has the advantage of testing a voltage role independent of chloride *per se*.

No measurable differences in cell proliferation were noted between melanocytes cultured in standard vs high- $K^+$  media (data not shown). However, cells grown in high- $K^+$  medium demonstrated a striking shape change similar to *Xenopus* melanocytes exposed to ivermectin. Following 2 days of culture in 50 mM potassium-gluconate-supplemented medium, human melanocytes developed a highly arborized morphology, with many cells showing five or more projections (compare Figure 3.7A with B). Quantification showed that culturing cells in high- $K^+$  medium had a significant effect on the number of projections on melanocytes (2-way ANOVA,  $F_3=18.29$ ,  $P\leq 0.001$ ). To verify that melanocytes grown in high- $K^+$  medium were in fact depolarized, we made use of ratiometric  $V_{mem}$  imaging using CC2-DMPE and DiBAC<sub>4</sub>(3) dyes to visualize the membrane potential (Figure 3.7D,E). Comparison of treatments showed depolarization of treated cells compared with controls (Figure 3.7F,  $t_{22}=3.77$ ,  $P=0.001$ ). We conclude that some of the novel mechanisms that we observed in *Xenopus* larvae are not restricted to embryogenesis and might be relevant to human adult melanocytes.

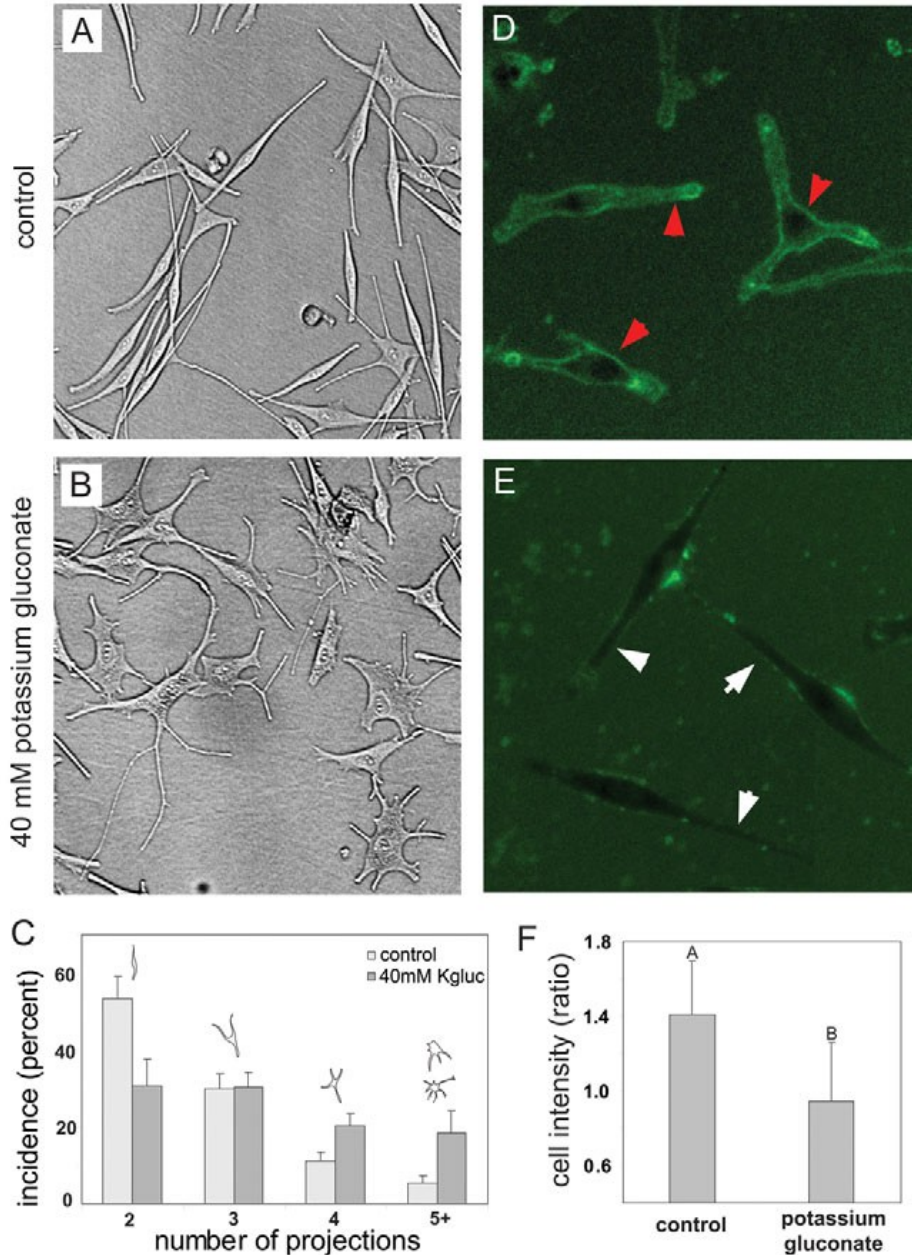


**Figure 3.7. Human melanocytes exhibit arborization when the membrane is depolarized.**

In normal culture medium, human melanocytes typically develop two or three projections (A). When grown in media supplemented with 50 mM potassium gluconate, cells develop a more arborized morphology, with many cells having four or five, or more, projections (B). Comparisons between treatments (C) demonstrate a significant effect of potassium gluconate on arborization of melanocytes. Error bars indicate one standard deviation. Image analysis (using the membrane voltage sensor pair CC2-DMPE and DiBAC4) comparing controls (D) and cells cultured in high-potassium medium (E) revealed the predicted depolarization (lower intensity of pixels) in response to the high-potassium media (F). Red arrowheads indicate depolarized cell membranes; white arrows indicate lack of depolarization in membrane.

## Discussion

### ***Control of melanocyte behavior by $V_{mem}$***

Prior work has examined the behavior of melanocytes within exogenous electrical fields [237, 238]. However, the role of transmembrane potential in the regulation of neural crest derivatives or the molecular basis for any bioelectrical controls of melanocyte behavior has not previously been examined. Our fundamental finding is that modulation of membrane potential by changing the direction of chloride flux in GlyCl-positive cells robustly and non-cell-autonomously confers a hyperproliferative, inappropriately colonizing phenotype upon melanocytes in *Xenopus* larvae (Figure 3.1A-C). Changes in  $V_{mem}$  were induced by forcing chloride channels open with the specific agonist ivermectin, followed by control of  $Cl^-$  concentration in the medium, a convenient technique with which transmembrane potential can be increased or decreased as desired. The resulting hyperpigmentation in depolarized tadpoles is a result of inappropriate MMP-dependent migration, cell shape change and greater melanocyte number (Figure 3.1D; Figures 3.2, 3); depolarization induced no increase in the amount of melanin pigment per melanocyte. The altered behavior of melanocytes includes arborization, the ability to penetrate and colonize internal organs and neural structures, and the formation of long processes that are highly uncharacteristic of normal melanocytes (Figure 3.2). Future work tracing the behavior of small numbers of labeled, depolarized instructor cells transplanted into a wild-type host will be necessary to determine whether the metastasis of ivermectin-treated melanocytes to inappropriate locations is due to altered control of pathfinding at the single-cell level or to a community ('population pressure') effect [239] among high numbers of melanocytes that

repel one another [183].

There are two phases to the effect. When treatment with depolarizing agent occurs during neurulation, significant increases in pre-melanocyte number occur (a 1.5-fold increase in melanocyte number is observed in periocular skin and a 2.8-fold increase in mitotic melanocytes is observed when all tissues in section are analyzed via H3B-P staining). The effect seems to be mediated by increased proliferation of melanocytes, not recruitment of additional cells into the melanocyte lineage (Figure 3.3D-G). By contrast, treatment beginning later at organogenesis stages does not induce significant increases in proliferation (Figure 3.3C), demonstrating that mitosis and shape and/or migration change in melanocytes are separable processes. Although both changes of melanocyte behavior result from depolarization of transmembrane potential in GlyCl-positive cells, the distinct natures of the two phenotypes is underlined by the fact that, although excess melanocytes do not disappear following withdrawal of ivermectin, shape rapidly returns to normal following washout (Figure 2G,H).

The early phase might be cell-autonomous, because the chloride channel target is expressed in neural crest cells (precursors of melanocytes) during the time of exposure (Figure 3.4A,B). By contrast, the effects of later depolarization are likely to be non-cell-autonomous, because (1) at somite stages the receptor is expressed in cells that are at a considerable distance from the melanocytes whose behavior is altered by induced chloride efflux (Figure 3.4F,G), (2) hyperpolarization of cells via Kir4.1 on half of the embryo inhibits hyperpigmentation on both sides (Figure 3.5H) and (3) depolarization of posterior cells on one side of the midline results in the appearance of ectopic melanocytes in the head of the embryo on the opposite side even when migration is inhibited

(Figure 3.4H-I'). Such long-range effects of biophysical changes are a fascinating aspect for future investigation because they suggest opportunities for biomedicine as well as potential sources of unexpected problems in patients taking drugs targeting ion channels.

A connection between ion transport proteins and pigment cell behavior has been observed in zebrafish, specifically between Kir7.1 and melanosomes [240], as well as between connexin 41.8 and pigment cells (in a diffusion-reaction patterning system) [241, 242]. However, our data specifically connect the control of  $V_{\text{mem}}$  in one cell population (GlyCI-expressing instructor cells) with migration, morphology, and proliferation in another (pigment cells). Indeed we show that the phenomenon of membrane-voltage-based signaling is even more directly recapitulated in human pigment cells (Figure 3.8), suggesting that the previously observed stimulatory effects of bee venom on human melanocytes [243] is due to the ion-channel-targeting properties of its apamin protein component [244]. More broadly, the voltage control mechanism might be a plausible candidate for biomedical intervention in the pigmentation disorder vitiligo [245, 246], in melanoma [247, 248] and, more broadly, in neurocristopathies (developmental birth defects involving neural crest stem cell derivatives) [176, 177, 249].

### ***GlyCI as a marker of a unique cell population in embryos***

One of the advantages of ivermectin-based depolarization is that the target cells can easily be identified. Ivermectin is a highly specific agonist for GlyCI [217], and our phenotype results from the effects on GlyCI rather than off-target side effects of this compound, because its native ligand, glycine, can induce the same effect (supplementary material Figure S3.2). Whereas GlyCI is normally expressed in some neurons (spinal cord, retina) and sperm [250], we detected a

dynamic and highly interesting distribution during frog embryogenesis. It is first expressed in the dorsal neural tube during stage 15 (Figure 3.4A,B) and is later enriched in the ventral neural tube (Figure 3.4C-F), at the same location from which N-tubulin-positive motor neurons arise [251]. At post-neurula stages (e.g. stage 30), it is also present in a unique pattern throughout the interior of the embryo, in a sparse population of small cells resembling macrophages in size [252]. It is specifically not expressed in melanocytes (Figure 3.4G). Importantly, nearly all ivermectin-treated embryos acquire the hyperpigmented phenotype; by contrast, depolarizing arbitrary (even large) groups of cells by forcing KCNE1 overexpression only affects ~20% of the embryos [33], underscoring the significance of the native GlyCl-expressing cells.

This speckled arrangement of the ivermectin-sensitive cells is especially useful for research because it facilitates exploration of a highly mosaic depolarization effect, a powerful technique resembling the mosaic analysis that has been capitalized on by the *Drosophila* community and is difficult to achieve with ubiquitous  $V_{\text{mem}}$ -modulating methods such as ionophores. Inducing chloride efflux in a small population of cells induced a highly specific phenotype in which the behavior of melanocytes was radically affected despite completely normal development of the anterior-posterior axis, major organs and other neural crest derivatives such as branchial arches. It is remarkable that depolarization of a rare cell population is able to induce a very specific but almost 100%-penetrant phenotype in just one cell type during embryogenesis.

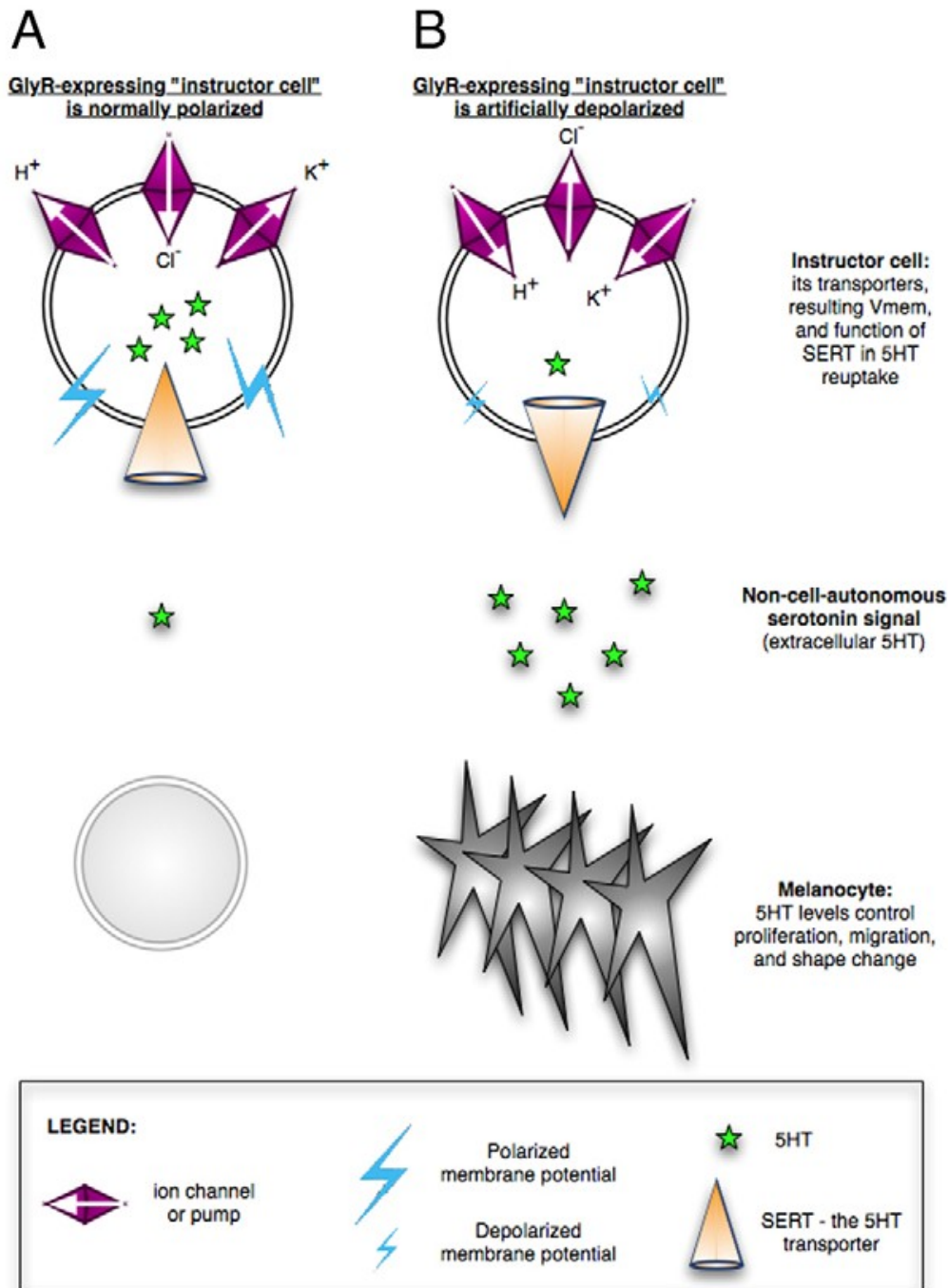


**Figure 3.8. A model of melanocyte control by transmembrane potential of cells in the neural crest's environment.**

(A) In unperturbed embryos, several classes of ion transporters keep the plasma membrane polarized. This transmembrane potential powers the reuptake of extracellular serotonin through its transporter SERT, resulting in normal melanocyte behavior. (B) By contrast, when the instructor cell population (demarcated by GlyCl expression) is depolarized by targeted modulation of  $H^+$ ,  $Cl^-$  or  $K^+$  channel/pump function, the SERT runs backwards and not only fails to clear the extracellular space of serotonin, but actually exports additional

serotonin. The higher serotonin level in the milieu of the neoblasts induces neoplastic-like behavior in melanocytes, as occurs in human cancers. This pathway can be manipulated at a number of points. Consistent with this model, our data show that, although direct serotonin exposure or depolarization of GlyCl-expressing cells can induce hyperpigmentation, the depolarization phenotype can be prevented by overexpression of hyperpolarizing channels or inhibition of SERT. Central features of this model are the regulation of cell behavior by transmembrane potential, regardless of which specific gene product achieves it, and non-cell-autonomous effects of a cell subpopulation specifically instructing, at considerable distance, one derivative of neural crest to undergo the stem-cell-to-neoplastic-cell-like phenotype.

### ***Transduction, voltage sensing and melanocyte regulation by serotonin***

Chloride influx (induced by activation of GlyCl and demonstrated directly using ion chromatography analysis) induces an increase in melanocyte number.

Although chloride channels have been linked to mitotic control [253, 254], the pathway resulting in hyperpigmentation is not restricted to chloride-specific signaling but is rather controlled by  $V_{\text{mem}}$ . This is indicated by the fact that other methods for depolarizing cells, such as inhibition of hyperpolarizing  $\text{H}^+$  pumps (Figure 3.5A-D) or potassium channels (Figure 3.8) [33], result in the same phenotype. Moreover, the phenotype can be rescued by misexpression of a hyperpolarizing channel (Figure 3.5F-H). Thus, the modulation of melanocyte behavior is not a consequence of some cryptic role of ivermectin, nor of the  $\text{Cl}^-$  ion, but of  $V_{\text{mem}}$ . However, chloride channels are a tractable mechanism (endogenously, and experimentally) for controlling  $V_{\text{mem}}$  in distinct cell groups.

It is known that prolonged depolarization activates proliferation of some cell types [49, 204, 255], as we observed in human melanocytes, although the mechanism is largely unknown. Interestingly, sustained ivermectin treatment in *Xenopus* does not result in generalized runaway hyperproliferation but affects a specific cell type; it remains to be understood why the GlyCl-expressing cells instruct only melanocytes and not other cell types. Depolarization induced approximately one extra cell cycle (Figure 3.5D and Figure 3.3C), which is a very strong effect because it occurred within about a day of exposure, whereas melanocyte doubling normally takes 8-10 days in *Xenopus* [256]. Thus, depolarization might not be a generalized and direct inducer of mitosis but rather a signal that can stimulate specific instructor cells to trigger a defined and limited change in cell number of specific other cell populations.

Our data are also consistent with previous observations showing abnormal neural crest migration in embryos exposed to electric fields [257]. Although direct application of fields to complex tissues is a somewhat blunter tool than molecular changes of ion fluxes in defined cells, applied electric fields can depolarize cells, and such a treatment also results in hyperpigmentation (data not shown). Because melanocytes do not migrate directionally in physiological direct current (DC) electric fields [237, 258] these effects are probably mediated by transmembrane potential and not long-range electric fields induced by ion channel activity.

How are changes in transmembrane voltage transduced into alterations of cell behavior? Activation of voltage-gated calcium channels is a common mechanism [259], although our data (Table 3.3) offer no support for the role of  $\text{Ca}^{2+}$  in the depolarization effect. Instead, a serotonin-dependent mechanism is implicated downstream of chloride-dependent  $V_{\text{mem}}$  changes. Blockade of the serotonin transporter SERT suppresses the hyperpigmentation phenotype (Table 3.3). Moreover, the well-established role of SERT as part of the reuptake mechanism that lowers extracellular levels of serotonin suggests that high external levels of serotonin ought to mimic the hyperpigmentation effect. This was indeed observed (Figure 3.6D,E). The direction of serotonin transport by SERT is controlled by transmembrane potential [231], and serotonin is a known mitogen [260, 261]. Consistently, melanocytes are known to express serotonin receptors [262], and serotonergic signaling has been reported to induce a doubling of melanocytes in human skin [263], precisely as we observed.

Together, the data suggest a model in which modulation of serotonin levels (by SERT-dependent clearance of serotonin from intercellular spaces) is a

mechanism by which depolarization can activate proliferation. This is particularly plausible for melanocytes because serotonergic signaling has been linked to secretion of  $\alpha$ -melanocyte-stimulating hormone [264, 265]; thus, we propose the following model. In unperturbed embryos (Figure 3.8A), the ‘instructor’ cells are polarized by the activity of several ion transporters. The resulting transmembrane gradient powers the function of coexpressed SERT, allowing this reuptake to reduce the level of extracellular serotonin (as occurs in synapses). In the absence of elevated extracellular serotonin levels, melanocytes maintain their normal levels of proliferation, obey normal migration cues and exhibit a rounded shape. By contrast (Figure 3.8B), if the membrane is depolarized (by targeting  $H^+$ ,  $K^+$  or  $Cl^-$  transport; Figs 1, 5), SERT cannot clear the surrounding space. Indeed, it runs backwards [266, 267] to enrich the milieu with excess serotonin content (Figure 3.6D,E). This is a non-cell-autonomous signal and is consistent with a number of serotonin receptors being expressed in melanocytes [265] as well as classical data on serotonergic control of melanocytes in frog skin [268].

As in left-right patterning [41, 60], serotonin acts in this system as a small-molecule messenger mediating cell-cell instructive signaling downstream of changes in transmembrane potential. Indeed, animals injected with serotonin developed neural crest tumors [269], suggesting that serotonergic signaling is an important component of tumorigenesis. Future work will identify the receptor mechanisms by which melanocytes respond to serotonin or potential downstream factors to acquire a neoplastic-like phenotype.

### ***Voltage changes in development and cancer***

Most cancer cell types exhibit a characteristic depolarization of membrane potential compared with healthy tissue [22, 79]. However, our *in vivo* experiments

revealed a non-cell-autonomous instructive function for GlyCl-expressing cells that would not be apparent from *in vitro* experiments: depolarization can induce a neoplastic-like phenotype in cells that themselves are not (yet) depolarized (Figure 3.4). Strikingly, human melanocytes exhibit an even more direct, cell-autonomous component of the depolarization phenotype (Figure 3.7). One of the interesting features of the melanocyte phenotype is the appearance of very long projections (Figure 3.2J); it is not yet known whether this is associated with nerves, for example using axons as guidance cues. This might also be related to the striking finding that highly aggressive melanoma cells can be coaxed to produce vascular networks in three-dimensional culture [186].

Indeed, there is a fascinating and still poorly understood relationship between cancer and developmental processes [68, 270, 271]. On transplantation of human metastatic melanoma cells into premigratory neural crest of chick embryos, the melanoma cells became distributed along neural crest migratory pathways, lost tumorigenic potential and acquired normal neural crest features [272, 273]. Our data illustrate the flip side of normalizing metastatic tumor cells with embryonic microenvironments [100, 273, 274]: depolarization of somatic cells is a physiological (epigenetic) component of the embryonic microenvironment that, like acidification [275], can contribute to a transformation of the behavior of embryonic stem cell derivatives into cancer-like cells.

Neural crest stem cell derivatives are known to contribute to several tumor types, including melanoma, neuroblastoma and pheochromocytoma [179]. The depolarization phenotype is neoplastic-like – although there is no primary tumor (as in small-cell lung carcinoma, for example), the effect fulfils three classic criteria for cancer: cell shape change, invasiveness and overproliferation.

Moreover, the drug NSC-84093 – an MMP inhibitor [221] – prevents colonization of ectopic sites in the embryo, as it does in adult animal cancer models [276]. Thus, the hyperpigmentation phenotype seems to be similar in mechanistic ways to the metastatic phase of cancer.

What is the relevance of our data for cancer, and melanoma specifically? Uncontrolled growth and dispersal of melanocytes can lead to melanoma [94, 277, 278]. Melanoma cell migration [279], as well as migration of other cell types [280], is known to be dependent on potassium channels [281-287] and a number of ion channels have been characterized as markers and likely causes of neoplasm [81, 88, 89, 205, 288-294]. Indeed, ion channels are increasingly becoming high-priority targets for anti-neoplastic therapy [79, 206, 295], and monitoring of electrical properties is being used as a diagnostic tool [296-299]. Our data suggest that control of  $V_{mem}$  is a key component of this set of pathways, and as such is a promising target of treatments for melanoma as well as other types of neoplasm. In particular,  $V_{mem}$  might be an important and novel regulator of the stem cell-cancer cell transition [300-304]. We are currently pursuing strategies for early, non-invasive cancer detection using voltage-sensitive fluorescent reporter dyes and techniques to normalize cancer by repolarizing neoplastic cells and instructor cell populations.

***GlyCl as a target for rational modulation of bioelectric signals in regenerative medicine***

It is important to note that the effect described by the above data is not simply a function of the GlyCl protein, nor is it inherently tied to chloride flux (Figure 3.5). Although GlyCl is a convenient target for voltage modulation, this pathway is not limited to any one gene product but rather is driven by changes in a biophysical

parameter,  $V_{\text{mem}}$ , that is determined by the activity of multiple transporters. Our data shed light on a control mechanism operating during normal embryogenesis that can regulate neural crest stem cell dynamics, as well as identifying a new environmental parameter that might be involved in neoplastic processes.

Indeed, the data suggest a new strategy for rational control of cell behavior in regenerative medicine. Our method was to identify an ion channel that is present in a specific cell population, and modulate  $V_{\text{mem}}$  by opening that channel while designing the external medium in such a way as to direct ion flux towards the desired  $V_{\text{mem}}$  change. We used ivermectin-sensitive GlyCl, which works very well, plus ivermectin is already approved for human use as an antiparasitic [305]. However, this strategy can be used with any channel (especially potassium channels) for which openers and closers are available, and the above data show that it is possible to use the Goldman-Katz equation to quantitatively design a strategy to rationally modulate transmembrane potential. Previously, we have shown that control of transmembrane potential is a powerful tool for understanding and inducing complex regenerative responses [21, 29, 34, 52]. This approach can be used to control  $V_{\text{mem}}$  changes in well-defined cell groups *in vivo* with temporal modulation.

Moreover, the unique and unusual expression pattern reveals GlyCl as a marker for a potentially highly important cell type: a kind of 'instructor cell' that can signal other populations (e.g. neural crest) and drastically change their behavior at considerable distance (Figure 3.4H-I', Figure 3.5G,H). Analysis of expression of other ion channels and pumps might reveal yet other subsets of otherwise homogenous-seeming cell groups, which, like the GlyCl-expressing cells, could be tractable targets for modulation in regenerative medicine. For

example, melanocytes can build vessels through vasculogenic mimicry [161, 186], and voltage control should be investigated as a technique for controlling shape in bioengineering contexts [20].

Future work will surely reveal additional fascinating roles for specific ion flows in morphogenesis. Taken together, our data reveal  $V_{\text{mem}}$  as a tractable mechanism of morphogenetic regulation, with relevance to normal embryonic development and neoplasm, and suggest a pharmacological strategy for  $V_{\text{mem}}$  modulation that might be of use in several branches of biomedicine.

## **Translational impact**

### ***Clinical issue***

Understanding how stem cells function in the creation and maintenance of biological shape is fundamental to three main areas of biomedicine: birth defects, which result from failure to build appropriate structures during embryonic development; regeneration after injury or disease, which requires the proper shape of the damaged structure to be rebuilt in adulthood; and, finally, cancer, which can be seen as a failure to obey the patterning cues that continuously act to impose three-dimensional order against neoplasia and aging. The neural crest is a key population of stem cells that migrate throughout the embryo and contribute to structures such as the heart, face and skin. Neurocristopathies, which are defects in neural crest development, form an important class of congenital defects.

Although the genetic and biochemical signaling pathways that regulate the conversion from normal developmental patterning to cancer have been intensively studied, an important class of signals remains poorly understood:

endogenous bioelectric cues produced by ion channels and transmembrane voltage gradients.

### **Results**

Owing to their ease of manipulation and relative transparency, *Xenopus laevis* embryos are a particularly convenient model for understanding the signals directing neural crest cells and their progeny. To determine how changes in membrane voltage regulate cell behavior and interactions *in vivo*, the authors target a population of cells expressing the glycine-gated chloride channel (GlyCl). By opening the channel pharmacologically and manipulating ion levels to hyperpolarize or depolarize these cells, they show that GlyCl-expressing cells can trigger a neoplastic-like phenotype in an important class of neural crest derivatives – the pigment cells known as melanocytes. The GlyCl-expressing ‘instructor’ cells trigger hyperproliferation, and cause increased dendricity and invasiveness into neural tissues, blood vessels and gut. Crucially, the induction of this metastatic phenotype occurs at long range and is mediated by serotonergic signaling.

### **Implications and future directions**

This work demonstrates that the bioelectrical state of specific cells in the host can trigger the stem cell to neoplastic cell transition in pigment cells, resulting in a phenotype that is similar to that of metastatic melanoma. Crucially, the relevant signal is not tied to GlyCl per se, or even chloride, but is truly carried by a physiological parameter – voltage. These data reveal a new role for ion flow and serotonergic signaling in melanocyte regulation, with potential uses in the treatment of vitiligo and melanoma. Furthermore, they uncover a newly identified population of ‘instructor’ cells (characterized by GlyCl expression) that can

control the fate of neural crest derivatives with exquisite specificity. The ability to modulate membrane voltage without the need for gene therapy, and the identification of cell types that can direct the function of stem cells, are powerful approaches through which to better understand and address the *in vivo* control of patterning in cancer, the regenerative response and the repair of birth defects.

## **Methods**

### ***Animal husbandry***

*Xenopus* embryos were maintained according to standard protocols [122] in 0.1X MMR, pH 7.8, plus 0.1% gentamicin. *Xenopus* embryos were staged according to Nieuwkoop and Faber [154].

### ***Expression analysis***

*In situ* hybridization was performed as previously described [157]. *Xenopus* embryos were collected and fixed in MEMFA ([122]). Prior to *in situ* hybridization, embryos were washed in phosphate buffered saline (PBS) + 0.1% Tween-20 (PBST) and then transferred to methanol through a 25%/50%/75% series.

Probes for *in situ* hybridization were generated *in vitro* from linearized templates using a DIG labeling mix from Roche. Chromogenic reaction times optimized signal:background ratio. Analyses represent consistent patterns from 50-60 embryos for each marker. Probes used for *in situ* hybridization include: sense and antisense GlyCl-a (NCBI accession #CX801861), and GlyCl-b (NCBI accession #BC121237). Anti-GlyCl (Chemicon 5052 used at 1:200 dilution) and -SERT (Chemicon MAB5618 used at 1:100 dilution) antibodies were used for

immunohistochemistry using previously described protocols [306].

### ***Microinjection***

Capped, synthetic mRNAs were dissolved in water and injected into embryos in 3% Ficoll using standard methods [122]. After 3 hours, embryos were washed and cultured in 0.1X MMR until the desired stages were reached. Constructs used for misexpression included: dominant-negative E140K mutant of ductin (the 16 kDa subunit of the V-ATPase) [65, 307], the KCNE1 accessory subunit [33], the GlyCl wild-type channel [308] and the potassium channel Kir4.1 [123].

### ***Drug exposure***

Stocks of ivermectin (Sigma) were kept at 10 mM concentration in dimethyl sulfoxide (DMSO). Embryos were exposed in 0.1X MMR for the stages indicated to: ivermectin, 1 mM; cadmium chloride, 0.1 mM; verapamil, 10 mM; fluoxetine, 10 mM; lindane, 1.7 mM; NSC-84093, 2 mM; and glycine, 0.13 mM.

### ***Elemental analysis***

For elemental analysis, cohorts of stage 13 embryos were either untreated or exposed to a combination of 10 mM ivermectin + MMR containing 60 mM Cl<sup>-</sup>. At stage 30, 2 ml of packed embryo were collected from each cohort and washed three times in 0.1X MMR. Excess media was removed from the samples and the embryos were stored at -80°C before shipping to Galbraith Laboratories (Knoxville, TN) for dry analysis of chlorine concentration. Samples were prepared by Parr oxygen bomb combustion and analyzed by ion chromatography. Results are reported as percent chloride in total sample based on dry mass.

### ***Measurement of melanocyte numbers***

Melanocytes were counted by cellAnalyst software (AssaySoft) on digital photographs of anesthetized larvae. Adobe Illustrator was used to define the dorsal region between the eyes used for counting. Tail regions were defined using digital photographs: all melanocytes within a 400X400 pixel box, extending anteriorly from the tip of the tail, were counted.

### ***Immunohistochemistry***

Spatial detection of apoptosis and proliferation was performed by immunohistochemistry in section. We chose caspase-3 staining as a more specific detector of apoptosis [309-311] than classical methods such as TUNEL, which gives considerable levels of false positive signal [312]. Briefly, larvae were fixed overnight in MEMFA [122], embedded in agarose and sectioned at 100  $\mu$ m using a Leica vibratome. The sections were permeabilized in PBS + 0.1% Triton X-100 for 30 minutes, blocked with 10% goat serum PBST for 1 hour, and incubated at 4°C overnight with primary antibody (anti-activated-caspase-3; Abcam #AB13847) for apoptosis [313], or anti-H3B-P, Upstate #05-598) for proliferation, diluted 1:1000 in PBST + 10% goat serum. They were then washed six times with PBST (1 hour each at room temperature) and incubated with Alexa-Fluor-555-conjugated secondary antibody at 1:1000 in PBST + 10% goat serum overnight at 4°C. Sections were photographed using the appropriate filter set on a Nikon SMZ-1500 scope with epifluorescence after six 1-hour washes in PBST.

### ***Direct measurement of melanin content***

Melanin content of embryos was measured as described previously [314] with slight modification. In brief, five stage-45 embryos were hydrolyzed in 0.2 ml 1 M NaOH for 96 hours at 37°C, and 0.15 ml was diluted to 1 ml with H<sub>2</sub>O, and used for spectrophotometric determination of the absorption at 414 nm.

### ***Human melanocyte culture***

Human melanocytes were obtained commercially and cultured in DermaLife M Melanocyte culture medium (cells and media provided by Lifeline Cell Technology, Walkersville, MD). Cells were maintained in standard 25-cm<sup>2</sup> culture flasks; the 10 ml of media was replaced every other day. On reaching confluence, melanocytes were passaged using a standard trypsinization protocol, and new colonies were seeded at approximately 5000 cells/cm<sup>2</sup>. For high-potassium-media experiments, DermaLife M media was supplemented with 40 mM potassium gluconate, a level determined during a preliminary potassium dose-response screen to be non-inhibitory to growth while inducing morphological changes.

For cell shape analysis, cells were imaged on a Nikon AZ100M stereomicroscope and the numbers of filopodia on all cells within the field of vision were counted. Cell culture in high-potassium media was repeated three times and the results averaged for statistical analysis.

### ***Imaging $V_{mem}$ using CC2-DMPE and DiBAC<sub>4</sub>(3)***

CC2-DMPE [N-(6-chloro-7-hydroxycoumarin-3-carbonyl)-dimyristoylphosphatidyl ethanolamine], a cationic coumarin phospholipid, and the anionic oxonol DiBAC<sub>4</sub>(3) [bis-(1,3- dibutylbarbituric acid) trimethine oxonol] were purchased

from Invitrogen. Using two dyes with opposite emission profiles simultaneously provides an internal control and allows results to be corrected for artifact by ratiometric normalization. Stock CC2-DMPE solution was prepared according to manufacturer's directions: a 5 mM stock (in DMSO) was prepared, aliquoted and stored at  $-20^{\circ}\text{C}$  until immediately before use. DiBAC<sub>4</sub>(3) stock (1.9 mM in DMSO) was prepared and stored at room temperature. CC2-DMPE stock was dissolved 1:1000 directly into culture medium. DiBAC<sub>4</sub>(3) stock was dissolved 1:2 in DMSO, then spun at RCF 20,800 for 10 minutes to remove undissolved particles of dye. Supernatant was then diluted 1:4000 in culture media. 1 ml of CC2-DMPE was added to cells grown in 35-mm FluoroDish Sterile Culture Dishes. Cells were incubated for 30 minutes, then washed twice with plain culture media. 1-2 ml of DiBAC<sub>4</sub>(3) were then added to the dish. Cells were incubated at least 30 minutes before imaging began; cells were imaged while in the DiBAC<sub>4</sub>(3) bath. A round coverslip was dropped into the dish, and any medium outside the well was removed. The dish was then turned over and the cells imaged through the glass bottom of the dish.

An Olympus BX-61 equipped with a Hamamatsu ORCA AG CCD camera, and controlled by IPLabs, was used for imaging. CC2-DMPE is imaged with the following filters: EX 405/20; BS 425; EM 460/50 (Chroma filter set 31036). DiBAC<sub>4</sub>(3) is imaged with: EX 470/20; BS 485; EM 517/23 (Chroma filter set 41001). After dark-field (to remove camera noise) and flat-field (to correct for uneven illumination) corrections, image arithmetic was used to take the ratio of CC2-DMPE intensity over DiBAC<sub>4</sub>(3) intensity. The result is an artifact-corrected picture of  $V_{\text{mem}}$ ; the brighter the pixel, the more polarized the region it represents. Images were pseudocolored to make the contrast between different regions more

easily visible. No calibration was performed; nonetheless, pixel intensity within and among images can be compared for relative quantification. Except for resizing during figure preparation, no other changes were made to the images; thus, pixel intensity or color are reliable reporters of  $V_{\text{mem}}$ . Original images are available on request.

### ***Statistics***

All statistical analyses were performed using Prism v.5 (GraphPad Software, La Jolla, CA). Student's *t*-tests were used for comparisons of melanocyte number, incidence of hyperpigmented tadpoles and cell intensity for microscopy experiments. Filopodial numbers in human melanocytes were compared using a two-way ANOVA. Data conformed to parametric requirements; no corrections were needed for normality or variance.

## **Acknowledgements**

We thank Punita Koustubhan and Amber Currier for *Xenopus* husbandry, and Dayong Qiu and Norman Lautsch for histology. We are grateful to the Drug Synthesis and Chemistry Branch, Developmental Therapeutics program, Division of Cancer Treatment and Diagnosis, National Cancer Institute, for providing NSC-84093 compound, Daryl Davies and Miriam Fine for the GlyCI expression construct, John Mihic for useful discussions and for the overactive D97R mutant of human glyR $\alpha$ 1, Nancy Papalopulu for helpful comments on the manuscript, and Carole Labonne for Sox10 plasmid. M. Levin gratefully acknowledges the support of the NIH (grant GM078484), NHTSA (grant DTNH22-06-G-00001) and DOD (grant W81XWH-10-2-0058). D.B. was supported by Forsyth Institute's T32-DE-007327 training grant. D.S.A. was supported by the NIH/NIDCR (grant K22DE016633).

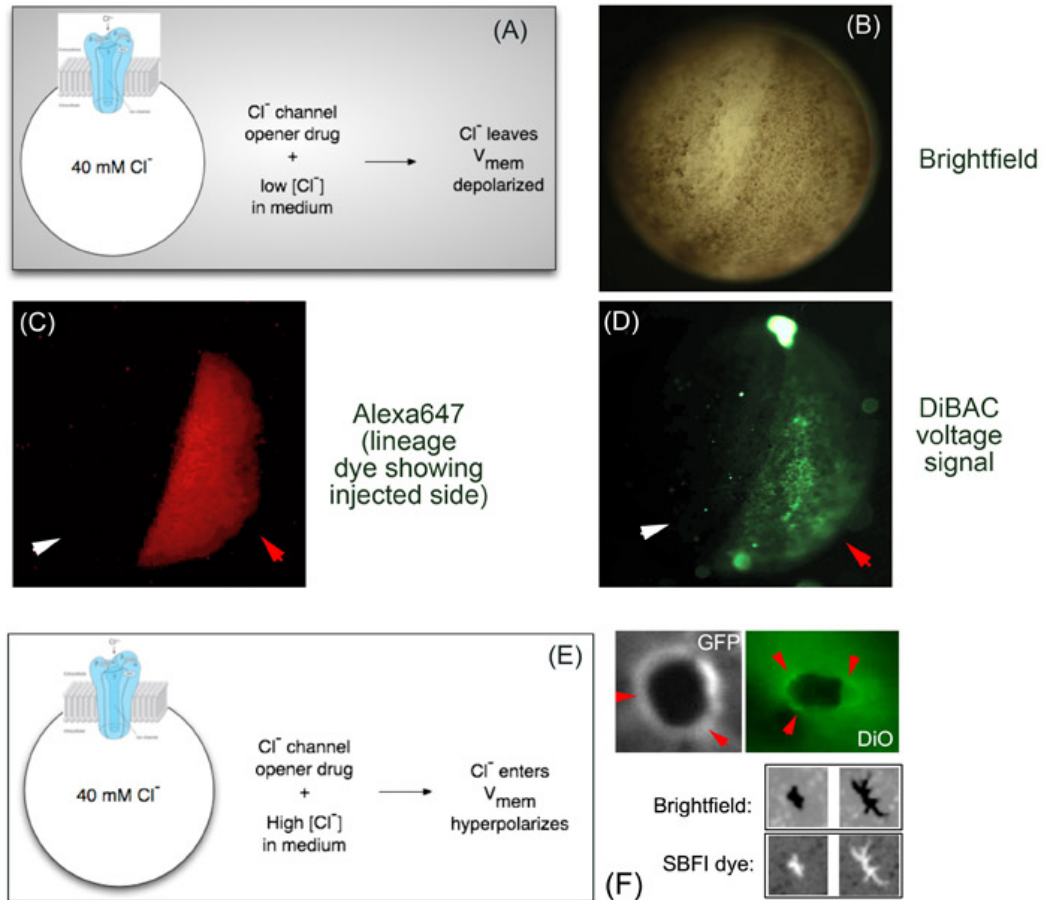
## **Competing interests**

The authors declare no competing financial interests.

## **Supplementary material**

Supplementary material for this article is available at

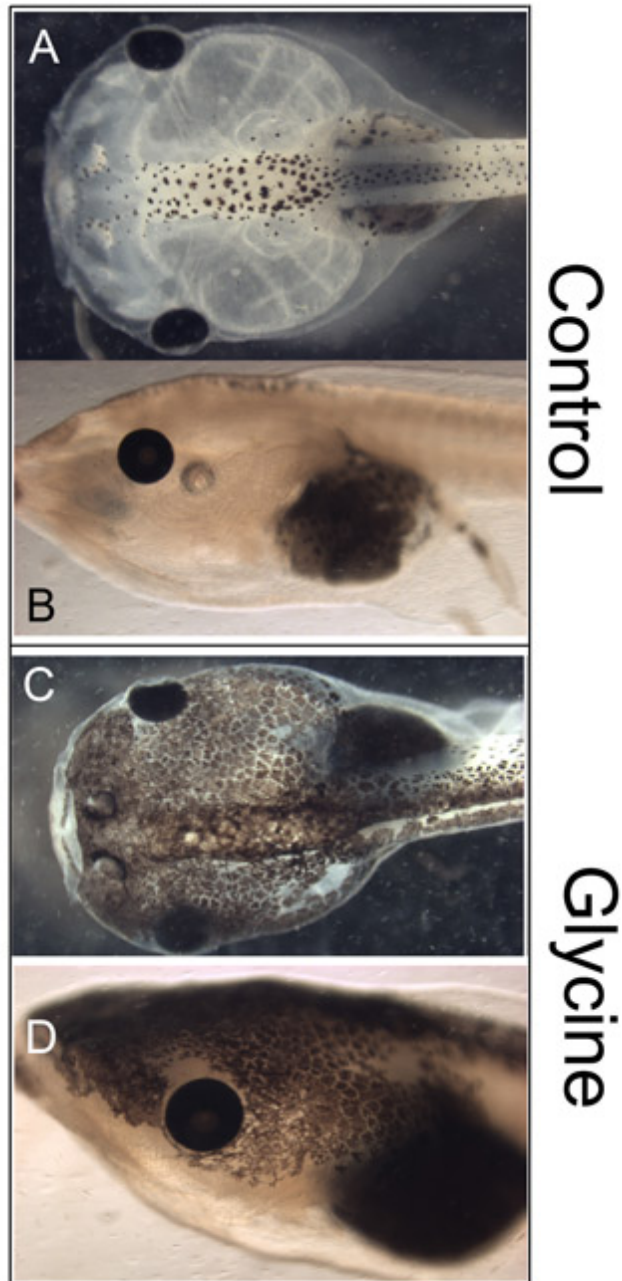
<http://dmm.biologists.org/lookup/suppl/doi:10.1242/dmm.005561/-/DC1>



**Supplemental Figure 3.1. Depolarization by ivermectin exposure.**

(A) A schematic of the strategy for depolarizing specific cells. In *Xenopus* cells, the chloride concentration is significantly higher than in the external medium (10 mM in 0.1× MMR). Thus, if chloride channels are forced open pharmacologically, the Cl<sup>-</sup> ions flow outwards down their concentration gradient and depolarize cells expressing this channel. In wild-type embryos, relatively few cells express GlyCl (Figure 4). This is an advantage (allows mosaic analysis) in functional experiments, but makes it very difficult to observe depolarization directly. Indeed, we observed that most cells did not depolarize after ivermectin exposure (data not shown and left side of panel D), demonstrating that ivermectin is not a general depolarizer (as expected from its specificity for GlyCl). To show directly that our strategy of ivermectin-based depolarization works as expected to target the GlyCl, we misexpressed GlyCl throughout half of each embryo prior to ivermectin treatment and detection of transmembrane potential by a fluorescent voltage reporter dye. (B) A sample neurula-stage frog embryo in which one blastomere at the 2-cell stage was injected with GlyCl-α mRNA. (C) Lineage dye label shows that half of the embryo (red arrowhead, compare to contralateral internal control, white arrowhead) was indeed targeted with GlyCl expression construct mRNA. (D) Signal from the DiBAC voltage dye reveals that when the same embryo was treated with ivermectin, GlyCl-expressing cells were depolarized (red arrowhead, compare to contralateral control not expressing GlyCl – white arrow – which is not depolarized). (E) A schematic of the inverse

strategy to hyperpolarize specific cells: augmentation of external medium with excess chloride causes cells to take up negative ions thus becoming hyperpolarized. Thus, once GlyCl is opened in cells expressing this channel, their transmembrane potential can be controlled by modulating extracellular chloride concentration. (F) Close-up of wild-type melanocytes (with edge demarcated by cell surface markers GFP and DiO), demonstrating that the rounded appearance (which changes to an arborized one upon depolarization of GlyCl-expressing cells) is in fact the true shape of these cells (and is not an artifact of a tight spot of pigment within a normally highly-arborized melanocyte). Red arrows indicate cell boundary, which is not arborized in cells in which melanocyte distribution is compact. The same is seen when rounded vs. arborized melanocytes are imaged with the SBF1 dye, which fills cells and reveals that actual cell boundaries closely match pigment pattern in both rounded and more arborized melanocytes.



**Supplemental Figure 3.2. Glycine exposure induces hyperpigmentation.** Compared to wild-type embryos (A,B) exposure to the GlyCI receptor ligand glycine from st. 10 to st. 41 induced the same hyperpigmentation phenotype as did ivermectin exposure (C,D).

## Chapter 4

### **Resting Potential, Oncogene-induced Tumorigenesis, and Metastasis: The Bioelectric Basis of Cancer *in vivo***

Maria Lobikin, Brook Chernet, Daniel Lobo and Michael Levin

Physical Biology (2012) 9(6): p. 065002

**Data contributions:** I contributed data to figures 4.1, 4.2, 4.3, 4.4, and tables 4.2-4. Brook Chernet contributed data to the figures 4.5, 4.6, 4.7, 4.8, and supplement 2. Daniel Lobo modeled serotonergic signaling in melanocytes (supplement 4.1).

## Abstract

Cancer may result from localized failure of instructive cues that normally orchestrate cell behaviors towards the patterning needs of the organism. Steady-state gradients of transmembrane voltage ( $V_{\text{mem}}$ ) in non-neural cells are instructive, epigenetic signals that regulate pattern formation during embryogenesis and morphostatic repair. Here, we review molecular data on the role of bioelectric cues in cancer and present new findings in the *Xenopus laevis* model on how the microenvironment's biophysical properties contribute to cancer *in vivo*. First, we investigated the melanoma-like phenotype arising from serotonergic signaling by “instructor” cells – a cell population that is able to induce a metastatic phenotype in normal melanocytes. We show that when these instructor cells are depolarized, blood vessel patterning is disrupted in addition to the metastatic phenotype induced in melanocytes. Surprisingly, very few instructor cells need to be depolarized for the hyperpigmentation phenotype to occur; we present a model of antagonistic signaling by serotonin receptors that explains the unusual all-or-none nature of this effect. In addition to the body-wide depolarization-induced metastatic phenotype, we investigated the bioelectrical properties of tumor-like structures induced by canonical oncogenes and cancer-causing compounds. Exposure to carcinogen 4-Nitroquinoline 1-oxide (4NQO) induces localized tumors, but has a broad (and variable) effect on the bioelectric properties of the whole body. Tumors induced by oncogenes show aberrantly high sodium content, representing a non-invasive diagnostic modality. Importantly, depolarized transmembrane potential is not only a marker of cancer but is functionally instructive: susceptibility to oncogene-induced tumorigenesis is significantly reduced by forced prior expression of hyperpolarizing ion channels.

Importantly, the same effect can be achieved by pharmacological manipulation of endogenous chloride channels, suggesting a strategy for cancer suppression that does not require gene therapy. Together, these data extend our understanding of the recently-demonstrated role of transmembrane potential in tumor formation and metastatic cell behavior.  $V_{\text{mem}}$  is an important non-genetic biophysical aspect of the microenvironment that regulates the balance between normally patterned growth and carcinogenesis.

## **Introduction**

### ***Cancer as a developmental disorder***

Cancer may be fundamentally a developmental disorder [68, 69, 315-318], and may occur when cells stop obeying the normal patterning cues of the body [319-321]. Cancer is thus 'part of an inexorable process in which the organism falls behind in its ceaseless effort to maintain order' [68]. The signals that establish and maintain anatomy during embryogenesis and adult life comprise both genetic and epigenetic pathways, and much debate has occurred about the relative contributions of genetic vs. epigenetic disruptions to cancer [100, 103, 194, 274, 322-326]. The view of cancer as a reversible physiological state has significant medical implications because learning to modulate the impact of the cellular environment on neoplastic progression could impact prevention and detection strategies. Moreover, a mechanistic dissection of pathways by which the host reboots cancer cells may give rise to strategies that normalize cancer [273, 327, 328], in contrast to current approaches that seek to kill tumors and thus risk a compensatory proliferation response by any remaining cancer cells [329].

The phenomenon of tumor reversion (e.g., observed when cancer cells are

placed in normal embryonic or regenerative environments) contradicts irreversible, cell-autonomous genetically-deterministic models of the origin of cancer, and emphasizes the role of tissue structure [327, 330-333]. Biologists are beginning to explore [334] the idea that cancer is a kind of attractor in a multi-dimensional transcriptional state space: 'The topology of the attractor is the "invisible hand" driving the system functions into coherent behavioral states: they are self-organizing structures and can capture the gene expression profiles associated with cell fates' [335]. However, such models are also compatible with state spaces in which the dimensions correspond to physical properties and not only transcriptional states. If cancer is indeed best understood as part of the interplay between the host organism and individual cell regulation, it thus becomes crucial to dissect the endogenous physiological signals used to coordinate cell growth with the large-scale patterning needs of the body.

### ***Gradients of Transmembrane Potential Mediate Patterning Cues***

In addition to the biochemical gradients and gene-regulatory networks that underlie cell-cell communication, the complex field of patterning information that impinges upon all cells within a host organism [336] also contains an important biophysical component. "Bioelectricity" refers to the slowly-changing gradients of transmembrane (resting) potential, ion fluxes, and electric fields produced and sensed by non-excitabile cells [337-339]. While classical work has long suggested the importance of bioelectric gradients for regeneration, development, and cancer [340-344], molecular-resolution tools have recently been developed for real-time detection and manipulation of bioelectrical properties *in vivo* [345, 346]. This work has identified novel roles for bioelectricity in cellular regulation and dissected the pathways linking ion flows to transcriptional responses and

changes in cell behavior [18, 347-349]. Indeed, transmembrane voltage gradients are now known to control cell proliferation, migration, differentiation, and orientation [22, 350]. Moreover, the information stored in physiological networks (dynamic spatio-temporal patterns of ion flows through cell membranes and among connected cell groups) is instructive for anatomical identity of newly produced tissue, and mediates size control and positional information during organ formation, large-scale organ/appendage regeneration, and axial patterning [24, 26, 29, 61, 63, 351].

### ***Bioelectricity as a Non-genetic Aspect of Cancer Microenvironment***

The view that cancer is a developmental disorder predicts that molecular mechanisms known to be important mediators of the morphogenetic field would be involved in tumorigenesis. Indeed, there is mounting evidence that the bioelectric cues that establish normal pattern can go awry and result in cancerous growth. The unique bioelectrical properties of tumor tissue have been long-recognized [75, 76, 343, 352-364]; specifically, cancer cells are generally depolarized with respect to normal healthy tissue [365-368]. Modern molecular data have confirmed the physiological observations, and several pathways of high relevance to cancer have now been shown to be under bioelectrical control, including apoptosis [369], epigenetic chromatin modification [370, 371], stem cell regulation [52, 372, 373], and the transfer of signals through gap junctions [374]. A number of ion channel, pump, and gap junction genes are now recognized as bona-fide oncogenes (Table 1). Importantly, ion translocators are not only markers associated with neoplastic processes but are functional determinants of cancerous progression.

**Table 4.1. Known ion translocators as oncogenes.**

Several ion transporters are now recognized as causal agents in carcinogenesis, consistent with the role of  $V_{mem}$  in regulating cell proliferation, migration, and differentiation. Future work remains to test the hypothesis that the patterning roles of voltage gradients are an important component of pattern dysregulation as a fundamental cause of neoplasia [317, 334]

<b>Protein</b>	<b>Species</b>	<b>Reference</b>
NaV1.5 sodium channel	Human	[375]
EAG-1 potassium channel	Human	[293]
KCNK9 potassium channel	Mouse	[376]
Ductin (proton V-ATPase component)	Mouse	[377]
SLC5A8 sodium/butyrate transporter	Human	[378]
KCNE2 potassium channel	Mouse	[379]
Connexin26 (gap junctions)	Mouse	[380]

### ***Recent molecular data implicates ion translocator proteins in cancer***

The proliferation of some tumor cells is dependent on voltage-gated potassium channels [289, 381]. hERG channels are particularly implicated [205, 290, 369, 382-384], as are 2-pore channels such as KCNK9 [291, 385]. While roles other than ion transport have been proposed for some channels, in the case of KCNK9, it is known that its oncogenic potential depends on K<sup>+</sup> transport function, and not some other role of the protein [386]. A screen of several cervical cancers found the K<sup>+</sup> channel EAG expressed in 100% of the biopsies analyzed, and overexpression of EAG in human cells resulted in more quickly dividing progeny in culture [293, 387]. This result was replicated *in vivo* using mice implanted with human EAG-expressing CHO cells [293, 387]. hEAG-1 is a true oncogene since its overexpression drives mammalian cells into uncontrolled proliferation and favors tumor progression in cells injected into immune-suppressed mice [293]. Likewise, hERG is not normally present in most differentiated cells other than in the heart but has been observed in a number of human cancers and during neoplastic transformation in prostate epithelium [384, 388]. In these cells, hERG appears to recruit tumor necrosis factor receptor (TNFR) to the plasma membrane and cause a subsequent increase in NFκB, a known regulator of proliferation. In addition to modulations of single channels, some cancers are characterized by the activation of multiple potassium currents, such as human melanoma lines that express both hEAG1 and Ca<sup>2+</sup>-activated K<sup>+</sup> channels [389]. Indeed, complex interactions by multiple channels likely exist, and trans-membrane currents driven by diverse families of potassium channels (including calcium activated, inward rectifying K<sub>ir</sub>, EAG, and ERG) have all been correlated with cancerous tissue.

In addition to potassium, a number of other ions can play similar roles [390, 391]. Manipulation of membrane  $H^+$  flux confers a neoplastic phenotype upon cells [392], while studies in glioma cell lines have revealed a role of chloride channels [393, 394]. Inhibition of Clc-3 through hairpin RNA constructs resulted in the loss of premitotic condensation and arrest of the cell cycle in glioma cells [394]. In studies of human prostate cancer lines, these results support the role of chloride channels as key regulators of proliferation through cell size regulation [395, 396].

Sodium channels are a particularly important set of targets for cancer. The human knockout APC<sup>min/+</sup> cell line shares a mutation found in many human colorectal cancers, and when introduced into mice subsequently results in the development of multiple intestinal neoplasias [397]. *In vivo* transepithelial voltage recordings in this line revealed an increase in  $Na^+$  levels compared to wild type mice that was the result of an increase in expression of the ENaC  $Na^+$  channel. Metastatic potential correlates with voltage-gated inward sodium current and it has been convincingly argued that some sodium channels may be oncofetal genes [398-402]. Indeed, a sodium-channel gene was identified as the top node of a genetic network that regulates colon cancer invasion [295].

### ***Investigating the biophysics of cancer in vivo: the frog model***

Ion translocators are both predictive markers [391], and an important set of targets for new cancer drugs [206, 403, 404]. Dissecting the molecular mechanisms by which biophysical properties regulate oncogenesis and metastatic processes during morphogenesis requires a model system that is tractable to both biophysical/physiological techniques and state-of-the-art molecular genetics. Recent work in the *Xenopus* tadpole has both confirmed the

role of ion flow in oncogenesis *in vivo*, and identified bioelectricity as an important aspect of non-local signaling of the cellular microenvironment that can induce and suppress cancer-like cell behavior.

An expression analysis revealed a widely-distributed, sparse population of cells expressing glycine-gated chloride channels (GlyCl). By exposing embryos to the specific GlyCl channel activator ivermectin, and controlling the extracellular levels of chloride, the membrane potential of these specific cells could be set to any desired level (and confirmed with voltage-reporting fluorescent dyes; strategy is shown in Figure 4.1A). We took advantage of this finding to probe the consequences of bioelectrical dysregulation *in vivo* and to investigate the consequences of depolarizing select cell groups in the tadpole [31].

When depolarized, these cells signal, at significant distance, to melanocytes – pigment cell derivatives of the neural crest [405]. The melanocytes then acquire 3 properties commonly associated with metastasis: they hyper-proliferate, change to a highly dendritic morphology, and invade tissues throughout the animal (such as blood vessels, gut, and neural tube) in a matrix metalloprotease-dependent manner. The ability of these cells to direct the activity of an entirely different set of cells led us to call the depolarizing GlyCl-expressing population “instructor cells”. Lineage and marker analysis was used to show that the hyperpigmentation phenotype did not result from other cells being abnormally shifted into becoming melanocytes, but rather that this change affected mature, existing, differentiated melanocytes [31]. Crucially, the phenotype could also be induced with the native ligand of GlyCl (glycine), ruling out off-target effects of ivermectin. Indeed, the effect could be induced or suppressed by modulating extracellular chloride levels, precisely

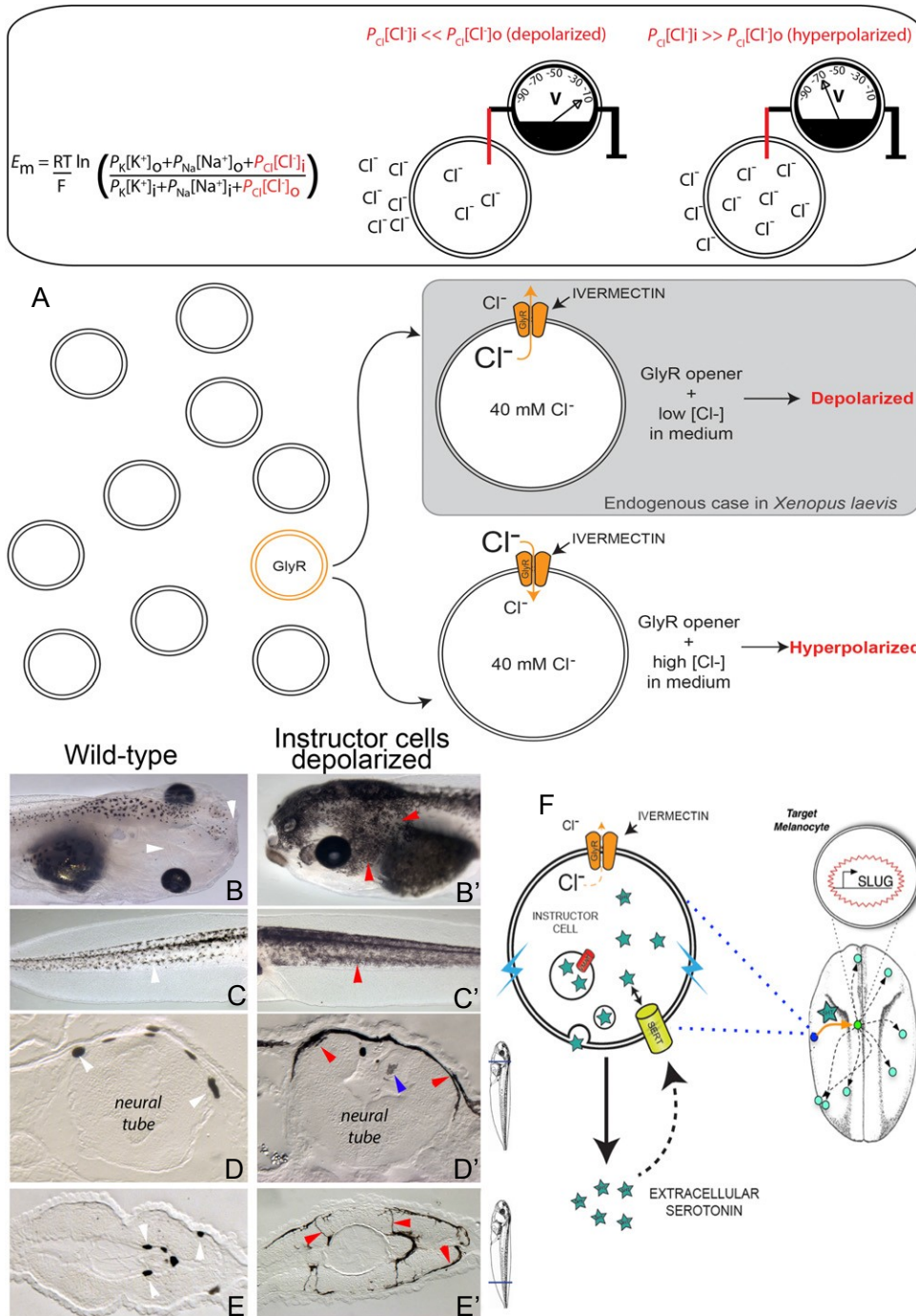


**Figure 4.1. Depolarization of instructor cells induces a metastatic phenotype in melanocytes.**

The Goldman equation reveals how resting potential  $V_{mem}$  depends on the internal and external  $K^+$ ,  $Na^+$  and  $Cl^-$  concentrations, ambient temperature ( $T$ ), and permeability of each ion ( $P$ ). (A) Manipulation of endogenous chloride channels as a means for selective probing of  $V_{mem}$ -based signaling. Ivermectin treatment targets GlyCl-expressing (“instructor”) cells, opening these chloride channels. Then, by manipulating external chloride levels, chloride ions can be made to enter or exit the GlyCl-expressing cells, thus controlling their

transmembrane potential. Normal tadpoles exhibit small numbers of black melanocytes over their neural tubes but not around their eyes or mouth (B, white arrowheads). In contrast, tadpoles whose instructor cells were depolarized for as little as 12 hours exhibit excess melanocytes, which possess a much more arborized appearance, and colonize areas normally devoid of melanocytes (B', red arrowheads). The same change in shape is seen in the tail (compare normal tail in panel C with the tail of a depolarized tadpole in C'); this change was quantified and mitotic indices were calculated in [31]. Sectioning of these tadpoles reveals that in contrast to the small number of round melanocytes normally present in the neural tube (D, white arrowheads), depolarization of instructor cells causes melanocytes to acquire a highly aberrant spread-out morphology (D, red arrowheads) as well as to invade the nervous tissue (blue arrowhead). This is also seen in more posterior sections through the tail/trunk, where the normally round melanocytes (E, white arrowheads) are far more numerous and extend long abnormal projections (E', red arrowheads). (F) Because the phenotype can be recapitulated by gain-of-function of serotonin signaling, and prevented by blockade of the serotonin transporter SERT, the data suggest a model of how instructor-cell signaling affects melanocyte morphology: depolarized instructor cells' SERT runs backwards, secreting serotonin into the extracellular space where it can diffuse and activate melanocytes to acquire 3 basic properties of metastasis: overgrowth, abnormal cell shape, and invasion of other tissues.

as predicted by the Goldman Equation (which links overall transmembrane potential to the concentrations and permeabilities of various ion species), ruling out ion-independent roles of GlyCl protein. Finally, it was found that misexpression of mRNAs encoding depolarizing sodium, potassium, or proton translocators could also phenocopy the highly specific change in melanocyte behavior induced by efflux of chloride through GlyCl. Moreover, the effect of GlyCl opening in the presence of low extracellular chloride could be rescued by expressing a hyperpolarizing potassium channel in the exposed embryos. Together these results demonstrated that the melanocyte-transforming effect is truly initiated by a change in voltage and independent of any specific ion or channel protein. This finding is consistent with the published data in mammalian systems, which implicate many different ion channels in cancer (as all of them can contribute to the regulation and dysregulation of resting potential). One interesting aspect of the phenotype is its all-or-none character: in the induction and rescue/suppression experiments, some percentage of the treated population become hyperpigmented while the rest do not, but any one tadpole is either hyperpigmented or not – there appear to be no in-between (partial) states.

It was shown that depolarization induces the up-regulation of cancer-relevant genes such as Sox10 and SLUG [405], but how do depolarized instructor cells signal to the distant melanocytes to induce the metastasis-like phenotype? A suppression screen tested known mechanisms by which transmembrane voltage changes were transduced into transcriptional responses, and implicated serotonergic signaling (a mechanism which also mediates long-range bioelectric signaling in left-right patterning [351, 371, 406]). Inhibition of the voltage-regulated serotonin transporter SERT abolished the hyperpigmenting

defect of depolarization, and SERT was seen to co-localize with the GlyCl channel (be expressed in instructor cells). Moreover, direct application of serotonin recapitulated the metastatic phenotype, suggesting a model in which membrane voltage regulated the dynamics of serotonin secretion by instructor cells, allowing non-cell-autonomous regulation of melanocyte function (Figure 4.1F).

The above data illustrated the power of depolarized  $V_{\text{mem}}$  as an epigenetic initiator of widespread metastatic behavior in the absence of a centralized tumor. More recently [407], we investigated the role of bioelectricity in tumor-like foci induced by canonical oncogenes. Tumors induced in *Xenopus* by oncogenes such as Gli1 and Rel3, or mutant tumor suppressors such as DNp53 and KRAS<sup>G12D</sup> [408-411] exhibit the predicted depolarized potential, but additional metrics are needed to refine a more narrow physiological signature that can distinguish prospective tumor sites from normal depolarized cells (e.g., stem cells). Further, while depolarization has been associated with cancer in the literature, it is now necessary to explore the extent to which forced hyperpolarization could prevent or revert tumor development *in vivo*.

### ***Open questions and new data***

Thus, transmembrane potential can both induce a metastatic phenotype in widespread normal somatic cells, and participate in localized carcinogenesis induced by canonical pathways. Here, we investigated several key questions brought up by the remarkable effects of localized depolarization in *Xenopus*. What other cell types, besides the melanocytes, may be affected by depolarization of instructor cells? How many depolarized instructor cells are sufficient to induce hyperpigmentation (metastatic conversion of normal

melanocytes) throughout the animal? What serotonin receptors mediate the non-cell-autonomous signaling between the instructor cells and melanocytes, and what model can explain the puzzling all-or-none character of melanoma-like transformation in depolarized tadpoles? What bioelectric changes are induced by carcinogens and oncogene expression? Are such changes localized to the tumor site, and how consistent are these changes among individual animals? Can such tumors be identified by a specific physiological signature, and could artificial control of the resting potential (either by transgenes or by pharmacological modulation of native ion channels) change the incidence of induced tumors? Here we present new data that fill in important details of this fascinating epigenetic pathway and highlight novel aspects of the bioelectric control of cancer.

## **Materials and methods**

### ***Animal Husbandry***

*Xenopus* embryos were maintained according to standard protocols [122] in 0.1X Modified Marc's Ringers (MMR), pH 7.8, plus 0.1% gentamycin. *Xenopus* embryos were staged according to Nieuwkoop and Faber [154].

### ***Microinjection***

Capped, synthetic mRNAs were dissolved in water and injected into embryos at cleavage stages in 3% Ficoll using standard methods [122]. mRNA injections were made into the locations indicated using borosilicate glass needles calibrated to bubble pressures of 50-70 kPa in water, delivering 70 ms pulses. After 30 min, embryos were washed in 0.75X MMR for 30 and cultured in 0.1X

MMR until desired stages. Constructs used included: GlyCl-A288G-tom [412], Gli1 [409], Xrel3 [410], KRASG12D [408], and Kir4.1 [413].

### ***Transgenics***

PT2xflk-1:GFP transgenic embryos were prepared using the *sleeping beauty* transposon system [414]. Transgenic embryos were treated with 1  $\mu$ M ivermectin, and imaged on an Olympus BX-61 using a FITC filter. Adobe Illustrator was used to define a 200  $\mu$ m region on the tail tip region, and vascular cells in this region were counted.

### ***Drug Exposure***

Stocks of ivermectin (Sigma) were stored at 10 mM concentration in dimethyl sulfoxide (DMSO). Embryos were exposed in 0.1X MMR for the stages indicated to: ivermectin, 0.05 - 1  $\mu$ M; reserpine 100  $\mu$ M; methiothepin 10 nM; cyanopridolol 50  $\mu$ M, altanserin, 10  $\mu$ M; tropisetron, 10  $\mu$ M; GR113808, 1  $\mu$ M; SB 699551, 2.5  $\mu$ M; Ro 04-6790, 50  $\mu$ M; SB 258719, 50  $\mu$ M. All compounds were obtained from Tocris unless otherwise noted. A stock of 4NQO (Sigma) was stored at 175 mM concentration in acetone. Embryos were exposed to 42  $\mu$ M 4NQO in 0.1X MMR for the stages indicated.

### ***Voltage and sodium dye imaging***

Transmembrane potential (Figure 4.5E) was imaged as previously described [19, 31, 415]. For sodium imaging, a stock of CoroNa green (Invitrogen) was stored at 5 mM concentration in DMSO. Embryos were incubated for 1 hr in 100  $\mu$ M of CoroNa Green in 0.1x MMR. Embryos were washed with fresh 0.1x MMR and directly visualized using a FITC filter set of a fluorescent microscope.

### ***Predictive screening***

*Gli1* injected *Xenopus* embryos were collected at the neurula stage (st. 15), before ITLSs are morphologically and histologically apparent. Collected embryos were imaged using CoroNa green (as described above), and divided into two categories based on the presence of group of cells with high Na<sup>+</sup> content. The effectiveness of unique Na<sup>+</sup> content in predicting ITLS formation was quantified by calculating: false positives (how many of the embryos exhibited increased Na<sup>+</sup> foci but never developed ITLSs), false negatives (how many did our technique miss), sensitivity (how many of the ITLS were preceded by unique Na<sup>+</sup> content), and specificity values (how many of the non-ITLS forming cells were not preceded by unique Na<sup>+</sup> content).

### ***Electroporation***

The method used is described in detail in [416]. Here, poring and driving pulse parameter values of volt (v) = 35/7; length (ms) = 50/50; interval (ms) = 50/50; and repeat count = 3/10 were used.

## **Results**

### ***Depolarization-induced metastasis-like conversion of melanocytes***

In order to better understand the neoplastic-like phenotype induced by changes in the transmembrane potential ( $V_{mem}$ ) *in vivo*, we took advantage of the glycine gated chloride (GlyCl) channel, specifically expressed in a sparse yet widely distributed cell population, whose  $V_{mem}$  can be specifically modulated by pharmacologically opening the channel and then altering the extracellular chloride levels (Figure 4.1A). To open these GlyCl channels, we utilized

ivermectin, a well-characterized antiparasitic that is known to specifically affect GlyCl channels [31, 32]. In unperturbed *Xenopus laevis* embryos, the extracellular medium contains a lower chloride concentration than inside the cell. Thus, treatment of *Xenopus* embryos with 1  $\mu$ M ivermectin depolarizes cells expressing the GlyCl channel (because negative chloride ions leave those cells down their concentration gradient). We first confirmed the remarkable hyperpigmentation phenotype in almost all treated individuals, resulting from a change of normal melanocyte behavior in three ways characteristic of cancerous transformation: an increase in proliferation, a change in their morphology (extensive arborization), and an extensive colonization of ectopic regions including blood vessels and neural tissues (Figure 4.1B-E). This effect is quite specific and the embryos appear to have no abnormalities of morphogenesis in any of the major organ systems or overall axial development. Furthermore, this effect is non-cell autonomous, the GlyCl-expressing instructor cells are being depolarized, whereas melanocyte behavior is being affected. However, the strong melanocyte phenotype suggests the possibility that other cell types are affected but not easily detected if they lack pigment. We specifically asked whether another important aspect of cancer – vascularization – might also be affected.

***Depolarization of instructor cells causes dysregulation of vascular patterning***

Transgenic frog embryos (Figure 4.2A-B) whose endothelial cells are labeled with fluorescent protein using the flk-1 promoter [414] were exposed to 1  $\mu$ M ivermectin from gastrulation to organogenesis (stages 10-46), and the blood vessel-specific fluorescence was imaged and compared to control embryos of

the same stage. In untreated embryos, the intersomitic vessels extending between the major tail veins resemble evenly-spaced rungs on a ladder (Figure 4.2C,C'). However, embryos whose GlyCl-expressing cells had been depolarized by ivermectin treatment (electrophysiology shown in [31]) displayed disorganized intersomitic vessels (Figure 4.2D). This phenotype was marked by a decrease in the overall number of vessels (Figure 4.2G) as well as an increase in vessels that displayed aberrant morphologies (branching, tilting, and truncations; Figure 4.2D). An increase in amount of small, blind-end vessels extending from the posterior cardinal vein on the tail was also observed in embryos whose instructor cells had been depolarized (Figure 4.2D',H). To determine whether there was an overall increase in endothelial precursors of blood vessels in the tail tip of the tadpoles, the numbers of GFP-positive cells in 200  $\mu\text{m}$  square regions were counted. While ivermectin treatment did not affect the number of vascular cells present (Figure 4.2I), the vascular cells did appear more arborized and larger following depolarization (compare Figure 4.2E-F). We conclude that the instructor cells regulate not only the behavior of melanocytes, but also the morphogenesis of the vasculature.

### ***Depolarization of Very Few Instructor Cells is Sufficient to Transform Melanocytes***

Hyperpigmentation is an all-or-none effect: if affected, the whole tadpole becomes colonized and all of the melanocytes abandon their normal round appearance in favor of a highly arborized morphology. Interestingly, prior work showed that it is not necessary to depolarize all of the instructor cells to induce the hyperpigmentation phenotype: it is sufficient to misexpress depolarizing channels in parts of the embryo [405]. Hyperpigmentation is initiated by global

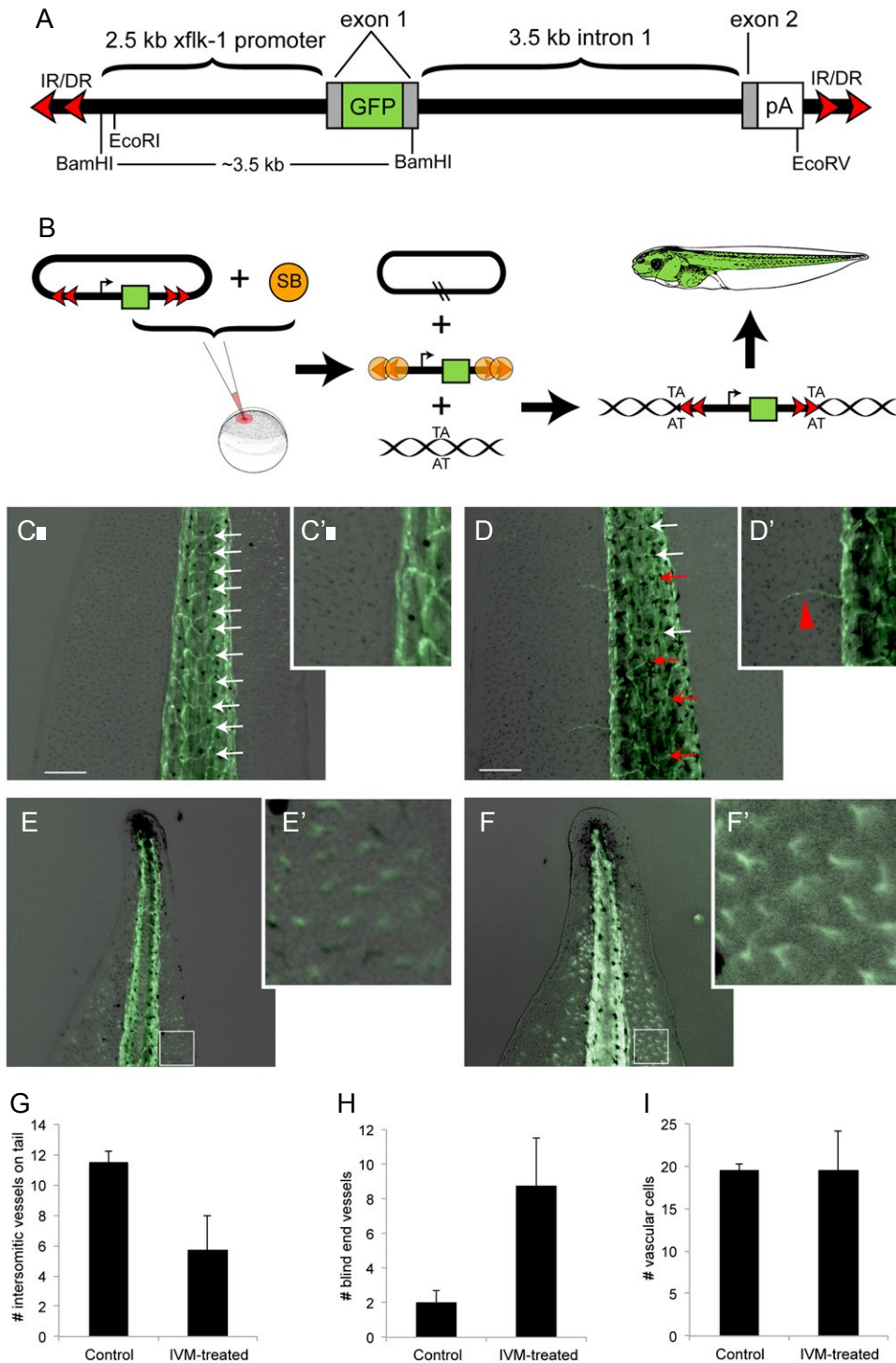


**Figure 4.2 GlyCl-mediated depolarization induces abnormal vascular structure *in vivo*.**

(A) Schematic of the pT2xflk-1:GFP transposon gene, adapted from [414] and not drawn to scale. The green fluorescent protein (GFP) on exon 1 is driven by a flk-1 promoter 2.5 kb upstream. A polyadenylation signal (pA) was cloned to maintain the integrity of the splice acceptor. The xflk-1:GFP construct was cloned

into the pT2 non-autonomous transposon between the invert-direct repeats (IR/DR). (B) Mechanism of SB-mediated transposition. The pT2flk-1:GFP was injected together with *Sleeping Beauty* (SB) transposase mRNA into fertilized eggs at the one-cell stage. SB transposase binds to the IR/DRs as shown and cuts the transposon (containing the flk-1 promoter driving GFP expression) out of the plasmid (the cut sites are indicated by the two black slashed lines in the remaining plasmid). A DNA molecule with a 'TA' sequence becomes the recipient of a transposed transposon; transgenic animals bearing this fluorescent marker of vasculature were used in experiments where instructor cells were depolarized with ivermectin. (C, C') In untreated pT2flk-1:GFP *Xenopus laevis* transgenic tadpoles, the intersomitic vessels on the tail are evenly spaced (white arrows) and tail regions largely lack blind end vessels. (D, D') Ivermectin-treated embryos display an overall decrease the number of intersomitic vessels (G), as well as an increase in disrupted intersomitic vessels (red arrows), and an increase in the amount of small blind-end vessels extending into the tail fin region (H). To determine whether there was an increase in vascular cells in the tail tip between control and ivermectin-treated embryos (E,F), the number of GFP-positive cells in a 200  $\mu\text{m}$  square region (white boxes) was counted. While there is no difference in the number of vascular cells in the tail tip between treatments (I), the shape of the vascular cells in ivermectin-treated embryos (F') compared to controls (E') reveals an increase in arborization. Scale bars, 250  $\mu\text{m}$ .

depolarization of a very sparse but widespread cell population, but what is not known is the size of the minimal signaling unit: how small an area can be depolarized, and how far from the dorsal neural tube (the site of the melanocyte precursors) can it be, in order to activate the transformation of all (or most) of the melanocytes in the embryo?

We selectively depolarized cell groups of differing size and location to determine which can produce the hyperpigmented phenotype. In order to do so, we took advantage of a mutant GlyCl-channel (GlyCl-A288G) that has increased sensitivity to ivermectin. GlyCl channels normally have a threshold of activation of roughly 100 – 300 nM for ivermectin [217]. However, the introduction of the A288G mutation increases ivermectin sensitivity almost 100-fold [412]. Thus, through microinjection of the GlyCl-A288G mutant mRNA into *Xenopus* embryos followed by exposure to doses of ivermectin too low to activate native GlyCl receptors, we were able to systematically depolarize only those cells expressing the injected super-sensitive mutant, and not endogenous GlyCl-expressing cells (Figure 4.3A).

Synthetic mRNA encoding the GlyCl-A288G mutant fused to a tdTomato fluorescent tag (tom) was injected into *Xenopus* embryo blastomeres at the 32-cell stage (allowing for the targeting of progressively smaller regions of the developing embryo) as schematized in Figure 4.3B. These embryos were then treated 0.05  $\mu$ M ivermectin. At this concentration, ivermectin does not affect endogenous GlyCl channels (confirmed by lack of hyperpigmented effect in uninjected tadpoles treated with this low ivermectin dose); however, we observed hyperpigmentation when embryos were pre-injected with the GlyCl-A288G-tom mutant and then exposed to the lower ivermectin level. Embryos were reared to

stage 22, at which point they were sorted for tdTomato expression (Figure 3C) to determine which regions had been affected by the depolarizing treatment, and allowed to develop to tadpole stage (stage 45), at which point they were scored for hyperpigmentation.

By correlating the degree of hyperpigmentation with the location and size of the region rendered sensitive to low ivermectin-induced depolarization, we performed a survey of the spatial limits of the depolarization → hyperpigmentation effect. tdTomato expression in hyperpigmented tadpoles was highly variable. However, even very small depolarized regions at the very posterior of the tadpole were able to produce embryo-wide hyperpigmentation (Figure 4.3D-F). Depolarization of small regions of GlyR-A288G-tom injected cells produced hyperpigmentation in 48.3% (N=267) of embryos treated with low dose of ivermectin. Thus, depolarization-induced hyperpigmentation of large and distant body regions only requires a small number of instructor cells to be depolarized.

### ***Monoamine vesicle transporter regulates transformation-relevant serotonin levels***

Depolarization functions non-cell-autonomously to affect melanocyte behavior. The long-range signal is mediated by serotonin [31]. Serotonin is an important signaling molecule that participates in a wide range of physiological systems. Increasing evidence also indicates that serotonin plays a developmental role before it becomes a neurotransmitter, affecting craniofacial, gastrointestinal, and cardiovascular morphogenesis [60, 417-419]. Our prior work showed that regulation of serotonin levels by the voltage-regulated serotonin transporter SERT is essential for the transduction of  $V_{mem}$  changes into changes in cell

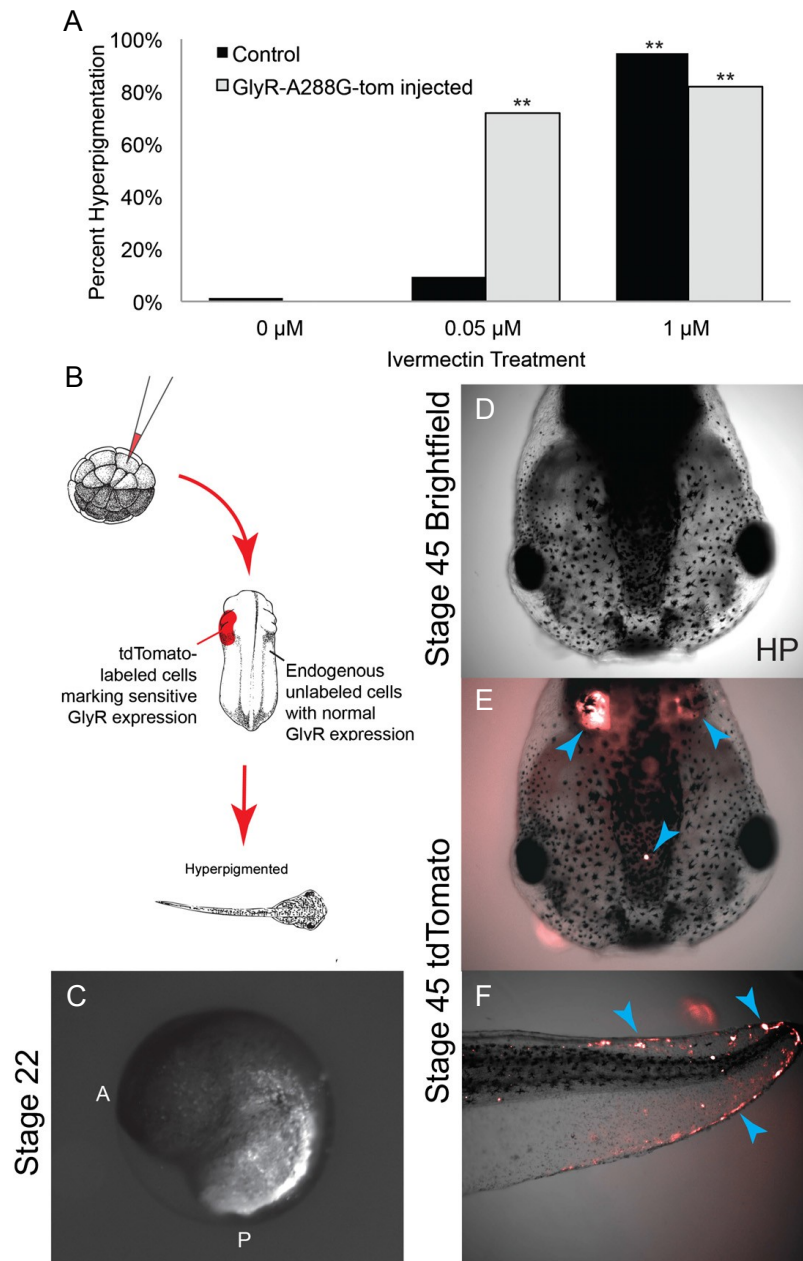


**Figure 4.3. Hyperpigmentation requires the depolarization of only a small number of instructor cells.**

(A) Embryos that had been injected at the 1-cell stage with GlyCI-A288G-tom, a GlyCI channel with increased sensitivity to ivermectin fused to a tdTomato fluorescent label, were treated with 0.05  $\mu\text{M}$  ivermectin. This resulted in significant rates of hyperpigmentation, while uninjected control embryos had no phenotype, demonstrating that this level of ivermectin does not trigger native GlyCI in instructor cells. (B) Injections of GlyCI-A288G-tom were done into a randomly chosen 1 cell of stage 6 *Xenopus* embryos. Embryos were then treated with 0.05  $\mu\text{M}$  ivermectin, sorted at stage 22 for discrete tdTomato signal localization (C), then reared to stage 45 and scored for hyperpigmentation. (D-F) Analysis of stage 45 hyperpigmented tadpoles reveals that only a small number of GlyCI-A288G-tom-expressing cells (blue arrows) are necessary to induce hyperpigmentation.

behavior observed during hyperpigmentation [31]. One model (Figure 4.1F) is that when the membrane of instructor cells is depolarized, SERT not only fails to clear the extracellular space of excess serotonin, but exports additional serotonin [266, 267]. The excess serotonin level surrounding the developing melanocytes induces their neoplastic-like behavior [31].

We next sought to determine whether intracellular stores of serotonin were also involved in the depolarization-induced hyperpigmentation. The vesicular monoamine transporter (VMAT) is responsible for the translocation of monoamines (including serotonin) from the cytoplasm into storage vesicles [420]. As part of a suppression screen [47, 346], we applied a VMAT antagonist together with ivermectin treatment to determine whether VMAT function was required for depolarization to be effectively transduced into changes in melanocyte behavior. Treatment with the VMAT blocker, reserpine, reduced ivermectin-induced hyperpigmentation significantly (Table 4.2), without other apparent effects on overall patterning or embryo health. It is likely that the intracellular packaging of serotonin in GlyCI-expressing cells is important, as it is in synapses, for cooperating with SERT to regulate tissue serotonin levels needed to activate melanocytes

### ***A model of serotonin receptors for signal transduction during hyperpigmentation***

The levels of serotonin are regulated by SERT and VMAT, but its activation of melanocytes must be transduced by a receptor. Thus, we next sought to deduce which serotonin receptor is required for the depolarization of instructor cells to be effectively transduced into changes in melanocyte behavior. Extracellular serotonin receptors can be divided into 7 classes based on their pharmacological

**Table 4.2. Hyperpigmentation involves VMAT function.**

Embryos were exposed to either 1  $\mu$ M ivermectin, 100  $\mu$ M reserpine (a VMAT antagonist), or a combination of both agents from stage 10 to 46 (from gastrulation to organogenesis). Ivermectin exposure alone resulted in a high incidence of hyperpigmentation, not seen in control embryos. Concurrent exposure to ivermectin and reserpine significantly reduced the rate of ivermectin-induced hyperpigmentation. \*  $p < 0.01$  compared to ivermectin treatment alone, students t-test.

	Control	Ivermectin	Reserpine	Ivermectin + Reserpine
Normally-pigmented tadpoles	124	5	46	16
Hyperpigmented tadpoles	1	97	0	54
% hyperpigmented	0.8%	95.1%	0%	77.1%*
<i>N</i>	125	102	46	70

**Table 4.3. Blocking multiple 5-HT receptors induces hyperpigmentation, but inhibits depolarization-induced hyperpigmentation.**

Embryos were exposed to either 1  $\mu$ M ivermectin, 10 nM methiothepin (antagonist to serotonin receptors 1, 2,5,6 and 7), or a combination of both agents from stage 10 to 46 (from gastrulation to organogenesis). Ivermectin exposure alone resulted in a high incidence of hyperpigmentation, not seen in control embryos. Exposure to methiothepin significantly reduced ivermectin-induced hyperpigmentation, but was also able to induce hyperpigmentation on its own. \*  $p < 0.01$  compared to ivermectin treatment alone, #  $p < 0.01$  compared to control, students t-test.

	Control	Ivermectin	Methiothepin	Ivermectin + Methiothepin
Normally-pigmented tadpoles	331	7	67	27
Hyperpigmented tadpoles	8	151	129	78
% hyperpigmented	2.4%	95.6%	65.8%#	74.3%*
<i>N</i>	339	158	196	105

profiles, primary sequences, and signal transduction mechanisms; with the exception of 5-HT<sub>3</sub>, a ligand-gated ion channel, all other 5HT receptors are G-coupled protein receptors that activate intracellular second messenger cascades [421]. Using the same suppression screen strategy that implicated both SERT and VMAT, individual inhibitors of serotonin receptors were used together with ivermectin treatment to investigate whether receptor inhibition could suppress the depolarization-induced hyperpigmentation.

We began the screen with the broad-spectrum receptor antagonist, methiothepin, which blocks 5-HT receptor types 1, 2, 5, 6, and 7 [422]. Treatment with methiothepin was successful in significantly reducing hyperpigmentation rates when embryos were exposed to both this serotonin antagonist alongside depolarizing ivermectin (Table 4.3). However, surprisingly, treating embryos with this receptor antagonist alone (i.e. without ivermectin) resulted in hyperpigmentation in 65.8% of embryos! The ability of a receptor blocker to suppress the transformation phenotype when it is being induced by depolarization, but also to induce it on a wild-type background animal suggested the involvement of multiple serotonin receptors that antagonized each other's activity. We thus went on to test the involvement of each serotonin receptor subtype by targeting them individually using receptor specific antagonists. Treatment with blockers of receptors 3, 4, 5, 6, or 7 (10  $\mu$ M tropisetron, 1  $\mu$ M GR 113808, 2.5  $\mu$ M SB 699551, 50  $\mu$ M Ro 04-6790, and 50  $\mu$ M SB 258719 respectively) did not result in any reduction in ivermectin-induced hyperpigmentation (Table 4.4). However, exposure to both 5-HT receptor 1 and receptor 2 antagonists (50  $\mu$ M Cyanopridolol and 10  $\mu$ M Altanserin, respectively) significantly reduced hyperpigmentation in embryos also treated with ivermectin.

**Table 4.4. Rescue of hyperpigmentation reveals involvement of 5-HT receptors 1, 2, and 5.**

Embryos were exposed to either 1  $\mu$ M ivermectin concurrent with a selective serotonin (5-HT) receptor antagonist, or a serotonin receptor antagonist alone from stage 10 to 46 (from gastrulation to organogenesis). Ivermectin exposure alone resulted in a high incidence of hyperpigmentation (HP), not seen in control embryos. Exposure to tropisetron, GR113808, Ro 04-6790, or SB 258719 did not inhibit hyperpigmentation or induce hyperpigmentation. However, exposure to either cyanopridolol or altanserine effectively reduced ivermectin-induced hyperpigmentation, while treatment of SB699551 was able to hyperpigment on its own. \*  $p < 0.01$  compared to ivermectin treatment alone, #  $p < 0.01$  compared to control, students t-test.

<b>5-HT Receptor Blocked</b>	<b>Control</b>	<b>R1</b>	<b>R2</b>	<b>R3</b>	<b>R4</b>	<b>R5</b>	<b>R6</b>	<b>R7</b>
Antagonist	None	Cyano- pridolol	Altan- serin	Trop- isetron	GR 113808	SB 699551	Ro 04- 6790	SB 258719
% HP w/ ivermectin	95.6%	83.6%*	70.9%*	96.2%	96.6%	92.0%	92.6%	93.8%
% HP w/o ivermectin treatment	2.4%	5.9%	3.5%	1.4%	0%	30.4%#	0%	0%

Treatments of receptor antagonists without ivermectin revealed that blocking 5-HTR-5 and blocking 5-HTR-1 led to significant levels of hyperpigmentation (30.4% with 2.5  $\mu$ M SB 699551, and 22% with 10  $\mu$ M cyanopridolol). Taken together, these data presented a complex serotonergic signal transduction network operating between changes in  $V_{mem}$  and hyperpigmentation.

The results of the suppression screen revealed that blocking serotonin receptors could both suppress depolarization-induced hyperpigmentation, and hyperpigment on its own. Even more puzzling was the stochastic nature of the all-or-none phenotype; some individuals in the treated population would become hyperpigmented, and some would not, but none exhibited a partial phenotype: the whole body behaves as a “unit” with respect to melanocyte behavior, but the decision whether to express the transformed melanocyte phenotype is variable among the identically-treated population. In order to formulate a model that quantitatively predicts and explains this complex counter-intuitive dataset, we undertook a computational approach. The specific details of the method will be published in a subsequent manuscript highlighting the application of network searches to difficult problems in developmental signaling. We began with a network of possible functional relationships between serotonin and its receptors (Supplement 4.1), and constrained it using known data on the interplay between antagonistic serotonin receptors in mammary cell development [423, 424]. Using simulated annealing to find connectivity values that correctly predict the results of all of our experiments, we arrived at a model consistent with our data (Figure 4.4). It explains the observation that using an antagonist to multiple serotonin receptors can suppress hyperpigmentation when used with ivermectin treatment, yet, induce hyperpigmentation even when instructor cells are not depolarized. In

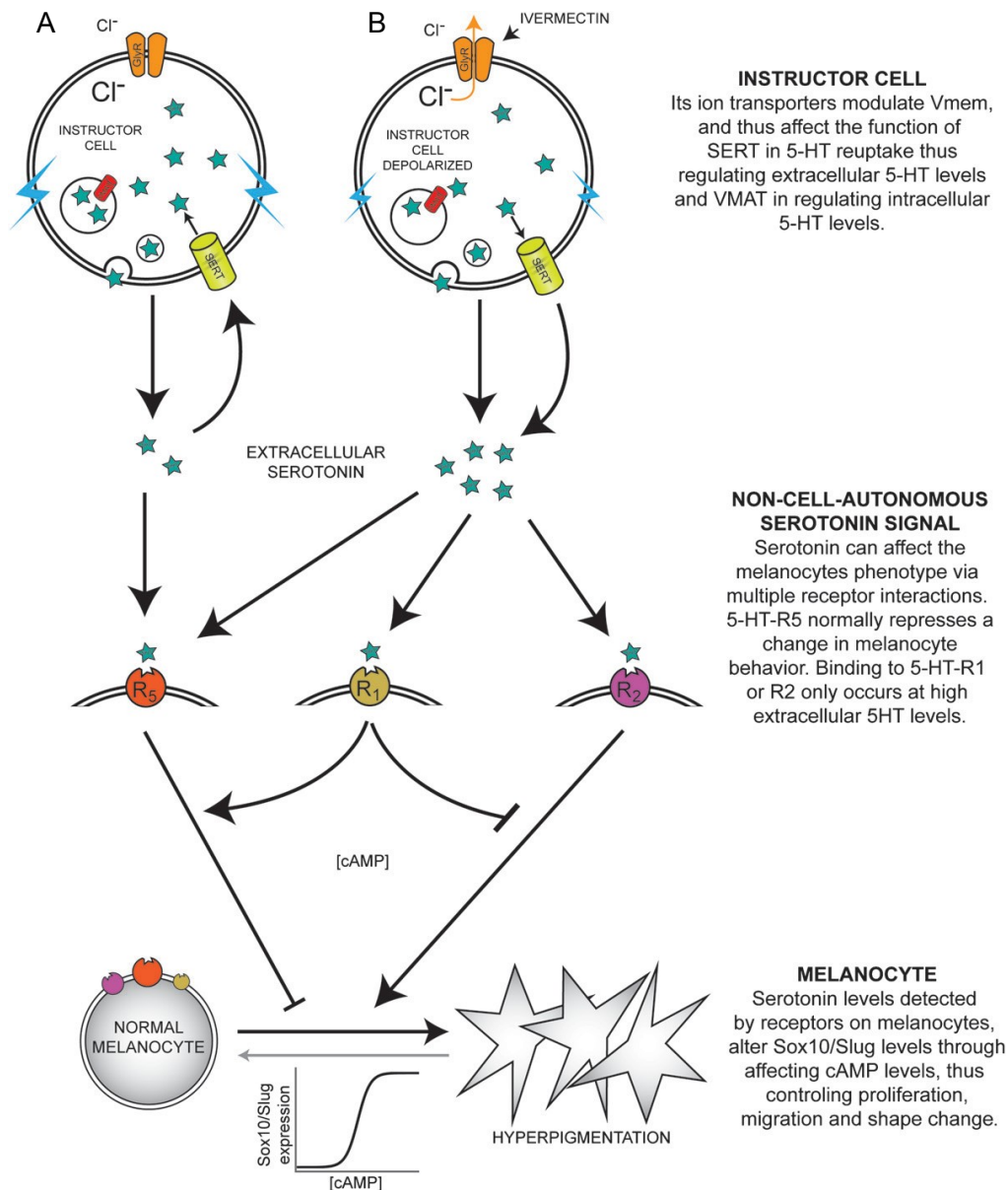


**Figure 4.4. A model of melanocyte control by serotonergic signaling downstream of voltage change.**

(A) In unperturbed embryos, ion transporters keep the plasma membrane in a state where it is able to power the reuptake of extracellular 5-HT through its transporter, SERT, and regulate intracellular 5-HT levels with VMAT. With normal extracellular 5-HT levels, binding to 5-HT-R5 maintains normal melanocyte behavior by regulating cAMP levels, which in turn maintain low Sox10 and Slug levels and suppress melanocyte transformation. (B) When the instructor cell population is depolarized, VMAT no longer functions properly to sequester serotonin inside vesicles, and SERT runs backwards, exporting additional 5-HT into the microenvironment of the melanocytes. At high extracellular 5-HT levels, 5-HT activates 5HT-R1 and 5HT-R2. Binding to 5-HT-R2 induces the transformation of melanocytes. R1-binding (which induces hyperpigmentation) functions to partially suppress the effects of R2-binding, and increase the effects of R5-binding through the regulation of intracellular cAMP levels.

the endogenous case, when instructor cells are not depolarized, extracellular serotonin levels remain low. Under these conditions, blocking multiple receptors also blocks the serotonin receptor that normally maintains correct melanocyte morphology (receptor 5 – a suppressor of transformation), inducing hyperpigmentation in a significant proportion of treated embryos. Following instructor cell depolarization, excess serotonin is expelled into the milieu of the developing melanocytes, resulting in binding to receptors that are not normally activated (receptors 1 and 2). Binding to receptors 1 and 2 overcomes baseline inhibitory activity of receptor 5. Thus, blocking receptors 1 and 2 with a broad serotonin receptor antagonist can decrease hyperpigmentation rates, but not completely, since it is also blocking the serotonin receptor involved in maintaining melanocyte behavior. The multiple competing levels of inhibition and activation among elements in this model and the sigmoidal response curve of the transforming transcription factors Slug and Sox10 [405] to the cAMP output of the serotonin receptor account for the pharmacology data and the bi-modal behavior of the output (all-or-none character of the hyperpigmentation phenotype); this scheme makes a number of specific, quantitative predictions that can be tested to refine the model in subsequent investigations

### ***Global voltage change during chemically-induced tumorigenesis***

Our previous data focused on metastatic-like phenotypes induced by voltage change in the absence of chemical or genetic insult. We next sought to characterize the voltage changes that may function during the processes initiated by traditional carcinogens. Exposure to 42  $\mu$ M 4-nitroquinolin-1-oxide (4NQO), a known carcinogen [425-428], induced global hyperpigmentation (Figure 4.5A,B), consistent with the above-described effects of depolarization (Figure 4.1B').

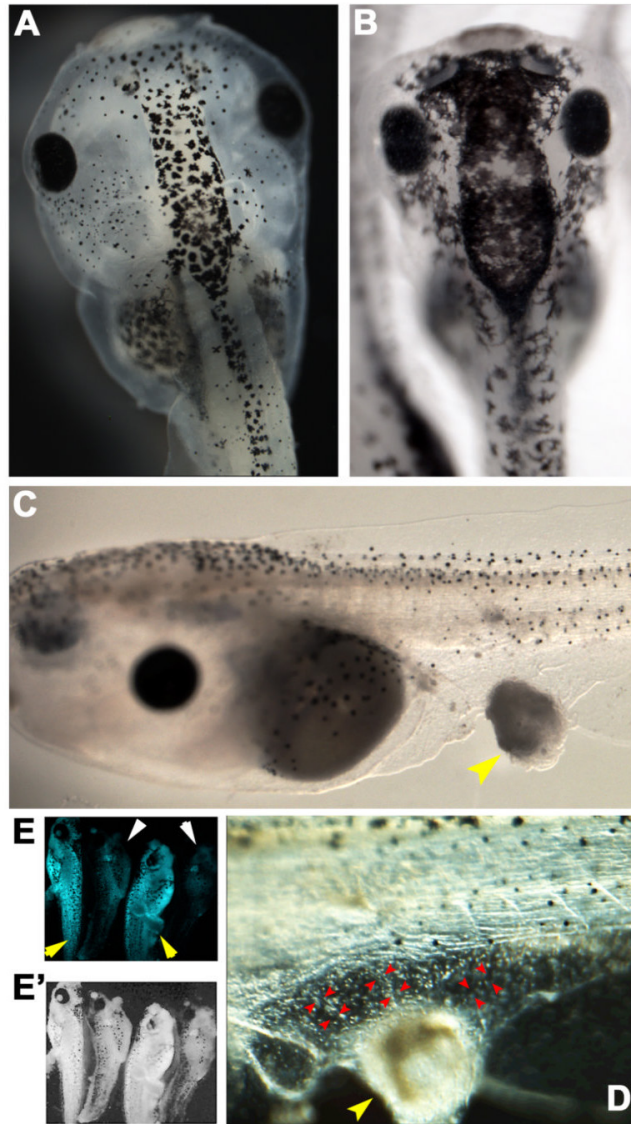


**Figure 4.5. Exposure to carcinogen 4NQO induces hyperpigmentation, embryo-wide depolarization, and tumor-like structures.** (A) Unperturbed stage 45 embryo showing normal pigmentation in the dorsoanterior region. (B) Stage 45 embryos treated with 42  $\mu\text{M}$  4NQO for 24 hours exhibited the hyperpigmentation. Following exposure, hyperproliferative melanocytes migrated and colonized regions that are normally devoid of melanocytes. (C) A stage 47 embryo with a typical induced tumor-like structure (ITLS, yellow arrowhead). To generate this phenotype, embryos were treated with 42  $\mu\text{M}$  4NQO for 24 hours; ITLSs were observed 48 hours post termination of 4NQO treatment. (D) A stage 48 embryo showing vascularization (red arrowheads) of an ITLS (yellow arrowhead). See Supplement 2 for a movie of the blood flow that more clearly reveals the attraction of vasculature by this tumor-like structure. (E) Imaging with DiBAC<sub>4</sub>(3) (a fluorescent  $V_{\text{mem}}$  reporter) using fluorescent confocal microscopy as previously described [415] reveals that 53.3% of hyperpigmented embryos ( $n=21$ ) are relatively depolarized (the panel shows 4 embryos, side by side, as shown by white ring-light view of the same 4 embryos in panel E').

Unlike the instructor-cell depolarization, this also caused discrete tumor-like structures (ITLSs) to be formed (Figure 4.5C, yellow arrowhead), which also attracted vasculature (Figure 4.5D, red arrowheads, Supplement 4.2). We specifically examined transmembrane potential in the exposed tadpoles using voltage-sensitive fluorescent reporter dye, DiBAC<sub>4</sub>(3) [24, 415]. We observed an embryo-wide depolarization, but only in approximately half of the treated tadpoles (Figure 4.5E,E'). We conclude that exposure to carcinogens affects the bioelectrical state of many more cells than those in the resulting tumor; however, this effect is highly variable among a population of individuals.

### ***Sodium content reveals tumors***

It has long been noted that tumor cells can be distinguished from normal cells by their aberrant transmembrane potential [343, 429]. However, a number of normal patterning events are also driven by localized depolarizations [24, 52, 372]; thus, non-invasive detection of incipient tumors will depend on the discovery of additional biophysical criteria that would allow the defining of a narrower physiological signature by which to distinguish prospective cancer sites from normal.

*Gli1* mRNA, encoding a known human oncogene [409, 430], was injected into one blastomere of *Xenopus* embryos at the 2-cell stage. Embryos were then raised to early tadpole stages (stage 35), at which point induced tumor-like structures (ITLSs) were clearly visible (Figure 6A). We then imaged these *Gli1*-induced tumors with the sodium reporter dye CoroNa Green, which revealed that such tumors are indeed enriched for sodium (Figure 4.6A'-A"). To determine whether elevated sodium levels could be a predictor of future tumor development, we imaged neurula-stage (stage 15) embryos with CoroNa Green.

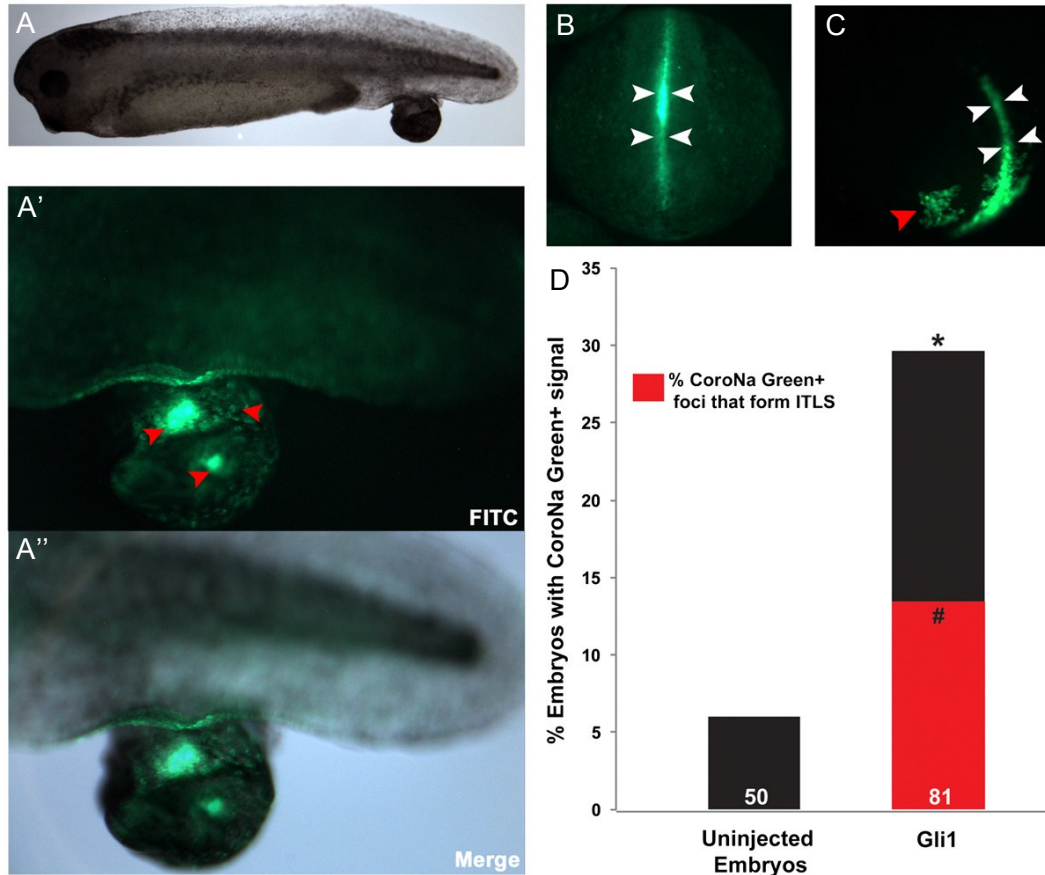


**Figure 4.6. Overexpression of *Gli1* results in ITLSs with unique  $\text{Na}^+$  signature**

(A) A stage 35 embryo showing *Gli1* ITLS on its tail. To generate this phenotype, embryos were injected with 2ng of *Gli1* mRNA into 1 of 2 cell stage embryos. Injected embryos were raised to stage 35 and were imaged using bright-field microscopy. (A') Imaging using CoroNa green (fluorescent  $\text{Na}^+$  content reporter) reveals that tumor cells have relatively higher (but heterogeneous)  $\text{Na}^+$  content as compared with healthy surrounding tissue. (A'') Overlay of bright field and FITC (CoroNa green) images showing co-localization of ITLS and unique  $\text{Na}^+$  fluorescent signal, confirming that foci of ITLS and unique  $\text{Na}^+$  signature are identical. (B) An unperturbed stage 15 embryo showing the normal  $\text{Na}^+$  content along the neural tube (white arrowheads). (C) At stage 15, when there is no histological and morphological signs of ITLS, *Gli1*-injected embryos exhibit foci with unique  $\text{Na}^+$  content (red arrowheads) as well as the normal  $\text{Na}^+$  signal within the neural tube (white arrowheads). (D) At stage 15, unique  $\text{Na}^+$  content foci were present in 29.6% (black bar) of *Gli1* injected embryos (n=81), 45.8% of which (red bar) formed morphologically apparent ITLSs by stage 35. In unperturbed embryos, unique  $\text{Na}^+$  content foci were observed in only 6% (black bar) of all treatments (n=50), and no ITLS formation was observed. #p<0.001; \*p<0.001;  $\chi^2$  test compared to uninjected embryos.

At this stage, there were no histological or morphological signs of incipient tumors; however, *Gli1*-injected embryos exhibited foci with unique sodium content (compare Figure 4.6B-C). Out of the ~30% of *Gli1*-injected embryos displaying CoroNa foci (N=81), 46% (sensitivity value) formed morphologically apparent ITLSs by stage 35 (Figure 4.6D). Other predictive parameters tested include: specificity (82%), false positive (44%), and false negative (18%). Together, data collected suggest that unique bioelectric sodium signal is indicative of prospective tumor formation.

### ***Forced hyperpolarization reduces tumor incidence***

If transmembrane potential is a causal factor in tumorigenesis, as it is in metastatic transformation of melanocytes, then artificial hyperpolarization of cells ought to reduce the incidence of tumorigenesis. We used two canonical oncogenes that induce tumors (rhabdomyosarcoma, lymphoma, and various solid cancers) in *Xenopus*, *Xrel3* [410] and *KRASG12D* [408]. Electroporation of either mRNA consistently induced tumor-like structures (ITLSs) in ~45% of electroporated embryos (Figure 4.7A-C). Remarkably, pre-injection of the embryos with mRNA encoding a hyperpolarizing Kir4.1 channel (previously characterized and shown to persist in the animal for days and hyperpolarize cells [24, 431]) significantly reduced the percentage of embryos that develop tumors (by roughly 25% and 75% in *Xrel3* and *KRAS12D*, respectively; Figure 4.7D). We conclude that depolarized transmembrane potential is a causative factor in tumor induction by two canonical oncogenes, and that this signal can be counteracted by hyperpolarizing ion flows.

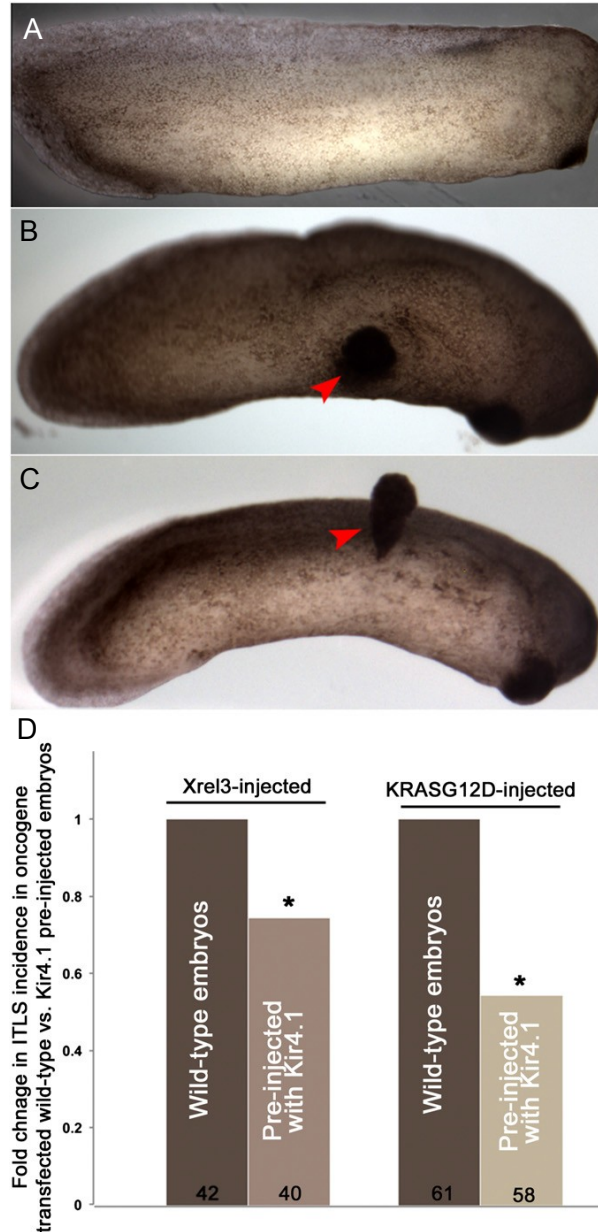


**Figure 4.7. Oncogene-induced ITLSs can be suppressed by prior injection of hyperpolarizing channel mRNA**

(A) An unperturbed (control) stage 29 embryo showing normal development. (B) Embryos that are electroporated with Xrel3 DNA at stage 10 exhibit ITLSs by stage 29 (red arrowhead). (C) Embryos that are electroporated with KRASG12D DNA at stage 10 exhibit ITLSs by stage 30 (red arrowhead). (D) Xrel3 and KRASG12D ITLS formation can be partially blocked by forced pre-hyperpolarization via molecular expression of *Kir4.1* (a hyperpolarizing channel). Injection of *Kir4.1* mRNA at the one-cell stage followed by electroporating with oncogene DNA at stage 10 results in 25.8% fewer embryos with ITLSs compared with Xrel3 electroporation on a wild-type background and 46% fewer embryos with ITLSs compared with KRASG12D electroporation on a wild-type background. \* $p < 0.05$  One-sample t-test to a normalized ITLS incidence (set to 1) in Xrel3 or KRASG12D electroporated embryos.

### ***Hyperpolarization without gene therapy***

If hyperpolarization is to become a viable treatment modality to reduce tumor incidence, it will be beneficial to avoid the need for introduction of transgenes, as biomedical gene therapy involves a number of safety and efficacy hurdles. Following the same strategy we used to regulate voltage levels to induce organ regeneration without introduction of transgenes [63], we sought to use pharmacological reagents to capitalize on ion channels already natively expressed in the relevant tissues. Overexpression of *Xrel1* using mRNA injections directed into 1 blastomere of 2-cell embryos results in ITLSs in 65% of embryos. Raising the extracellular chloride level of the tadpoles' medium, thus hyperpolarizing via chloride channels, significantly reduced the incidence of tumors in embryos that had been pre-injected with *Xrel3* (Figure 4.8), suggesting the presence of an endogenous depolarizing chloride channel that contributes to tumorigenesis. Consistently with this, application of indanyloxy acetic acid (IAA), a potent pharmacological blocker of chloride channels, abolished the high-chloride inhibition of tumorigenesis. We conclude that endogenous chloride channels contribute to the voltage regulation that mediates oncogene-induced tumor formation, and these channels represent a potentially convenient target for modulation of this process.

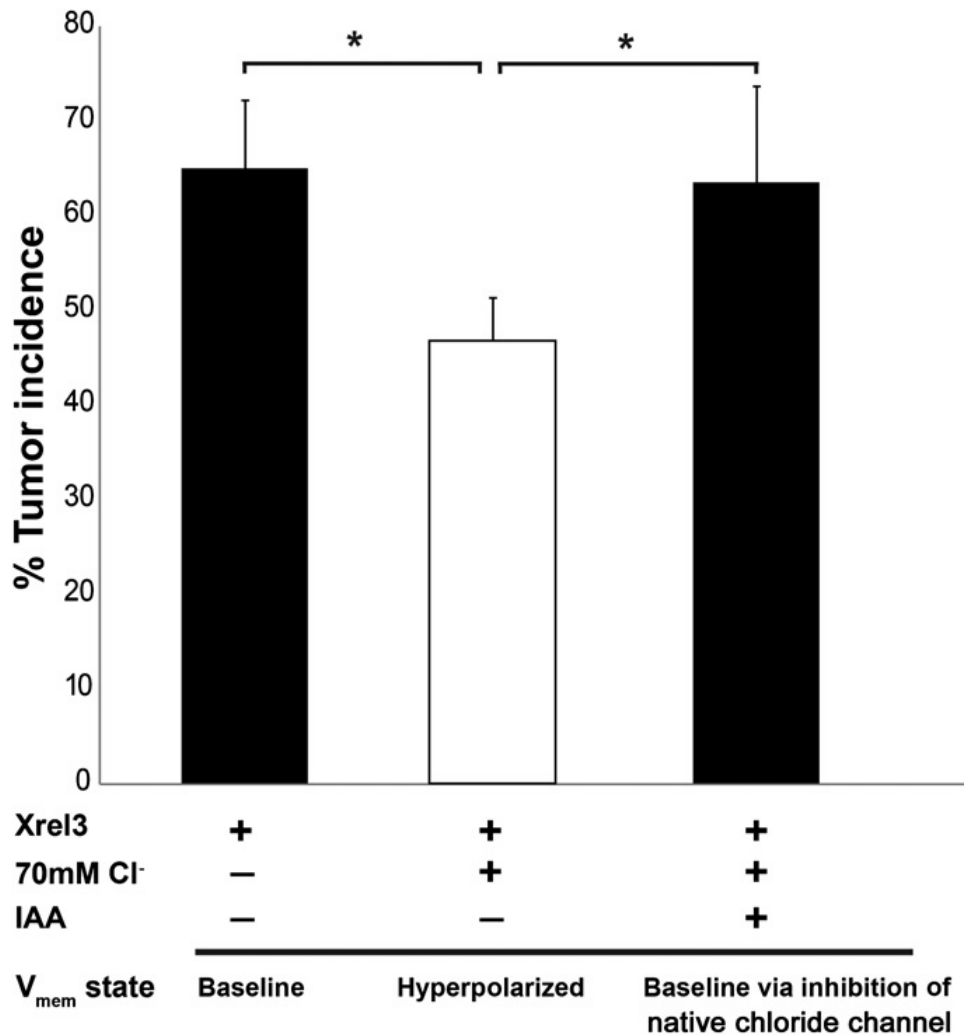


**Figure 4.8. Pharmacological targeting of endogenous Cl<sup>-</sup> channels suppresses *Xre/3* ITLSs.**

Overexpression of *Xre/3* in 1 of 2 cell stage embryos results in ITLSs in 65% of the embryos. When *Xre/3*-injected embryos are exposed to a medium containing high chloride levels (70 mM), ITLS incidence is reduced to 46.8%, suggesting the presence of a native chloride channel that would mediate the hyperpolarization by influx of Cl<sup>-</sup> ions. The ITLS suppression effect can be blocked by pharmacological blockade of Cl<sup>-</sup> channels – exposure to indanyloxy acetic acid (IAA) along with the high chloride results in the baseline ITLS incidence of 63.5%, similar to that of *Xre/3* only treatment. \*p<0.01; One-way ANOVA; Bonferroni post hoc.

## Discussion

### ***Cancer in an in vivo model: developmental dysregulation***

The *Xenopus* tadpole is an ideal model for understanding the interplay between normal developmental cues and the defects of morphostasis that manifest as cancer. Its amenability to physiology, molecular genetics, cell biology, and pharmacology techniques allowed us to investigate two very different aspects of malignancy. The first was a widespread metastatic conversion affecting many mature cells (melanocytes) throughout the body with no definable “tumor” at its source. Our data suggest that even in the absence of a primary tumor, the main properties of metastasis (overproliferation, cell shape change that facilitates invasion, and colonization of other organs and tissues) can be conferred upon a mature cell type. While originally the phenotype was discovered by its obvious effect on melanocytes, we found that vascular patterning was also affected (Figure 4.2), consistent with the well-known role of aberrant vasculogenesis as a hallmark of cancer. While tadpoles with depolarized instructor cells have no obvious anatomical defects, it is possible that other, even more subtle changes still remain undetected. Future studies in transgenic animals with other fluorescently-marked cell types, or detailed marker analysis in sections, may identify additional cell populations that are regulated by the instructor cells.

### ***Bioelectric aspects of the microenvironment – melanoma at a distance***

Resting potential across the plasma membrane is a crucial parameter regulating many aspects of cell behavior [22, 55, 350, 432]. Spatio-temporal changes in  $V_{\text{mem}}$  occur due to the opening and closing of existing ion translocators (post-translational regulation by physiological cues). These alterations of biophysical cell state (bioelectric signals) are thus a source of non-genetic information during

development and regeneration, and are now increasingly understood as an important factor in cancer. The signal from depolarized neighbors that confers metastatic-like behavior upon melanocytes is mediated by serotonin. This neurotransmitter has been shown to mediate bioelectric signals into transcriptional cascades in other aspects of developmental regulation [371, 433], and has been linked to carcinogenesis through studies of serotonergic drugs and activity of serotonin pathway enzymes in tumors [425, 434-439]. Interestingly, only a very small region of the embryo has to be depolarized for all of the melanocytes to become activated (Figure 4.3). Indeed, the minimal signaling unit is likely to be even somewhat smaller than revealed by the fluorescence in Figure 3E,F because not every targeted cell is going to be maximally depolarized.

While the few millimeter length of a tadpole is not considered very long distance on the size scale of human tumors, the ability of a few cells on the tail to influence all of the melanocytes in the animal's head region is a remarkably long-range developmental signal. Serotonin is difficult to image *in vivo* because any tag placed on could significantly change its size and thus diffusion/transport dynamics; the development of novel techniques that would allow molecular tracking of serotonin movement in living embryos represents an important area for future work, since dissecting the dynamics of cross-body transfer of this important signaling molecule is likely to shed light on both developmental regulation and cancer. Interestingly, it is now known that transglutaminase is an important component of transformation-conferring microvesicles from cancer cells [426, 440]; transglutaminase is important for serotonin signaling [441-443], and future work will test the hypothesis that serotonin is involved in microvesicle-mediated passage of transformation among cells in biomedical settings.

The endpoint of the serotonergic signaling triggered by depolarization is a change in behavior of melanocytes towards metastatic melanoma. Because melanocytes are derivatives of the migratory neural crest, they have conserved significant neuronal characteristics, including production of neurotransmitters and expression of their functional receptors [444, 445]. Indeed, the skin of amphibians, rodents, and humans has been shown to contain endogenous serotonin receptors [446-448]. Human cutaneous melanocytes are also immunoreactive to serotonin [449] and express multiple serotonin receptor subtypes [444]. Taken together, melanocytes can be thought to act as the 'neurons of the skin' – a hypothesis that is quite similar to the “acquisition of excitability” that has been suggested as underlying the role of onco-fetal sodium channels in cancerous transformation [399, 450]. We hypothesize that the extension of abnormal long projections (Figure 4.1E vs. E') may be another indicator that melanocytes have assumed some nerve-like properties as part of this transformation, much as melanoma cells have been described to mimic vascular cells [97, 163, 186].

***Serotonin: transducing voltage change into cellular effectors***

In addition to its roles in development, serotonin also has well-established functions as a regulator of mitosis and tumor growth in adult human tissue. The ability of serotonin signaling to cause melanocytes to proliferate is consistent with its proposed role as an unconventional mitogen [261, 451-453], while the induced change of shape to a highly arborized appearance has been also observed in human melanocytes [31] and breast cells [425]. Our pharmacological data relied on well-characterized inhibitors to suggest VMAT as an important regulator of serotonin availability for export by instructor cells, as well as several receptor

proteins; future studies using gene-specific knockdown will be necessary to conclusively confirm the identity of the gene products involved.

The inhibitor data painted a complex picture: how can inhibition of a receptor suppress hyperpigmentation from depolarizing treatments but induce hyperpigmentation when used on its own? A model (Figure 4.4) based on the competing interactions between serotonin receptors and the downstream cAMP signaling in the breast cell field [425] was our basis for a model that explains these data. The model also has the advantage that it explains the bistable (all-or-none) hyperpigmentation phenotype: the dynamics of such networks, together with the known variable initial serotonin concentration among animals [406], results in two stable “attractor” states with respect to final output [454-457], corresponding to activation of transformation or maintenance of normal melanocyte state. Our future work will be focused on refining a quantitative model of this network, developing our method into a general-purpose bioinformatics tool to help scientists formulate predictive models from puzzling functional data, and building a detailed picture of cAMP signaling among cells *in vivo*, using optogenetic control of cAMP levels [458]. Regardless of the specifics of the model, the opposing activity of several serotonin receptors suggests that therapeutic approaches must be based on quantitative simulation of the relevant physiology – the desired outcome will unfortunately not be as simple as applying serotonergic blocker drugs to melanoma.

### ***Localized tumorigenesis and bioelectric cues***

Transmembrane voltage level is not only an initiator of dispersed metastasis but is involved in formation of discrete tumor-like structures. Exposure to well-known carcinogen 4NQO results in tumors with functional blood vessels (Figure 4.5C,D,

Supplement 4.2); interestingly, the directly-detected (Figure 4.5E) change of transmembrane potential throughout the organism, and its attendant hyperpigmentation (Figure 4.5A) reveal a kind of field carcinogenesis [459-461] – a change in the physiology of cells well outside of the region containing an anatomically-apparent tumor. While the channels responsible for cancer-relevant sodium (Figure 4.6) and chloride (Figure 4.7) fluxes remain to be genetically identified in this system, all of the data indicate that it is the voltage and ion content, not the molecular identity of the translocator protein, that is crucial for determining cell behavior. Thus, systems of fluorescent voltage- and sodium-reporter dyes may be a useful modality for identification of the transformed field prior to, and around the site of, tumor formation in clinical settings.

Interestingly, we observed considerable heterogeneity in the voltage responses of animals treated with 4NQO. We found about half the number of animals to be largely depolarized throughout their bodies, while the other half appeared unaffected. This bi-stability, similar to that discussed for the hyperpigmentation serotonin signaling pathway above, may be a common feature of physiological networks [462] and could underlie the well-known heterogeneity among human patients with respect to cancer susceptibility and response to treatments. We suggest that in addition to the epigenetic profiling currently under way to help understand differences among the population, the states of physiological (not genetic) networks should play an important part in understanding inherent variability in cancer-relevant processes [68, 192].

### ***Conclusions and future prospects***

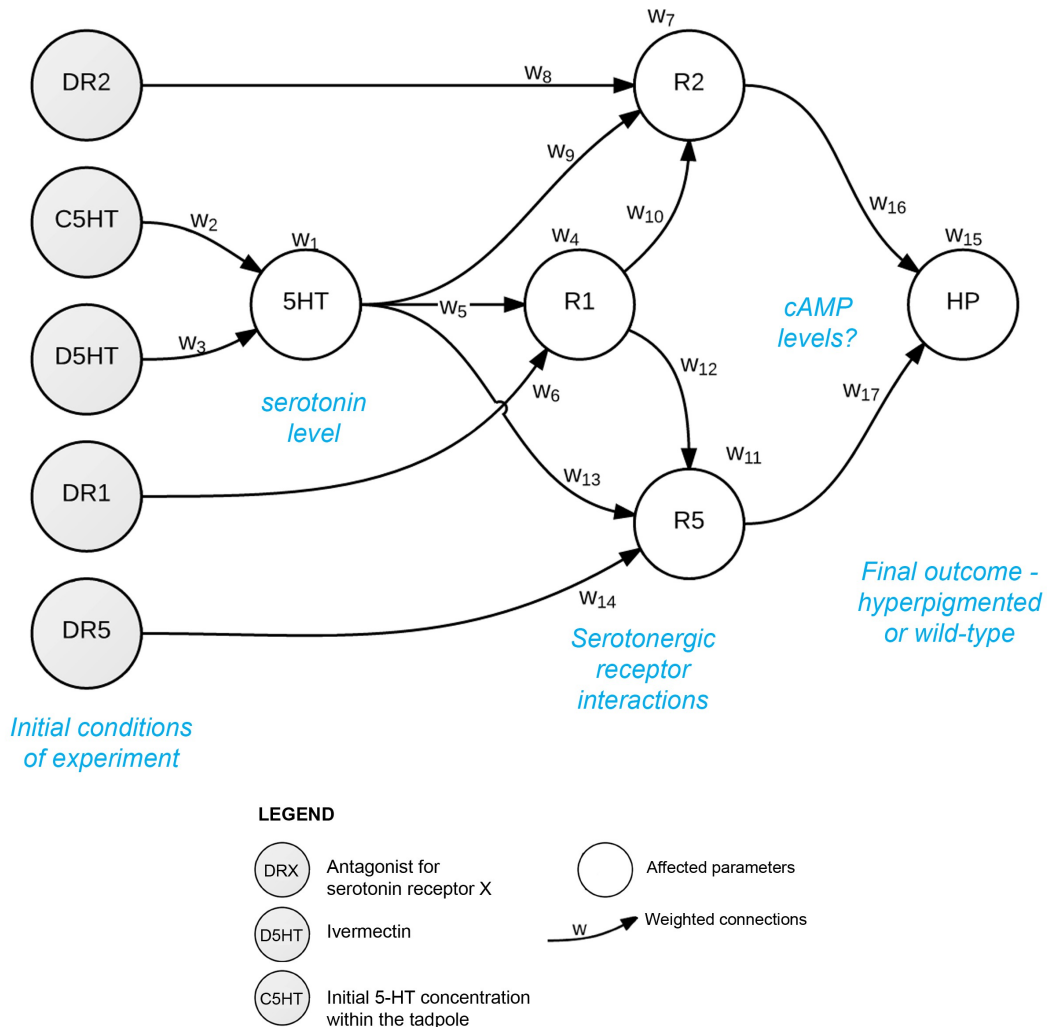
These studies have provided important details on the fascinating novel area of voltage regulation of cancer; however, many new questions now arise. The

spatial properties of voltage-regulated serotonergic long-range signaling, and the complex dynamics of physiological networks upstream of key cell decisions are both likely to be of relevance not only to developmental patterning but also to a new understanding of the biophysics of the tumor microenvironment. In addition to the basic biology revealed by this pathway, these data suggest a number of approaches with biomedical applications. The search for new types of instructor cells adds an interesting dimension to the current focus on stem cells as a uniquely important cancer cell population. Moreover, the ability to visualize tumor and carcinogen-modified cells via physiological dyes likely represent interesting non-invasive diagnostic modalities to identify tissues at risk or tumor margins during surgery. Most excitingly, forced hyperpolarization (Figures 4.7,4.8) via either molecular-genetic or pharmacological means can functionally reduce tumor incidence. It is likely that capitalizing on the functional significance of transmembrane potential as a mediator of pattern maintenance and tumor suppression *in vivo* represents an exciting and important future approach for cancer management. It is hoped that by unraveling fundamental roles of bioelectricity in pattern formation, biomedicine will someday be able to activate at will the remarkable pathways that highly regenerative model species use to normalize, not kill, tumor tissue [463-466].

## **Acknowledgements**

We thank Paul Mead for his kind assistance and gift of the transgenic flk1-GFP frogs, John Adelman for the Kir4.1 construct, Ruiz I Altaba for the Gli1 construct, Leonard Zon for the KRAS mutant construct, Punita Koustubhan and Amber Carrier for general lab assistance and frog husbandry, Joan Lemire and Claire Stevenson for molecular biology assistance, Vaibhav Pai for advice on serotonergic signaling pathways, Joan Lemire for valuable comments on the manuscript, and the members of the Levin lab and the bioelectricity community for many useful discussions. M.L. is grateful for support of the NIH (awards AR061988, AR055993) and the G. Harold and Leila Y. Mathers Charitable Foundation.

## Supplementary material



### Supplemental Figure 4.1. A network model of serotonergic signaling downstream of voltage.

A feed-forward network can represent a wide variety of signaling relationships between initial conditions (DR2 representing 5-HT receptor 2 antagonist presence; C5HT, initial 5-HT concentration; D5HT, ivermectin; DR1, receptor 1 antagonist; DR5, receptor 5 antagonist) determining serotonin concentration (5HT), several serotonin receptors (R1, R2, and R5), and the final output of melanocyte state (HP). Nodes are activated with a sigmoid function, and each connecting arrow bears a weight whose value (between -10.0 and 10.0) represents the normalized strength with which it up- or down-regulates the next node to which it is connected. For example,  $w_{12}$  represents the strength with which R1 activity can induce or repress 5HT<sub>R5</sub>, while  $w_{11}$  represents the bias value of the activation function of R5. A set of values for the weights of each

arrow represents (unambiguously specifies) a model for one possible relationship among these components. Then, each experiment (consisting of a set of treatments, which can perturb voltage and perhaps block one of the receptors, and a hyperpigmented or normal outcome of the experiment) can be compared to the prediction of any model: given a set of treatments and initial 5-HT concentration, what degree of hyperpigmentation phenotype is expected? Computing the output of the network and using a suitable formalism for capturing our experimental results in a database, a model can be ranked based upon how well its predictions match the outcomes of all our experiments. A simulated annealing search algorithm was used to identify networks whose predictions best match the results; such networks represent good models that can make new predictions for experimental conditions that have not yet been attempted.

### Model description

Inputs:

$$x = \begin{bmatrix} c^{5HT} \\ d^{5HT} \\ d^{R1} \\ d^{R2} \\ d^{R5} \end{bmatrix}$$

$d^{5HT}$ ,  $d^{R1}$ ,  $d^{R2}$ ,  $d^{R5}$ : quantitative effect of drugs on extracellular serotonin level ( $d^{5HT}$ ) and serotonin receptors sensitivity ( $d^{R1}$ ,  $d^{R2}$ , and  $d^{R5}$ ). Depending on the treatment, values are set to 0 (block), 1 (normal level), or 2 (enhance).

$c^{5HT}$ : initial concentration (value between 1 and 2; 100 values tested during training).

Parameters:

$$\theta^{5HT} = \begin{bmatrix} w_1 \\ w_2 \\ w_3 \end{bmatrix} \quad \theta^{R1} = \begin{bmatrix} w_4 \\ w_5 \\ w_6 \end{bmatrix} \quad \theta^{R2} = \begin{bmatrix} w_7 \\ w_8 \\ w_9 \\ w_{10} \end{bmatrix} \quad \theta^{R5} = \begin{bmatrix} w_{11} \\ w_{12} \\ w_{13} \\ w_{14} \end{bmatrix} \quad \theta^{HP} = \begin{bmatrix} w_{15} \\ w_{16} \\ w_{17} \end{bmatrix} \quad \theta = \begin{bmatrix} \theta^{5HT} \\ \theta^{R1} \\ \theta^{R2} \\ \theta^{R5} \\ \theta^{HP} \end{bmatrix}$$

$$\begin{cases} 0 < w_i < 10 & \text{if } i = \{1,2,3,5,6,8,9,13,14\} \\ -10 < w_i < 10 & \text{otherwise} \end{cases}$$

Output:

$$a^{5HT} = [1 \ c^{5HT} \ d^{5HT}] \theta^{5HT}$$

$$a^{R1} = \text{sigmoid}([1 \ a^{5HT} \ d^{R1}] \theta^{R1})$$

$$a^{R2} = \text{sigmoid}([1 \ d^{R2} \ a^{5HT} \ a^{R1}] \theta^{R2})$$

$$a^{R5} = \text{sigmoid}([1 \ a^{R1} \ a^{5HT} \ d^{R5}] \theta^{R5})$$

$$h_{\theta}(x) = a^{HP} = \text{sigmoid}([1 \ a^{R2} \ a^{R5}] \theta^{HP})$$

$$\text{sigmoid}(z) = \frac{1}{1 + e^{-z}}$$

Penetrance:

$$x_d = \begin{bmatrix} d^{5HT} \\ d^{R1} \\ d^{R2} \\ d^{RX} \end{bmatrix}$$

$$P_{\theta}(x_d) = \frac{1}{100} \sum_{c^{5HT}=1,1.01,\dots,2} \text{step}\left(h_{\theta}\left(\begin{bmatrix} c^{5HT} \\ x_d \end{bmatrix}\right)\right)$$

$$\text{step}(z) = \begin{cases} 1 & \text{if } z \geq 0.5 \\ 0 & \text{otherwise} \end{cases}$$

Bistability:

$$B_{\theta}(x_d) = \frac{1}{100} \sum_{c^{5HT}=1,1.01,\dots,2} \text{gauss}\left(h_{\theta}\left(\begin{bmatrix} c^{5HT} \\ x_d \end{bmatrix}\right)\right)$$

$$\text{gauss}(z) = e^{-\frac{(z-0.5)^2}{2 \cdot 0.1^2}}$$

Cst function (error):

$$J(\theta) = \frac{1}{m} \sum_{i=1}^m \left( P_{\theta}(x_d^{(i)}) - y^{(i)} \right)^2 + 0.1 \cdot B_{\theta}(x_d^{(i)})$$

**Best model found by simulated annealing search (error = 0.0538)**

Parameters:

Parameter Value	$w_1$	$w_2$	$w_3$	$w_4$	$w_5$	$w_6$	$w_7$	$w_8$	$w_9$
	3.8	1.0	3.7	-8.4	8.4	2.3	-7.8	1.2	1.5
Parameter Value	$w_{10}$	$w_{11}$	$w_{12}$	$w_{13}$	$w_{14}$	$w_{15}$	$w_{16}$	$w_{17}$	
	-8.0	-3.7	9.9	9.7	3.1	0.7	8.2	-4.3	

Predictions:

TREATMENT:	5HT	R1	R2	R5		Exp. result	Model result
WT	1	1	1	1		0%	33%
IVM	2	2	2	2		100%	100%
IVM + R1 block	2	0	2	2		84%	100%
R1 block	1	0	1	1		22%	33%
IVM + R2 block	2	2	0	2		71%	100%
R2 Block	1	1	0	1		0%	0%
IVM + R5 block	2	2	2	0		100%	100%
R5 block	1	1	1	0		30%	33%
IVM + MTP	2	0	0	0		74%	100%
MTP	1	0	0	0		66%	0%
IVM + Fluoxetine	0	1	1	1		0%	0%

**Supplement 4.2. movie of blood flow in chemically-induced tumor**

This movie (<http://iopscience.iop.org/1478-3975/9/6/065002/media>) shows blood flowing through ectopic blood vessels that have grown into a 4NQO-induced ITLS.

## Chapter 5

### **Selective depolarization of transmembrane potential alters muscle patterning and muscle cell localization in embryonic *Xenopus laevis***

Maria Lobikin, Jean-François Paré, David L. Kaplan, and  
Michael Levin

International Journal of Developmental Biology (In Press, 2015)

**Data contributions:** I contributed data and performed statistical analyses on all figures in this chapter.

## **Abstract**

The correct anatomical placement and precise determination of specific cell types is required for the establishment of normal embryonic patterning. Understanding these processes is also important for research in regenerative medicine and cancer biology. Transmembrane voltage gradients across embryonic tissues can mediate cellular communication to regulate the processes of proliferation, migration, and differentiation. Our past work showed that selective depolarization of an endogenous instructor cell population in *Xenopus laevis in vivo* induced a melanoma-like phenotype in the absence of genetic damage. Here, we use a hypersensitive glycine-gated chloride channel (GlyR) under control of tissue-specific promoters to show that instructor cells resident within muscle are more effective at triggering the metastatic conversion of ectodermal melanocytes than those similar cells within the nervous system. Moreover, depolarization of muscle cells results in aberrant muscle patterning and the appearance of cells expressing muscle markers within the neural tube, which impacts but does not abolish the animals' ability to learn in an associative conditioning assay. Taken together, our data reveal new details of long-range (non-cell-autonomous) reprogramming of cell behavior via alteration of the resting potential of specific embryonic subpopulations.

## Introduction

How cells adopt and maintain their fate is a crucial question in developmental biology. The proper regulation of cell fate and anatomical localization is also an important component of carcinogenesis and metastasis. Alongside the well-studied biochemical signaling cues present *in vivo*, several types of endogenous bioelectrical signals have also been shown to act as instructive cues for proper tissue patterning and maintenance [49, 339, 467].

Previous work in *Xenopus laevis* embryos revealed the sensitivity of melanocytes (the pigmented cell derivatives of the embryonic stem cell population known as the neural crest) to the resting potential of specific other cells [31, 33]. Artificially depolarizing a widely-distributed cell population expressing the glycine-gated chloride channel (GlyR) in the developing frog embryo results in the neoplastic-like conversion of melanocytes in the absence of genetic damage or carcinogen exposure. The melanocytes acquire properties associated with cancer: they over-proliferate, change their morphology toward a more dendritic shape, and become highly invasive, targeting heart, neural tube, blood vessels, and visceral organs; aberrant vasculogenesis is also observed [31, 468]. The GlyR-expressing cells were termed “instructor” cells, since they proved able to activate melanocyte metastatic conversion at a distance (non-cell-autonomously).

Remarkably, depolarizing even very small regions of developing *Xenopus* embryos is sufficient to induce an embryo-wide change in melanocyte behavior [468]. However, two major questions were not answered by body-wide or regional depolarization of instructor cells in their endogenous locations. First, given that the instructor cells are present throughout the embryo but enriched in neural regions such as the ventral neural tube, might one specific sub-population

be responsible for the effects we observed? Second, aside from the clearly visible melanocyte phenotype, might additional phenotypes have gone undetected, if they affected non-pigmented cells?

Here, we used tissue-specific promoters to investigate the effects of neural- or muscle-specific instructor cell activation, for the first time addressing individual subsets of this fascinating cell population that is ubiquitous in tissues. In order to depolarize different embryonic lineages, we misexpressed the GlyR channel exclusively in muscle or neural cells. To avoid triggering native instructor cells in other regions of the embryo, we used a hyper-sensitive mutant GlyR which would afford selective targeting of muscle or neural lineages and very low doses of Ivermectin (the GlyR channel opener), which would not depolarize endogenous instructor cells. Depolarizing either muscle or neural-specific instructor cells was sufficient to produce the embryo-wide conversion of melanocyte behavior. Surprisingly, the muscle lineage was more efficient at doing so than the neural lineage. Depolarization resulted in abnormal development of skeletal muscle, and also had the remarkable effect of changing the localization of affected cells to neural regions; cells positive for muscle markers began to appear in the neural tubes of treated animals. These data demonstrate that (1) depolarization of muscle precursors results in abnormal muscle development *in vivo*, (2) depolarization of even restricted lineages can result in whole-body hyperpigmentation, and (3) depolarization of muscle-specific cells results in their dramatic relocalization to neural regions.

## Results

### ***Depolarization of instructor cells results in a metastatic-like conversion of melanocytes***

We sought to investigate additional effects of selective depolarization of GlyR-expressing cells besides the previously-reported metastatic conversion of melanocytes [31]. GlyR-expressing cells comprise a sparse, yet widely distributed cell population in the developing tadpole [31] and can be selectively targeted with the drug ivermectin [32]. The extracellular chloride concentration in the *Xenopus* extracellular media is lower than that of the cytoplasm; thus, when embryos are treated with 1  $\mu$ M ivermectin, native GlyR-channels are opened and chloride ions will flow down their concentration gradient out of the expressing cell, depolarizing it. This depolarizing treatment results in the remarkable embryo-wide conversion of melanocytes, leading to hyperpigmentation in nearly all embryos. We have previously shown that this depolarizing treatment changes three major characteristics of melanocyte behavior: increased proliferation, a more arborized morphology and invasion into ectopic regions [31]. It should be noted that hyperpigmentation is an all-or-none phenotype, with no partial cases observed.

Importantly, the hyperpigmentation phenotype is due to voltage depolarization, and not due to specific effects of chloride concentration, off-target effects of ivermectin, or possible unknown non-channel roles of GlyR. To confirm this, we reproduced the same phenotype using sodium flux – a strategy often used to interrogate bioelectric signaling [469]. TPC3 is a newly identified two-pore channel, selective for sodium ions, that has an activity profile similar to that of native Na<sub>v</sub> channels when injected into *Xenopus* oocytes [470]. Injection of this

depolarizing voltage-gated sodium channel, TPC3, into one cell of two-cell stage (NF stage 2) embryos also results in the same embryo-wide hyperpigmentation phenotype in 18% of embryos (Figure S5.1). The incidence of hyperpigmentation phenotype was lower than that produced by Ivermectin, since TPC3 mRNA levels had to be kept very low, to avoid major effects on overall development.

### ***Instructor cell depolarization disrupts muscle patterning***

While the change in melanocyte behavior following depolarization is clearly evident through their black pigmentation, effects on other cell types or transparent tissues could have escaped notice. Elegant work previously revealed that mammalian muscle differentiation relied on the function of the potassium channel Kir2.1 [50, 471], which suggests voltage-dependence of myogenesis *in vivo*. Thus, we next asked whether skeletal muscle patterning might be affected by instructor cells. Because the pigmentation on the tails of hyperpigmented *Xenopus* tadpoles obscured visualization of muscle patterning, we examined albino embryos using polarized birefringence imaging.

Birefringence is an intrinsic optical property of the collagen fibers that make up the axial skeletal muscle in the *Xenopus* tail [472]. Using polarized light microscopy, tails of albino tadpoles (NF stage 45) that had either been treated with 1  $\mu$ M ivermectin from pre-neurula stage (NF stage 10) onwards, decapitated at NF stage 25/26 (to control for effects of ivermectin-induced paralysis on muscle development), or left untreated (controls), were photographed. In normal, untreated tadpoles, the axial muscle of the tail was highly organized - divided into concrete and highly regular segments along the anterior-posterior axis, forming chevron-like structures (Figure 5.1A, yellow arrows). Following instructor cell depolarization, the muscle segment peripheries no longer appeared as regular

and smooth as in control embryos, and there was a marked loss of muscle collagen signal from some regions in (Figure 5.1C-D). This abnormal muscle phenotype was observed in 74% (N=39) of animals examined (Figure 5.1E).

Ivermectin treatment has the side effect of paralyzing *Xenopus* tadpoles. To determine whether the muscle phenotype seen following ivermectin treatment was due to this paralysis, untreated tailbud embryos (NF stage 25/26) were paralyzed via decapitation, and muscle structure was observed at tadpole stages. The collagen organization and chevron pattern of the decapitated tadpoles appeared smooth and organized, as in control embryos (Figure 5.1B, yellow arrows), suggesting the muscle phenotype seen following ivermectin treatment is due to depolarization, and not an artifact of the paralysis that this treatment induces. The decapitation, however, did result in a decrease in overall collagen density, as quantified by calculating the brightness (Figure 5.1D). We conclude that polarized resting potentials are required for normal muscle development *in vivo*, and that paralysis induces an overall subtle reduction in collagen level but not the large-scale contiguous defects produced by  $V_{\text{mem}}$  depolarization.

The depolarization-induced hyperpigmentation in *Xenopus* tadpoles is mediated by serotonin signaling. Inhibition of the voltage-regulated serotonin transporter (SERT) is able to completely prevent depolarization-induced hyperpigmentation [31]. To determine whether serotonin signaling also mediates proper muscle development, embryos were treated with ivermectin together with the SERT inhibitor, fluoxetine, from NF stage 10 onwards, photographed under polarized light at tadpole stages (NF stage 45) and scored for abnormal muscle phenotypes. Exposure to 10  $\mu\text{M}$  fluoxetine blocked the ivermectin-induced

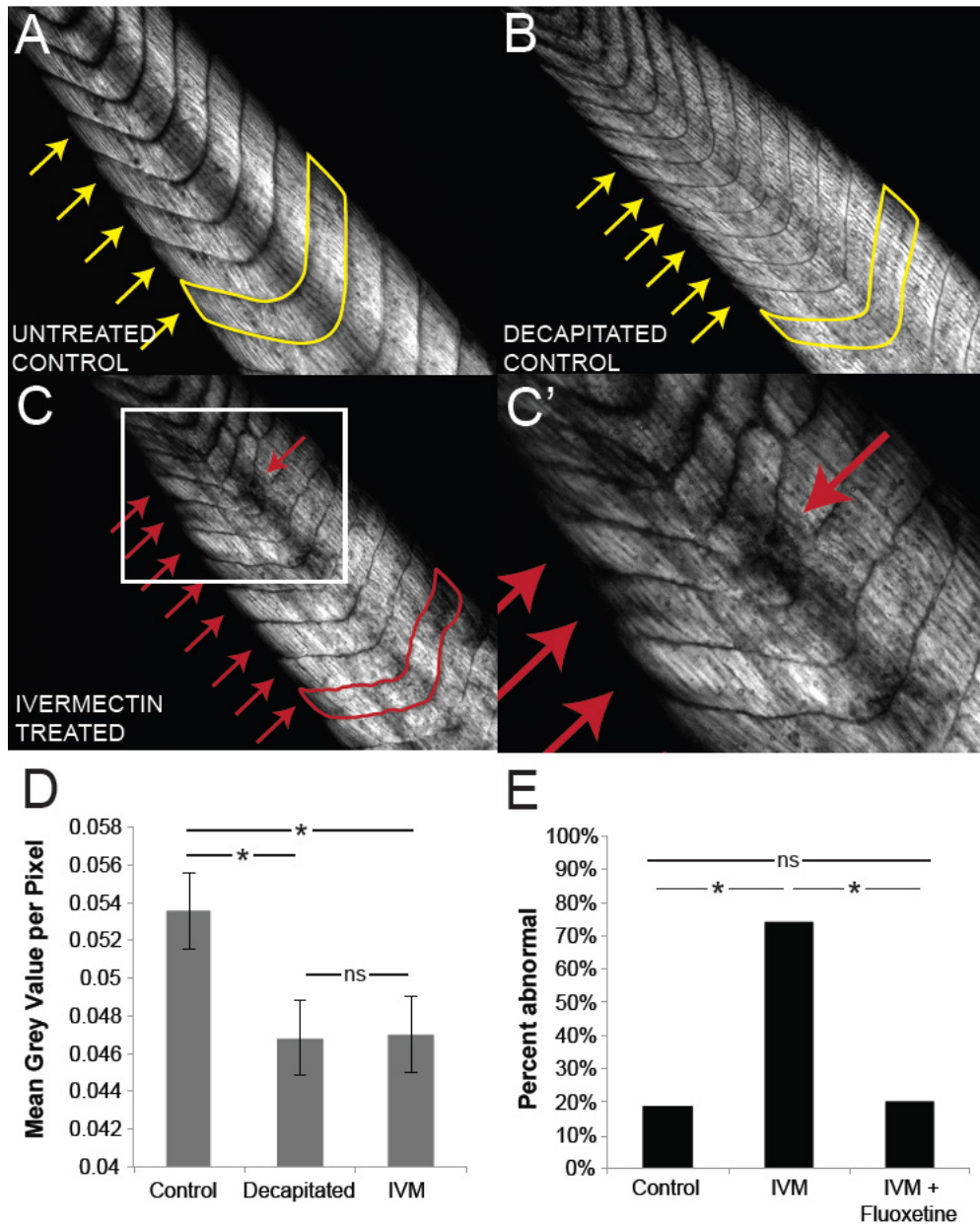


**Figure 5.1. Depolarization of instructor cells results in abnormal muscle structure independent of immobilization.**

Birefringence imaging of wildtype (A), decapitated (B) and ivermectin-treated (C, C') tadpole tails reveals disruption of muscle patterning (yellow, red arrows) with depolarizing ivermectin treatment, but not in immobilized tadpoles that had been decapitated at tailbud stage. D) Quantification of the mean grey value per pixel of area in examined tails reveals a significant decrease in overall collagen density in paralyzed ivermectin-treated and decapitated embryos. (E) Concurrent treatment of 1  $\mu$ M ivermectin with 10  $\mu$ M fluoxetine significantly inhibited ivermectin-induced muscle disorganization (20% abnormal, N=20,  $p < 0.01$  compared to ivermectin treatment alone). Error bars denote standard deviation. \*,  $p < 0.01$ .

muscle disorganization, and reduced the percent of abnormal tadpole tails to control levels (20% abnormal, N=20, Figure 5.1E). These data suggest that serotonin signaling is important for transducing changes in  $V_{mem}$  to changes in skeletal muscle patterning.

***Tissue-specific instructor cells are sufficient for embryo-wide depolarization***

Hyperpigmentation is an embryo-wide phenotype, and GlyR<sup>+</sup> instructor cells are present throughout the body. Since it was not known whether one subset of the instructor cells was responsible for the phenotypes (such as the denser enrichment found within the ventral neural tube), we next sought to determine whether the depolarization of tissue-specific regions is sufficient to induce this embryo-wide change in melanocyte behavior. In order to induce depolarization in specific regions, we took advantage of a Tol2 transposase system and the neural beta tubulin (NBT2) promoter to drive the expression of a hypersensitive GlyR mutant, GlyR-A288G [412], fused to the red fluorescent protein tdTomato, in neural tissue. We confirmed neural-specific expression of GlyR-A288G in embryos that had been injected in one cell at the two-cell stage (NF stage 2) by monitoring fluorescence expression in NF Stage 45 tadpoles (Figure 5.2A, white arrow).

By using the GlyR-A288G mutant, we were able to take advantage of its increased sensitivity to ivermectin, and thus open only the introduced (ectopic) channels by using a low dose of ivermectin that does not affect the native GlyR-channels (Figure 5.2B). While injection of the Tol2-NBT2pr-GlyR-A288G-tom itself had no effect on overall hyperpigmentation rates, treating injected embryos with 0.05  $\mu$ M ivermectin led to a significant increase in hyperpigmented embryos

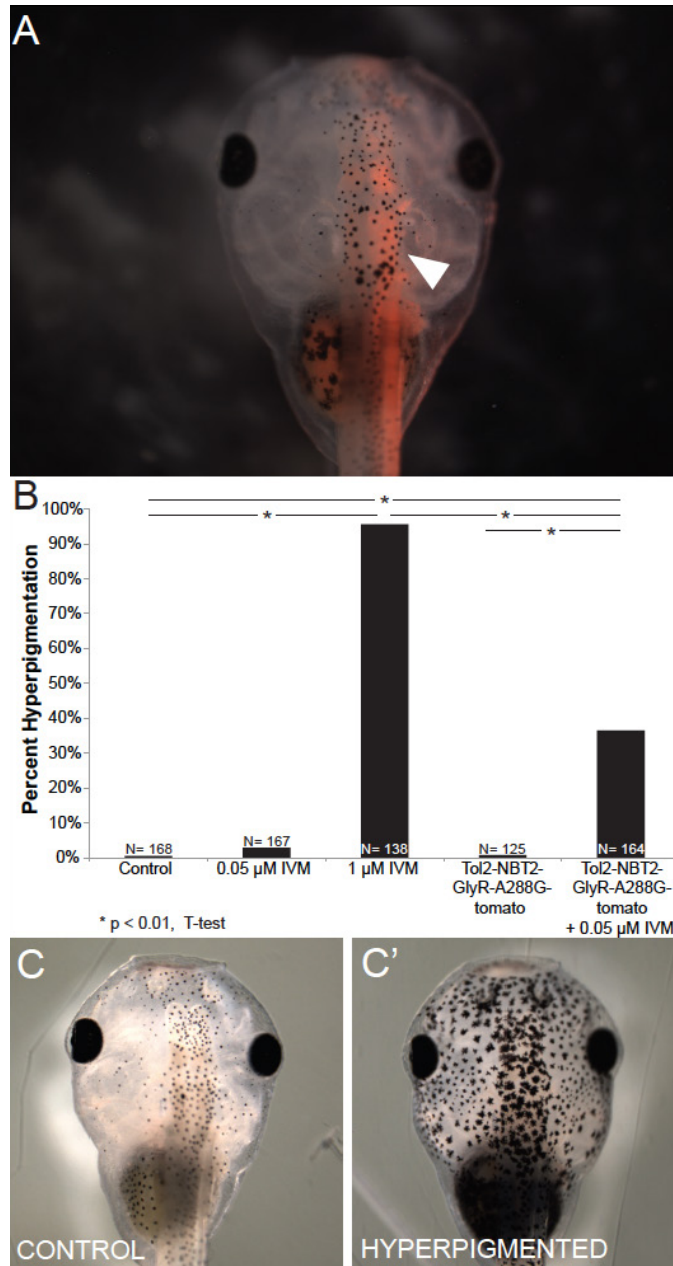


**Figure 5.2. Driving GlyR-A288G expression in neural tissue is sufficient to induce hyperpigmentation.**

Embryos were injected with Tol2-NBT2-GlyR-A288G-tomato (driving the neural-specific expression of a GlyCl channel with increased sensitivity to ivermectin fused to a tdTomato fluorescent reporter) into 1 cell of 2-cell embryo (NF stage 2). A) Neural-specific expression was confirmed in NF stage 45 tadpoles (white arrow). B) Embryos that had been injected with Tol2-NBT2-GlyR-A288G-tom and treated with 0.05  $\mu$ M ivermectin displayed significant levels (36.3%, N=164,  $P < 0.01$  in injected & treated embryos) of hyperpigmentation (C') compared to control embryos (C) and those that had been injected and not exposed to ivermectin (0.8% hyperpigmented, N=125).

(Figure 5.2B-C, 36.6% hyperpigmented, N=164,  $p < 0.01$ ). However, the percentage of hyperpigmented embryos was far less than when embryo-wide instructor cells were targeted (compared to 95.7% hyperpigmented with 1  $\mu\text{M}$  ivermectin treatment of uninjected embryos, Figure 5.2B). These data suggest that neural-specific instructor cells are sufficient to induce embryo-wide hyperpigmentation, but not as efficiently as embryo-wide instructor cell depolarization, within the context of the range of expression levels observed in this transgenic system.

Melanocytes themselves are derivatives of a neural embryonic stem cell population known as the neural crest. This cell population forms shortly after neurulation, and then migrates to form a variety of different tissue including neurons, glia, connective tissue, cartilage and melanocytes. Thus, we next wanted to determine whether depolarization of non-neural (and in particular, mesodermal) instructor cells would be sufficient to induce embryo-wide hyperpigmentation. In order to do so, we once again used the Tol2 system, this time driving the expression of the hypersensitive GlyR-A288G mutant in muscle tissue fused to a GFP reporter controlled by the cardiac actin ( $\rho\text{Car}$ ) promoter [473, 474]. The introduced transgene was first detectable at NF stage 17 [475] and then expressed throughout the life of the animal (data not shown). We confirmed muscle-specific expression in NF stage 45 embryos via fluorescent imaging of tadpole-stage embryos that had been injected with the Tol2-CarPr-GlyR-A288G-GFP3 construct into one cell of the two-cell stage (NF stage 2, Figure 5.3A).

While Car promoter-driven GlyR-A288G-GFP3 on its own had no effect on hyperpigmentation rates, treating injected embryos with 0.05  $\mu\text{M}$  ivermectin (a

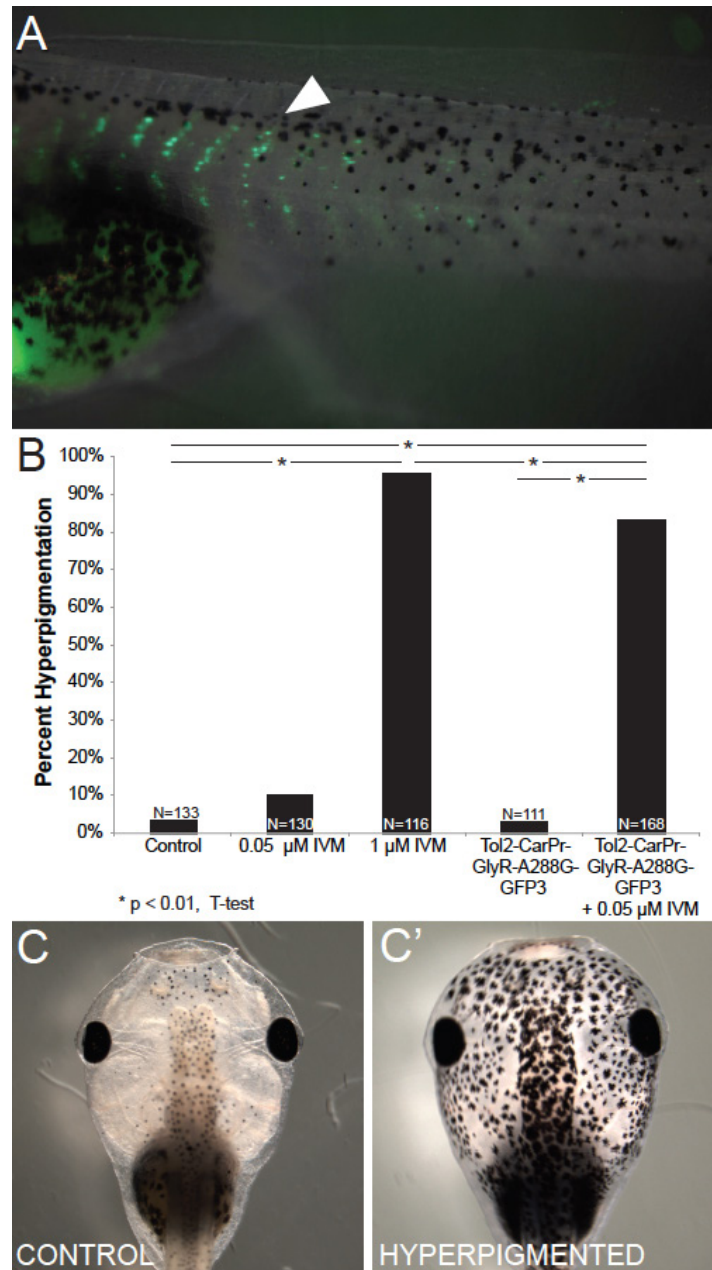


**Figure 5.3. Driving GlyR-A288G expression in muscle tissue is sufficient to induce hyperpigmentation.**

Embryos were injected with Tol2-CarPr-GlyR-A288G-GFP3 (driving the muscle-specific expression of a GlyR channel with increased sensitivity to ivermectin, fused to a GFP fluorescent reporter) into 1 cell of a 2-cell embryo (NF stage 2). A) Muscle specific expression of GlyR mutant confirmed in NF stage 45 tadpoles (white arrow). B) Embryos that had been injected with Tol2-CarPr-GlyR-A288G-GFP3 and treated with a low dose of ivermectin (0.05  $\mu$ M) displayed significant levels (83.3%, N=168, P<<0.01) of hyperpigmentation (C'') compared to control embryos (C') and those that had been injected and not exposed to ivermectin (2.7% hyperpigmented, N=111).

dose that does not affect endogenous GlyR channels, Fig. 5.3B) resulted in a significant percentage of hyperpigmented animals at tadpole stage (Figure 5.3B, 83.3% hyperpigmented, N=168,  $p < 0.01$ ). Surprisingly, depolarizing non-neural instructor cells resulted in more efficient hyperpigmentation than when neural-specific instructor cells were targeted (83.3% vs. 36.6%, respectively). Taken together, our data suggest that either muscle- or nerve-specific depolarized cells are able to trigger melanocyte conversion, but that muscle-specific targeting was far more effective (although not quite as effective as depolarizing all of the native instructor cells).

#### ***Depolarizing muscle-specific cells results in their partial reprogramming***

While confirming that Tol2-CarPr-GlyR-A288G-GFP3 injections were truly specific to muscle tissue, we looked at the internal localization of the transgenic GFP reporter. Embryos that had been injected with either Tol2-CarPr-GFP3 (as a control) or with Tol2-CarPr-GlyR-A288G-GFP3 into one cell at the two-cell stage (NF stage 2) and later treated with ivermectin from NF stage 10 onwards were fixed, sectioned, and processed for immunohistochemistry at tailbud stages (NF stage 28/29) with an anti-GFP antibody. In the control, Tol2-CarPr-GFP-injected embryos, localization of the GFP signal was confined to the somites (Figure 5.4A,C), as expected. Surprisingly, in embryos in which these muscle-specific cells had been selectively depolarized, Car promoter-driven GFP expression was observed within the neural tube (Figure 5.4B) – a location devoid of muscle cells during normal embryogenesis. This improper localization of muscle cells was observed in 76% of embryo sections examined (Figure 5.4D). There was no overall difference in the number of pCar-cells present between sections of embryos that had been injected with Tol2-pCar-GFP and embryos injected with

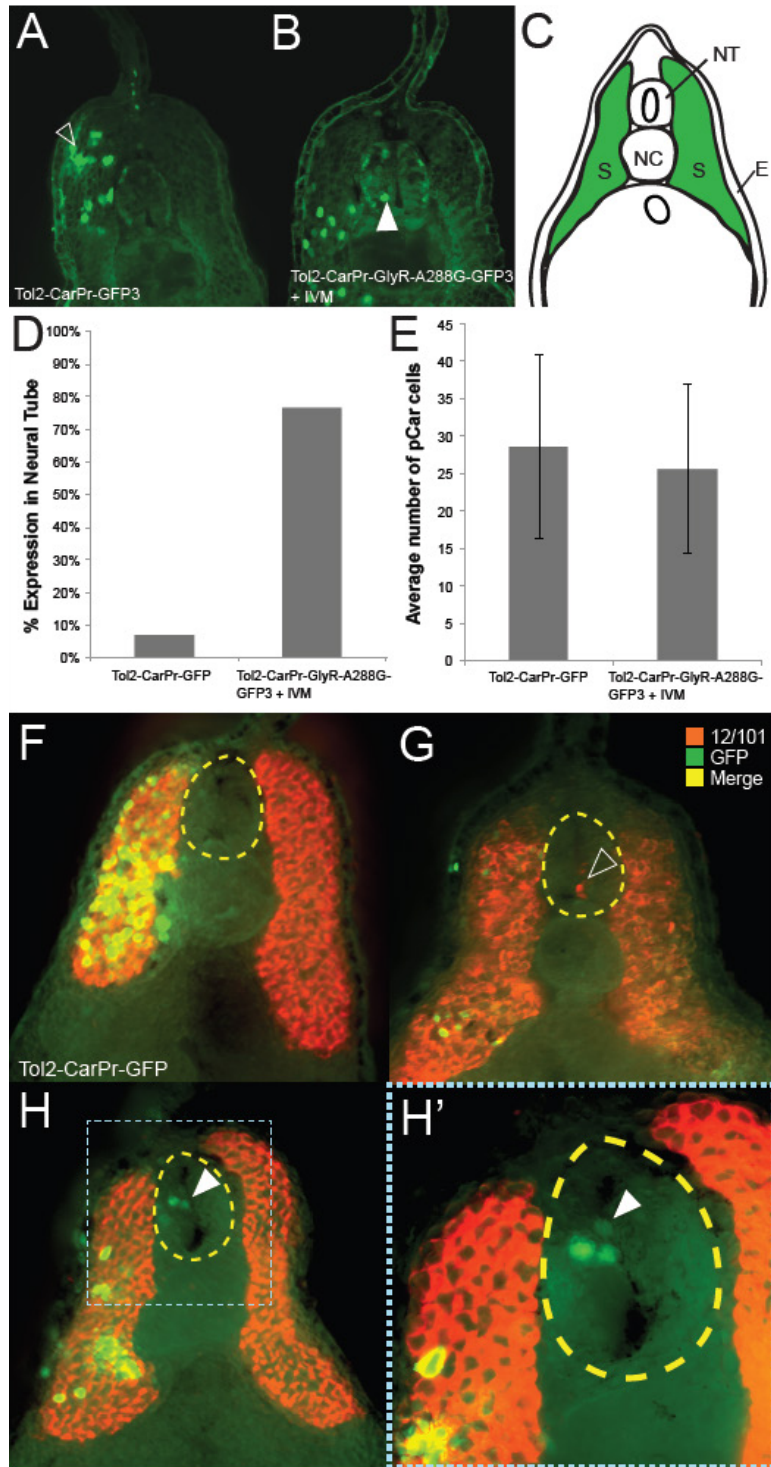


**Figure 5.4. Expressing GlyR-A288G and selectively depolarizing muscle-specific cells results in abnormal localization.**

(A) Immunohistochemistry performed on sections of tailbud stage (NF stage 28/29) *Xenopus laevis* embryos that had been injected with Tol2 construct driving GFP expression in muscle cells using cardiac actin promoter, Car, using GFP-specific antibodies revealed normal muscle specific localization of GFP signal (in

somatic tissue, C, green). (B) Driving hypersensitive GlyR expression (GlyR-A288G) in muscle tissue using Car promoter and subsequent depolarization resulted in GFP signal appearing in neural tissue (white arrow). (D) Abnormal localization of GFP<sup>+</sup> cells to the neural tube occurred in 76% of embryos that had been injected with Tol2-Car-pRGlyR-A288G-GFP3 and treated with 0.05  $\mu$ M ivermectin, but overall number of GFP<sup>+</sup> cells was not significantly different between injected and treated embryos and control embryos that had been injected with Tol2-CarPr-GFP3 (E). Co-immunohistochemistry using an anti-GFP antibody to track cells expressing GFP in response to the Car promoter and a 12/101 antibody labeling skeletal muscle confirmed GFP<sup>+</sup> cells of Tol2-CarPr-GFP3 injected embryos are localized in somatic muscle tissue (F). Co-immunohistochemistry on embryos that had been injected with Tol2-CarPr-GlyR-A288G-GFP3 and treated with ivermectin displayed either 12/101 signal in the neural tube (G), or Car-regulated GFP signal in the neural tube (H, H', white arrow) or but no overlapping signal in the neural tube. Scale bars represent 100  $\mu$ m.

Tol2-CarPr-GlyR-A288G-GFP3 and treated with 0.05  $\mu$ M ivermectin (Figure 5.4E). This suggests that depolarization does not produce excess GFP<sup>+</sup> cells in the neural tube but rather causes these muscle cells to occupy the neural tube at the expense of their presence in their native locations.

To determine whether these improperly localized muscle cells are also positive for other muscle markers, we performed co-immunohistochemistry at tailbud stage (NF stage 28/29) with 2 antibodies: anti-GFP to label injected Car promoter-driven GFP<sup>+</sup> cells, and anti-12/101 [476], which labels mature skeletal muscle. The co-immunohistochemistry data confirmed the proper localization of injected cells driven by the pCar promoter in Tol2-CarPr-GFP3 controls (Figure 5.4F). In sections of embryos that had been injected with Tol2-CarPr-GlyR-A288G-GFP3, and treated with 0.05  $\mu$ M ivermectin, while GFP<sup>+</sup> cells are seen in the neural tube (Figure 5.4H, H'), they do not overlap with 12/101 localization. In some instances, 12/101 was observed within the neural tube, confirming the presence of ectopic muscle, but not overlapping with the localization of injected and depolarized pCar cells (Figure 5.4G). Taken together, these data suggest that depolarizing Car promoter-driven muscle cells results in their reprogramming, causing them to ectopically occupy the neural tube, but that the effect is partial, such that cells never simultaneously express both GFP (and thus Car-driven expression) and 12/101 muscle markers.

We next asked whether these ectopic muscle cells acquire a neural-like character when located in the neural tube. Co-immunohistochemistry was performed on sections of tailbud stage embryos (NF stage 28/29) that had been injected into one cell at the two-cell stage (NF stage 2) with either Tol2-CarPr-GFP3 or Tol2-CarPr-GlyR-A288G-GFP3 and later treated with 0.05  $\mu$ M ivermectin using anti-GFP to label the Car promoter-driven cells, and anti-

acetylated alpha tubulin to label neural cells. In control embryos that had been injected with Tol2-CarPr-GFP3, the pCar cells (green) do not co-localize with the neural tissue labeled in red (Figure 5.5A). The same is true for embryos that had been injected with Tol2-CarPr-GlyR-A288G-GFP3 but not treated with ivermectin (Figure 5.5B). In sections of embryos that had been injected with Tol2-CarPr-GlyR-A288G-GFP3, then treated with 0.05  $\mu$ M ivermectin, while Car promoter driven muscle cells did appear in the neural tube region, they too, did not co-localize with the neural signal, suggesting that these depolarized pCar<sup>+</sup> cells that end up in the neural tube are not being completely reprogrammed into neural cells. We were unable to track the anatomical fate of these cells long-term, as the fluorescence of our injected markers disappeared after 1 week. Further studies using transgenic animals, at single-cell and multiple timepoint resolution, are now in progress, to understand the transcriptional and anatomical course of these cells throughout development and subsequent growth.

Strikingly, these muscle-promoter driven cells were found to comprise between 2.6% and 27.3% (1-6 of  $30 \pm 8$  cells) of the cells in a given neural tube (Figure 5.5D, D'). Given the large number of muscle cells colonizing neural regions, we sought to determine whether these embryos display any behavioral changes. Thus, behavior testing was performed using an automated training apparatus that implemented an associative learning paradigm: tadpoles (NF stage 45/46) were to avoid a (moving) red-light section of their petri dish, or receive weak electric shocks (Figure S5.2A, [477]). Surprisingly, both embryos that had been treated with low doses of ivermectin, and those that had been injected with Tol2-CarPr-GlyR-A288G-GFP3 (at NF stage 2) and then treated with low doses of ivermectin, were able to learn to avoid the red portions of the dish (Figure S2B). However, embryos that had been both injected with the

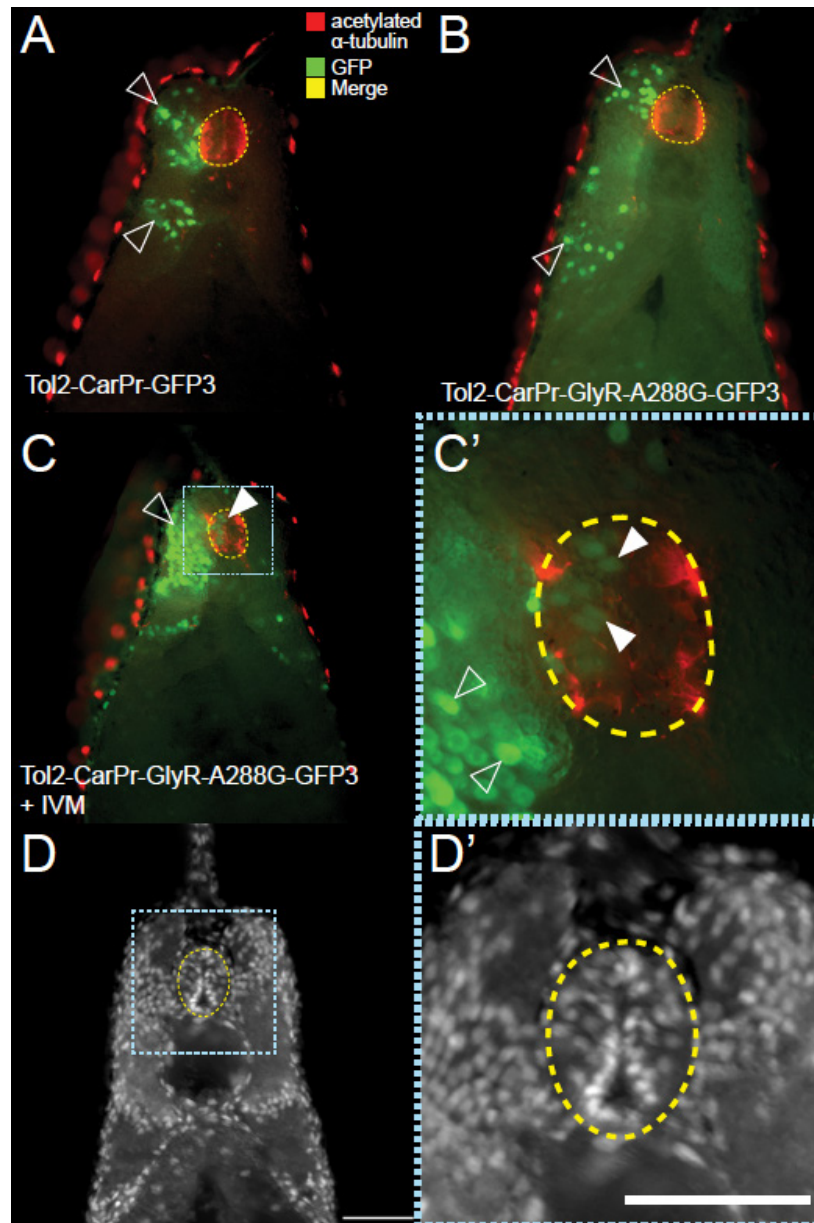


**Figure 5.5. Mislocalized Car promoter-driven GFP+ cells in neural tube are not completely neural.**

(A) Double labeling co-immunohistochemistry was performed on sections of tailbud stage (NF stage 28/29) *Xenopus* embryos that had been injected with Tol2-CarPr-GFP3 using an anti-GFP antibody to track cells that have been activated by the cardiac actin promoter alongside an anti-acetylated  $\alpha$ -tubulin, labeling neural tissue. This revealed normal expression of GFP in the somatic tissue. (B) Co-immunos on sections of embryos that had been injected with a Tol2-pCar construct driving expression of hypersensitive GlyR-A288G mutant also revealed normal localization of injected construct. (C) Embryos injected with Tol2-CarPr-GlyR-A288G-GFP3 and treated with 0.05  $\mu$ M ivermectin displayed abnormal neural localization (white arrow), however, the GFP<sup>+</sup> cells in the neural tube did not co-localize with acetylated  $\alpha$ -tubulin cells (C', white arrows). (D, D') Hoechst nuclear staining of sections.

hypersensitive GlyR channel driven by the CarPr promoter did not learn as effectively as controls. After two training sessions, the uninjected animals displayed a significant aversion to red light, while injected and treated embryos displayed the induced significant aversion to red light following three training sessions (Figure S5.2B). No significant differences were observed in average speed or average time being punished during training (Figure S2C,D).

Taken together, our data show that depolarizing muscle-specific cells results in their improper colonization of neural regions of the developing *Xenopus* embryo. Surprisingly, these cells express only one muscle marker at a time (the mature skeletal muscle marker, 12/101, or the pCAR marker), and do not express acetylated alpha tubulin as do real neural tissues. These data suggest that these migrating cells may be partially reprogrammed into an intermediate cell type, or alternatively, that depolarization results in the migration of a non-fully differentiated cell that has already committed to the muscle lineage. Despite the replacement of considerable proportions of neural cells with muscle, learning ability remains (although the speed of learning is decreased).

## **Discussion**

Melanocyte behavior can be affected by the non-cell-autonomous depolarization of a population of GlyR-expressing instructor cells [31]. In addition to changes in melanocyte behavior and vasculature structure [468], here we demonstrate that GlyR-mediated depolarization also disrupts normal muscle development (Figure 5.1). There is both a loss of density in collagen fibers characteristic of muscular dystrophy and a disorganization of tail muscle patterning. This abnormal muscle phenotype can be rescued by treatment with the specific inhibitor of the serotonin transporter, fluoxetine (Figure 5.1E), suggesting that serotonin can prevent the

development of the depolarization-induced dystrophic-like muscle phenotype. Serotonin has been previously implicated with instructive signaling downstream of changes in  $V_{\text{mem}}$ , mediating changes in melanocyte behavior [31] as well as in left-right patterning [62, 478]. These data also corroborate a recent finding that fluoxetine treatment can prevent dystrophy in a zebrafish model of Duchenne muscular dystrophy, possibly acting on skeletal muscle to enhance membrane integrity [479]. Taken together, these data demonstrate an important role for serotonin in skeletal muscle and suggest a potential therapeutic benefit of serotonin modulation for treating muscular dystrophy.

Existing data have shown that depolarization of even a few cells, a long distance away from the melanocytes is sufficient to radically change their behavior leading to a metastatic-like phenotype through serotonergic signaling [33, 468]. However, the question as to which subpopulations of cells have the potential to transform these stem cell derivatives remained heretofore unanswered. Here, we demonstrate that these instructor cells do not need to be of a particular cell lineage in order to be able to induce embryo-wide hyperpigmentation: the depolarization of either muscle and neural instructor cells is sufficient (Figure 5.2B, 5.3B). The depolarization of muscle-specific cells may be more potent in producing the change in melanocyte phenotype than is the depolarization of cells of a neural lineage (Figure 5.2B, 5.3B). This is especially interesting since it is known that the expression pattern of GlyR-expressing cells in *Xenopus* is denser in the ventral marginal zone of the neural tube than the punctate distribution of these cells throughout the entire embryo [31], and it is that region which initially was thought to be responsible for the hyperpigmentation induced by embryos' exposure to ivermectin. These differences in hyperpigmentation phenotype penetrance could formally be due to

differences in expression levels, as we could not verify that in every embryo injected with the NBT-promoter driven there was strong expression across the entire central nervous system. However, in our hands, the overall expression levels from each of these promoters were quite comparable. Another possibility, that the difference in number of cells expressing the neural vs. muscle promoter is what accounts for the different penetrance of phenotype, is probably unlikely since we have previously shown that very few depolarized instructor cells are needed to trigger the animal-wide hyperpigmentation phenotype [468].

Importantly, the depolarized muscle cells that induce hyperpigmentation are themselves being altered while signaling to the melanocytes. Here, we demonstrate for the first time, how driving the specific depolarization of muscle cells during development leads to their partial reprogramming *in vivo*. While these cells driving the pCar promoter are normally found in muscle-specific regions of the developing *Xenopus* tadpole (Figure 5.4C), selective depolarization caused them to take up residence in the neural tube (Figure 5.4B, 5.4H, 5.5C) – a highly abnormal location for muscle cells. These ectopic cells only express one muscle marker at a time of the pair tested (pCAR and 12/101) (Figure 5.4H,H'), and do not express the neural-specific marker acetylated alpha-tubulin (Figure 5.5C, C'). These ectopic cells also have a modest effect on the ability of tadpoles in learning studies, as it takes embryos subjected muscle-specific depolarization one extra training period to learn to avoid red light (Figure S5.2A). While there was no significant difference in the behavior of these tadpoles from control tadpoles that had been treated with low doses of ivermectin alone, it is important to note that there is an increase in variance of recall performance between the injected and treated tadpoles, suggesting that a subset of tadpoles were indeed affected by the presence of ectopic cells in neural

regions.

The cells migrating into the neural tube may be partially reprogrammed into an intermediate cell type, or may result from the migration of a non-fully differentiated cell that has already committed to the muscle lineage. The latter alternative suggests that only non-differentiated cells are targeted for depolarization. Neural beta-tubulin is expressed exclusively in differentiated neurons in *Xenopus*, whereas cardiac actin in the embryo is expressed in the myotomes, which will later become muscles. Therefore, what may be occurring in injected and treated embryos is a change in migration of cells that have committed enough towards muscle lineage that by the time they migrate into the neural tube, they can no longer become neural. These migrating cells are removed from the regular muscular environment and so no longer commit to muscle, while the rest of the cells in the somites carry on down muscular differentiation pathways. This may explain the difference in penetrance of the two Tol2 constructs; one is expressed in a differentiated environment whereas the other is in a precursor cell that is committed to a certain pathway but has not yet terminally differentiated.

The ultimate fate of these misplaced muscle cells remains unknown, as tracking these cells at late stages has proven to be difficult due to progressive disappearance of the GFP protein with developmental time. Future work will seek to determine whether these cells move to the neural tube from an initially normal location or whether existing neural tube cells become more muscle-like. While *in vivo* cell motility data are not yet available, we favor the former hypothesis because of the unchanged total number of pCAR<sup>+</sup> cells in depolarized embryos.

In normal development, embryonic stem cells gradually progress from a multipotent state, capable of generating all cell types, to a highly restricted state

by sequential restriction of differentiation potential [480]. These differentiation processes have been shown to be subject to manipulation from various signaling cues, such as transcription factor expression [481, 482] but have also been shown to be directed by bioelectrical events [48, 483, 484]. While much of this work has been done *in vitro*, our data suggest that *in vivo* depolarization can also affect cell fate determination. The depolarization of cells in which gene expression is driven by the cardiac actin promoter (i.e. specific to muscle tissue) results in these cells no longer being confined to the segmented blocks of mesoderm destined to become muscle (i.e. the somites), but rather in the ectodermal region of the neural tube. This suggests that bioelectric state may be an important component of proper germ cell layer specification events that occur during gastrulation in the developing frog embryo.

It is now clear that the misregulation of stem cell fate and division is also an important component of cancer [485]. Given its characteristic morphogenetic derangement, cancer can also be thought of as a developmental disorder [165, 486], and the *Xenopus* tadpole system is an ideal model for understanding this interplay between normal developmental signals and those as manifest as cancer. Perturbations that induce metastatic-like phenotypes during development may provide great insight into the signals that create cancer stem cells. We see here that in addition to observations of the main properties of metastasis (overproliferation, cell shape change promoting invasion, and ectopic colonization) seen in altered melanocytes, overall muscle structure is also affected (Figure 1). Interestingly, despite this subtle deficiency, tadpoles with depolarized instructor cells appear to have no gross anatomical defects. However, future work with animals with other fluorescently-labeled cell types or with more detailed marker analysis in sections may reveal additional cell

populations that respond to bioelectric changes in instructor cells. Of course, the search for new instructor cells (demarcated by other characteristic ion channels through which they can be selectively depolarized) is another active area of research.

Taken together, these studies reveal how changes in  $V_{\text{mem}}$  can function in the morphogenetic regulation of both melanocytes and muscle cells, relevant not only to developmental patterning but also to cancer. Hopefully, a better understanding of how these bioelectrical signals function together with the well studied molecular and biochemical pathways will provide insights to several branches of biomedicine.

### **Acknowledgements**

We thank Amanda Allen and Erin Switzer for general lab assistance and frog husbandry, Gufa Lin for the CarPr-GFP transgenic frogs [487], Joan Lemire for molecular biology assistance, Doug Blackiston for behavior testing assistance, and the members of the Levin lab and the bioelectricity community for many useful discussions. We thank Doug Blackiston, Gary McDowell, and Joan Lemire for comments on a draft of the manuscript. We gratefully acknowledge the support of AHA (14IRG18570000), (DARPA #W911NF-11-2-0054), NIH (AR061988; AR00559I), The G. Harold and Leila Y. Mathers Charitable Foundation and the W.M. Keck Foundation.

## **Materials & methods**

### ***Animal Husbandry***

*Xenopus* embryos were maintained according to standard protocols (Sive *et al*, 2000) in 0.1× Modified Marc's Ringers (MMR), pH 7.8. *Xenopus* embryos were staged according to Nieuwkoop and Faber (Nieuwkoop and Faber, 1994).

Transgenic *Xenopus laevis* embryos were prepared by Gufa Lin using plasmids from Enrique Amaya. Animal handling conducted in accordance with protocol M2014-79.

### ***Microinjection***

Capped, synthetic mRNAs were dissolved in water and injected into embryos at cleavage stages in 3% Ficoll using standard methods (Sive *et al* 2000). mRNA injections were made into specific locations using borosilicate glass needles calibrated to bubble pressures of 50–70 kPa in water, delivering 50-70 ms pulses. After 30 min, embryos were washed and cultured in 0.1X MMR until desired stages. eGFP-TPC3 construct was received from Chunlei Cang [470] and subcloned into PCS2 for the synthesis of messenger RNA. Other constructs used included Tol2-CarPr-GFP3, Tol2-CarPr-GlyR-A288G-GFP3 (in which human GlyR-A288G [412, 468] was inserted into Tol2-CarPr-GFP3), Tol2-NBT2-GlyR-A288G-tomto (made by replacing GFP3 in Tol2-NBT2-GFP3 [488] with GlyR-A288G-tomato). Cardiac actin promoter and neural tubulin promoters were the same as those used for transgenic frogs. Tol2 constructs were injected as DNA following the same protocol used for mRNA injections.

### ***Drug exposure***

Stocks of ivermectin (Sigma) were stored at 10 mM concentration in dimethyl

sulfoxide (DMSO). Embryos were exposed in 0.1 X MMR from pre-neurulation (NF stage 10) to tadpole stage (NF stage 45) to ivermectin, 1  $\mu$ M or 0.05  $\mu$ M, or fluoxetine, 10  $\mu$ M.

### ***Immunohistochemistry***

*Xenopus* embryos were collected and fixed in MEMFA [100 mM 3-(N morpholino) propanesulfonic acid (pH 7.4), 2 mM ethylene glycol tetraacetic acid, 1 mM MgSO<sub>4</sub>, 3.7 % (v/v) formaldehyde] at tailbud stage (NF stage 28/29) for 1 hr (Sive et al., 2000), washed twice in phosphate buffered saline Tween-20 (PBST), embedded into Agarose and sectioned at 200  $\mu$ m using a vibratome (Leica VT1000S) according to previously described protocols [31]. Samples were then blocked with 10% normal goat serum in PBST for 1 hr at room temperature. Samples were rocked overnight at 4°C using the following antibodies: Anti-GFP (AbCam AB290, used at 1:500 dilution), 12/101 (DHSB, concentrate used at 1:100) and Anti-acetylated alpha tubulin (Sigma T7451 used at 1:500 dilution) antibodies were used for immunohistochemistry using previously described protocols (Levin, 2004). Following primary exposure, samples were washed three times in PBST before a 60-min secondary incubation with either AlexaFluor-555 or AlexaFluor-488 conjugated secondary used at 1:1000 diluted in PBST. Following secondary incubation, samples were washed three times for 15 min in PBST and imaged on an Olympus BX-61 microscope.

### ***Birefringence Imaging & Analysis***

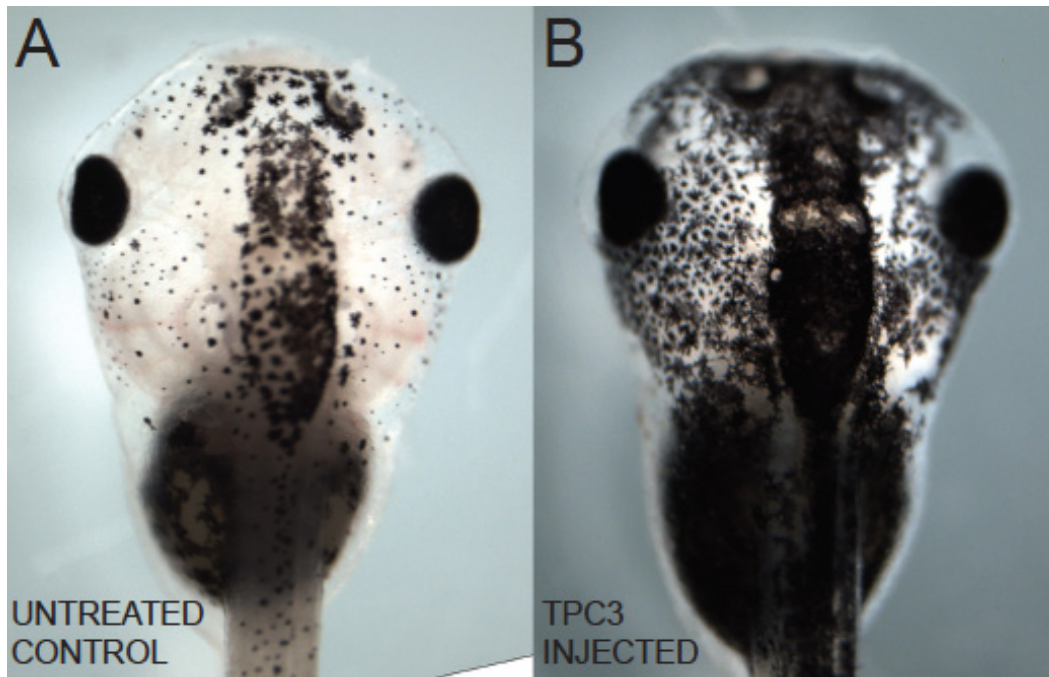
Birefringence microscopy was performed on an Olympus BX-61 compound microscope with a universal condenser (U-UCD8). The transmitted light DIC slider (U-DICTS) was pulled out and the polarizing filter was rotated such the background appeared darkest. Embryo tails were positioned at a 45° angle for

imaging. Analysis of birefringence images was performed in ImageJ. The mean grey value of each tail section was calculated, and normalized to tail fragment size.

### ***Behavior Testing***

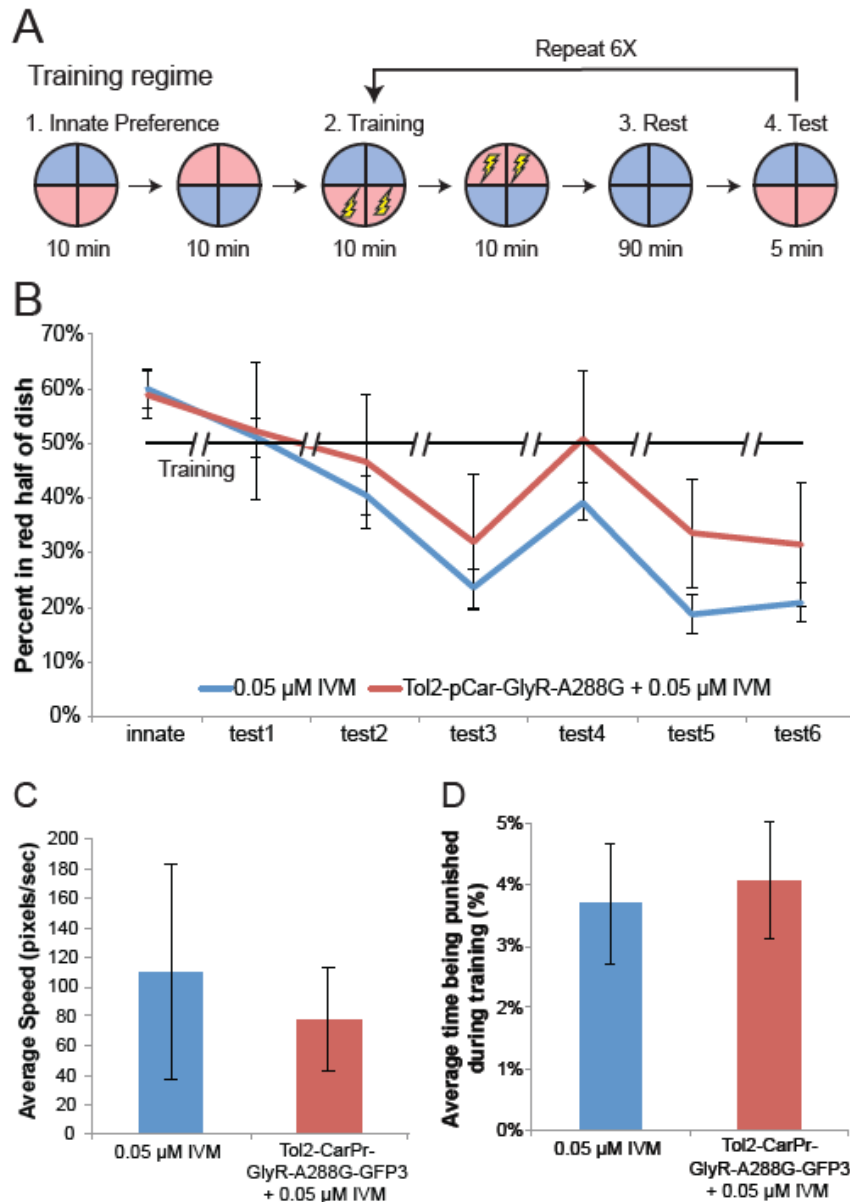
Behavioral testing was conducted using an automated training apparatus that has been documented previously [477, 489]. The overall structure of the device includes a rectangular array of cells, each with a disposable Petri dish in the field of vision of a machine vision camera (Insight-Micro 1400, Cognex Corporation, Natick, MA, USA). Each Petri dish housed a single animal that can be subjected to a series of individual conditions, with external illumination of each dish provided by red and/or blue LEDs (Osram Semiconductors, Sunnyvale, CA, USA; blue LED, 470 nm, part no. LBW5SM; red LED, 635 nm, part no. LRG6SP) housed in an illumination control module (ICM). In this device, illumination is delivered from above the experimental environment and can vary both by quadrant and intensity, ranging between maximum or off in fifteen even steps. Within each cell is also a set of six iridium oxide-coated titanium electrodes, allowing the delivery of mild to strong electric shocks. All shocks delivered during light-mediated training experiments were 1.2 mA AC currents, pulsed for 100 ms, followed by 300 ms of no shock. Computer-controlled software executed an experiment autonomously, recording the animal's position and speed in the dish, as well as changing lighting conditions or delivering shock as a result of time and/or behavior criteria specified in the training paradigm. All positional data during each trial were written to a log file, which was parsed and analyzed in Excel over discrete time blocks.

**Supplementary material**



**Supplemental Figure 5.1. Injection of depolarizing TPC3 channel induces embryo-wide hyperpigmentation.**

Embryos were either treated with 1 $\mu$ M ivermectin at NF stage 10 or injected with the depolarizing sodium ion channel, TPC3 into one cell of a two-cell stage (NF stage 2) embryo. Treated embryos were incubated to allow development to free-swimming tadpole stage and scored for hyperpigmentation (A). Depolarizing injections resulted in observation of the hyperpigmentation phenotype (C), compared to control phenotype (B).



**Supplemental Figure 5.2. Tadpoles with mislocalized muscle cells in neural regions can learn associated stimulus avoidance in an automated assay.**

Embryos that were either injected with Tol2-CarPr-GlyR-A288G-GFP3 and treated with 0.05  $\mu$ M ivermectin at NF stage 10 or uninjected and treated with 0.05  $\mu$ M ivermectin were placed individually into the behavior apparatus, and the automated software executed a training cycle (A). Prior to training, all animals displayed a slight preference for the red side of the dish; however, by two trainings the uninjected animals displayed a significant aversion to red light (B). Injected and treated embryos displayed a significant aversion to red light following three trainings. There was no significant difference in average speed in both treatments (C). During the training periods, when tadpoles are punished for occupying red halves of the arena, embryos from both treatments spent similar time in punishing areas (D). Error bars indicate  $\pm 1$  S.E.M. N=12 for both treatment types.

## Chapter 6

### **Serotonergic regulation of metastatic potential in melanocytes: a bioelectric network explains all-or-none stochastic hyperpigmentation**

Maria Lobikin, Daniel Lobo, Douglas J. Blackiston, Christopher Martyniuk, Elizabeth Tkachenko, and Michael Levin

Submitted to Science Signaling (2015)

**Data contributions:** I contributed data to figures 6.1, 6.3, 6.5, 6.6, supplemental figures S6.1, S6.3 and supplemental tables S6.1 and S6.2. Daniel Lobo contributed data to figures 6.5, 6.6, 6.7, and supplemental figure S6.2. Doug Blackiston contributed data to figure 6.2, Chris Martyniuk contributed data to figure 6.4 and supplemental table S6.3. Elizabeth Tkachenko contributed data to figure 6.3.

## Abstract

Depolarization of resting membrane potential in select cells in *Xenopus* larvae induces normal melanocytes to undergo a conversion to a metastatic phenotype. Here, we show that this non-cell-autonomous process is mediated by cAMP, CREB, and the transcription factors Sox10 and Slug, which have been previously shown to be implicated in various cancers, including melanoma. Our microarray analysis reveals specific transcripts responsive to  $V_{\text{mem}}$  levels within a few hours of depolarization, and a set of 517 transcripts whose expression remains altered during the full hyperpigmented phenotype over a week later, linking instructor cell-depolarization to a range of developmental processes and disease states. We also show that voltage-dependent conversion of melanocytes involves the MSH-secreting melanotrope cells of the pituitary, and formulate a model for the molecular pathway linking the bioelectric properties of melanocyte cells' microenvironment *in vivo* to the genetic and cellular changes induced in this melanoma-like phenotype. Remarkably, the phenotype is all-or-none: each individual animal either undergoes melanocyte conversion or not, as a whole. This group decision is stochastic, resulting in varying percentages of hyperpigmented individuals for a given experimental treatment. To explain the observed stochasticity as an inherent dynamic property of this complex signaling system, we developed a novel computational method that reverse-engineered a dynamic regulatory network that quantitatively explained our complex dataset, and made correct predictions for new experiments. Taken together, these data (1) reveal new molecular details about a novel trigger of metastatic cell behavior *in vivo*, (2) suggest new targets for biomedical intervention, and (3) demonstrate proof-of-principle of a computational method for understanding stochastic decision-making by cells during development and cancer.

## Introduction

In addition to well-characterized biochemical and genetic pathways coordinating cell-to cell communication and large-scale pattern-formation processes, there exists an important and powerful signaling system functioning through bioelectrical mechanisms. Slowly-changing endogenous ion currents, voltage gradients, and electric fields serve instructive roles in the signaling pathways that control cell proliferation [6, 84], differentiation [48, 490, 491], and migration [31, 492]. Mounting functional evidence suggests that spatio-temporal gradients of transmembrane potential ( $V_{mem}$ ) may be a key regulating-component of many patterning processes during embryogenesis and regeneration [349, 493-496]. Importantly, bioelectric signaling is also increasingly implicated in cancer biology [390, 497-499], via the recognition of ion channels as both oncogenes [500-502] and as cancer drug targets [403, 503, 504], as well as the identification of specific bioelectrical states with neoplastic transformation and tumor prevention [299, 343, 432, 505].

Recently, we showed that forced hyperpolarization can suppress oncogene-mediated tumorigenesis despite the strong continued presence of the oncogene [505, 506]. In order to better understand the role of endogenous bioelectrical patterning mechanisms in cancer, we utilize the *Xenopus laevis* embryonic model, which provides an ideal system in which biophysical cues, molecular-genetic signaling, and cell-tissue outcomes can be readily studied. In past work, we showed that specific depolarization can non-cell autonomously induce increased melanocyte invasiveness and proliferation in the absence of DNA damage, oncogenic mutation, or carcinogen exposure [31, 33, 468]. Tadpoles in which an instructor cell population was depolarized acquired a hyperpigmented phenotype: the melanocytes over-proliferated, acquired an

arborized cell shape, and drastically invaded all the other organs. The instructor cells are characterized by their expression of the glycine-gated chloride channel (which provides a convenient method for altering their  $V_{\text{mem}}$ ), are present throughout the body, and are able to induce otherwise normal melanocytes to acquire three basic hallmarks of metastatic cells: overgrowth, cell shape change, and invasiveness.

$V_{\text{mem}}$  depolarization is transduced into cell behavior changes by a serotonin-dependent mechanism, involving a complex interplay of several serotonin receptors, the serotonin transporter SERT, and the vesicular monoamine transporter, VMAT [31, 468]. These findings implicated biophysical properties of the plasma membrane and identified extracellular ion flows and serotonergic signaling as potential novel control points for biomedical intervention in melanoma and other pigmentation disorders [507, 508]. Thus, it is important to better understand the downstream signaling mechanisms mediating the transforming effects of this novel aspect of the microenvironment [509-512]. Here, we address a number of open questions concerning the bioelectrical induction of metastatic behavior. We show that depolarization of instructor cells signals to melanocytes via canonical cascades involving cyclic adenosine monophosphate (cAMP) production, the cAMP response binding element (CREB)-mediated transcriptional activation, and the transcription factors Sox10 and Slug, all of which have been previously shown to be implicated in various cancers, including melanoma [513-518]

One of our goals is to understand fundamental principles of developmental cell:cell signaling via biophysical events, including morphogenetic cues that keep cells away from carcinogenesis *in vivo*. Probing further into the long-range nature of such signaling, in which depolarization of instructor cells

activates an entirely distinct cell population (melanocytes) at a distance, we also show that voltage-based conversion is mediated by the melanocyte stimulating hormone (MSH)-secreting melanotrope cells of the pituitary. To uncover novel targets of this depolarization, we performed a genome-wide analysis of transcriptional changes downstream of instructor cell depolarization, which revealed numerous similarities to known cancer pathways. Finally, we used an automated computational approach to derive the first predictive stochastic dynamic network model explaining the most puzzling aspects of this phenotype: the stochastic phenotype penetrance of each condition among a treated population. Taken together, these data fill in important knowledge gaps in our understanding of the molecular steps by which voltage change in specific cell populations can drastically affect the behavior of other cell types. The computational approach taken here is a proof-of-principle of using artificial intelligence techniques to assist human scientists to derive quantitatively-predictive models of complex functional datasets with surprising dynamics such as stochastic decision-making by cell populations.

## **Results**

### ***Ivermectin-induced instructor cell signaling is mediated by cAMP, PKA, and CREB***

The exact same hyperpigmentation phenotype can be induced by any genetic or pharmacological method that depolarizes instructor cells (e.g., via sodium channels), and can be blocked (rescued) by potassium or proton-mediated strong hyperpolarization, confirming that the effect depends on voltage itself, not on off-target effects of ivermectin or any chloride-specific signaling. For these

studies, we used ivermectin as the simplest way to depolarize instructor cells. In *Xenopus laevis* medium (0.1X MMR), this specific and irreversible glycine-gated chloride channel (GlyR, also known as GlyCl) opener results in the exit of chloride ions from the GlyR-expressing instructor cells depolarizing them [31, 519]. The readout in all of the pathway experiments below was percent hyperpigmentation (Figure 6.1A, A'), i.e., what percent of the experimental population became hyperpigmented. Each individual animal either converts entirely or does not – we observed no cases of partial phenotype, and animals were scored as either being hyperpigmented or not, for calculation of penetrance of each treatment. Careful inspection of morphology, behavior, and survival indicated no overt toxicity or teratogenesis, as in prior studies [31].

The induction of hyperpigmentation requires the serotonin receptors 5HT-R1, 5HT-R2, and 5HT-R5 [31, 468]. Most serotonin receptors are coupled to G-proteins, and signal through either the second messenger systems of adenylyl cyclase (AC) and cyclic adenosine monophosphate (cAMP) or phospholipase C (PLC). Since both R1 and R5 are inhibitory G-coupled protein receptors, and increasing evidence suggests that cAMP signaling plays a role in melanoma [518], we sought to examine whether the cAMP signaling cascade was necessary for the depolarization of instructor cells to induce changes in melanocyte behavior.

Using the same suppression screen strategy previously employed to dissect transduction machinery [31, 468, 469], individual inhibitors of the cAMP signaling process were used together alongside ivermectin treatment to investigate whether this inhibition could suppress depolarization-induced hyperpigmentation. Treatment with the potent cell-permeable cAMP antagonist 2'5'-dideoxyadenosine alongside the depolarizing agent ivermectin reduced the

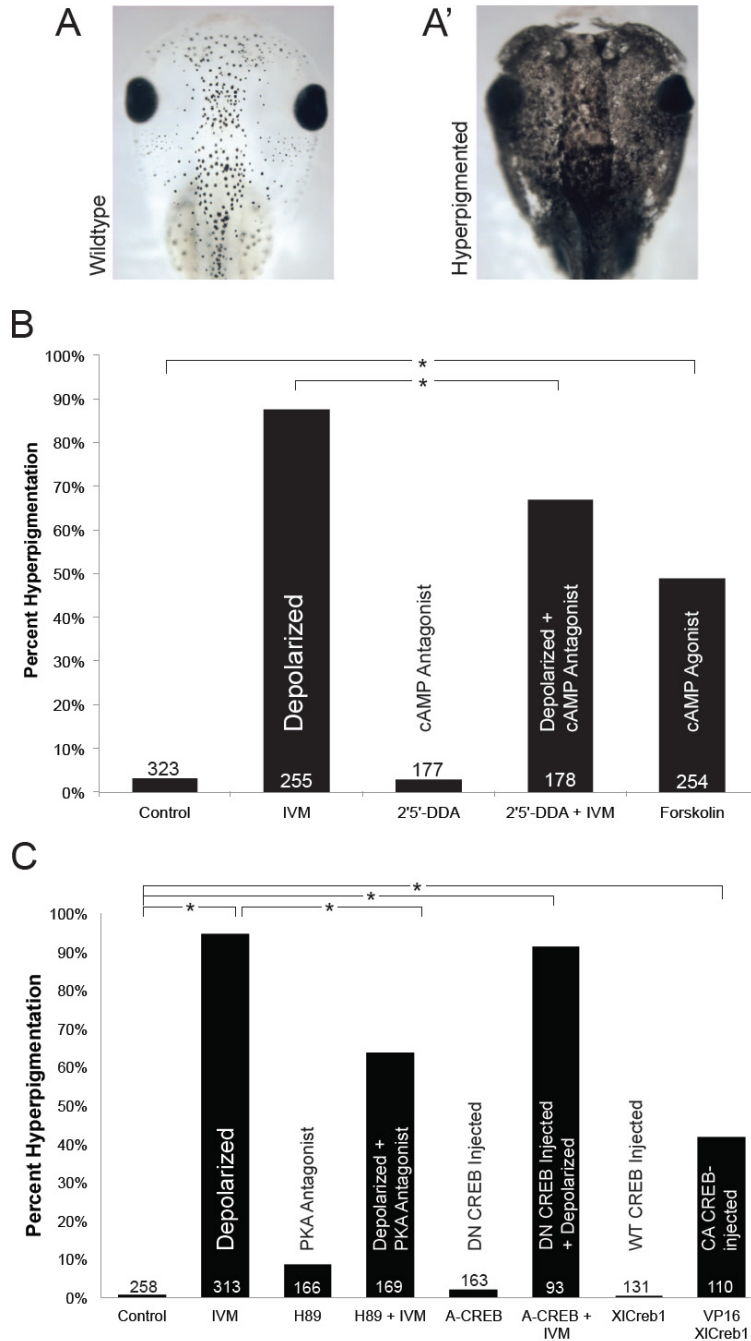


**Figure 6.1. Cyclic AMP (cAMP) and cAMP response mediating protein (CREB) are involved in mediating instructor cell signaling**

Frogs treated with pharmacological agents at NF Stage 10 are scored for pigmentation phenotypes (either wildtype, A, or hyperpigmented, A'). B) A schematic of intracellular signaling downstream of 5HT. Adenylyl cyclase activity is regulated by G-protein receptors (R). Binding to Gs (stimulatory G-protein) increases cAMP by activating adenylyl cyclase which then activates PKA (cAMP stimulated protein kinase), resulting in nuclear translocation of PKA. In the nucleus, PKA phosphorylates the transcription factor CREB resulting in

transcriptional activation of CREB target genes. Activation of Gi proteins (inhibitory G-proteins) decreases cAMP (through adenylyl cyclase inhibition). C) Treatment of NF stage 10 *Xenopus* embryos with the cAMP antagonist, 2'5'-Dideoxyadenosine (2'5'-DDA) alongside depolarizing ivermectin significantly decreases the percent of depolarization-induced hyperpigmentation, while treatment of 2'5'-DDA alone has no effect on hyperpigmentation. Treatment of embryos with the cAMP antagonist forskolin results in a significant increase in percent of hyperpigmentation. D) Treatment of NF Stage 10 embryos with the PKA antagonist, H89, significantly decreased levels of hyperpigmentation when used in conjunction with depolarizing ivermectin. Embryos that had been injected at the 1/4-cell stage with either dominant negative CREB (ACREB) or wild type CREB (XICreb1) had no hyperpigmented phenotype, while injection of the constitutively active CREB (VP16 XICreb1) resulted in significantly increased levels of hyperpigmentation.

incidence of hyperpigmentation by 20% (87% hyperpigmented with 1  $\mu$ M ivermectin alone, 67% hyperpigmented with 500  $\mu$ M 2'5'-Dideoxyadenoside and ivermectin; Figure 6.1B). In order to confirm the involvement of cAMP, ivermectin-treated embryos were exposed to the potent cAMP agonist, Forskolin. Exposure alone (without depolarizing reagent) led to significant levels of hyperpigmentation (49%, N=254,  $p < 0.01$ ; Figure 6.1B). These results suggest the involvement of cAMP in  $V_{mem}$ -induced changes in melanocyte behavior.

Changes in intercellular cAMP levels are known to regulate the activity of the cAMP-dependent protein kinase A (PKA). PKA has been implicated in many cellular processes including proliferation, ion transport, regulation of metabolism, and gene transcription and has been proposed as a cancer therapeutic target [520-524]. To determine whether PKA was involved in the signal transduction from instructor cell depolarization to changes in melanocyte behavior, *Xenopus* embryos were subjected to depolarizing ivermectin treatment alongside treatment with the PKA antagonist H89 dihydrochloride. This resulted in a 31% reduction in the incidence of hyperpigmentation (from 94.9%, N=313 in ivermectin-treated embryos, to 63.9%, N=169 in embryos treated with ivermectin and H89; Figure 6.1C), suggesting that PKA is involved in this signaling process.

A proposed method by which this cAMP and PKA signaling can be translated into changes in gene transcription levels is through the cAMP response element binding protein (CREB). Upon activation, PKA is able to translocate to the nucleus and trigger phosphorylation of Ser133 in CREB, thus activating CREB. CREB is a member of a leucine zipper class of transcription factors with binding sites found within the promoter and enhancer regions of hundreds of genes [525]. To address whether CREB is involved in mediating the hyperpigmentation phenotype in *Xenopus*, synthetic mRNAs encoding either

wildtype CREB (XICreb1), dominant negative CREB (A-CREB, [526]) or a constitutively active version of CREB (VP16-XICreb1, [527]) were injected into NF stage 5 (32-cell) embryos using standard methods [122]. While injection of excess wild-type CREB mRNA had no effect, introduction of the constitutively active CREB into developing embryos resulted in hyperpigmentation in 41.8% of embryos injected (N=110; Figure 6.1C). Surprisingly, injection of the dominant negative inhibitor of CREB (A-CREB) into 1 cell of NF stage 5 embryo, had no significant effect on hyperpigmentation rate (alone or with ivermectin, Figure 6.1D), similar to N-methyl-D- CREB signaling which is sensitive to gain-of-function approaches, but resistant to CREB inhibition [528]. Taken together, these results implicate the involvement of a cAMP-PKA-CREB pathway in transducing the depolarization of instructor cells into an embryo-wide change in melanocyte regulation.

***Hyperpigmentation phenotype is mediated by the involvement of the intermediate pituitary***

Melanocytes themselves do not express GlyR [529]. Given the long-range signaling [31, 468] between the depolarized instructor cell population, which is sparse, yet widely distributed throughout the entire embryo, and the responding neural crest-derived melanocytes, which can be many cell lengths away, we wanted to determine whether there were any other cells involved in this signaling process. This was especially suggested by the observation (data not shown) that in batches of animals treated with ivermectin, the only ones that would not hyperpigment would be the rare spontaneous individuals with narrow heads (midline defects). Two possible regions we suspected as necessary for instructor cell signaling were the *Xenopus* pineal and pituitary glands. The pineal gland

regulates circadian rhythms and hormone production [530], and is associated with the photoreceptive pineal eye, which produces and releases the serotonin derivative, melatonin, in response to darkness [531]. It was previously demonstrated that melanocytes in hyperpigmented embryos avoid colonizing the region below the pineal eye [31], suggesting the cells in this area may be responsible for mediating instructor cell signaling. The intermediate pituitary is home to melanotrope cells that secrete alpha melanocyte stimulating hormone ( $\alpha$ MSH), which, in turn, is known to modulate the melanin granule dispersion in *Xenopus* [532]. Thus, it was hypothesized that instructor cell signaling may function through these two regions.

In order to investigate the relation of the pineal and pituitary to depolarization-induced hyperpigmentation, each of these regions was individually dissected out of tail bud-stage (NF stage 32) embryos that had been treated with ivermectin from neurula-stage (NF stage 10) onwards. These cuts were performed on embryos prior to the first melanocytes developing at NF stage 33/34. Cuts removed either the pineal area, a section containing the pituitary, or a control cut below the cement gland and away from either of these areas (Figure 6.2A,B,B',B''). The embryos were then reared to free-swimming tadpole stage and scored for hyperpigmentation. These dissections revealed that removing the pineal gland had no significant effect on ivermectin-mediated hyperpigmentation, while removing the pituitary decreased hyperpigmentation rates by nearly 50% (Figure 6.2C,D''). These results suggest that signaling driving hyperpigmentation is mediated by the intermediate pituitary and reveals that depolarization-induced metastatic signaling can be interrupted until at least stage 32.

In order to confirm the involvement of  $\alpha$ MSH in the hyperpigmentation phenotype, *Xenopus* embryos were exposed to  $\alpha$ MSH agonists and antagonists.

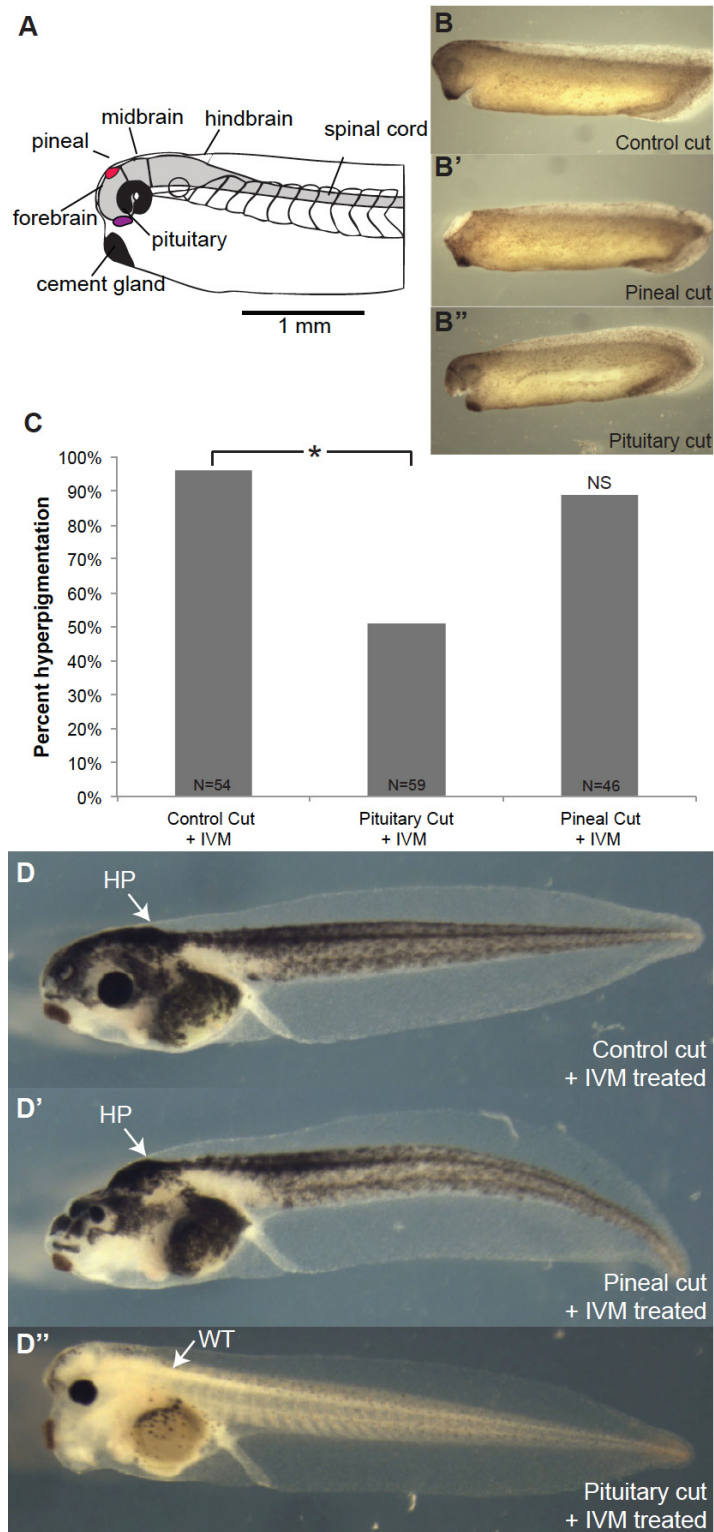


**Figure 6.2. The pituitary gland is necessary for ivermectin-mediated hyperpigmentation.**

A) Side view showing main regions of *Xenopus* tadpole brain. B) *Xenopus* embryos were treated with ivermectin from neurula stage (NF Stage 10), cut at

tailbud stage (NF Stage 32), raised to tadpole stage (NF Stage 45), and scored for hyperpigmentation. Cuts were performed on tailbud stage (NF Stage 32) removing the pineal gland, pituitary gland, or a control region below the cement gland and away from both the pituitary and pineal. C) Control cuts and pineal cuts both failed to suppress ivermectin-mediated hyperpigmentation, while pineal cuts significantly reduced the percent of hyperpigmented tadpoles. D) Resulting phenotypes of ivermectin-treated embryos that had undergone either control (D), pineal (D') or pituitary (D'') cuts.

As predicted, embryos exposed to the potent  $\alpha$ MSH agonist SHU 9119 from neurula to tadpoles stages developed a hyperpigmented phenotype 93.6% of the time (similar to the potency of depolarizing ivermectin treatment, Figure S6.1). Embryos treated with  $\alpha$ MSH-release inhibiting factor (MSH-RIF) together with depolarizing ivermectin treatment, displayed 32.5% less hyperpigmentation than when treated with ivermectin alone.

To determine whether serotonin signaling and  $\alpha$ MSH-involvement were part of the same pathway, we performed epistasis experiments with a combination of  $\alpha$ MSH and 5HT drugs. Both MSH-RIF and the serotonin receptor 2 (5HT-R2) antagonist, altanserin, significantly decreased ivermectin-induced depolarization on their own (Figure S6.1). If these two pathways (5HT and MSH) had two distinct roles in the hyperpigmentation signaling pathway, we would expect to see additive effects of combining MSH-RIF and altanserin with ivermectin treatment. Instead, the combination of all three pharmacological agents (Ivermectin + MSH-RIF + altanserin) failed to significantly reduce hyperpigmentation levels (Figure S6.1). Based on the epistasis analysis, we conclude that both serotonin and  $\alpha$ MSH-signaling are part of the same signaling pathway.

### ***Instructor cell depolarization results in transient upregulation of Sox10 expression***

Previous work demonstrated that depolarization of specific regions of developing embryos by misexpression of depolarizing ion channels results in the local upregulation of several important transcription factors [33]. Specifically, the region of depolarizing mRNA injection exhibits ectopic induction of *Sox10* (key in neural crest progenitor specification to the melanocyte lineage [533], Figure

6.3A), which has recently been shown to be involved in melanoma invasion [514]), and *Slug* (a member of the SNAIL family of transcription factors important in the epithelial to mesenchymal transition in neural crest cells and implicated with tumor metastasis [516, 534]). However, unlike mRNA injection into an early blastomere, ivermectin depolarizes a very sparse, widely distributed cell population. Under those conditions, would cells also up-regulate these key transcription factors and, if so, in what geometrical arrangement?

Initial surveys via *in situ* hybridization done on stage 25 embryos treated with ivermectin from neurula stage onwards failed to detect distributed upregulation of either transcription factor (data not shown). However, *in situ* hybridization is not quantitative and makes it difficult to detect widespread, small regions of ectopic up-regulation. We therefore quantified transcription factor expression by quantitative RT-PCR (qPCR). qPCR performed on tail bud stage embryos revealed that both Sox10 and Slug were up-regulated more than 2-fold following instructor cell depolarization and confirmed that injection of XminK (a depolarizing potassium channel subunit) resulted in a significant upregulation of expression of these transcription factors (Figure 6.3B).

To determine whether the time course of ectopic up-regulation was responsible for the lower than expected upregulation of Sox10, embryos treated with ivermectin at stage 10 were fixed at different stages and processed for qPCR. This analysis revealed that Sox10 expression was up-regulated very early after ivermectin exposure, and normalized to a steady state in later stages (Figure 6.3C). To determine the spatial profile of this strong upregulation, NF stage 15 embryos that had been treated with ivermectin were processed for *in situ* hybridization under optimized conditions, and sectioned. Compared to control embryos, in which Sox10 expression was limited to its endogenous

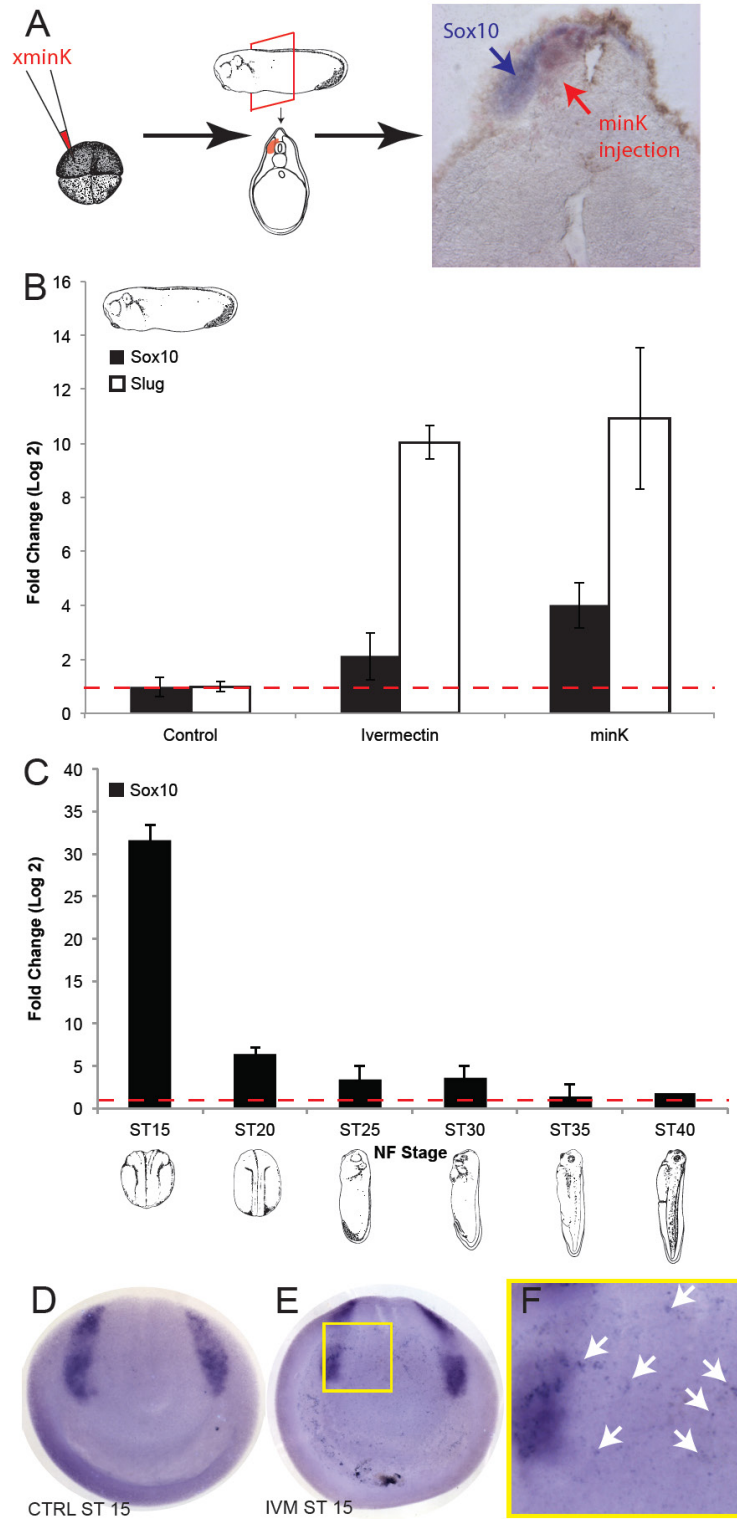


**Figure 6.3. Both concentrated and sparse, widely distributed depolarization results in upregulation of Sox10.**

A) Embryos injected with a mixture of XminK and  $\beta$ -gal mRNAs at the 4-cell stage were fixed at tailbud stages and processed for in situ hybridization for

Sox10 expression. Sections of these embryos revealed Sox10 overexpression near the region of depolarization. B) Qualitative PCR (qPCR) on tailbud stage embryos (NF Stage 25) confirmed XminK injection results in upregulation of Sox10 and Slug. qPCR also revealed that embryos subjected to ivermectin treatment from neurula stage (NF Stage 10) onwards resulted in significant upregulation of Sox10 and Slug compared to controls (red dashed line denotes no fold change). C) Embryos treated with ivermectin at neurula stage were collected at various stages, and processed for qPCR revealing that Sox10 overexpression is highest immediately following depolarization, and normalized at later stages. D-F) In situ hybridization for Sox10 performed on NF Stage 15 embryos confirmed that ivermectin treatment results in upregulation of Sox10 in a sparse, punctate pattern (F, compared to D).

domains of expression directly along the neural fold, depolarized embryos displayed ectopic Sox10 expression present in a punctate pattern throughout the embryo, reminiscent of the expression pattern for the GlyR-expressing instructor cells (Figure 6.3D-F, [31]). Moreover, while the endogenous Sox10 signal in controls is solid and thick, there are breaks in the band seen in IVM treated embryos, suggesting a reduction of signal. We conclude that, just as with contiguous regions ectopically depolarized, foci of abnormally low  $V_{\text{mem}}$  give rise to foci of ectopic, and loss of endogenous Sox10 expression soon after depolarization.

### ***The effect of instructor cell depolarization on overall gene expression***

Given the marked effects that instructor cell depolarization had on the expression of neural crest-specific transcription factors, and the current lack of knowledge about the genome-wide effects of selective cell depolarization during development, we asked what genes' steady state mRNA levels are increased or decreased following depolarization of instructor cells. To address this question, we collected whole embryos at early neurula (NF stage 15) and tadpole (NF stage 45) stages, and performed a differential microarray analysis using the Affymetrix *Xenopus* genome chip V2.0 comparing controls and embryos treated with ivermectin from stage 10. The gene expression of treated embryos was compared to stage-matched controls. Functional enrichment analysis for differentially expressed genes was then conducted using the GOrilla database [535] with *Homo sapiens* as the reference species.

We found that there were 45 gene probes differentially expressed (irrespective of the direction of change) by stage 15 and 517 gene probes differentially expressed in stage 45 embryos (Figure 6.4A). Three expressed

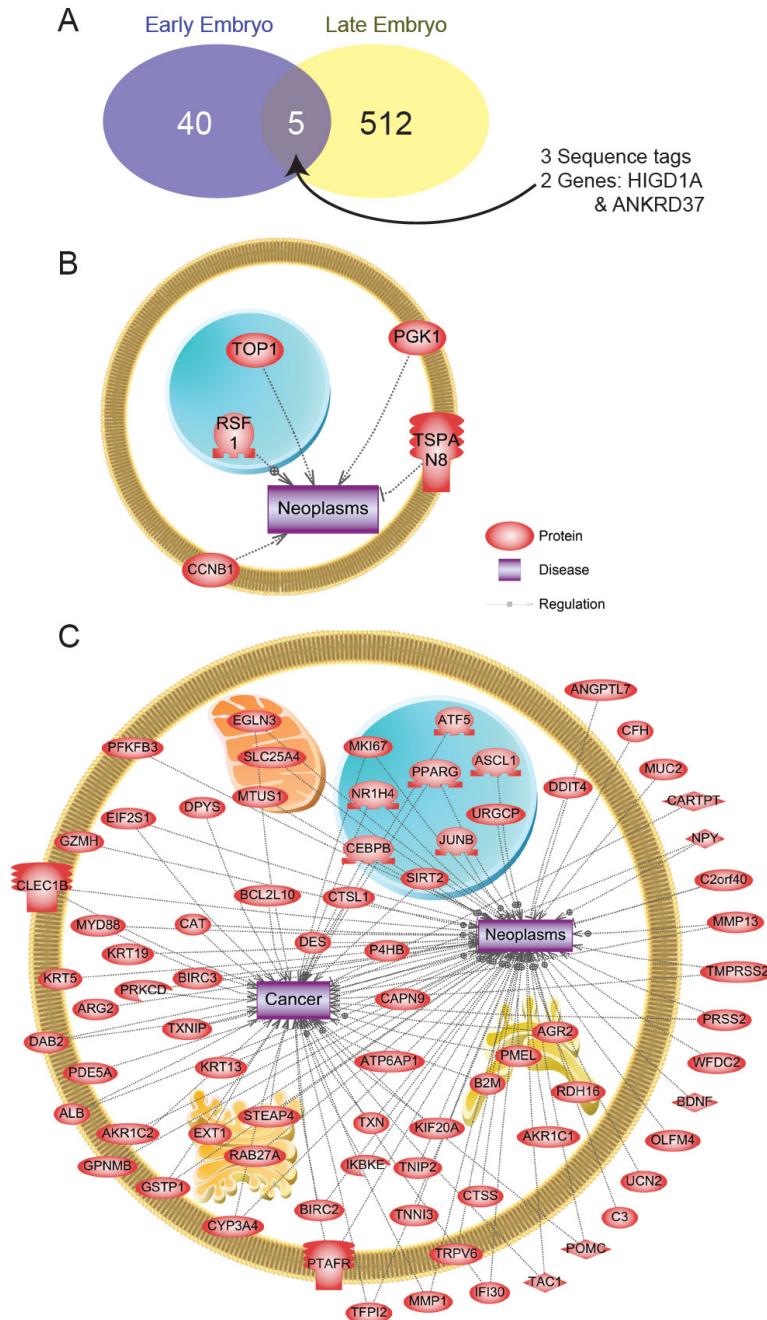


**Figure 6.4. Ivermectin-induced depolarization results in upregulation of neoplasm-related, and cancer-related genes at early and late stages, respectively.**

A) Microarray analysis on *Xenopus* tadpoles treated with ivermectin collected at early (NF Stage 15) and late (NF Stage 45) stages found 45 gene probes differentially expressed in the early embryos and 517 gene probes differentially expressed in the late-stage embryos. B) Pathway analysis revealed that 5 genes differentially expressed in the early embryo were related to neoplasms. C) In late-stage embryos, pathway analysis found 45 differentially expressed cancer-related genes.

sequence tags were found in common between the two developmental stages. However, two known genes were identified as differentially regulated in both the early and late stages. These two genes were *HIG1 hypoxia inducible domain family, member 1A* (2.4-fold increase in the early embryos, and a 4.5 fold increase in late embryos) and *ankyrin repeat domain 37* (2.9-fold increase in the early embryos, and 9-fold increase in the late embryos). There were too few genes differentially expressed in the early embryos for a functional enrichment analysis; nevertheless, our data show that some transcripts are altered in abundance by instructor cells' depolarization after only a few hours of depolarization, and remain altered for over 1 week.

Analysis of the altered transcripts at stage 45 (when the hyperpigmentation phenotype is strongly evident) revealed a number of processes enriched by depolarization (Table S6.2). GOrilla recognized 14,190 genes out of 17,337 gene terms entered and there were 5,587 duplicate genes removed, resulting in a total of 8,603 genes. Of these, 8,327 genes were associated with a gene ontology term(s) and served as the background list for functional enrichment. There were three major biological themes enriched in the late embryos: immune (e.g. regulation of complement activation, regulation of humoral immune response, protein activation cascade, innate immune response, and others), metabolism (e.g. carbohydrate biosynthetic process, monosaccharide biosynthetic process, gluconeogenesis, ATP hydrolysis coupled proton transport, and others), and ion regulation (e.g. regulation of pH, proton transport, cellular iron ion homeostasis, organic anion transport, among others).

Pathway analysis revealed that genes differentially expressed in the early embryos were involved in the cell processes of chromatin remodeling, apoptosis, cell differentiation, and mitosis. Importantly, diseases related to the differentially

expressed genes included cancer and neoplasms (Figure 4B). Based on the sub-network enrichment analysis (SNEA), 8.7% of genes (45 out of 517) differentially expressed in stage 45 embryos treated with ivermectin, were associated with cancer, consistent with the metastatic phenotype triggered by this depolarization [468, 529]. Sub-network enrichment analysis suggested that transcripts related to the cell process of cell differentiation and apoptosis and the diseases of “Neoplasms” were preferentially regulated in early embryos (Table S6.3). Pathway analysis also revealed that genes differentially expressed in the late embryos were involved in the cell processes of cell growth, immune response, morphogenesis, apoptosis, inflammatory response, and others. Based on the pathway analysis, diseases related to the differentially expressed genes included cancer, neoplasms, diabetes, and atherosclerosis among others (Figure 6.4C). Sub-network enrichment analysis suggested that transcripts related to NO biosynthesis, contractile activity, immunoreactivity, inflammatory response, glucose metabolism and oxidative stress were preferentially regulated in early embryos while diseases enriched in the late embryo dataset included cancer, neoplasms, hypertrophy, leukemia, neuron toxicity, and autoimmune diseases (Table S6.3). We conclude that depolarization of instructor cells induces transcriptional alterations in genes related to several disease states, including cancer.

### ***Modeling the bistable and stochastic response to embryo-wide depolarization***

Surprisingly, this hyperpigmentation phenotype is bistable; no animals were ever seen to be partially hyperpigmented. However, at a population level, the phenotype is stochastic in that many of our treatments produced less than

100% penetrance of the phenotype. This appears to be a kind of cellular group dynamic: the stochastic decision of whether or not to proceed to metastatic-like conversion is not made at the level of individual cells (which would give a salt-and-pepper outcome in each tadpole) but rather at the level of the entire organism which converts to hyperpigmentation or not, at some frequency, as a whole. In order to better understand this fascinating stochastic process, we undertook a computational modeling approach. Any successful model of this system would have to quantitatively reproduce the percentage of hyperpigmented tadpoles observed in each treatment; this phenotype is more complex than what can be accurately modeled by a typical induction/repression pathway schematic. However, the complex emergent dynamics required for the correct stochastic outcomes of a proposed molecular signaling pathway make it extremely difficult to develop a quantitative model that correctly predicts a rich dataset such as ours. This is a general issue for many biological phenotypes that include a stochastic component [536-538]. Thus, we developed an artificial intelligence method to assist human scientists in discovering complex networks with behavior that matches their stochastic dataset (Figure S6.2). The goal was to show a proof-of-principle of a system that assists human scientists to discover constructive models whose behavior matches a complex functional dataset.

We first formulated a set of necessary regulatory links, based on known interaction pathways, that comprises some of the key steps from depolarization through melanocyte activation and the in-between components, as suggested by the functional experiments in this and prior papers [468, 517, 525, 529, 539-541]. We then automated the task of assigning specific link parameters, new necessary connections, and yet-to-be-discovered nodes within this dynamic network such that, when simulated with specific starting conditions in our dataset,

the network exhibits a bistable and stochastic behavior, resulting in wild-type (“wt”) or “hyperpigmented” outputs with correct frequencies matching experimental data. This task amounts to the discovery of a fully-specified regulatory network whose behavior, when simulated given diverse experimental conditions, correctly predicts existing and future data.

Our automatic method works with dynamic signaling networks modeled as ordinary differential equations. Every element in the network is modeled according to its concentration value, whereas its dynamics include the interactions with other elements, a decay term, and a noise term. The first component of our system is a custom simulation engine able to simulate the same type of pharmacological experiments performed *in vivo*. This is a necessary advance over “arrow” diagrams since it forces all parameters to be specified and allows unambiguous testing of how well a given “model” of a pathway really explains the data. While our approach is general and can be applied to many problems in cell biology, the version reported here was used specifically to perform *in silico* experiments on virtual embryos in which the known, relevant signaling elements interact according to biochemically-plausible rules. The second component of the system provides candidate models to be thus tested, and is an artificial intelligence algorithm based on evolutionary computation [542].

The evolutionary algorithm maintains a population of signaling networks, including the initial set of fixed regulatory links in addition to new random links and random parameters. The algorithm adds periodically new networks to the population by crossing and mutating existing ones, using random operations for adding and deleting nodes and links and altering parameters. This allows the system to explore the enormous space of all possible models (usually traversed

by the intuition of the human experimenter), to identify networks with the correct stochastic behavior. Each network in the population receives a score by comparing the frequency of the phenotypes obtained during multiple simulations (N=100) for each of the experiments included in the training set with the frequencies obtained *in vivo* (see methods section). The networks with the best scores are kept in the population, while the worst networks are removed. This process of creating, evaluating, and replacing networks in the population and is iterated for a specific number of generations. After which, the best network in the population is then returned by the algorithm. This strategy leverages the power of evolution to uncover models with the desired dynamics and high predictive value.

We employed our method to search for a simple, human-readable dynamic signaling network that could explain the bistable and stochastic behavior described in a selection of pharmacological experiments (Figure 6.5). Remarkably, our process found a network model that recapitulates the bistability and stochasticity characteristic of the experiments *in vivo*. Figure 6.5B illustrates the dynamics of the model with three different treatments which show the same stochastic behavior as observed in our experiments *in vivo*. While an experiment with no treatment results in a hyperpigmented phenotype in 3% of the simulations, an experiment with a cyanopindolol treatment (repressor of 5HT-R1) results in the hyperpigmentation phenotype produced 32% of the simulations; combining IVM and cyanopindolol together, the model produces hyperpigmented phenotypes 89% of the simulations. These stochastic results match precisely within 10% with what is seen in the *in vivo* experiments. Crucially, the network also recapitulates the all-or-none dynamics of the hyperpigmented phenotype. All the simulations using any experimental treatment converge to a steady-state where the hyperpigmentation is complete (values close to 1) or non-existent

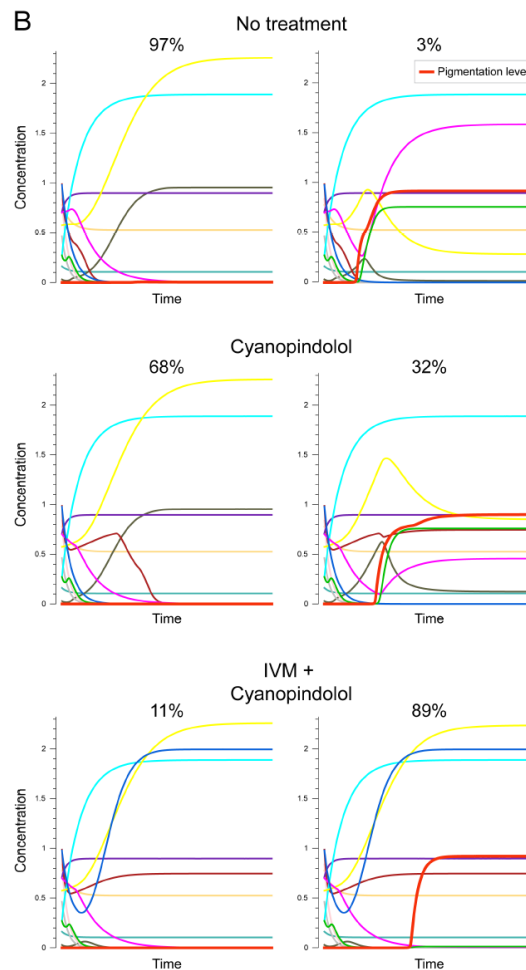
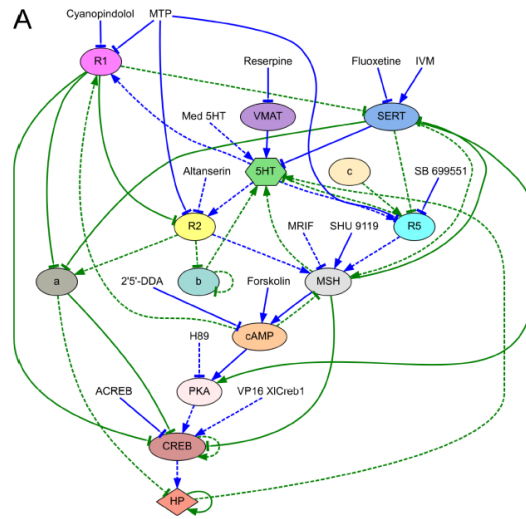


**Figure 6.5 Automatically discovered dynamic stochastic network.**  
 A) Starting with a basic network made of known components (named nodes and drugs) and pathways (blue links), the automatic algorithm found the unknown necessary components ('a'-'c' nodes) and pathways (green links), as well as all

the parameters in the dynamic system. B) Simulations show the stochastic and bistable dynamics of the network. While a no treatment assay results in 97% of simulations with no hyperpigmentation (pigmentation value of 0) and 3% with complete hyperpigmentation (pigmentation value of 1), the addition of cyanopindolol shifts the results to 68% of simulations with no hyperpigmentation, and 32% with hyperpigmentation. The combined effect of IVM together with cyanopindolol results in 11% of the simulations with no hyperpigmentation and 89% of simulations with hyperpigmentation..

(values close to 0); no simulation produces an intermediate pigmentation value, matching the surprising and heretofore unexplained all-or-none aspect of this phenotype *in vivo*. Indeed, this is an especially difficult feature to accommodate by hand-derived models.

The performance (as the percentage of correct outcomes) of the automatically reverse-engineered network compared to the experimental results *in vivo* is higher than 85% for all the experiments we used in the training set during the network search (Figure 6.6A). Thus, the model uncovered by this process correctly predicts both the large-scale dynamics and the quantitative stochastic outcomes of the dataset. To explore its predictive value further, we asked how well this model would do in explaining experimental results that were *not* in the set against which it was evaluated during its evolution – completely new experiments that it had never seen, which we then validated *in vivo*. Strikingly, all the outcomes predicted by the model for the novel experiments, which were not used during the reverse-engineering of the network, have a performance higher than 75% (Figure 6.6B). Together, these results validate both the specific found dynamic signaling network as a good mechanistic model of melanocyte hyperpigmentation, and our computational approach to automatically discover such dynamic models from stochastic experimental data.

We then used the model to gain an intuitive understanding of the all-or-none dynamics of this process – an important adjunct to correct numerical predictions by the simulation. Projecting the trajectories of several experiments in the phase space revealed different attractors for the hyperpigmented and non-hyperpigmented phenotypes, as well as phase bifurcations after applying different treatments (Figure 6.7A-C). The attractors defined by the dynamical system always lay in any of the two extreme pigmentation levels (all or none),

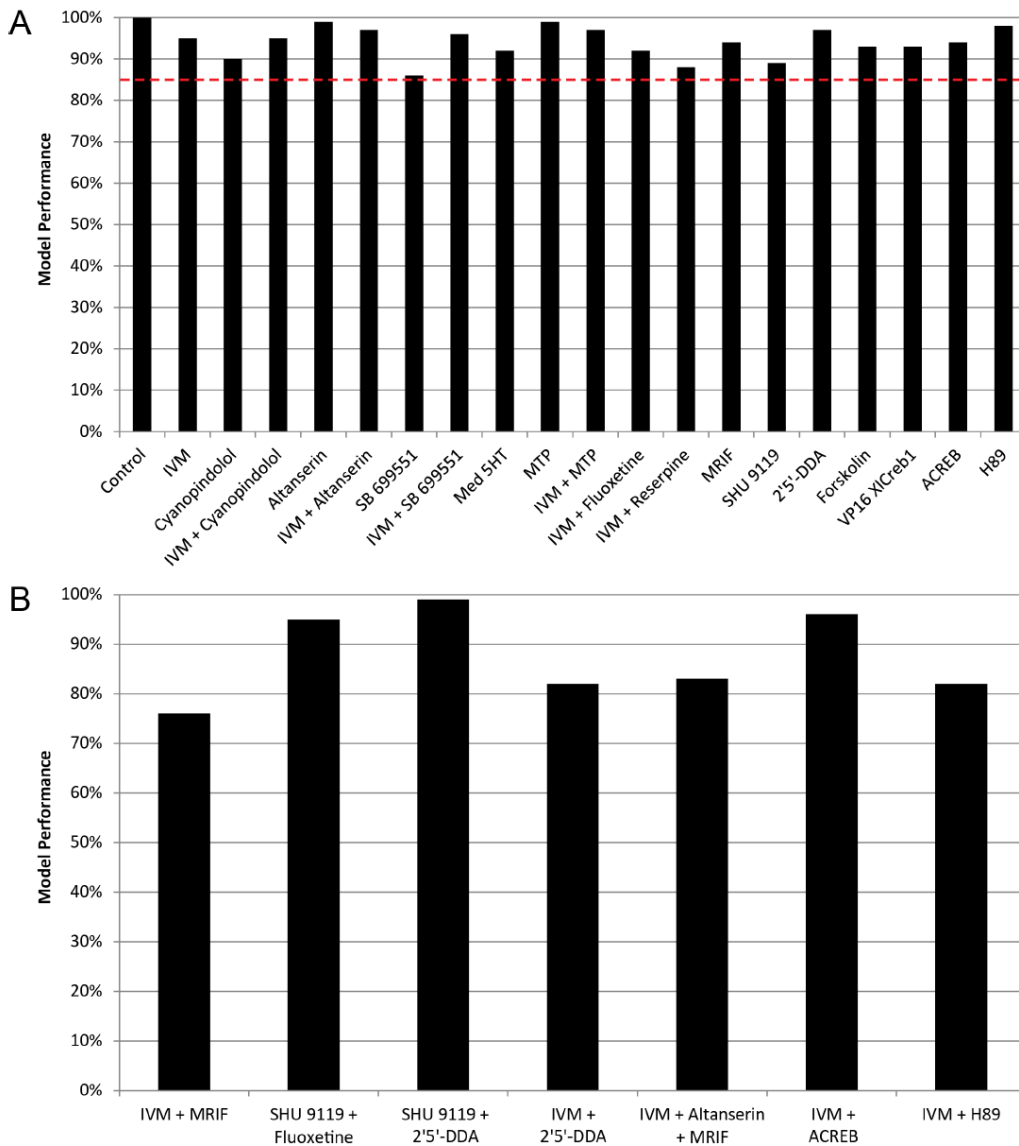


**Figure 6.6. Dynamic model performance with training experiments and novel predictions.**

Percentage of correct outcomes of the model for each of the training experiments used during the search. The dynamic model performance for all the experiments in the training set is higher than 85% (red line) B) Percentage of correct predictions of the model for a set of novel experiments. The results show that 70% of the novel experiments were predicted with more than 80% correct outcomes.

explaining the bistability observed for all treatments. In addition, the diagrams show how the trajectories pass near a separatrix, which, due to the stochastic noise included in the signaling network, explains how trajectories starting at the same initial conditions can converge to different attractors and hence obtain the observed stochastic penetrance of the hyperpigmented phenotype. The trajectory diagrams also reveal the creation of bifurcations in the state space due to the application of pharmacological treatments, which produces a variation in the location and basin of the attractors and explains the change in frequencies of the resultant phenotypes. Finally, a qualitative summary of the trajectories and attractors under different treatments highlights the bifurcations produced in the state space, the phenotypes associated with the different attractors, and their relative frequency for each treatment (Figure 6,7D). Interestingly, this analysis reveals how an apparently similar hyperpigmented phenotype is actually produced by two different molecular states: either a high level of R1 activity combined with a low level of SERT (bottom-right in Figure 6.7D) or a low level of R1 combined with a high level of SERT (top-left in Figure 6.7D).

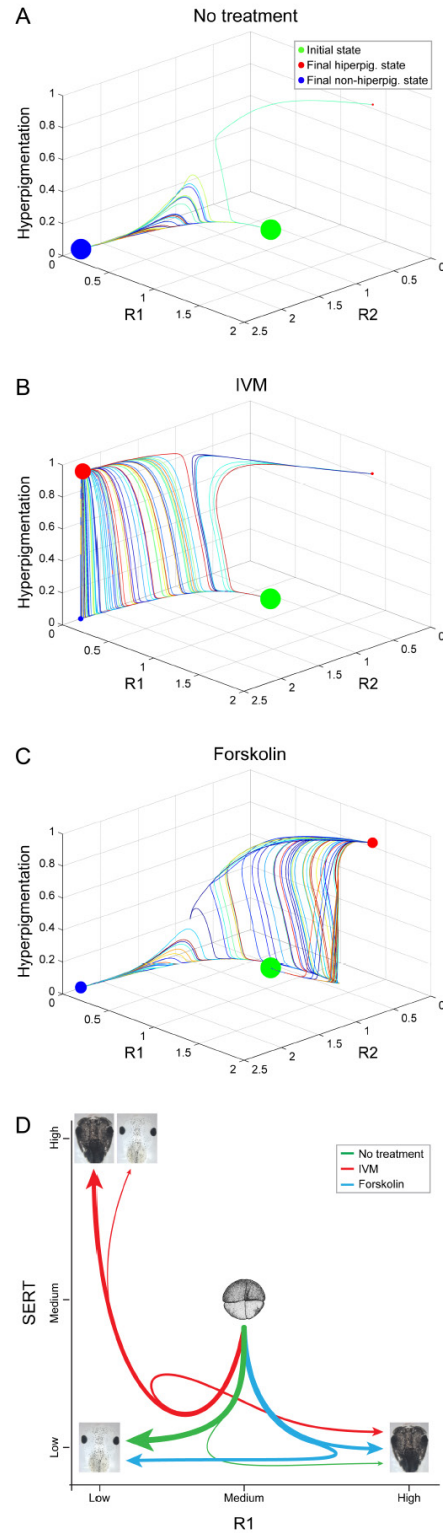


**Figure 6.7. Phase space of the dynamic model with stochastic developmental trajectories and pharmacological treatment bifurcations.** A-C) Trajectories of 100 simulations for each of three representative treatments. While the initial state (green dot) is the same for all the simulations, the

trajectories stochastically converge to different attractors, representing hyperpigmented phenotypes (red dots), and non-hyperpigmented phenotypes (blue dots). The attractor dot size is proportional to the number of converging trajectories. D) Qualitative phase space trajectories of three different treatments, which produce a bifurcation in the dynamic system and a change of attractors and the resultant phenotypes. The trajectories line widths are proportional to the frequency of simulations describing the trajectory.

## **Discussion**

Previous studies have examined the role that transmembrane potential has on regulating the pigmentation of *Xenopus laevis* embryos and have suggested serotonin signaling and the involvement of multiple serotonin receptors in translating the bioelectrical signal to a change in melanocyte behavior [31, 468]. Here we present a detailed model of these signaling processes (Figure S6.3). Most importantly, we identified a comprehensive computational dynamic model that quantitatively predicts the stochastic effects of altering various control points of this process. In order to discover the parameters and necessary links for the model (control network topology and coupling coefficients among nodes), we developed a novel automated method for reverse-engineering stochastic dynamic models directly from the phenotypic penetrance results of *in vivo* experiments. The reverse-engineered model can account for the bistable all-or-none hyperpigmentation phenotype as well as for the precise stochastic penetrance under multiple interventions. Moreover, we validated the model by correctly predicting the hyperpigmentation phenotype penetrance for a new set of combined interventions.

### ***Bioelectric control of melanocyte behavior is mediated by changes in gene expression***

Our results also demonstrate that the depolarization of a sparse, yet widely distributed cell population seems to result transcription factor up-regulation similar to that which occurs with hyperpigmentation mediated by the injection of depolarizing KCNE1 ion channel mRNA [33]. Both the transcription factors Sox10 and Slug were significantly upregulated following ivermectin-induced depolarization (Figure 6.3B). Sox10 is expressed in pre-migratory neural crest

cells, and its expression is gradually restricted to glia and melanocyte lineages [543, 544]. In the melanocyte, Sox10 plays an indispensable role in melanocyte survival, proliferation and migration [545], and has also been shown to be expressed in primary and metastatic melanoma [513-515, 546]. It is interesting to note that the upregulation of the transcription factor Sox10 is highest shortly after depolarization begins, and is reduced to a lower, stable baseline in later stages (Figure 6.3C). This novel finding suggests that this aberrant signal is being normalized via signaling of normal, unaffected neighboring cells.

Notably, in addition to upregulation of *Sox10* and *Slug*, pathway analysis performed on microarray results revealed differential gene expression in 45 genes in late stage embryos that have previously shown to be implicated in a variety of different cancers, including melanoma (Table S6.1). For example, ivermectin exposure resulted in a 3.59-fold overexpression of pro-opiomelanocortin (POMC). POMC, a precursor to  $\alpha$ MSH, has been linked to a number of disorders related to metabolic disorders [547], as well as a number of cancers including lung cancer [548] and melanoma [549-551]. POMC overexpression has also been shown to be induced in response to elevated p53 levels in the regulation of the pigmentation response to UV damage [552]. Interestingly, the melanocortin receptor gene is associated with depressive disorder, and is implicated in serotonergic signaling in human disease [553]. Microarray analysis also suggested that there was a ~30-fold increase of the transmembrane serine 2 protease (TMPRSS2), a gene commonly expressed in prostate cancer [554] and an almost 12-fold down-regulation of albumin, a soluble, monomeric protein which comprises about one-half of the blood serum protein, and has been implicated in breast cancer [555-557]. These were significant and dramatic changes within the embryo.

Skin pigmentation and the tanning response in humans is a dynamic system. Pigmentation results from the synthesis of melanin from the melanocytes, followed by the distribution of this pigment granules by keratinocytes [558]. Hyperpigmentation is characterized by increases in pigment production and deposition, both characteristics of hyperpigmentation in the *Xenopus laevis* tadpole. It is interesting to note that both UV-induced, p53-mediated hyperpigmentation in mice, and depolarization-induced hyperpigmentation in this tadpole system, are both mediated by the upregulation of POMC transcription [552, 559]. As previously noted, POMC has also been shown to be upregulated in melanoma [549], confirming conserved molecular players mediating the relationship between instructor cell depolarization and the neoplastic-like conversion of melanocytes.

***From a biophysical signal to a change in cell behavior; modeling a bi-phasic, stochastic response to changes in  $V_{mem}$***

Taken together, the data presented here on the signaling cascade downstream of instructor-cell depolarization describe how this bioelectric manipulation can be used to control many aspects of melanocyte behavior. This bioelectric signal is first transduced into an increase of serotonin release from the instructor cell [31] which, in turn, via complex signaling involving multiple serotonin receptors [468] is transduced into upregulation of POMC expression in the pituitary melanotrope cell. This leads to an increase in the release of MSH, which, then via CREB activated transcription factors is responsible for melanocyte migration, and proliferation. CREB has been shown to be important in *Xenopus* embryogenesis [541], and also functions to regulate the expression of many genes mediating inflammation and tumor metastasis including interleukin-8 and matrix

metalloproteinase-2 [560-562]. Additionally, the involvement of CREB in tumor growth and metastasis has been demonstrated to be pivotal in human melanoma [563-566]. This increased understanding of the mechanism by which changes in transmembrane potential can relate morphogenesis, provide useful information for the creation of future therapeutic techniques.

The goal of many mechanistic studies is to arrive at a model that would predict system behavior and reveal what perturbations must be made to achieve a specific outcome. It is important to note that typical functional “arrow diagram models” are useful knowledge, but are not constructive: they are not sufficiently specified to be able to be tested against quantitative datasets, and usually do not directly facilitate the understanding of complex behaviors like stochastic outcomes. As with many systems, our hyperpigmentation penetrance dataset was too rich to allow inference of a well-fitting network model by hand. To identify a predictive model that can facilitate future research, and understand the stochastic character of hyperpigmentation outcomes, we sought to uncover the first fully-specified model of this process that can be directly simulated in a virtual embryo context. Such a model is useful for *in silico* screening of strategies for manipulation of outcome (e.g., in a cancer context) and for understanding the developmental dynamics of cell-cell signaling events.

One of the most curious aspects of this phenotype is its all-or-none character. Tadpoles were never seen to be partially hyperpigmented: each tadpole is either normal or is covered with metastatic-like melanocytes. This type of bistable phenomena has been reported in bacteria [567], synaptic plasticity [568], developmental processes, including the epithelial to mesenchymal transition [569], the specification of neuron cell types [570], and the maturation of *Xenopus* oocytes [571], and cancer [572]. Signaling networks with feedback

loops can act as irreversible switch-like responses [573], explaining these all-or-none phenomena. Indeed, bistable switches are fundamental components used in synthetic biology to engineer regulatory circuits with memory for the control of desired cell functions [574-576].

However, at a population level, the hyperpigmented phenotype is stochastic in that many of our treatments produced less than 100% penetrance of the phenotype; the decision as to whether to succumb to conversion was implemented not at the level of individual cells (resulting in a mixed population within each host) but at the level of the individual (resulting in a group of normal and hyperpigmented animals but no in-between cases). Stochastic regulation of cell and organism fate is widespread, from bacteria to humans [537, 577]. For example, the cell types in the retina of *Drosophila* differentiates stochastically into one of two possible cell types with a ratio of 30:70 [578-580]; similarly, the differentiation into epiblast and endoderm lineages in the early mouse embryo is stochastic [538], as is the expression of odorant receptor genes in olfactory neurons [581]. Similarly, during left-right patterning, expression of normally left-sided transcripts can be randomized, resulting in double-left, right-only, or double-right outcomes, but these decisions are made by the whole lateral tissue – not individual cells but a whole region deciding to function as a Left or Right side [61, 351, 582-584]. How this coordination takes place (and avoids speckling – randomization at the level of single cells which in the end have to express a transcript or not) is still unknown.

Formulating dynamic regulatory networks whose behavior, when quantitatively simulated, gives the correct phenotypes for the various experimental conditions is a significant challenge due to the non-linear interactions in signaling networks [585-587]. Automated reverse-engineering

methods have been proposed to discover such pathways from experimental data [588-597]; however, there are no generalized methods for discovering pathway models that have bistable and stochastic phenotypes. Identifying such networks matching complex functional datasets is crucial, in order to have explanatory power in our models of embryogenesis, and also for knowing what signals to provide in order to achieve a desired outcome *in vivo*.

Here we presented a novel computational method for reverse-engineering dynamic signaling networks that can explain both bistable and stochastic resultant phenotypes. Starting with a dataset containing the incidence data on hyperpigmentation under 20 different pharmacological perturbations, the automated method discovered a dynamic network that can recapitulate precisely the bistability and stochasticity showed in the set of experiments performed *in vivo*. Finding the parameters and links necessary for a stochastic dynamic network to produce precise stochastic results after certain perturbations is a very hard problem, almost impossible for a human scientist facing a non-trivial dataset. Indeed, our automated method needed to evaluate more than 20 million different networks, comprising a grand total of N=40 billion virtual experiments, during 36 hours run-time on a high-performance parallel computer to reverse-engineer the dynamic network that could precisely recapitulate the stochastic phenotypes in 20 pharmacological assays [598]. The network model includes candidates for global coordination of cell state within each embryo (the diffusible factors MSH and cAMP), and has only two unknown nodes, which can be identified via candidate approaches (based on known protein-protein interaction databases) or by screening.

The current model facilitates *in silico* testing of proposed biomedical interventions; indeed one surprising prediction – that serotonin transporter

inhibitors could suppress tumorigenesis, have already been borne out by data in independent mammalian systems [598]. Our model also fits with recent proposals that cancer-promoting stimuli such as UV exposure mediate their effects via changes of resting potential [599, 600].

Furthermore, we evaluated the predictive power of the network found by our method by generating testable predictions regarding the stochastic penetrance of the hyperpigmented phenotypes for seven additional perturbations not used during the search. Remarkably, the model was able to correctly predict the outcomes of brand new experiments; after we performed the same experiments *in vivo*, we found that the precise stochastic penetrance values of the resultant phenotypes predicted by the network were correct to a high degree for all the seven experiments, validating the method and its reverse-engineered network. The model was also able to predict that cAMP signaling did not occur through the serotonin receptors (5HT-R1, 5HT-R2 and 5HT-R5) involved in the hyperpigmentation response, which are either inhibitory or function through IP3-DAG and PKC rather than cAMP. In summary, the method we presented here represents a powerful new method to assist scientists in the discovery of dynamic signaling networks to explain in mechanistic and functional terms any given dataset of complex stochastic resultant phenotypes.

### ***Future implications***

We present a quantitative, constructive model of the pathway mediating bioelectrical conversion of genetically-normal melanocytes to an invasive metastatic-like phenotype. This suggests strategies for intervention at several points (e.g., serotonin receptor signaling) which could be tested in clinical or epidemiological contexts. Moreover, the model correctly exhibits a fascinating

aspect of this effect *in vivo*: the complex attractor dynamics that allow a signaling pathway to stochastically select one of several discrete outcomes. The simulation approach facilitates next-generation models that are constructive in the sense that they reveal the steps sufficient to reach specific outcomes (whereas simple arrow diagrams are usually showing necessary elements, not sufficient algorithmic steps). Similar models could be applied to numerous other contexts in developmental or regenerative pattern formation, and used for *in silico* simulations to screen candidate reagents for achieving specific outcomes. Derivation of such networks could also greatly assist the efforts to understand why quite different outcomes can be obtained within a population treated with antipsychotic or cancer drugs – a major problem in pharmacogenetics [601-603]; the dynamics of our model suggests that the observed variability may not be due to straightforward differences in patients' genomes but an intrinsic part of some signaling networks' dynamics.

This computational approach is a component of our efforts towards bioinformatics of complex phenotypes [604-607], and a contribution to the robot scientist field [608-611], illustrating how the power of evolution can be harnessed to identify models of important signaling events that are too difficult to guess directly from complex and ever-increasing datasets. Not only did this process find a good, predictive model explaining the details and overall stochastic dynamics of this pathway, but the model thus identified is not overly-complex and easily understood by human scientists. This suggests that future application of AI methods to problems of development and cancer will give rise not only to correct predictions but also to deep understanding of the complex dynamics we seek to control and repair.

## **Acknowledgments**

We thank Amanda Allen and Erin Switzer for general lab assistance and frog husbandry, Joan Lemire for molecular biology assistance, Shawn Doughty for high-performance computation support, and the members of the Levin lab and the bioelectricity community for many useful discussions. We thank Vaibhav Pai and Chris Fields for comments on a draft of the manuscript. Computation used a cluster computer awarded by Silicon Mechanics and the Campus Champion Allocation for Tufts University TG-TRA130003 at the Extreme Science and Engineering Discovery Environment (XSEDE), which is supported by NSF grant ACI-1053575. This work was supported by the G. Harold and Leila Y. Mathers Charitable Foundation.

## **Materials and Methods**

### ***Animal husbandry***

*Xenopus* embryos were maintained according to standard protocols [122] in 0.1X Modified Marc's Ringers (MMR), pH 7.8, plus 0.1% gentamycin. *Xenopus* embryos were staged according to Nieuwkoop and Faber [612]. All experimental procedures involving *Xenopus* embryos were approved by the institutional animal care and use committees and Tufts University Department of Laboratory Animal Medicine under protocol M2014-79.

### ***Microinjection***

Capped, synthetic mRNAs were dissolved in Millipure (18 M $\Omega$ ) water and injected into embryos at cleavage stages in 3% Ficoll using standard methods [122]. The mRNA injections were made using borosilicate glass needles calibrated to

bubble pressures of 50–70 kPa in water, delivering 50-70 msec pulses. After 30 min, embryos were washed and cultured in 0.1X MMR until desired stages.

Constructs used included XICreb1 (BC041206), VP16 XICreb1 [527, 613], injected into 1 cell of NF stage 5 (32-cell) embryos; and XminK (also known as KCNE1 and isK [33, 614]), injected into 1 cell of NF stage 3 (4-cell) embryos (Figure 3A).

### ***Drug exposure***

Stocks of ivermectin (Sigma) were stored at 10 mM concentration in dimethyl sulfoxide (DMSO). Embryos were exposed in 0.1 X MMR from NF Stage 10 to NF Stage 45 to ivermectin (Sigma), 1  $\mu$ M; 2'5'-Dideoxyadenosine (Sigma), 500  $\mu$ M; Forskolin, 5  $\mu$ M; Melanocyte stimulating hormone release inhibiting factor, 25  $\mu$ M; SHU 9119, 500 nM. All compounds were obtained from Tocris, unless otherwise noted and prepared in Millipure (18 M $\Omega$ ) water unless indicated.

### ***Microsurgery***

Prior to microsurgery, stage 32 embryos were anesthetized in a 0.02% tricaine solution, pH 7.5, in 0.1x MMR. Using a surgical blade (Feather #11, Osaka JP), tissue was excised from one of three regions depending on the treatment. In the first experimental group, a wedge shaped cut was made between the eye and the cement gland, corresponding to the region of the developing pituitary. In the second experimental group, a single cut removed the entire anterodorsal region of the head (above the eye), corresponding to the region of the developing pineal gland. In the third experimental group, a wedge shaped cut removed the tissue between the cement gland and stomach, which served as a control for wounding. Following tissue removal, animals were kept anesthetized for 30 minutes after which they were washed twice with 0.1x MMR. After washing, operated animals

were raised at 16 °C under a 12h:12h light:dark cycle and were scored for the presence or absence of hyperpigmentation at stage 46.

### ***Expression analysis***

In situ hybridization was performed as previously described [615]. *Xenopus* embryos were collected and fixed in MEMFA for 30 min [122]. Prior to in situ hybridization, embryos were washed in phosphate buffered saline (PBS) + 0.1% Tween-20 (PBST) and then transferred to methanol through a 25%/50%/75% series. Probes for in situ hybridization were generated in vitro from linearized templates using a DIG labeling mix (Roche). Chromogenic reaction times optimized signal:background ratio. Analyses represent consistent patterns from 50–60 embryos for each marker. Probes used for in situ hybridization include: Sox10 (GenBank Accession #AY149116) and Slug (GenBank Accession #AF368040).

### ***RNA extraction & cDNA synthesis***

Embryos (collected N=10 per eppendorf tube, 2 biological replicates) washed in RNase/DNase free water were homogenized in TRIzol reagent (Life Technologies). Homogenized samples were stored at -80°C for up to one month. Total RNA was extracted according to the manufacturer's instructions (Life Technologies). RNA yield and quality were assessed by spectrophotometry (NanoDrop ND-1000) and gel electrophoresis respectively to assess integrity of 28S and 18S RNA.

Reverse transcription was performed using ThermoScript™ RT-PCR system (Life Technologies). Each in vitro reverse transcription reaction was performed using 1 µg total RNA and 50 µg Oligo(dT)<sub>20</sub> primers (Life Technologies). RNA and primers were mixed, denatured 5 min at 65°C, and

placed on ice before adding the reaction mix according to the manufacturer's instructions. Reverse transcription reaction was carried out at 50°C for 45 min. The reaction was terminated by incubating at 85°C for 5 min, followed by RNA degradation using 1 µg of RNase H for 20 min at 37°C. cDNA was stored at -20°C until use. The quality and quantity of cDNA was validated using Advantage® 2 PCR kit (Clontech) on cDNA samples using alpha-tubulin primers [93].

### **RT-qPCR**

Primers were designed using Primer3Plus enhanced web interface [616] for Sox10 (AY149116) and Slug (AF368040). Ornithine decarboxylase (ODC), a widely used endogenous control for *Xenopus* was used to normalize target gene expression, and primer sequences have been previously published [617]. The PCR specificity was verified by Blast (<http://blast.ncbi.nlm.nih.gov/Blast.cgi>) using NCBI *X. laevis* reference sequence. Desalted primers were obtained from Invitrogen by Life Technologies™

For each primer pair, standard curve primer analysis was performed using serial dilutions of cDNA from NF stage 25 control embryos (1 (undiluted), 10<sup>-1</sup>, 10<sup>-2</sup>, 10<sup>-3</sup>). Formation of primer-dimer and amplification specificity was assessed by efficiency and melt curve analysis.

The cDNA from validated RNA was used to perform qualitative real-time PCR assays (RT-qPCR). For each biological sample, three technical replicates were run in each RT-qPCR experiment. Each treatment contained 2 biological replicates. Triplicate NTCs were also run for each cDNA sample for each reaction.

The 20 µL PCR reactions were assembled manually. Samples were

prepared by adding 1  $\mu$ l cDNA, 10  $\mu$ l 2X PowerSYBR® Green PCR Master Mix (Applied Biosystems) and 0.5  $\mu$ l of each primer (diluted to 10  $\mu$ M). Reactions were incubated in 96-well MicroAmp® Optical Reaction plates at 95°C for 10 min followed by 40 cycles at 95°C for 15 s and 60°C for 1 min in a StepOnePlus™ qPCR instrument (Applied Biosystems).

The RT-qPCR data were analyzed using the StepOne software v.2.3 and  $\Delta\Delta C_T$  values were calculated (Applied Biosystems). Fold change of target genes relative to the normalized ODC was calculated as  $-2^{\Delta\Delta C_T}$ .

### **Microarray analysis**

Gene expression analysis was performed using samples treated with ivermectin from NF stage 10 onwards, collected at two developmental stages; stage 15 (early neurula) and stage 45 (free-swimming tadpole). Embryos were collected in eppendorf tubes (N=50 for stage 15, N=5 for stage 45) and frozen at -80°C. RNA extraction and microarray analysis were performed by the Beth Israel Deaconess Medical Center Genomics and Proteomics Center (Harvard) according to standard Affymetrix protocol, using a high throughput hybridization and scanning system. Microarray hybridization was performed using the Affy 3' IVT Express Kit. Fragmented and biotin labeled/amplified RNA was hybridized to the GeneChip® *Xenopus laevis* Genome 2.0 array as per manufacturer's protocol. The Affymetrix GeneChip® *X. laevis* Genome 2.0 Array, has 32,400 probe sets representing more than 29,900 *X. laevis* transcripts.

All microarray data were analyzed using Bioconductor packages in R. The quality of hybridized arrays was assessed using Affymetrix guidelines on the basis of scaling factor, background value, mean intensity of chip, and 3' to 5' ratios for spike-in control transcripts. The outlier analysis was performed using

unsupervised clustering and principal component analysis. All high quality arrays were normalized using the MAS5 algorithm developed by Affymetrix. The absent/present calls for the transcripts were calculated using the MAS5 algorithm. The differentially expressed transcripts were identified on basis of fold change and Affymetrix transcripts calls. Up-regulated transcripts were considered to be those that changed >2 fold in the experimental group compared to the control group, with present call in the experimental group. Down-regulated transcripts were considered to be those that changed >2 fold in the experimental group compared to the control group, with present call in control group. Differentially expressed transcripts were identified using customized script in R. The list of differentially expressed genes were annotated by Affymetrix.

### ***Bioinformatics***

Functional enrichment for differentially expressed genes was conducted using the GOrilla database [535] (updated on Aug 2, 2014). *Xenopus laevis* gene names were uploaded and mapped using the official gene symbol. *Homo sapiens* was used as the reference species for gene ontology assignments. Pathway Studio 9.0 (Ariadne, Rockville, MD, USA) was used for pathway analysis to construct gene interaction networks. For early embryos, 21 genes were mapped to annotated pathway in the database while in the late embryo experiments, 210 genes were successfully mapped to annotated pathway (see [618] for additional details on pathway analysis).

### **Computational modeling and reverse-engineering method**

Our goal was to identify a signaling network whose stochastic behavior, given experimental initial starting conditions, matched the observed dataset. We modeled dynamical signaling networks as systems of stochastic ordinary

differential equations (ODE). A signaling network is made of a set of interconnected elements, including the products perturbed during the experiments, the pharmacological drugs employed, an element representing the degree of pigmentation in the tadpole, and any additional unknown products necessary for the correct dynamics of the network. Each element in a network is represented with an equation modeling its production rate as the linear relation between a production term, a decay term, and a noise term. The production term is modeled with a combination of Hill functions, commonly used for modeling biochemical interactions [619], grouped together as sufficient (max operator) or necessary (min operator). The following equation illustrates a model of the production of product  $a$  as regulated by two necessary products (activator  $b$  and inhibitor  $c$ ) and two sufficient products (activator  $d$  and inhibitor  $e$ ):

$$\frac{da}{dt} = \rho_a \min \left( \frac{b^{\eta_1}}{\alpha_1^{\eta_1} + b^{\eta_1}}, \frac{\alpha_2^{\eta_2}}{\alpha_2^{\eta_2} + c^{\eta_2}}, \max \left( \frac{d^{\eta_3}}{\alpha_3^{\eta_3} + d^{\eta_3}}, \frac{\alpha_4^{\eta_4}}{\alpha_4^{\eta_4} + e^{\eta_4}} \right) \right) - \lambda_a a + \xi(t)$$

where  $\rho_a$  is the production constant,  $\eta_i$  are the Hill coefficients,  $\alpha_i$  are the dissociation constants in the Hill functions,  $\lambda_a$  is the decay constant, and  $\xi(t)$  is a Gaussian random noise of zero mean.

Given a signaling model network described as a system of PDEs, an experiment can be simulated *in silico* by numerically integrating the system with a set of initial conditions. The initial conditions include any pharmacological element used in the experiment as a constant equal to 1 in the case of being used or equal to 0 in the case of its absence. Due to the stochastic nature of the system of equations, the pigmentation level resultant from a simulation for a given set of initial conditions can vary among different runs.

In order to calculate the predictive power of a given signaling network

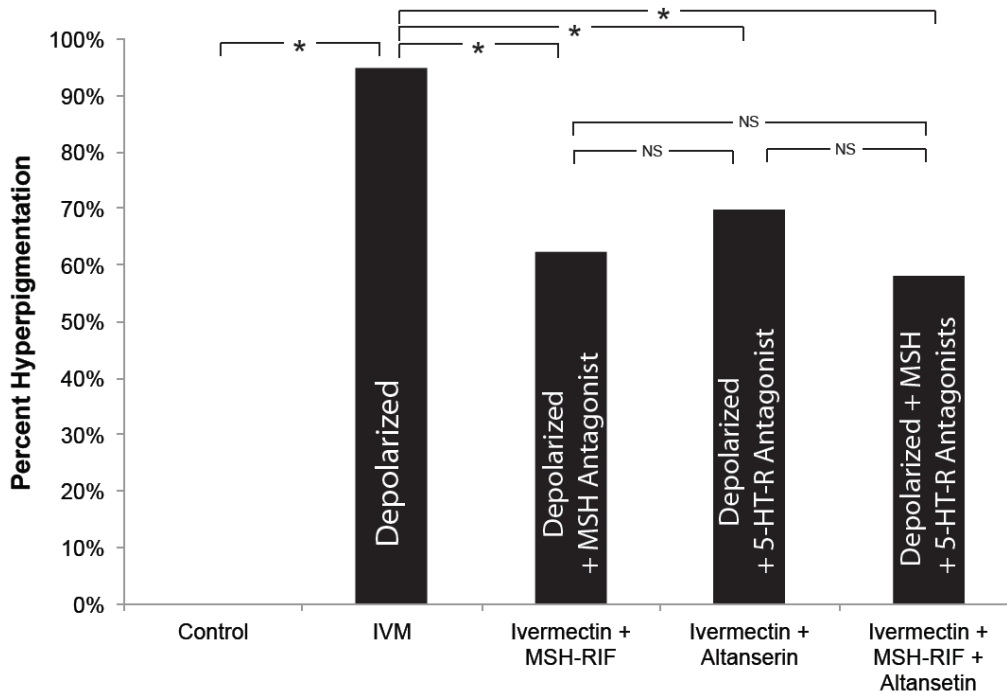
model, each pharmacological treatment is simulated 100 times. A resultant phenotype is considered hyperpigmented if the level of the corresponding product is above 0.9 and non-hyperpigmented if it is below 0.1. Then, we define the error of a signaling network model  $M$  for a set  $E$  of  $n$  experiments as the mean square error between the *in silico* and *in vivo* outcomes for each of the experiments:

$$\text{error}(M, E) = \frac{1}{2n} \sum_{i=1}^n ((H_i - H'_i)^2 + (N_i - N'_i)^2)$$

where  $H_i$  and  $N_i$  are the resultant frequency of hyperpigmented and non-hyperpigmented phenotypes in the *in silico* simulation of experiment  $i$ , and  $H'_i$  and  $N'_i$  are the resultant frequency of hyperpigmented and non-hyperpigmented phenotypes in the *in vivo* assay of experiment  $i$ .

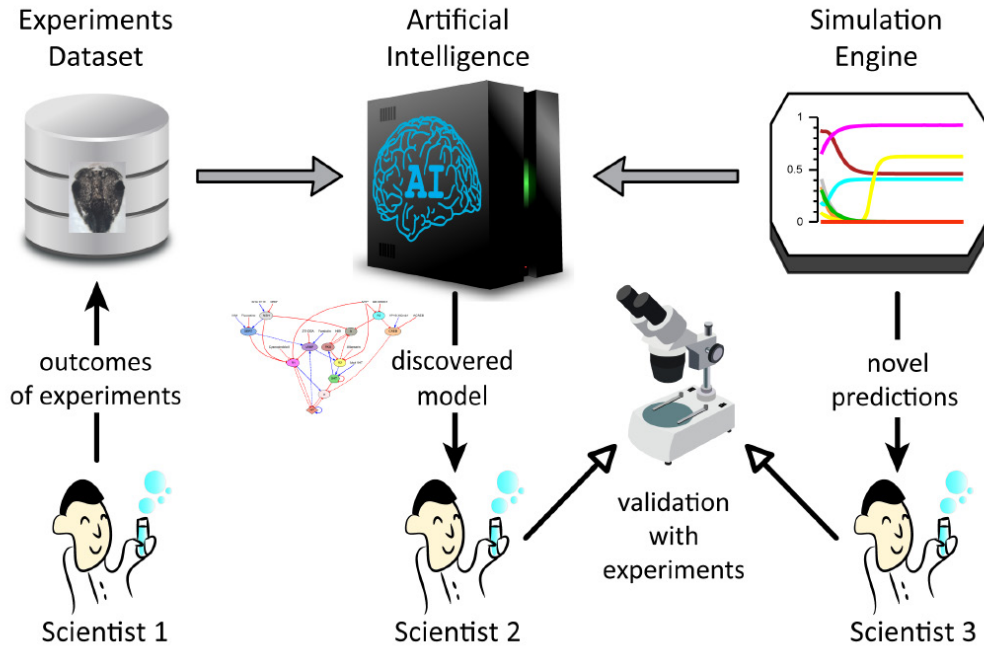
We implemented a computational method based on [620] to automate the discovery of the topology and parameters of signaling networks that minimize the error for a given set of training experiments. The method uses an evolutionary algorithm approach, where a set of signaling networks evolve *in silico* by crossing over and mutating them, and replacing those with worse error [621, 622]. After a fixed number of 10,000 generations, the best network is returned by the algorithm. The simulation and search method was implemented in C++ using the Standard Library. Visualizations used the Qt libraries (The Qt Company Ltd.) and the Qwt library (Uwe Rathmann and Josef Wilgen).

## Supplemental Material



### Supplemental Figure 6.1. Serotonin and $\alpha$ MSH signaling mediating instructor cell depolarization are part of a single pathway

Treatment of embryos with either MSH-release inhibiting factor (MSH-RIF) or the serotonin receptor 2 antagonist, altanserin, alongside ivermectin from NF stage 10 onwards significantly reduced ivermectin-induced hyperpigmentation. Treating embryos with all three pharmacologicals (ivermectin + MSH-RIF + altanserin), failed to further reduce hyperpigmentation rates.

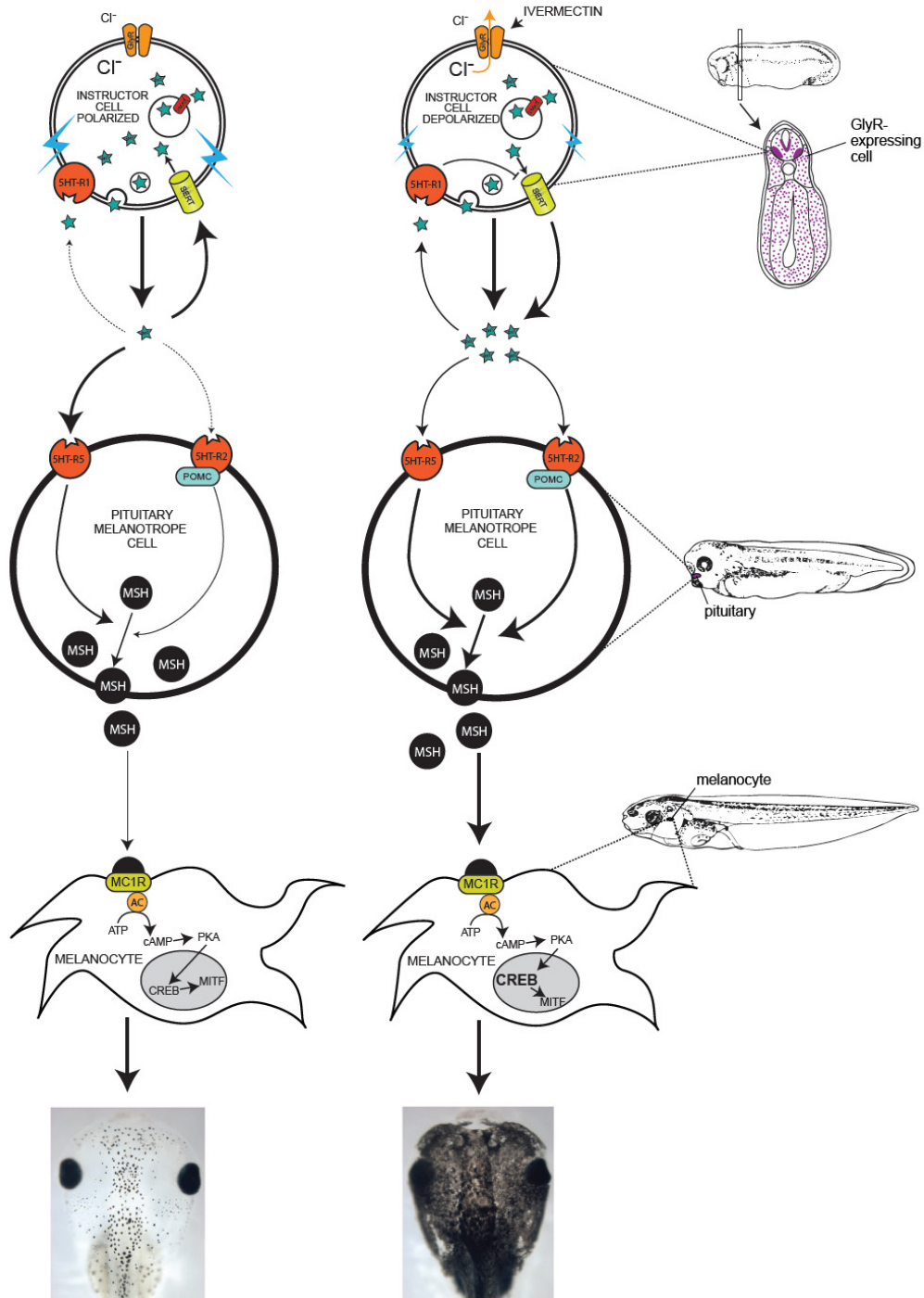


**Supplemental Figure 6.2 Methodology to reverse-engineer dynamic signaling networks.**

The resultant phenotype frequencies from the pharmacological treatments are encoded in a dataset of experiments. An artificial intelligence algorithm automates the discovery of models with the use of a simulation engine to reproduce *in silico* the dynamics of the experiments stored in the dataset. Scientists then validate the discovered model using novel predictions with the simulation engine and *in vivo* experiments.

**NORMAL**  
Polarized Instructor Cell

**IVERMECTIN**  
Depolarized Instructor Cell



**Supplemental Figure 6.3. Pathway model for melanocyte control downstream of serotonin signaling**

When the instructor cell population is depolarized, the serotonin transporter, SERT, runs backwards, exporting additional 5-HT into the microenvironment of

the melanocytes. At these high extracellular 5-HT levels, 5-HT activates receptors on both the pituitary melanotrope cells and on melanocyte cells. In the melanotrope cells, binding of 5-HT to receptors regulates adenylyl cyclase activity, which, in turn, effects calcium-mediated melanocyte stimulating hormone (MSH) release. 5HT binding may also facilitate the cleavage of Pro-opiomelanocortin (POMC) into MSH. MSH binding to MC1R receptors on melanocytes affects adenylyl cyclase activity in the melanocyte leading to increased cAMP activity, CREB phosphorylation, and an increase in gene transcription (i.e. upregulation of Sox10/Slug). 5-HT binding directly on melanocytes can also affect adenylyl cyclase-mediated cAMP levels, thus controlling proliferation, migration, and shape change.

**Supplemental Table 6.1. Cancer-related genes shown to be differentially expressed in stage 45 *Xenopus* tadpole embryos following depolarizing ivermectin treatment**

<b>Name</b>	<b>Description</b>	<b>Related cancer(s) (according to Oncomine)</b>	<b>Fold Change</b>
AGR2	anterior gradient homolog 2 ( <i>Xenopus laevis</i> )	Breast Cancer	-2.79
ALB	albumin	Breast Cancer	-11.91
ATF5	activating transcription factor 5	Lymphoma, Breast Cancer	-2.27
ATP6AP1	ATPase, H <sup>+</sup> transporting, lysosomal accessory protein 1	Leukemia	-4.07
B2M	beta-2-microglobulin	Brain & CNS Cancer	2.43
BCL2L10	BCL2-like 10 (apoptosis facilitator)	Breast Cancer	2.15
BIRC2	baculoviral IAP repeat containing 2	Brain & CNS Cancer, Myeloma	2.6
C2orf40	chromosome 2 open reading frame 40	Breast Cancer	2.56
CARTPT	CART prepropeptide	Breast Cancer	-2.11
CAT	catalase	Breast Cancer, Lung Cancer, Leukemia	-3.31
CEBPB	CCAAT/enhancer binding protein (C/EBP), beta	Colorectal, Lymphoma	2.11
CTSL1	cathepsin L1	Lymphoma	-2.73
CTSS	cathepsin S	Kidney	2.71
CYP3A4	cytochrome P450, family 3, subfamily A, polypeptide 4	Breast Cancer	2.11
DPYS	dihydropyrimidinase	Breast Cancer, Leukemia	-2.53
EGLN3	egl nine homolog 3 ( <i>C. elegans</i> )	Kidney	5.1
EIF2S1	eukaryotic translation initiation factor 2, subunit 1 alpha, 35kDa	Colorectal, Sarcoma	2.03
EXT1	exostosin 1	Head and Neck	-2.39
GPNMB	glycoprotein (transmembrane) nmb	Lymphoma, Melanoma	-3.18
GSTP1	glutathione S-transferase pi 1	Prostate Cancer	3.61
IFI30	interferon, gamma-inducible protein 30	Breast Cancer	4.24
IKBKE	inhibitor of kappa light polypeptide gene enhancer in B-cells, kinase epsilon	Breast Cancer	2.76

KIF20A	kinesin family member 20A	Breast Cancer, Sarcoma	2.32
MKI67	antigen identified by monoclonal antibody Ki-67	Lung Cancer	3.95
MMP1	matrix metalloproteinase 1 (interstitial collagenase)	Colorectal	3.75
MYD88	myeloid differentiation primary response gene (88)	Lung Cancer	-4.05
NPY	neuropeptide Y	Leukemia	-4.05
NR1H4	nuclear receptor subfamily 1, group H, member 4	Colorectal	-2.39
P4HB	prolyl 4-hydroxylase, beta polypeptide	Brain & CNS Cancer, Lymphoma	2.24
PDE5A	phosphodiesterase 5A, cGMP-specific	Colorectal	-2.16
PFKFB3	6-phosphofructo-2-kinase/fructose-2,6-biphosphatase 3	Breast Cancer, Leukemia	2
PMEL	premelanosome protein	Melanoma	2.91
POMC	proopiomelanocortin	Brain & CNS Cancer, Lung Cancer	3.59
PPARG	peroxisome proliferator-activated receptor gamma	Breast Cancer, Sarcoma	2.2
PRKCD	protein kinase C, delta	Leukemia	2.3
PRSS2	protease, serine, 2 (trypsin 2)	Cervical Cancer	-3.67
SIRT2	sirtuin 2	Lymphoma	2.48
STEAP4	STEAP family member 4	Lung Cancer	16.96
TAC1	tachykinin, precursor 1	Breast Cancer	-3.2
TFPI2	tissue factor pathway inhibitor 2	Kidney, Melanoma	-2.1
TMPRSS2	transmembrane protease, serine 2	Kidney, Colorectal	30.12
TXN	thioredoxin	Lymphoma, Melanoma	6.26
TXNIP	thioredoxin interacting protein	Breast Cancer	-2.18
URGCP	upregulator of cell proliferation	Myeloma	3.65

**Supplemental Table 6.2. Reference genes & primers for qPCR**

Gene	GenBank Acc no	Function	Primer F	Primer R
Sox10	AY149116	Regulation of embryonic development, determination of the cell fate	TCAGCATTTCCTCCATCTC	GGCCGAATGGCTGTAATAAG
Slug	AF368040	Neural crest formation	ACACTGCAACAGAGCATTTCG	AGCAACCAGATTTCCTCATGC
ODC	NM_001086698.1	Housekeeping gene	TCCATTGAGAGCGTAGGACTTG	GAGGCTCGCCGGTGAATA

**Supplemental Table 6.3. Enriched gene ontology categories affected in late embryos. FDR q is the multiple testing correction using the Benjamini and Hochberg (1995) method. Enrichment score (ES) is calculated using the formula  $ES = (b/n) / (B/N)$** 

GO term	GO accession	P-value	FDR q-value	Enrichment Score (N, B, n, b)
regulation of acute inflammatory response	GO:0002673	7.35E-10	8.17E-06	12.06 (8327,36,211,11)
regulation of complement activation	GO:0030449	8.23E-10	4.57E-06	21.05 (8327,15,211,8)
regulation of humoral immune response	GO:0002920	1.36E-09	5.03E-06	16.14 (8327,22,211,9)
regulation of protein activation cascade	GO:2000257	2.98E-09	8.27E-06	18.57 (8327,17,211,8)
complement activation	GO:0006956	7.81E-09	1.74E-05	13.66 (8327,26,211,9)
carboxylic acid metabolic process	GO:0019752	1.10E-08	2.03E-05	2.77 (8327,528,211,37)
oxoacid metabolic process	GO:0043436	2.09E-08	3.33E-05	2.61 (8327,590,211,39)
organic acid metabolic process	GO:0006082	2.90E-08	4.02E-05	2.58 (8327,597,211,39)
regulation of inflammatory response	GO:0050727	4.40E-08	5.43E-05	5.31 (8327,119,211,16)

regulation of defense response	GO:0031347	8.53E-08	9.48E-05	3.60 (8327,252,211,23)
small molecule metabolic process	GO:0044281	3.89E-07	3.93E-04	1.75 (8327,1603,211,71)
single-organism process	GO:0044699	4.33E-07	4.01E-04	1.22 (8327,5747,211,177)
monocarboxylic acid metabolic process	GO:0032787	4.44E-07	3.80E-04	3.29 (8327,276,211,23)
complement activation, alternative pathway	GO:0006957	5.25E-07	4.17E-04	24.67 (8327,8,211,5)
protein activation cascade	GO:0072376	6.29E-07	4.66E-04	8.66 (8327,41,211,9)
defense response	GO:0006952	8.08E-07	5.61E-04	2.55 (8327,496,211,32)
regulation of response to external stimulus	GO:0032101	1.61E-06	1.05E-03	3.06 (8327,297,211,23)
humoral immune response	GO:0006959	2.58E-06	1.60E-03	7.40 (8327,48,211,9)
single-organism metabolic process	GO:0044710	3.46E-06	2.03E-03	1.48 (8327,2558,211,96)
carbohydrate biosynthetic process	GO:0016051	3.51E-06	1.95E-03	5.09 (8327,93,211,12)
regulation of response to wounding	GO:1903034	5.43E-06	2.87E-03	3.74 (8327,169,211,16)
cytolysis	GO:0019835	6.83E-06	3.45E-03	16.44 (8327,12,211,5)
hexose biosynthetic process	GO:0019319	8.37E-06	4.04E-03	7.52 (8327,42,211,8)
positive regulation of immune response	GO:0050778	8.49E-06	3.93E-03	3.29 (8327,216,211,18)
monosaccharide metabolic process	GO:0005996	8.85E-06	3.94E-03	4.03 (8327,137,211,14)
ion transport	GO:0006811	1.10E-05	4.69E-03	2.29 (8327,534,211,31)
alpha-amino acid metabolic process	GO:1901605	1.34E-05	5.52E-03	3.89 (8327,142,211,14)
activation of immune response	GO:0002253	1.40E-05	5.56E-03	3.47 (8327,182,211,16)
glutamine family amino acid metabolic process	GO:0009064	2.00E-05	7.66E-03	6.72 (8327,47,211,8)
monosaccharide biosynthetic process	GO:0046364	2.35E-05	8.70E-03	6.58 (8327,48,211,8)
glutamine metabolic process	GO:0006541	2.43E-05	8.72E-03	13.15 (8327,15,211,5)
iron ion homeostasis	GO:0055072	3.20E-05	1.11E-02	6.31 (8327,50,211,8)

innate immune response	GO:0045087	3.28E-05	1.11E-02	2.62 (8327,332,211,22)
single-organism biosynthetic process	GO:0044711	4.38E-05	1.43E-02	2.02 (8327,685,211,35)
gluconeogenesis	GO:0006094	4.69E-05	1.49E-02	7.08 (8327,39,211,7)
complement activation, classical pathway	GO:0006958	4.81E-05	1.48E-02	11.61 (8327,17,211,5)
immune effector process	GO:0002252	5.22E-05	1.57E-02	3.27 (8327,181,211,15)
immune response	GO:0006955	6.83E-05	2.00E-02	2.32 (8327,425,211,25)
positive regulation of immune system process	GO:0002684	7.68E-05	2.19E-02	2.61 (8327,302,211,20)
proton transport	GO:0015992	7.74E-05	2.15E-02	4.93 (8327,72,211,9)
interaction with host	GO:0051701	8.45E-05	2.29E-02	5.54 (8327,57,211,8)
hydrogen transport	GO:0006818	8.64E-05	2.29E-02	4.87 (8327,73,211,9)
cellular response to interferon-gamma	GO:0071346	9.01E-05	2.33E-02	6.42 (8327,43,211,7)
monovalent inorganic cation homeostasis	GO:0055067	9.01E-05	2.28E-02	6.42 (8327,43,211,7)
single-organism carbohydrate metabolic process	GO:0044723	9.78E-05	2.42E-02	2.50 (8327,332,211,21)
immune system process	GO:0002376	1.03E-04	2.49E-02	1.89 (8327,773,211,37)
cation homeostasis	GO:0055080	1.07E-04	2.53E-02	2.94 (8327,215,211,16)
regulation of immune effector process	GO:0002697	1.19E-04	2.75E-02	3.88 (8327,112,211,11)
regulation of pH	GO:0006885	1.29E-04	2.92E-02	7.40 (8327,32,211,6)
cellular amino acid metabolic process	GO:0006520	1.29E-04	2.86E-02	2.68 (8327,265,211,18)
positive regulation of humoral immune response	GO:0002922	1.54E-04	3.37E-02	23.68 (8327,5,211,3)
transition metal ion homeostasis	GO:0055076	1.55E-04	3.32E-02	5.09 (8327,62,211,8)
energy coupled proton transmembrane transport, against electrochemical	GO:0015988	1.85E-04	3.87E-02	8.97 (8327,22,211,5)

gradient				
ATP hydrolysis coupled proton transport	GO:0015991	1.85E-04	3.80E-02	8.97 (8327,22,211,5)
regulation of immune response	GO:0050776	1.89E-04	3.82E-02	2.38 (8327,348,211,21)
response to interferon-gamma	GO:0034341	2.11E-04	4.19E-02	5.64 (8327,49,211,7)
transmembrane transport	GO:0055085	2.21E-04	4.31E-02	2.12 (8327,485,211,26)
glucose metabolic process	GO:0006006	2.27E-04	4.35E-02	3.91 (8327,101,211,10)
ferric iron transport	GO:0015682	2.31E-04	4.35E-02	8.58 (8327,23,211,5)
transferrin transport	GO:0033572	2.31E-04	4.28E-02	8.58 (8327,23,211,5)
trivalent inorganic cation transport	GO:0072512	2.31E-04	4.21E-02	8.58 (8327,23,211,5)
hexose metabolic process	GO:0019318	2.37E-04	4.25E-02	3.59 (8327,121,211,11)
organic anion transport	GO:0015711	2.43E-04	4.29E-02	3.15 (8327,163,211,13)

N - is the total number of genes

B - is the total number of genes associated with a specific GO term

n - is the number of genes in the top of the user's input list or in the target set when appropriate

b - is the number of genes in the intersection

## **Chapter 7**

### **Conclusions and Future Prospects**

## Conclusion

Embryonic patterning, regenerative repair and suppression of cancerous dysregulation all require continuous signal exchange among cells, tissues and organ systems within the body. Alongside well-characterized biochemical modes of cellular communication that regulate cellular behavior during pattern formation, there exists an important and powerful bioelectrical signaling system that is only now beginning to be understood and integrated with canonical biochemical and genetic pathways. Mastery of these endogenous bioelectrical signaling pathways will have transformative implications for developmental biology, regenerative medicine, and synthetic bioengineering.

We present an in-depth literature review of classical and recent studies that support  $V_{\text{mem}}$  as a regulator of cell behavior instrumental in both development and cancer. Current studies are increasingly revealing endogenous bioelectric gradients to be among the most important sources of morphogenetic information *in vivo* [6, 23, 24, 104, 346] and are key determinants of cell migration, differentiation and proliferation. Targeted perturbations of  $V_{\text{mem}}$  result in specific, coherent changes of large-scale patterning that can function over a large range of scales [1, 22, 48]. Not surprisingly, a number of ion channels have also been implicated in enhanced cell migration, motility and invasion; all crucial components of cancer metastasis [87-89, 91].

The *Xenopus* tadpole is an ideal model for understanding the interplay between normal developmental cues during morphogenesis and the defects of morphostasis that manifest as cancer. We demonstrate first that the proper establishment of body axes during embryogenesis involves the proper alignment of cytoskeletal tubulin at very early cleavage stages, a mechanism that is remarkably conserved across kingdoms and many different body plans. This

cytoskeletal transport affects the bioelectrical gradients that are known to drive asymmetry [27, 42]. These data, thus, implicate tubulin as instrumental to overall morphogenesis during development.

Appreciating the role of  $V_{\text{mem}}$  as a regulator of cellular properties with high relevance to both embryonic development and cancer – affecting proliferation, migration and differentiation – we investigated the role of  $V_{\text{mem}}$  changes *in vivo*. We demonstrate how depolarization of glycine-gated chloride channel-expressing cells activates metastatic behavior in an entirely different cell population (melanocytes) through a serotonergic signaling mechanism. This hyperpigmentation phenotype is characterized by a drastic change in melanocyte behavior, affecting proliferation, shape change and migration. By taking advantage of a hypersensitive GlyCl mutant, we were able to define the amount and location of depolarized instructor cells necessary for this embryo-wide change in melanocyte morphology to occur. We demonstrate that depolarization of only a few instructor cells is sufficient to induce hyperpigmentation, and that instructor cell competency is not dependent of being of a neural origin; depolarization of muscle-tissue specific instructor cells also induce embryo-wide hyperpigmentation. Together, these data provide novel insights on this cancer-relevant long-range  $V_{\text{mem}}$  signaling system.

Given the strong melanocyte phenotype, we also sought to determine whether other cell types and tissues are being affected by instructor cell depolarization, but not as easily detected. We identified that depolarization also resulted in dysregulation of vascular patterning and in dystrophic-like development of skeletal muscle in a serotonin-dependent manner. A microarray analysis of gene expression at early and late stages following depolarization identified a number of differentially expressed genes at both developmental

stages including many related to cancers. Furthermore, driving depolarization to muscle-specific cells, resulted in the appearance of cells expressing muscle markers within the neural tube, a region normally devoid of muscle cells. Taken together, these studies reveal how changes in  $V_{mem}$  can function in the morphogenetic regulation of not only melanocytes, but also vasculature, muscle cells, and embryo-wide gene expression.

Finally, we deduced a model for the signaling mechanism by which changes in  $V_{mem}$  are transduced into changes in melanocyte behavior. We first identified the serotonin transporter, SERT, and extracellular serotonin levels in mediating this long-range communication resulting in the neoplastic conversion of melanocytes. In later pharmacological suppression experiments, we implicate the function of the vesicular monoamine transporter (VMAT) and serotonin receptors 1, 2, and 5 in transducing the change in  $V_{mem}$  to changes in melanocyte behavior. We found that the downstream signaling mechanisms are coordinated by cAMP, CREB, and PKA levels, resulting in upregulated expression of the neural crest transcription factors Sox10 and Slug. Furthermore, we demonstrate that the signal transduction involves the MSH-secreting melanotrope cells of the pituitary. Using a novel computational approach, we develop a model for this stochastic yet bi-stable signaling. These data fill in some important gaps in our understanding of how voltage change can affect the behavior of other cell types.

Collectively, the data presented in this dissertation characterize the bioelectric and serotonergic signaling pathway directing metastatic melanocyte behavior in *Xenopus* embryos, and implicate voltage regulation as a novel and tractable control point for cancer.

## Future Directions

Future work will aim to determine whether similar bioelectric and serotonergic signaling can affect the oncogenic properties of mammalian melanoma. A number of ion channels have been implicated with various functions in melanoma, summarized in Table 7.1, while data on channel expression in non-malignant melanocytes remains scarce [623].  $V_{\text{mem}}$  in general has also been linked to melanoma, for example the  $K^+$ -induced membrane voltage and intracellular  $Ca^{2+}$  are involved in the proliferation of the human melanoma cell line SK MEL 28 [624, 625]. Our initial work has demonstrated that exposing human melanocytes in culture to increased  $K^+$  levels by addition of potassium gluconate, thus depolarizing the cells, results in a shape change similar to that in *Xenopus* melanocytes (Figure 3.7). However it remains to be determined whether changes in  $V_{\text{mem}}$  are endogenous factors in melanoma. Furthermore, information relative to non-malignant melanocyte channel expression or function remain scarce, and would need to be continued for potential uses in the treatment of melanoma.

We are currently extending what we have learned in the *Xenopus* system to determine whether  $V_{\text{mem}}$  manipulation affects the oncogenic potential of human melanoma cells *in vitro*, see Appendix 1 for preliminary data. These initial experiments suggest that while the introduction of the hyperpolarizing Kv1.5 and Kir2.1 potassium channels into the A375 melanoma cell line decreases the cells' ability to produce anchorage-independent colonies, it leads to increases in migration. Future work will examine the effects of the introduction of these hyperpolarizing channels has in the *in vivo* melanoma xenograft mouse model.

Finally, while the work presented in this dissertation reveals a thorough characterization of how transmembrane voltage and serotonergic signaling affect melanocytes in *Xenopus laevis* tadpoles, the specifics of what makes an

**Table 7.1 Summary of ion channels expressed in melanoma. Adapted from [626]**

Ion Channel Name	Ion Channel type	Biological Function in Melanoma	Expression		References
			Melanocyte	Melanoma	
Na <sup>+</sup> /K <sup>+</sup> pump ( $\alpha$ 1 subunit)	<i>Ion transporter</i>	Cell survival, cell proliferation	n.d.	Human metastatic melanoma (clinical samples & cell lines)	[627]
TRPM8	<i>TRPC</i>	Cell death	n.d.	Human melanoma (clinical samples & cell lines)	[247]
EAG	<i>K<sup>+</sup> channel</i>	Cell proliferation	n.d.	Melanoma cell lines	[389, 628]
hERG	<i>K<sup>+</sup> channel</i>	Cell proliferation, migration, invasion	n.d.	MDA-MB-435S cell line	[629]
SK3/KCa 2.3	<i>K<sup>+</sup> channel</i>	Cell migration and/or invasion	no	Human melanoma cell lines	[623]
Kv1.3	<i>K<sup>+</sup> channel</i>	Cell adherence	n.d.	Human melanoma (LOX) cell line	[630]
Cav1.3	<i>Voltage-gated Ca<sup>2+</sup> channel</i>	Cell migration and/or invasion	n.d.	Human (A375M, C8161) melanoma cell lines	[631]
TASK-3	<i>Two-pore K<sup>+</sup> channel</i>	Unknown	yes	Human melanoma cell lines	[632, 633]
TRPM2	<i>TRPC</i>	Unknown	no	Melanoma cell lines	[634]
ENaC delta	<i>Na<sup>+</sup> channel</i>	Unknown	n.d.	Human melanoma cell lines	[248]

TRPC: Transient Receptor Potential Channel; n.d.: not determined

instructor cell population remains unknown. It is possible that serotonergic signaling is not necessary for communication between instructor cell and target, in which case the discovery of other signaling mechanisms for this conversation would be necessary. It is also entirely probable that this signaling mechanism is not specifically tied to melanocytes, and may be present among other neural crest derivatives or other cell types in general. Detailed information on what is required to create an instructor cell would aid in the search for other instructor cells that converse with different targets to direct morphological changes in cell behavior, presenting exciting possibilities for the expansion of several branches of biomedicine.

### **Biomedical Implications**

Our data reveals the importance of resting transmembrane potential as a mediator of developmental signals, and show a disruption of these gradients affects not only the metastatic conversion of melanocytes, but also muscle and vascular patterning. In addition to the basic biology revealed by the pathways directing this long-range communication between depolarized cells and those affected, these data suggest a number of candidates for biomedical approaches of relevance not only to developmental patterning, but also to a new understanding of the biophysics of cancer microenvironments. The search for novel types of instructor cells affecting other stem cell populations also adds an interesting dimension to the current focus on stem cells as an important cancer cell population. The ability to modulate membrane voltage without the need for gene therapy is a powerful approach through which to better understand and address the *in vivo* control of patterning in cancer, and represents an exciting future approach for cancer management.

Additionally, transmembrane potential presents an interesting non-invasive diagnostic modality to identify tissues at risk or tumor margins during surgery. Bioelectrical impedance analysis, which determines tissue electrical properties, has shown promise as a prognostic indicator to monitor cancer progression [298, 353]. More recently, the development of non-invasive, voltage-sensitive optical probes provides a potential approach for *in vivo*  $V_{\text{mem}}$  measurement [19, 635]. By coupling voltage sensitive dyes, such as DiBAC<sub>4</sub>(3) with other imaging methods, such as magnetic resonance imaging (MRI) or positron emission tomography (PET), these scans can be analyzed on the basis of dye fluorescence. Such an approach would allow for the visualization of cellular and microenvironment-level bioelectric indicators of possible tumor formation, and may assist in classifying aggressive cancer types that have de-differentiated making them difficult to identify in routine histopathology, such as melanoma [96, 97].

Considering the vast array of therapeutic drugs that target ion channels [636-638], the modulation of  $V_{\text{mem}}$  of destructive tissues may be achieved by adjusting the activities of varied ion channels/transporters through use of well-established drugs, providing a convenient clinical approach for treating cancer. Approved ion channels drugs that work in excitable cells, may prove useful for treating cells outside of the nervous system for novel applications in cancer treatment.

Given that the mechanism by which depolarization can activate metastatic behavior in *Xenopus* melanocytes is modulated by serotonin levels, serotonin signaling may also be a possible target for cancer therapeutics. In addition to its known roles in development and as a neurotransmitter, serotonin also has well-established functions as a mitogenic factor for a wide range of

normal cells in culture, and is a proposed regulator of tumor growth in a wide range of cancers, supporting its proposed role as an unconventional mitogen [260, 451, 452, 639-641]. More often, the effect on serotonin on cell growth is mediated through serotonin receptors 5-HTR1 and 5HTR2 [641]. High levels of 5-HTR2 expression have been considered potentially oncogenic in transfected NIH3T3 fibroblasts and induced tumor formation in nude mice [642-644]. Moreover, the progression of some tumors is accompanied by the dysregulation of the pattern of serotonin receptor expressions. Serotonin receptors, SERT, serotonin synthesis pathways and downstream second messenger signaling thus represent a target for the prevention and treatment of several cancers. However, the use of serotonin receptor agonists and antagonists as anticancer agents is limited due to the many side effects of these compounds. The selective targeting of serotonin receptor agonists or antagonists to tumor cells, or development of serotonin transporter or receptor pharmacological agents that do not cross the blood-brain barrier is thus the challenge in developing serotonin-directed pharmaco-therapies for cancers.

Serotonin levels may also be prognostic marker. Serotonin has already been used as a tumor marker of gastrointestinal carcinoids, as well as bronchial, hepatic, ovarian carcinoids, and more recently, urological tumors [645]. Measurement of serotonin level is also clinically practicable; it is low cost, and easily interpreted when correctly obtained. Monitoring serotonin levels, thus may assist in classifying aggressive cancer types.

Together, ion channels (and bioelectricity in general), as well as serotonin signaling are potential therapeutic and prognostic targets for many types of cancers and at different stages of their progression.

## **Appendix 1**

### **Effect of introducing hyperpolarizing potassium channels into melanoma cell lines**

## Introduction

Bioelectric cues are essential in controlling cell behavior of high relevance to human cancer [22]. Remarkably,  $V_{\text{mem}}$  analysis of multiple cell types as shown that  $V_{\text{mem}}$  distinguishes between quiescent and plastic, uncommitted cells [34, 49]. Not surprisingly, expression patterns of ion channels that control  $V_{\text{mem}}$  have been shown to be altered in several types of cancer [78]. Data from several studies has revealed the possible role for  $V_{\text{mem}}$  as a physiological signal by which carcinogenesis can be regulated [22, 31, 33].

While melanocytes cells are considered to be electrically non-excitabile, they have been shown to express several types of voltage-activated ion channels [646], which is unusual for a non-excitabile cell. However, since melanocytes are derived from the same neural crest stem cell population that give rise to neurons and glia, it is not surprising that melanocytes (and thus melanoma) retain significant neuronal ability. Previous work has shown a number of ion channels are expressed by and active in melanoma cells and/or melanocytes (reviewed in [626]). For example,  $K^+$ -induced membrane voltage and intracellular  $Ca^{2+}$  are involved in the proliferation of the human melanoma cell lines SK MEL 28, A375 and C8161 [624, 625, 631]. Furthermore, work in human skin-derived mast cells has demonstrated the presence of multiple ion channels including the Kir2.1 inward rectifying  $K^+$  channel, the Nav1.8  $Na^+$  channel, and the ClC-3  $Cl^-$  channel [647]. Since the depolarization of GlyCl-expressing cells in *Xenopus* embryos leads to neoplastic-like conversion of melanocytes (a derivative of the neural crest that been shown to contribute to several tumor types including melanoma [31], we sought to determine whether changes in transmembrane potential are an endogenous factor in melanoma as well.

## **Material and Methods**

### ***Cell culture***

The mouse embryonic fibroblast cell line, NIH-3T3, and the human malignant melanoma cell line, A375, was purchased from the American Type Culture Collection (ATCC, Manassas, VA), routinely cultured in Dulbecco's modified Eagle's medium (DMEM, Gibco) supplemented with GlutaMAX (Gibco), 10% heat-inactivated fetal bovine serum (FBS) and 100 U/ml penicillin/streptomycin (Gibco) and incubated in a humidified (37°C, 5% CO<sub>2</sub>) incubator. The melanoma cell line Mel-ST, as well as the immortalized mouse embryonic fibroblast cell line (MEF/SV40) were a gift from N. Wajapeyee (Yale, New Haven, CT), and cultured in DMEM + 10% FBS. The metastatic melanoma cell line C8161 was kindly provided by T. Schatton (Brigham & Women's Hospital, Boston, MA), and cultured in RPMI 1640 (Gibco) supplemented with GlutaMAX (Gibco), 10% heat-inactivated fetal bovine serum (FBS) and 100 U/ml penicillin/streptomycin (Gibco).

### **Lentivirus production**

The hyperpolarizing potassium channels, Kir2.1-Y242F and Kv1.5-THG were cloned into pLenti plasmids containing the CMV promoter, eGFP fluorescent marker and blasticidin resistance gene (for selection). A control lentivirus driving the expression of eGFP alone under the control of the CMV promoter was made using the same pLenti backbone. Lentiviral particles were produced, purified and titrated by the Maine Medical Center Research Institute cell culture and viral vector core facility.

### ***Gene transduction with lentivirus***

Cells were plated onto 6 well plates at  $3 \times 10^5$  cells/well and incubated at 37°C, 5% CO<sub>2</sub> overnight. Cells were washed 1x with PBS and 1 ml of lentiviral supernatants (MOI = 1-2) containing either Kir2.1-Y242F-GFP or Kv1.5-THG-GFP or GFP control was added in each well. All viral supernatants were added with hexadimethrine bromide ((Sigma), final concentration 8 µg/ml) before use. After 24 hr incubation, supernatants were changed with fresh medium and cells were incubated for another 24 hrs before blasticidin selection. Blasticidin selection was performed by treating cell cultures with 5 µg/ml blasticidin for 7-10 days. Following selection, transduced cells were propagated and frozen down for future use.

### ***Colony formation assays***

For anchorage independent colony formation assay, A375 cells, and its derivatives (A375-GFP, A375-Kir2.1-GFP and A375-Kv1.5-GFP) were suspended in DMEM with 0.35% agarose solution (low gelling temperature agarose, Sigma), and plated onto solidified 0.7% agarose in 6 well plate at a density of 2500 cells per well in triplicate. A375 cells were maintained in culture by feeding with 0.5 ml fresh DMEM plus 10% FBS medium twice a week, for a total 3 weeks. Two independent assays were carried out and the number of colonies were counted after staining with 0.05% crystal violet solution at the end of each experiment.

### ***Transwell migration assay***

All A375-derived cell lines (A375, A375-GFP, A375-Kir2.1-GFP and A375-Kv1.5-GFP) were starved overnight in assay medium (DMEM containing GlutaMAX and Pen/Strep with no FBS). The starved cells were trypsinized,  $1 \times 10^5$  cells were

added to the top chambers of the transwell (6.5mm diameter inserts, 8  $\mu$ m pore size; Corning® Costar® Transwell®), and assay medium (DMEM containing 10% FBS) was added to the bottom chambers and incubated for 18 to 10 hours. After overnight incubation, the migratory cells were fixed, stained with 0.1% crystal violet, photographed, and number of migratory cells counted using image J. Each cell line was assayed in triplicate per experiment.

### ***Statistical analysis***

All statistical analyses were performed using the unpaired, two sided Student's *t*-test, and results considered significant when *P* values were less than 0.01.

### **Results**

In order to investigate the changes that  $V_{mem}$  has on melanocyte behavior, we have stably introduced the hyperpolarizing potassium channels Kir2.1-Y242F [648] and Kv1.5 [649] into various melanoma cell lines (A-375, Mel-ST, C-8161) and mouse embryonic fibroblast cell lines (NIH-3T3 and MEF/SV40) using lentiviral transduction. GFP along vector controls were generated for each cell line as well. These new cell lines now stably express these ion channels of interest and can be assayed for oncogenic potential.

One such assay is the soft agar assay for anchorage independent growth in which cells are plated on a semi-solid culture media. A cell's ability to proliferate without attachment to, or spreading onto, a substratum, is one of the hallmarks of transformation and the most accurate *in vitro* indication of tumorigenicity [650]. A soft agar performed on A-375 cells and those with introduced hyperpolarizing ion channels (Kir2.1 and Kv1.5) demonstrate that hyperpolarizing this melanoma cell line has a significant effect on it's growth in

soft agar, affecting both the number of colonies forming in soft agar as well as the distribution of colony size (Figure A1.1). Surprisingly, the GFP-alone vector control cell line displayed decreased growth in soft agar, suggesting that the concentration of blasticidin used to select for transduced cells affected overall growth rate. Future work will address the use of lower concentrations of blasticidin in order to reduce the difference of anchorage independent growth rate between control cell lines. As expected, soft agar assays performed using NIH-3T3 cells, and those derived from NIH-3T3 cells containing hyperpolarizing ion channels resulted in no colony growth (data not shown). Together, these data suggest that hyperpolarizing A375 cell  $V_{mem}$  affects this melanoma cell's ability to grow anchorage independent colonies.

The transwell migration assay is another assay of oncogenic potential, measuring the motility and migratory response of endothelial cells, a process that is critical to metastasis. As shown in Figure A1.2, the introduction of hyperpolarizing  $K^+$  channels into A375 melanoma cells significantly increases migration rates. The introduction of the GFP vector control also had an effect on A375 cell migration, further implying that the concentration of blasticidin used for selection may need to be reduced. This increase in migration is not entirely surprising, as it is well established for many cell types the cell migration is strongly influenced by potassium channels [285, 651-653], and hyperpolarizing melanoma cells has previously shown to increase migration [623]. These results suggest that introduction of potassium channels into melanoma cells may increase migration.

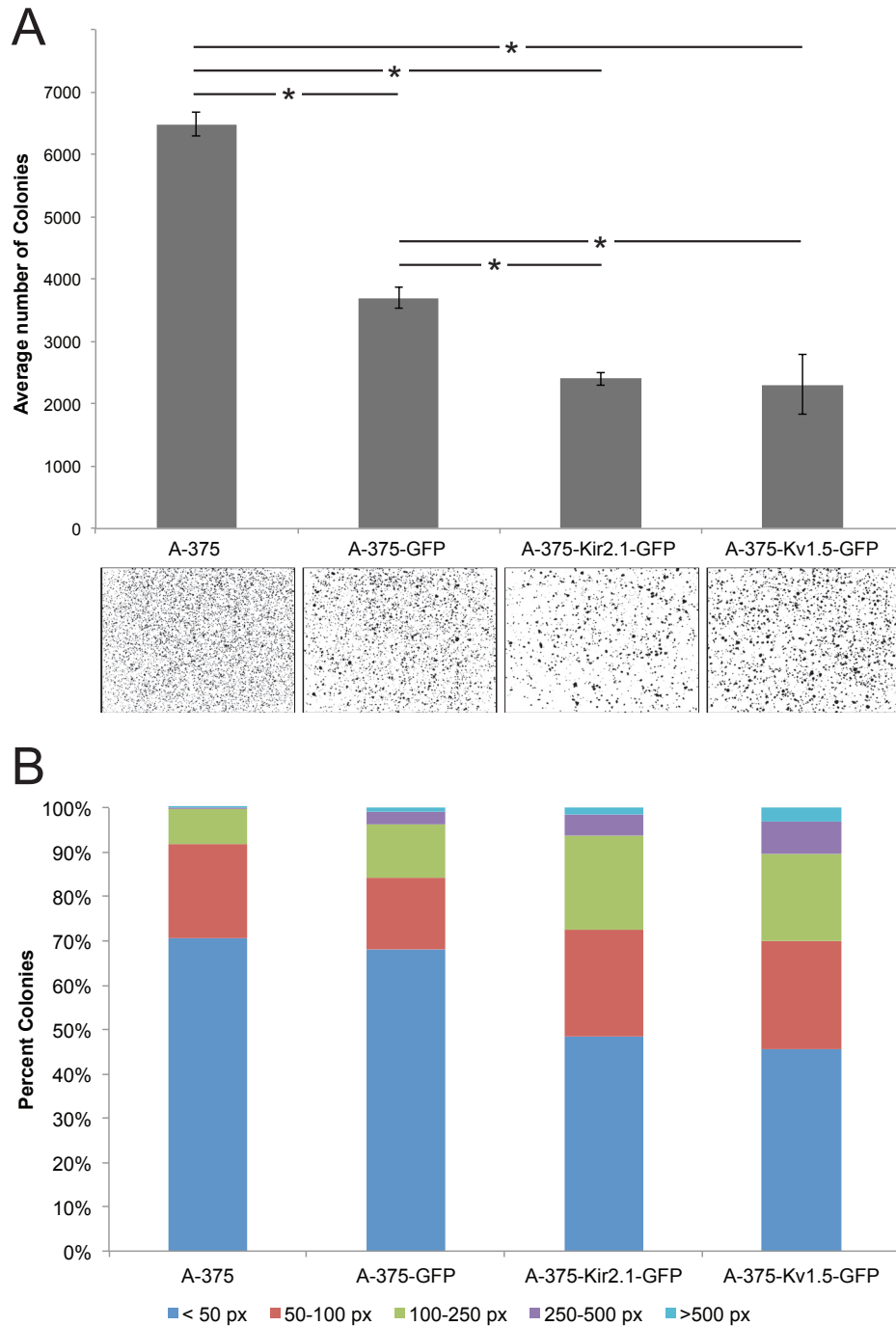


**Figure A1.1 Hyperpolarizing ion channel expression A-375 cells affects soft agar colony formation.**

A. Colony assays in soft agar were done using A-375 cells, A-375-GFP control cells, hyperpolarized A-375-Kir2.1-GFP cells and A-375-Kv1.5-GFP cells.

Representative results, showing sections of stained soft agar plates at 2 wks.

Columns represent mean, error bars represent standard deviation. B. Size

distribution of colony size. \*,  $P < 0.01$ , Student's T-test.

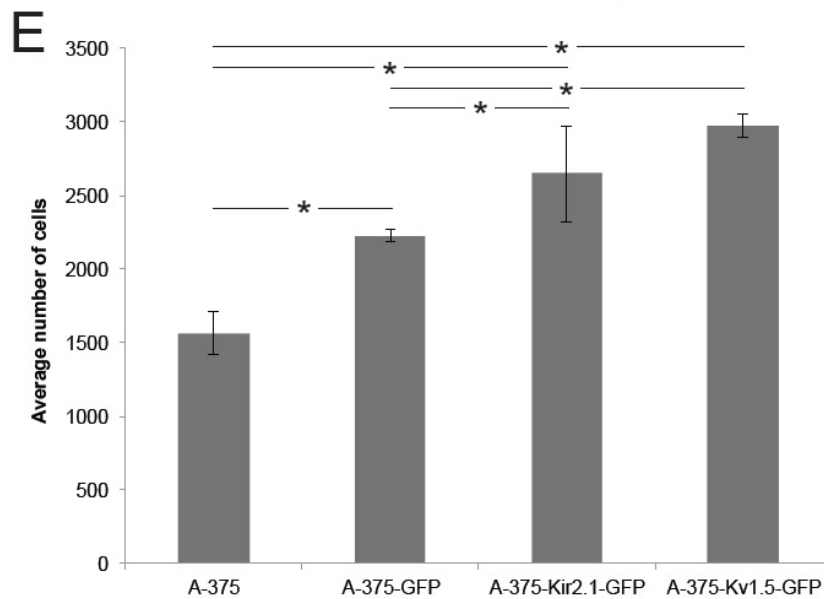
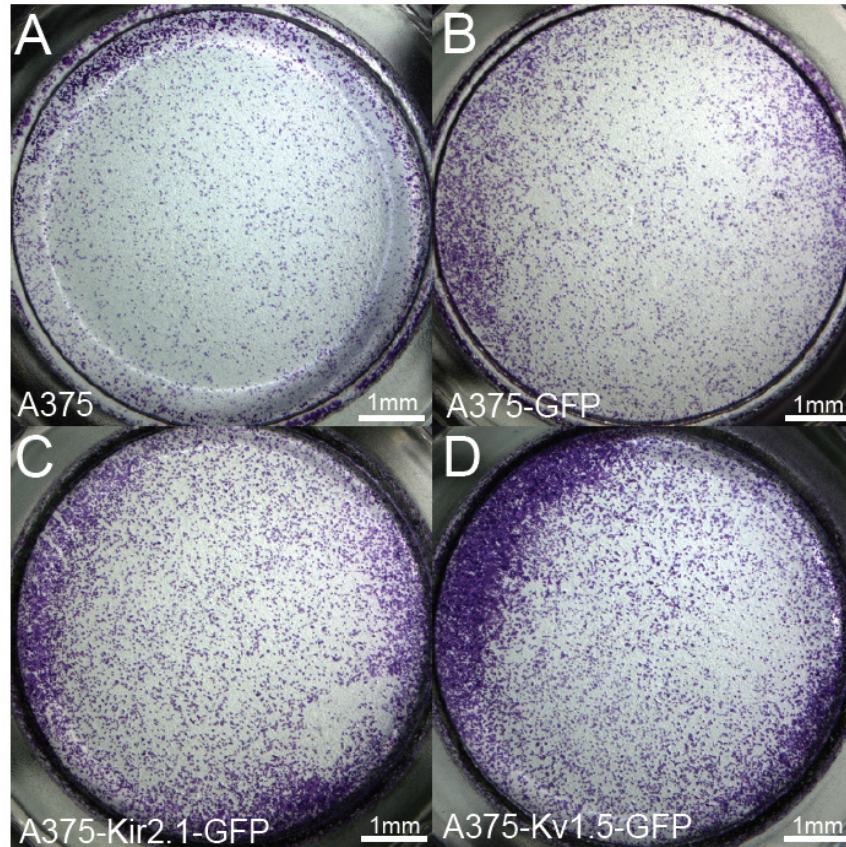


**Figure A1.2 Expression of Kv1.5 and Kir2.1 enhances the motility of melanoma cells**

A-D) Transwell migration assays were performed as described in the 'Materials and methods' section. Images were captured under 2.5X magnification; bars = 1 mm. E) Quantification of transwell migration efficiency. \*, P<0.01, Student's T-Test

## Conclusion

The aberrant expression of potassium channels is a frequent observation in tumors, affecting tumor behavior in often advantageous ways to the cancerous cells [653]. Here we demonstrate that while the introduction of the hyperpolarizing Kv1.5 and Kir2.1 potassium channels in the A375 melanoma cell line decreases their ability to produce anchorage independent colonies, it leads to increases in migration. Potassium channels have been shown to influence cell migration in a number of cell types [285, 651-653], and hyperpolarizing melanoma cells has previously shown to increase migration [623]. These results suggest that the function of these potassium channels function independently of their overall effect on  $V_{mem}$ . However, much further work is necessary to fully elucidate the function of these ion channels. Future experiments will confirm the effect of these ion channels on the overall  $V_{mem}$  of A375 cells, as well as assay the effect of introducing these  $K^+$  channels on melanoma cell invasion and cell proliferation.

Furthermore, future work will examine the effects the introduction of these hyperpolarizing ion channels has in the *in vivo* mouse xenograft model (Figure A1.3). In xenograft studies, cultured cells are generally injected subcutaneously into immunodeficient mice, which are then treated with a compound of interest for 2–6 weeks during which time subcutaneous tumours develop. The study is 'positive' if the compound of interest reduces the rate of growth of new tumors. Using this method we will address whether the  $V_{mem}$  of the host can affect the rate of metastasis of injected C8161 melanoma cells as well as what effect the introduction of ion channels into metastatic melanoma cell lines affects the outcome.

It is clear that potassium channels are involved in cancer; Abnormal

expression of potassium channels has been well documented for many tumor types [654]. While we have a good understanding of the physiological role of potassium channels during their canonical functions, many tumor types exhibit non-canonical potassium channel function [653], suggesting that a better understanding of potassium channel function is necessary for the development of therapeutic treatments. Collectively further investigation is necessary on the potential modulation of  $K^+$  channels as cancer therapy targets.

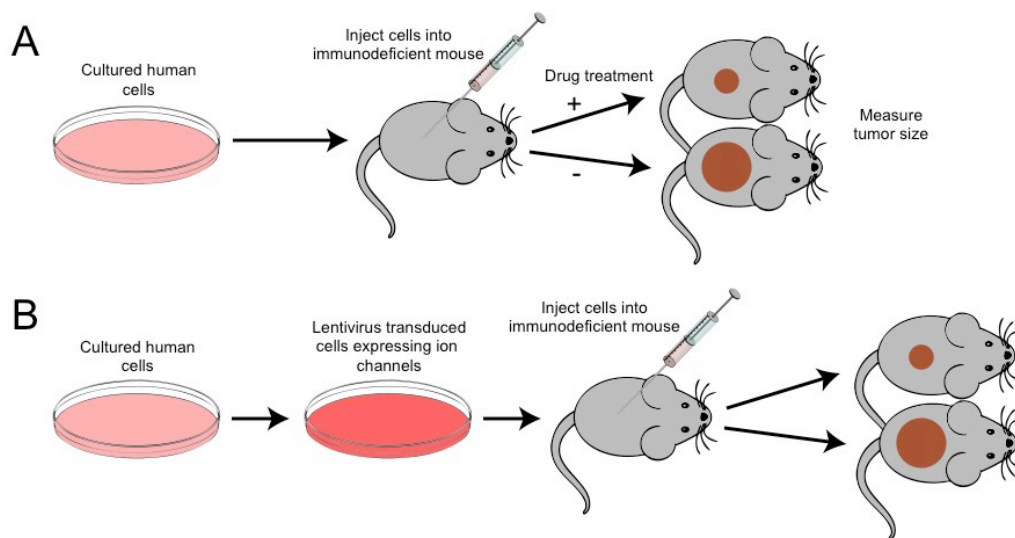


### Figure A1.3 The xenograft mouse model

(A) In xenograft studies, cultured human cells are usually injected subcutaneously into immunodeficient mice, which are then treated with the compound of interest for 2–6 weeks, during which time subcutaneous tumors develop. The tumor size in the treatment group is then compared to that in the control group. (B) To examine the cell-autonomous effect of introduction of ion channels into cell lines, these genes are stably introduced using lentiviral transduction, before being injected subcutaneously into immunodeficient mice. To determine the outcome of the assay, the tumor size in the treatment group is compared to that in the control group.

## References

1. Adams, D.S. and M. Levin, *Endogenous voltage gradients as mediators of cell-cell communication: strategies for investigating bioelectrical signals during pattern formation*. Cell Tissue Res, 2013. **352**(1): p. 95-122.
2. Cobb, M., *Timeline: exorcizing the animal spirits: Jan Swammerdam on nerve function*. Nature reviews. Neuroscience, 2002. **3**(5): p. 395-400.
3. McCaig, C.D., et al., *Controlling cell behavior electrically: current views and future potential*. Physiological reviews, 2005. **85**(3): p. 943-78.
4. Bresadola, M., *Medicine and science in the life of Luigi Galvani (1737-1798)*. Brain research bulletin, 1998. **46**(5): p. 367-80.
5. Abbott, A., *Hidden Treasures: Institute of Physiology collection*. Nature, 2008. **454**(7200): p. 31-31.
6. McCaig, C.D., B. Song, and A.M. Rajnicek, *Electrical dimensions in cell science*. Journal of cell science, 2009. **122**(23): p. 4267-4276.
7. Harold, F.M., *Chapter 26 Pumps and Currents: A Biological Perspective*, in *Current Topics in Membranes and Transport*, F.B. Arnost Kleinzeller and L.S. Clifford, Editors. 1982, Academic Press. p. 485-516.
8. Lund, E.J., *The bio-electric field of the cell and its significance*. Texas reports on biology and medicine, 1947. **5**(4): p. 370.
9. Jaffe, L.F., *The role of ionic currents in establishing developmental pattern*. Philosophical transactions of the Royal Society of London. Series B, Biological sciences, 1981. **295**(1078): p. 553-66.
10. Jaffe, L.F. and R. Nuccitelli, *Electrical controls of development*. Annual review of biophysics and bioengineering, 1977. **6**: p. 445-76.
11. Borgens, R.B., *What is the role of naturally produced electric current in vertebrate regeneration and healing*. Int Rev Cytol, 1982. **76**: p. 245-98.
12. Borgens, R.B., *The role of ionic current in the regeneration and development of the amphibian limb*. Prog Clin Biol Res, 1983. **110 Pt A**: p. 597-608.
13. Nuccitelli, R., *A Two-Dimensional Extracellular Vibrating Probe for the Detection of Trans-Cellular Ionic Currents*. Biophysical Journal, 1987. **51**(2): p. A447-A447.
14. Nuccitelli, R., K. Robinson, and L. Jaffe, *On electrical currents in development*. Bioessays, 1986. **5**(6): p. 292-4.
15. Robinson, K., Messerli, MA., *Electric embryos: the embryonic epithelium*

as a generator of developmental information, in *Nerve Growth and Guidance*, C.D. McCaig, Editor. 1996, Portland Press: London. p. 131-150.

16. Shi, R. and R.B. Borgens, *Three-dimensional gradients of voltage during development of the nervous system as invisible coordinates for the establishment of embryonic pattern*. *Developmental dynamics : an official publication of the American Association of Anatomists*, 1995. **202**(2): p. 101-14.
17. Levin, M., *Molecular bioelectricity in developmental biology: new tools and recent discoveries: control of cell behavior and pattern formation by transmembrane potential gradients*. *BioEssays : news and reviews in molecular, cellular and developmental biology*, 2012. **34**(3): p. 205-17.
18. Zhao, M., et al., *Electrical signals control wound healing through phosphatidylinositol-3-OH kinase-gamma and PTEN*. *Nature*, 2006. **442**(7101): p. 457-60.
19. Adams, D.S. and M. Levin, *General principles for measuring resting membrane potential and ion concentration using fluorescent bioelectricity reporters*. *Cold Spring Harb Protoc*, 2012. **2012**(4): p. 385-97.
20. Adams, D.S., *A new tool for tissue engineers: ions as regulators of morphogenesis during development and regeneration*. *Tissue Eng Part A*, 2008. **14**(9): p. 1461-8.
21. Levin, M., *Bioelectric mechanisms in regeneration: Unique aspects and future perspectives*. *Seminars in cell & developmental biology*, 2009. **20**(5): p. 543-56.
22. Blackiston, D.J., K.A. McLaughlin, and M. Levin, *Bioelectric controls of cell proliferation: ion channels, membrane voltage and the cell cycle*. *Cell cycle*, 2009. **8**(21): p. 3519-28.
23. Levin, M. and C.G. Stevenson, *Regulation of cell behavior and tissue patterning by bioelectrical signals: challenges and opportunities for biomedical engineering*. *Annu Rev Biomed Eng*, 2012. **14**: p. 295-323.
24. Pai, V.P., et al., *Transmembrane voltage potential controls embryonic eye patterning in *Xenopus laevis**. *Development*, 2012. **139**(2): p. 313-23.
25. Nuccitelli, R., *Ionic currents in morphogenesis*. *Experientia*, 1988. **44**(8): p. 657-66.
26. Beane, W.S., et al., *A Chemical Genetics Approach Reveals H,K-ATPase-Mediated Membrane Voltage Is Required for Planarian Head Regeneration*. *Chemistry & Biology*, 2011. **18**(1): p. 77-89.
27. Aw, S., et al., *The ATP-sensitive K(+)-channel (K(ATP)) controls early left-right patterning in *Xenopus* and chick embryos*. *Developmental*

- biology, 2010. **346**(1): p. 39-53.
28. Vandenberg, L.N., R.D. Morrie, and D.S. Adams, *V-ATPase-dependent ectodermal voltage and pH regionalization are required for craniofacial morphogenesis*. Developmental dynamics : an official publication of the American Association of Anatomists, 2011. **240**(8): p. 1889-904.
  29. Adams, D.S., A. Masi, and M. Levin, *H<sup>+</sup> pump-dependent changes in membrane voltage are an early mechanism necessary and sufficient to induce Xenopus tail regeneration*. Development, 2007. **134**(7): p. 1323-35.
  30. Tseng, A.S., et al., *Induction of vertebrate regeneration by a transient sodium current*. The Journal of neuroscience : the official journal of the Society for Neuroscience, 2010. **30**(39): p. 13192-200.
  31. Blackiston, D., et al., *Transmembrane potential of GlyCl-expressing instructor cells induces a neoplastic-like conversion of melanocytes via a serotonergic pathway*. Disease models & mechanisms, 2011. **4**(1): p. 67-85.
  32. Ottesen, E.A. and W.C. Campbell, *Ivermectin in human medicine*. The Journal of antimicrobial chemotherapy, 1994. **34**(2): p. 195-203.
  33. Morokuma, J., et al., *Modulation of potassium channel function confers a hyperproliferative invasive phenotype on embryonic stem cells*. Proceedings of the National Academy of Sciences of the United States of America, 2008. **105**(43): p. 16608-13.
  34. Levin, M., *Large-scale biophysics: ion flows and regeneration*. Trends in cell biology, 2007. **17**(6): p. 261-70.
  35. Arcangeli, A. and A. Becchetti, *Integrin structure and functional relation with ion channels*. Adv Exp Med Biol, 2010. **674**: p. 1-7.
  36. Arcangeli, A., et al., *Integrin-mediated neurite outgrowth in neuroblastoma cells depends on the activation of potassium channels*. J Cell Biol, 1993. **122**(5): p. 1131-43.
  37. Lacroix, J., et al., *Controlling the activity of a phosphatase and tensin homolog (PTEN) by membrane potential*. J Biol Chem, 2011. **286**(20): p. 17945-53.
  38. Okamura, Y. and J.E. Dixon, *Voltage-sensing phosphatase: its molecular relationship with PTEN*. Physiology (Bethesda), 2011. **26**(1): p. 6-13.
  39. Varga, Z., et al., *Switch of voltage-gated K<sup>+</sup> channel expression in the plasma membrane of chondrogenic cells affects cytosolic Ca<sup>2+</sup>-oscillations and cartilage formation*. PLoS One, 2011. **6**(11): p. e27957.
  40. Brooks, R.A. and R.I. Woodruff, *Calmodulin transmitted through gap*

- junctions stimulates endocytic incorporation of yolk precursors in insect oocytes.* Dev Biol, 2004. **271**(2): p. 339-49.
41. Fukumoto, T., I.P. Kema, and M. Levin, *Serotonin signaling is a very early step in patterning of the left-right axis in chick and frog embryos.* Current biology : CB, 2005. **15**(9): p. 794-803.
  42. Levin, M., *Is the early left-right axis like a plant, a kidney, or a neuron? The integration of physiological signals in embryonic asymmetry.* Birth defects research. Part C, Embryo today : reviews, 2006. **78**(3): p. 191-223.
  43. Bustamante, J.O., *Nuclear electrophysiology.* J Membr Biol, 1994. **138**(2): p. 105-12.
  44. Bustamante, J.O., A. Liepins, and J.A. Hanover, *Nuclear pore complex ion channels (review).* Mol Membr Biol, 1994. **11**(3): p. 141-50.
  45. Bustamante, J.O., J.A. Hanover, and A. Liepins, *The ion channel behavior of the nuclear pore complex.* J Membr Biol, 1995. **146**(3): p. 239-51.
  46. Mazzanti, M., J.O. Bustamante, and H. Oberleithner, *Electrical dimension of the nuclear envelope.* Physiol Rev, 2001. **81**(1): p. 1-19.
  47. Adams, D.S. and M. Levin, *Inverse drug screens: a rapid and inexpensive method for implicating molecular targets.* Genesis, 2006. **44**(11): p. 530-40.
  48. Sundelacruz, S., M. Levin, and D.L. Kaplan, *Role of membrane potential in the regulation of cell proliferation and differentiation.* Stem cell reviews, 2009. **5**(3): p. 231-46.
  49. Binggeli, R. and R.C. Weinstein, *Membrane potentials and sodium channels: hypotheses for growth regulation and cancer formation based on changes in sodium channels and gap junctions.* Journal of theoretical biology, 1986. **123**(4): p. 377-401.
  50. Konig, S., et al., *Membrane hyperpolarization triggers myogenin and myocyte enhancer factor-2 expression during human myoblast differentiation.* J Biol Chem, 2004. **279**(27): p. 28187-96.
  51. Konig, S., et al., *The calcineurin pathway links hyperpolarization (Kir2.1)-induced Ca<sup>2+</sup> signals to human myoblast differentiation and fusion.* Development, 2006. **133**(16): p. 3107-14.
  52. Sundelacruz, S., M. Levin, and D.L. Kaplan, *Membrane potential controls adipogenic and osteogenic differentiation of mesenchymal stem cells.* PLoS one, 2008. **3**(11): p. e3737.
  53. Ng, S.Y., et al., *Role of voltage-gated potassium channels in the fate*

- determination of embryonic stem cells*. Journal of cellular physiology, 2010. **224**(1): p. 165-77.
54. Cone, C.D., Jr., *Variation of the transmembrane potential level as a basic mechanism of mitosis control*. Oncology, 1970. **24**(6): p. 438-70.
  55. Cone, C.D. and C.M. Cone, *Induction of mitosis in mature neurons in central nervous system by sustained depolarization*. Science, 1976. **192**(4235): p. 155-8.
  56. Schwab, A., *Function and spatial distribution of ion channels and transporters in cell migration*. American journal of physiology. Renal physiology, 2001. **280**(5): p. F739-47.
  57. Pan, L. and R.B. Borgens, *Perpendicular organization of sympathetic neurons within a required physiological voltage*. Exp Neurol, 2010. **222**(1): p. 161-4.
  58. Marsh, G. and H.W. Beams, *Electrical control of growth polarity in regenerating Dugesia tigrina*. Fed Proc, 1947. **6**(1 Pt 2): p. 163.
  59. Marsh, G. and H.W. Beams, *Electrical control of morphogenesis in regenerating Dugesia tigrina. I. Relation of axial polarity to field strength*. J Cell Physiol, 1952. **39**(2): p. 191-213.
  60. Levin, M., G.A. Buznikov, and J.M. Lauder, *Of minds and embryos: left-right asymmetry and the serotonergic controls of pre-neural morphogenesis*. Developmental neuroscience, 2006. **28**(3): p. 171-85.
  61. Levin, M., et al., *Asymmetries in H<sup>+</sup>/K<sup>+</sup>-ATPase and cell membrane potentials comprise a very early step in left-right patterning*. Cell, 2002. **111**(1): p. 77-89.
  62. Fukumoto, T., R. Blakely, and M. Levin, *Serotonin transporter function is an early step in left-right patterning in chick and frog embryos*. Developmental neuroscience, 2005. **27**(6): p. 349-63.
  63. Tseng, A.S., et al., *Induction of vertebrate regeneration by a transient sodium current*. J Neurosci, 2010. **30**(39): p. 13192-200.
  64. Ring, H., et al., *GABA Maintains the Proliferation of Progenitors in the Developing Chick Ciliary Marginal Zone and Non-Pigmented Ciliary Epithelium*. PloS one, 2012. **7**(5): p. e36874.
  65. Adams, D.S., et al., *Early, H<sup>+</sup>-V-ATPase-dependent proton flux is necessary for consistent left-right patterning of non-mammalian vertebrates*. Development, 2006. **133**(9): p. 1657-71.
  66. Paul, S.M., M.J. Palladino, and G.J. Beitel, *A pump-independent function of the Na,K-ATPase is required for epithelial junction function and tracheal tube-size control*. Development, 2007. **134**(1): p. 147-55.

67. Oviedo, N.J. and W.S. Beane, *Regeneration: The origin of cancer or a possible cure?* Semin Cell Dev Biol, 2009. **20**(5): p. 557-64.
68. Rubin, H., *Cancer as a dynamic developmental disorder.* Cancer Res, 1985. **45**(7): p. 2935-42.
69. Tsonis, P.A., *Embryogenesis and carcinogenesis: order and disorder.* Anticancer Res, 1987. **7**(4A): p. 617-23.
70. Al-Hajj, M. and M.F. Clarke, *Self-renewal and solid tumor stem cells.* Oncogene, 2004. **23**(43): p. 7274-82.
71. Bjerkvig, R., et al., *Opinion: the origin of the cancer stem cell: current controversies and new insights.* Nature reviews. Cancer, 2005. **5**(11): p. 899-904.
72. Reya, T., et al., *Stem cells, cancer, and cancer stem cells.* Nature, 2001. **414**(6859): p. 105-11.
73. Wicha, M.S., *Cancer stem cells and metastasis: lethal seeds.* Clinical cancer research : an official journal of the American Association for Cancer Research, 2006. **12**(19): p. 5606-7.
74. Burr, H.S., *Changes in the Field Properties of Mice with Transplanted Tumors.* The Yale journal of biology and medicine, 1941. **13**(6): p. 783-8.
75. Cameron, I.L. and N.K. Smith, *Cellular concentration of magnesium and other ions in relation to protein synthesis, cell proliferation and cancer.* Magnesium, 1989. **8**(1): p. 31-44.
76. Koch, K.S. and H.L. Leffert, *Increased sodium ion influx is necessary to initiate rat hepatocyte proliferation.* Cell, 1979. **18**(1): p. 153-63.
77. Rozengurt, E. and S. Mendoza, *Monovalent ion fluxes and the control of cell proliferation in cultured fibroblasts.* Annals of the New York Academy of Sciences, 1980. **339**: p. 175-90.
78. Fiske, J.L., et al., *Voltage-sensitive ion channels and cancer.* Cancer metastasis reviews, 2006. **25**(3): p. 493-500.
79. Kunzelmann, K., *Ion channels and cancer.* The Journal of membrane biology, 2005. **205**(3): p. 159-73.
80. Pardo, L.A., et al., *Role of voltage-gated potassium channels in cancer.* The Journal of membrane biology, 2005. **205**(3): p. 115-24.
81. Prevarskaya, N., L. Zhang, and G. Barritt, *TRP channels in cancer.* Biochimica et biophysica acta, 2007. **1772**(8): p. 937-46.
82. Roger, S., et al., *Voltage-gated sodium channels: new targets in cancer therapy?* Current pharmaceutical design, 2006. **12**(28): p. 3681-95.

83. Hanahan, D. and R.A. Weinberg, *The hallmarks of cancer*. Cell, 2000. **100**(1): p. 57-70.
84. Prevarskaya, N., R. Skryma, and Y. Shuba, *Ion channels and the hallmarks of cancer*. Trends in molecular medicine, 2010. **16**(3): p. 107-21.
85. Freedman, B.D., M.A. Price, and C.J. Deutsch, *Evidence for voltage modulation of IL-2 production in mitogen-stimulated human peripheral blood lymphocytes*. Journal of immunology, 1992. **149**(12): p. 3784-94.
86. Cone, C.D., Jr. and M. Tongier, Jr., *Contact inhibition of division: involvement of the electrical transmembrane potential*. Journal of cellular physiology, 1973. **82**(3): p. 373-86.
87. Diaz, D., et al., *Functional expression of voltage-gated sodium channels in primary cultures of human cervical cancer*. Journal of cellular physiology, 2007. **210**(2): p. 469-78.
88. Diss, J.K., et al., *A potential novel marker for human prostate cancer: voltage-gated sodium channel expression in vivo*. Prostate cancer and prostatic diseases, 2005. **8**(3): p. 266-73.
89. Fraser, S.P., et al., *Voltage-gated sodium channel expression and potentiation of human breast cancer metastasis*. Clinical cancer research : an official journal of the American Association for Cancer Research, 2005. **11**(15): p. 5381-9.
90. Roger, S., et al., *Voltage-gated sodium channels potentiate the invasive capacities of human non-small-cell lung cancer cell lines*. The international journal of biochemistry & cell biology, 2007. **39**(4): p. 774-86.
91. McFerrin, M.B. and H. Sontheimer, *A role for ion channels in glioma cell invasion*. Neuron glia biology, 2006. **2**(1): p. 39-49.
92. Chernet, B.T. and M. Levin, *Transmembrane voltage potential is an essential cellular parameter for the detection and control of tumor development in a Xenopus model*. Dis Model Mech, 2013. **6**(3): p. 595-607.
93. Lobikin, M., et al., *Early, nonciliary role for microtubule proteins in left-right patterning is conserved across kingdoms*. Proceedings of the National Academy of Sciences of the United States of America, 2012. **109**(31): p. 12586-91.
94. White, R.M. and L.I. Zon, *Melanocytes in development, regeneration, and cancer*. Cell stem cell, 2008. **3**(3): p. 242-52.
95. Dean, M., T. Fojo, and S. Bates, *Tumour stem cells and drug resistance*. Nature reviews. Cancer, 2005. **5**(4): p. 275-84.

96. Bittner, M., et al., *Molecular classification of cutaneous malignant melanoma by gene expression profiling*. Nature, 2000. **406**(6795): p. 536-40.
97. Hendrix, M.J., et al., *Vasculogenic mimicry and tumour-cell plasticity: lessons from melanoma*. Nature reviews. Cancer, 2003. **3**(6): p. 411-21.
98. Vaux, D.L., *Response to "The tissue organization field theory of cancer: a testable replacement for the somatic mutation theory"*. DOI: 10.1002/bies.201100025. Bioessays, 2011. **33**(9): p. 660-1.
99. Vaux, D.L., *In defense of the somatic mutation theory of cancer*. Bioessays, 2011. **33**(5): p. 341-3.
100. Hendrix, M.J., et al., *Reprogramming metastatic tumour cells with embryonic microenvironments*. Nat Rev Cancer, 2007. **7**(4): p. 246-55.
101. Sonnenschein, C. and A.M. Soto, *The death of the cancer cell*. Cancer Res, 2011. **71**(13): p. 4334-7.
102. Soto, A.M. and C. Sonnenschein, *The tissue organization field theory of cancer: a testable replacement for the somatic mutation theory*. Bioessays, 2011. **33**(5): p. 332-40.
103. Soto, A.M. and C. Sonnenschein, *The somatic mutation theory of cancer: growing problems with the paradigm?* Bioessays, 2004. **26**(10): p. 1097-107.
104. Levin, M., *Morphogenetic fields in embryogenesis, regeneration, and cancer: non-local control of complex patterning*. Biosystems, 2012. **109**(3): p. 243-61.
105. Peeters, H. and K. Devriendt, *Human laterality disorders*. European journal of medical genetics, 2006. **49**(5): p. 349-62.
106. Tabin, C., *Do we know anything about how left-right asymmetry is first established in the vertebrate embryo?* Journal of molecular histology, 2005. **36**(5): p. 317-23.
107. Vandenberg, L.N. and M. Levin, *Perspectives and open problems in the early phases of left-right patterning*. Seminars in cell & developmental biology, 2009. **20**(4): p. 456-63.
108. Aw, S. and M. Levin, *Is left-right asymmetry a form of planar cell polarity?* Development, 2009. **136**(3): p. 355-66.
109. Wolpert, L., *Diffusible gradients are out - an interview with Lewis Wolpert. Interviewed by Richardson, Michael K*. Int J Dev Biol, 2009. **53**(5-6): p. 659-62.
110. Basu, B. and M. Bruedner, *Cilia: multifunctional organelles at the center*

- of vertebrate left-right asymmetry*, in *Ciliary Function in Mammalian Development*, B.K. Yoder, Editor. 2008, Elsevier Academic Press Inc: San Diego. p. 151-174.
111. Speder, P., et al., *Strategies to establish left/right asymmetry in vertebrates and invertebrates*. *Current opinion in genetics & development*, 2007. **17**(4): p. 351-8.
  112. Gros, J., et al., *Cell movements at Hensen's node establish left/right asymmetric gene expression in the chick*. *Science*, 2009. **324**(5929): p. 941-4.
  113. Armakolas, A. and A.J. Klar, *Left-right dynein motor implicated in selective chromatid segregation in mouse cells*. *Science*, 2007. **315**(5808): p. 100-1.
  114. Klar, A.J., *Support for the selective chromatid segregation hypothesis advanced for the mechanism of left-right body axis development in mice*. *Breast Dis*, 2008. **29**: p. 47-56.
  115. Zhang, Y. and M. Levin, *Left-right asymmetry in the chick embryo requires core planar cell polarity protein Vangl2*. *Genesis*, 2009. **47**(11): p. 719-28.
  116. Levin, M. and A.R. Palmer, *Left-right patterning from the inside out: widespread evidence for intracellular control*. *BioEssays : news and reviews in molecular, cellular and developmental biology*, 2007. **29**(3): p. 271-87.
  117. Vandenberg, L.N. and M. Levin, *Far from solved: a perspective on what we know about early mechanisms of left-right asymmetry*. *Developmental dynamics : an official publication of the American Association of Anatomists*, 2010. **239**(12): p. 3131-46.
  118. Abe, T., S. Thitamadee, and T. Hashimoto, *Microtubule defects and cell morphogenesis in the lefty1lefty2 tubulin mutant of Arabidopsis thaliana*. *Plant & cell physiology*, 2004. **45**(2): p. 211-20.
  119. Thitamadee, S., K. Tuchiara, and T. Hashimoto, *Microtubule basis for left-handed helical growth in Arabidopsis*. *Nature*, 2002. **417**(6885): p. 193-6.
  120. Nakamura, M. and T. Hashimoto, *A mutation in the Arabidopsis gamma-tubulin-containing complex causes helical growth and abnormal microtubule branching*. *Journal of cell science*, 2009. **122**(Pt 13): p. 2208-17.
  121. Ishida, T., et al., *Helical microtubule arrays in a collection of twisting tubulin mutants of Arabidopsis thaliana*. *Proc Natl Acad Sci U S A*, 2007. **104**(20): p. 8544-9.

122. Sive, H., Grainger RM., Harland RM., *Early Development of Xenopus Laevis: A Laboratory Manual*. 2000, New York: Cold Spring Harbor Laboratory Press.
123. Aw, S., et al., *H,K-ATPase protein localization and Kir4.1 function reveal concordance of three axes during early determination of left-right asymmetry*. *Mech Dev*, 2008. **125**(3-4): p. 353-72.
124. Vick, P., et al., *Flow on the right side of the gastrocoel roof plate is dispensable for symmetry breakage in the frog Xenopus laevis*. *Dev Biol*, 2009. **331**(2): p. 281-91.
125. Blum, M., et al., *Xenopus, an ideal model system to study vertebrate left-right asymmetry*. *Developmental dynamics : an official publication of the American Association of Anatomists*, 2009. **238**(6): p. 1215-25.
126. Toyozumi, R., et al., *Xenopus nodal related-1 is indispensable only for left-right axis determination*. *International Journal of Developmental Biology*, 2005. **49**(8): p. 923-938.
127. Sampath, K., et al., *Functional differences among Xenopus nodal-related genes in left-right axis determination*. *Development*, 1997. **124**(17): p. 3293-3302.
128. Levin, M., *Motor protein control of ion flux is an early step in embryonic left-right asymmetry*. *BioEssays : news and reviews in molecular, cellular and developmental biology*, 2003. **25**(10): p. 1002-10.
129. Qiu, D., et al., *Localization and loss-of-function implicates ciliary proteins in early, cytoplasmic roles in left-right asymmetry*. *Dev Dyn*, 2005. **234**(1): p. 176-89.
130. Clark, I., et al., *Transient posterior localization of a kinesin fusion protein reflects anteroposterior polarity of the Drosophila oocyte*. *Curr Biol*, 1994. **4**(4): p. 289-300.
131. Bernstein, B.W. and J.R. Bamberg, *ADF/Cofilin: a functional node in cell biology*. *Trends in cell biology*, 2010. **20**(4): p. 187-195.
132. Gu, J., et al., *ADF/cofilin-mediated actin dynamics regulate AMPA receptor trafficking during synaptic plasticity*. *Nat Neurosci*, 2010. **13**(10): p. 1208-15.
133. Roberts, R.M., et al., *Transcript profiling of individual twin blastomeres derived by splitting two-cell stage murine embryos*. *Biol Reprod*, 2011. **84**(3): p. 487-94.
134. Troemel, E.R., A. Sagasti, and C.I. Bargmann, *Lateral signaling mediated by axon contact and calcium entry regulates asymmetric odorant receptor expression in C. elegans*. *Cell*, 1999. **99**(4): p. 387-98.

135. Chang, C., et al., *Microtubule-based localization of a synaptic calcium-signaling complex is required for left-right neuronal asymmetry in C. elegans*. *Development*, 2011. **138**(16): p. 3509-18.
136. Wan, L.Q., et al., *Micropatterned mammalian cells exhibit phenotype-specific left-right asymmetry*. *Proc Natl Acad Sci U S A*, 2011. **108**(30): p. 12295-300.
137. Xu, J., et al., *Polarity reveals intrinsic cell chirality*. *Proceedings of the National Academy of Sciences of the United States of America*, 2007. **104**(22): p. 9296-300.
138. Manner, J., *Does an equivalent of the "ventral node" exist in chick embryos? A scanning electron microscopic study*. *Anat Embryol (Berl)*, 2001. **203**(6): p. 481-90.
139. Tian, T., et al., *Both foxj1a and foxj1b are implicated in left-right asymmetric development in zebrafish embryos*. *Biochem Biophys Res Commun*, 2009. **380**(3): p. 537-42.
140. Serluca, F.C., et al., *Mutations in zebrafish leucine-rich repeat-containing six-like affect cilia motility and result in pronephric cysts, but have variable effects on left-right patterning*. *Development*, 2009. **136**(10): p. 1621-31.
141. Zhao, C. and J. Malicki, *Genetic defects of pronephric cilia in zebrafish*. *Mech Dev*, 2007. **124**(7-8): p. 605-16.
142. Zeng, H., A.N. Hoover, and A. Liu, *PCP effector gene Inturned is an important regulator of cilia formation and embryonic development in mammals*. *Dev Biol*, 2010. **339**(2): p. 418-28.
143. Gardner, R.L., *Normal bias in the direction of fetal rotation depends on blastomere composition during early cleavage in the mouse*. *PLoS One*, 2010. **5**(3): p. e9610.
144. Deinum, E.E., S.H. Tindemans, and B.M. Mulder, *Taking directions: the role of microtubule-bound nucleation in the self-organization of the plant cortical array*. *Phys Biol*, 2011. **8**(5): p. 056002.
145. Brown, N.A. and L. Wolpert, *The development of handedness in left/right asymmetry*. *Development*, 1990. **109**(1): p. 1-9.
146. Carneiro, K., et al., *Histone deacetylase activity is necessary for left-right patterning during vertebrate development*. *BMC developmental biology*, 2011. **11**: p. 29.
147. Kuroda, R., et al., *Chiral blastomere arrangement dictates zygotic left-right asymmetry pathway in snails*. *Nature*, 2009. **462**(7274): p. 790-4.
148. Danilchik, M.V., E.E. Brown, and K. Riepert, *Intrinsic chiral properties of the Xenopus egg cortex: an early indicator of left-right asymmetry?*

- Development, 2006. **133**(22): p. 4517-26.
149. Yost, H.J., *Development of the left-right axis in amphibians*. Ciba Found Symp, 1991. **162**: p. 165-76; discussion 176-81.
  150. Klar, A.J., *A model for specification of the left-right axis in vertebrates*. Trends Genet, 1994. **10**(11): p. 392-6.
  151. Levin, M. and N. Nascone, *Two molecular models of initial left-right asymmetry generation*. Med Hypotheses, 1997. **49**(5): p. 429-35.
  152. Oviedo, N.J. and M. Levin, *Gap junctions provide new links in left-right patterning*. Cell, 2007. **129**(4): p. 645-7.
  153. Mello, C. and A. Fire, *DNA transformation*. Methods Cell Biol, 1995. **48**: p. 451-82.
  154. Nieuwkoop, P.D. and J. Faber, *Normal table of Xenopus laevis (Daudin)*. . Normal table of Xenopus laevis. 1967, Amsterdam: (North Holland Publ. Co.). pp. vi + 243.
  155. Brenner, S., *The genetics of Caenorhabditis elegans*. Genetics, 1974. **77**(1): p. 71-94.
  156. Levin, M. and M. Mercola, *Gap junctions are involved in the early generation of left-right asymmetry*. Developmental biology, 1998. **203**(1): p. 90-105.
  157. Harland, R.M., *In situ hybridization: an improved whole-mount method for Xenopus embryos*. Methods in Cell Biology, 1991. **36**: p. 685-695.
  158. Xu, J., et al., *Divergent signals and cytoskeletal assemblies regulate self-organizing polarity in neutrophils*. Cell, 2003. **114**(2): p. 201-14.
  159. Abe, T. and T. Hashimoto, *Altered microtubule dynamics by expression of modified alpha-tubulin protein causes right-handed helical growth in transgenic Arabidopsis plants*. The Plant journal : for cell and molecular biology, 2005. **43**(2): p. 191-204.
  160. Gonzalez, C., *Spindle orientation, asymmetric division and tumour suppression in Drosophila stem cells*. Nat Rev Genet, 2007. **8**(6): p. 462-72.
  161. Hess, A.R., et al., *Deciphering the signaling events that promote melanoma tumor cell vasculogenic mimicry and their link to embryonic vasculogenesis: role of the Eph receptors*. Dev Dyn, 2007. **236**(12): p. 3283-96.
  162. Kyrgidis, A., T.G. Tzellos, and S. Triaridis, *Melanoma: Stem cells, sun exposure and hallmarks for carcinogenesis, molecular concepts and future clinical implications*. J Carcinog, 2010. **9**: p. 3.

163. Lee, L.M., et al., *The fate of human malignant melanoma cells transplanted into zebrafish embryos: assessment of migration and cell division in the absence of tumor formation*. Dev Dyn, 2005. **233**(4): p. 1560-70.
164. Lee, M. and V. Vasioukhin, *Cell polarity and cancer--cell and tissue polarity as a non-canonical tumor suppressor*. J Cell Sci, 2008. **121**(Pt 8): p. 1141-50.
165. Levin, M., *Errors of geometry: regeneration in a broader perspective*. Seminars in cell & developmental biology, 2009. **20**(6): p. 643-5.
166. Al-Hajj, M., et al., *Therapeutic implications of cancer stem cells*. Curr Opin Genet Dev, 2004. **14**(1): p. 43-7.
167. Hong, J.H., et al., *K6PC-5, a direct activator of sphingosine kinase 1, promotes epidermal differentiation through intracellular Ca<sup>2+</sup> signaling*. J Invest Dermatol, 2008. **128**(9): p. 2166-78.
168. Domen, J., K.L. Gandy, and I.L. Weissman, *Systemic overexpression of BCL-2 in the hematopoietic system protects transgenic mice from the consequences of lethal irradiation*. Blood, 1998. **91**(7): p. 2272-82.
169. Domen, J. and I.L. Weissman, *Hematopoietic stem cells need two signals to prevent apoptosis; BCL-2 can provide one of these, Kitl/c-Kit signaling the other*. J Exp Med, 2000. **192**(12): p. 1707-18.
170. Taipale, J. and P.A. Beachy, *The Hedgehog and Wnt signalling pathways in cancer*. Nature, 2001. **411**(6835): p. 349-54.
171. Varnum-Finney, B., et al., *Pluripotent, cytokine-dependent, hematopoietic stem cells are immortalized by constitutive Notch1 signaling*. Nat Med, 2000. **6**(11): p. 1278-81.
172. Ingber, D.E. and M. Levin, *What lies at the interface of regenerative medicine and developmental biology?* Development, 2007. **134**(14): p. 2541-7.
173. Ingber, D.E., *Can cancer be reversed by engineering the tumor microenvironment?* Seminars in cancer biology, 2008. **18**(5): p. 356-64.
174. Sauka-Spengler, T. and M. Bronner-Fraser, *Evolution of the neural crest viewed from a gene regulatory perspective*. Genesis, 2008. **46**(11): p. 673-82.
175. Bergstrom, C.S., et al., *Iris hypoplasia and aorticopulmonary septal defect: a neurocristopathy*. J AAPOS, 2005. **9**(3): p. 264-7.
176. Bolande, R.P., *Neurocristopathy: its growth and development in 20 years*. Pediatric pathology & laboratory medicine : journal of the Society for Pediatric Pathology, affiliated with the International Paediatric Pathology

- Association, 1997. **17**(1): p. 1-25.
177. Inoue, K., et al., *Translation of SOX10 3' untranslated region causes a complex severe neurocristopathy by generation of a deleterious functional domain*. Hum Mol Genet, 2007. **16**(24): p. 3037-46.
  178. Crane, J.F. and P.A. Trainor, *Neural crest stem and progenitor cells*. Annual review of cell and developmental biology, 2006. **22**: p. 267-86.
  179. Fuchs, S. and L. Sommer, *The neural crest: understanding stem cell function in development and disease*. Neuro-degenerative diseases, 2007. **4**(1): p. 6-12.
  180. Tucker, R.P., *Neural crest cells: a model for invasive behavior*. Int J Biochem Cell Biol, 2004. **36**(2): p. 173-7.
  181. Cooper, C.D. and D.W. Raible, *Mechanisms for reaching the differentiated state: Insights from neural crest-derived melanocytes*. Semin Cell Dev Biol, 2009. **20**(1): p. 105-10.
  182. Kuriyama, S. and R. Mayor, *Molecular analysis of neural crest migration*. Philos Trans R Soc Lond B Biol Sci, 2008. **363**(1495): p. 1349-62.
  183. Macmillan, G.J., *Melanoblast-tissue interactions and the development of pigment pattern in Xenopus larvae*. J Embryol Exp Morphol, 1976. **35**(3): p. 463-84.
  184. Haass, N.K. and M. Herlyn, *Normal human melanocyte homeostasis as a paradigm for understanding melanoma*. J Investig Dermatol Symp Proc, 2005. **10**(2): p. 153-63.
  185. Haass, N.K., et al., *Adhesion, migration and communication in melanocytes and melanoma*. Pigment Cell Res, 2005. **18**(3): p. 150-9.
  186. Maniotis, A.J., et al., *Vascular channel formation by human melanoma cells in vivo and in vitro: vasculogenic mimicry*. Am J Pathol, 1999. **155**(3): p. 739-52.
  187. Baylin, S.B. and J.E. Ohm, *Epigenetic gene silencing in cancer - a mechanism for early oncogenic pathway addiction?* Nat Rev Cancer, 2006. **6**(2): p. 107-16.
  188. Bulic-Jakus, F., et al., *Of mice and men: teratomas and teratocarcinomas*. Coll Antropol, 2006. **30**(4): p. 921-4.
  189. Ducasse, M. and M.A. Brown, *Epigenetic aberrations and cancer*. Mol Cancer, 2006. **5**: p. 60.
  190. Jaffe, L.F., *Epigenetic theories of cancer initiation*. Adv Cancer Res, 2003. **90**: p. 209-30.

191. Park, P.C., et al., *Stem cell enrichment approaches*. Semin Cancer Biol, 2007. **17**(3): p. 257-64.
192. Rubin, H., *The significance of biological heterogeneity*. Cancer Metastasis Rev, 1990. **9**(1): p. 1-20.
193. Welsch, T., J. Kleeff, and H. Friess, *Molecular pathogenesis of pancreatic cancer: advances and challenges*. Curr Mol Med, 2007. **7**(5): p. 504-21.
194. Bissell, M.J. and M.A. Labarge, *Context, tissue plasticity, and cancer: are tumor stem cells also regulated by the microenvironment?* Cancer Cell, 2005. **7**(1): p. 17-23.
195. Uzman, J.A., et al., *The role of intracellular alkalinization in the establishment of anterior neural fate in Xenopus*. Dev Biol, 1998. **193**(1): p. 10-20.
196. Borgens, R.B., et al., *Electric Fields in Vertebrate Repair*. 1989, New York.
197. Jaffe, L., *Developmental currents, voltages, and gradients*, in *Developmental Order: its Origin and Regulation*, S. Subtelny, Editor. 1982, Alan R. Liss: New York. p. 183-215.
198. Nuccitelli, R., *A two-dimensional vibrating probe with a computerized graphics display*. Prog Clin Biol Res, 1986. **210**: p. 13-20.
199. Adams, D.S. and M. Levin, *Strategies and Techniques for investigations of biophysical signals in patterning*, in *Analysis of Growth Factor Signalling in Embryos*, M. Whitman and A.K. Sater, Editors. 2006, Taylor and Francis Books. p. 177-262.
200. Reid, B., R. Nuccitelli, and M. Zhao, *Non-invasive measurement of bioelectric currents with a vibrating probe*. Nat Protoc, 2007. **2**(3): p. 661-9.
201. Song, B., et al., *Application of direct current electric fields to cells and tissues in vitro and modulation of wound electric field in vivo*. Nat Protoc, 2007. **2**(6): p. 1479-89.
202. Pullar, C.E., et al., *beta4 integrin and epidermal growth factor coordinately regulate electric field-mediated directional migration via Rac1*. Mol Biol Cell, 2006. **17**(11): p. 4925-35.
203. Rajnicek, A.M., L.E. Foubister, and C.D. McCaig, *Growth cone steering by a physiological electric field requires dynamic microtubules, microfilaments and Rac-mediated filopodial asymmetry*. J Cell Sci, 2006. **119**(Pt 9): p. 1736-45.
204. Olivotto, M., et al., *Electric fields at the plasma membrane level: a neglected element in the mechanisms of cell signalling*. Bioessays, 1996.

18(6): p. 495-504.

205. Arcangeli, A., *Expression and role of hERG channels in cancer cells*. Novartis Found Symp, 2005. **266**: p. 225-32; discussion 232-4.
206. Arcangeli, A., et al., *Targeting ion channels in cancer: a novel frontier in antineoplastic therapy*. Curr Med Chem, 2009. **16**(1): p. 66-93.
207. Biagiotti, T., et al., *Cell renewing in neuroblastoma: electrophysiological and immunocytochemical characterization of stem cells and derivatives*. Stem cells, 2006. **24**(2): p. 443-53.
208. Cai, J., et al., *Membrane properties of rat embryonic multipotent neural stem cells*. Journal of neurochemistry, 2004. **88**(1): p. 212-26.
209. Gersdorff Korsgaard, M., et al., *Identification of a novel voltage-gated Na<sup>+</sup> channel rNav1.5a in the rat hippocampal progenitor stem cell line HiB5*. Pflügers Archiv, 2001. **443**(1): p. 18-30.
210. Heubach, J.F., et al., *Electrophysiological properties of human mesenchymal stem cells*. The Journal of physiology, 2004. **554**(Pt 3): p. 659-72.
211. van Kempen, M., et al., *Expression of the electrophysiological system during murine embryonic stem cell cardiac differentiation*. Cell Physiol Biochem, 2003. **13**(5): p. 263-70.
212. Cho, T., et al., *Human neural stem cells: electrophysiological properties of voltage-gated ion channels*. Neuroreport, 2002. **13**(11): p. 1447-52.
213. Sun, W., et al., *Voltage-sensitive and ligand-gated channels in differentiating neural stem-like cells derived from the nonhematopoietic fraction of human umbilical cord blood*. Stem Cells, 2005. **23**(7): p. 931-45.
214. Pfeifer, A. and I.M. Verma, *Gene therapy: promises and problems*. Annu Rev Genomics Hum Genet, 2001. **2**: p. 177-211.
215. Thomas, C.E., A. Ehrhardt, and M.A. Kay, *Progress and problems with the use of viral vectors for gene therapy*. Nat Rev Genet, 2003. **4**(5): p. 346-58.
216. Lerchner, W., et al., *Reversible silencing of neuronal excitability in behaving mice by a genetically targeted, ivermectin-gated Cl<sup>-</sup> channel*. Neuron, 2007. **54**(1): p. 35-49.
217. Shan, Q., J.L. Haddrill, and J.W. Lynch, *Ivermectin, an unconventional agonist of the glycine receptor chloride channel*. The Journal of biological chemistry, 2001. **276**(16): p. 12556-64.
218. Collazo, A., M. Bronner-Fraser, and S.E. Fraser, *Vital dye labelling of*

- Xenopus laevis* trunk neural crest reveals multipotency and novel pathways of migration. *Development*, 1993. **118**(2): p. 363-76.
219. Kumasaka, M., et al., *Regulation of melanoblast and retinal pigment epithelium development by Xenopus laevis Mitf*. *Developmental dynamics* : an official publication of the American Association of Anatomists, 2005. **234**(3): p. 523-34.
220. Tomlinson, M.L., et al., *Chemical genomics identifies compounds affecting Xenopus laevis pigment cell development*. *Mol Biosyst*, 2009. **5**(4): p. 376-84.
221. Tomlinson, M.L., et al., *A chemical genomic approach identifies matrix metalloproteinases as playing an essential and specific role in Xenopus melanophore migration*. *Chem Biol*, 2009. **16**(1): p. 93-104.
222. Tseng, A.S., et al., *Apoptosis is required during early stages of tail regeneration in Xenopus laevis*. *Developmental biology*, 2007. **301**(1): p. 62-9.
223. Kumasaka, M., et al., *Isolation and developmental expression of tyrosinase family genes in Xenopus laevis*. *Pigment Cell Res*, 2003. **16**(5): p. 455-62.
224. Saka, Y. and J.C. Smith, *Spatial and temporal patterns of cell division during early Xenopus embryogenesis*. *Developmental biology*, 2001. **229**(2): p. 307-18.
225. Sanchez Alvarado, A., *The freshwater planarian Schmidtea mediterranea: embryogenesis, stem cells and regeneration*. *Curr Opin Genet Dev*, 2003. **13**(4): p. 438-44.
226. Kumasaka, M., et al., *Isolation and developmental expression of Mitf in Xenopus laevis*. *Dev Dyn*, 2004. **230**(1): p. 107-13.
227. Beckstead, M.J., et al., *Anesthetic and ethanol effects on spontaneously opening glycine receptor channels*. *J Neurochem*, 2002. **82**(6): p. 1343-51.
228. Gillespie, J.I., *The distribution of small ions during the early development of Xenopus laevis and Ambystoma mexicanum embryos*. *J Physiol*, 1983. **344**: p. 359-77.
229. Higashimori, H. and H. Sontheimer, *Role of Kir4.1 channels in growth control of glia*. *Glia*, 2007. **55**(16): p. 1668-79.
230. Kucheryavykh, Y.V., et al., *Downregulation of Kir4.1 inward rectifying potassium channel subunits by RNAi impairs potassium transfer and glutamate uptake by cultured cortical astrocytes*. *Glia*, 2007. **55**(3): p. 274-81.

231. Li, C., et al., *Voltage and ionic regulation of human serotonin transporter in Xenopus oocytes*. Clin Exp Pharmacol Physiol, 2006. **33**(11): p. 1088-92.
232. Moran, D., *Voltage-dependent -L-type Ca<sup>2+</sup> channels participate in regulating neural crest migration and differentiation*. Am J Anat, 1991. **192**(1): p. 14-22.
233. Munaron, L., S. Antoniotti, and D. Lovisolo, *Intracellular calcium signals and control of cell proliferation: how many mechanisms?* J Cell Mol Med, 2004. **8**(2): p. 161-8.
234. Munaron, L., et al., *Blocking Ca<sup>2+</sup> entry: a way to control cell proliferation*. Curr Med Chem, 2004. **11**(12): p. 1533-43.
235. Anderson, K.L. and R.I. Woodruff, *A gap junctionally transmitted epithelial cell signal regulates endocytic yolk uptake in Oncopeltus fasciatus*. Dev Biol, 2001. **239**(1): p. 68-78.
236. Zhang, Y. and M. Levin, *Particle tracking model of electrophoretic morphogen movement reveals stochastic dynamics of embryonic gradient*. Developmental dynamics : an official publication of the American Association of Anatomists, 2009. **238**(8): p. 1923-35.
237. Grahn, J.C., et al., *Melanocytes do not migrate directionally in physiological DC electric fields*. Wound Repair Regen, 2003. **11**(1): p. 64-70.
238. Stump, R.F. and K.R. Robinson, *Xenopus neural crest cell migration in an applied electrical field*. J Cell Biol, 1983. **97**(4): p. 1226-33.
239. Barlow, A.J., et al., *Critical numbers of neural crest cells are required in the pathways from the neural tube to the foregut to ensure complete enteric nervous system formation*. Development, 2008. **135**(9): p. 1681-91.
240. Iwashita, M., et al., *Pigment pattern in jaguar/obelix zebrafish is caused by a Kir7.1 mutation: implications for the regulation of melanosome movement*. PLoS Genet, 2006. **2**(11): p. e197.
241. Asai, R., et al., *Zebrafish leopard gene as a component of the putative reaction-diffusion system*. Mech Dev, 1999. **89**(1-2): p. 87-92.
242. Watanabe, S., et al., *Crystallization and preliminary X-ray crystallographic studies of the oxidative-stress sensor SoxR and its complex with DNA*. Acta Crystallographica Section F-Structural Biology and Crystallization Communications, 2006. **62**: p. 1275-1277.
243. Jeon, S., et al., *Bee venom stimulates human melanocyte proliferation, melanogenesis, dendricity and migration*. Exp Mol Med, 2007. **39**(5): p. 603-13.

244. Seagar, M.J., C. Granier, and F. Couraud, *Interactions of the neurotoxin apamin with a Ca<sup>2+</sup>-activated K<sup>+</sup> channel in primary neuronal cultures*. J Biol Chem, 1984. **259**(3): p. 1491-5.
245. Lotti, T., et al., *Vitiligo: new and emerging treatments*. Dermatologic therapy, 2008. **21**(2): p. 110-7.
246. Whitton, M.E., D.M. Ashcroft, and U. Gonzalez, *Therapeutic interventions for vitiligo*. J Am Acad Dermatol, 2008. **59**(4): p. 713-7.
247. Yamamura, H., et al., *TRPM8 activation suppresses cellular viability in human melanoma*. Am J Physiol Cell Physiol, 2008. **295**(2): p. C296-301.
248. Yamamura, H., et al., *Expression analysis of the epithelial Na<sup>+</sup> channel delta subunit in human melanoma G-361 cells*. Biochem Biophys Res Commun, 2008. **366**(2): p. 489-92.
249. De Schepper, S., et al., *Pigment cell-related manifestations in neurofibromatosis type 1: an overview*. Pigment Cell Res, 2005. **18**(1): p. 13-24.
250. Lynch, J.W., *Native glycine receptor subtypes and their physiological roles*. Neuropharmacology, 2009. **56**(1): p. 303-9.
251. Schlosser, G., et al., *Eya1 and Six1 promote neurogenesis in the cranial placodes in a SoxB1-dependent fashion*. Dev Biol, 2008. **320**(1): p. 199-214.
252. Tomlinson, M.L., et al., *Three matrix metalloproteinases are required in vivo for macrophage migration during embryonic development*. Mech Dev, 2008. **125**(11-12): p. 1059-70.
253. Tang, Y.B., et al., *Silence of CIC-3 chloride channel inhibits cell proliferation and the cell cycle via G/S phase arrest in rat basilar arterial smooth muscle cells*. Cell Prolif, 2008. **41**(5): p. 775-85.
254. Tung, J.J., et al., *Chloride intracellular channel 4 is involved in endothelial proliferation and morphogenesis in vitro*. Angiogenesis, 2009. **12**(3): p. 209-20.
255. Cone, C.D., Jr. and M. Tongier, Jr., *Control of somatic cell mitosis by simulated changes in the transmembrane potential level*. Oncology, 1971. **25**(2): p. 168-82.
256. Fukuzawa, T. and H. Ide, *Proliferation in vitro of melanophores from Xenopus laevis*. J Exp Zool, 1983. **226**(2): p. 239-44.
257. Metcalf, M.E.M. and R.B. Borgens, *Weak applied voltages interfere with amphibian morphogenesis and pattern*. Journal of Experimental Zoology, 1994. **268**(4): p. 323-338.

258. Isseroff, R.R., et al., *Melanocytes do not exhibit directional migration in a DC electric field*. J. Invest. Dermatol., 2001. **117**(556).
259. Nishiyama, M., et al., *Membrane potential shifts caused by diffusible guidance signals direct growth-cone turning*. Nat Neurosci, 2008. **11**(7): p. 762-771.
260. Fanburg, B.L. and S.L. Lee, *A new role for an old molecule: serotonin as a mitogen*. Am J Physiol, 1997. **272**(5 Pt 1): p. L795-806.
261. Nebigil, C.G., et al., *5-hydroxytryptamine 2B receptor regulates cell-cycle progression: cross-talk with tyrosine kinase pathways*. Proc Natl Acad Sci U S A, 2000. **97**(6): p. 2591-6.
262. Slominski, A., et al., *Melanin pigmentation in mammalian skin and its hormonal regulation*. Physiol Rev, 2004. **84**(4): p. 1155-228.
263. Iyengar, B., *Photomodulation of the melanocyte cell cycle by indoleamines*. Biol Signals Recept, 1998. **7**(6): p. 345-50.
264. Carr, J.A., et al., *In vivo effects of serotonergic agents on alpha-melanocyte-stimulating hormone secretion*. Neuroendocrinology, 1991. **54**(6): p. 616-22.
265. Slominski, A., J. Wortsman, and D.J. Tobin, *The cutaneous serotonergic/melatonergic system: securing a place under the sun*. FASEB J, 2005. **19**(2): p. 176-94.
266. Adams, S.V. and L.J. DeFelice, *Flux coupling in the human serotonin transporter*. Biophys J, 2002. **83**(6): p. 3268-82.
267. Hilber, B., et al., *Serotonin-transporter mediated efflux: a pharmacological analysis of amphetamines and non-amphetamines*. Neuropharmacology, 2005. **49**(6): p. 811-9.
268. Van De Veerdonk, F.C.G., *Serotonin, a Melanocyte-stimulating Component in the Dorsal Skin Secretion of Xenopus laevis*. Nature, 1960. **187**(4741): p. 948-949.
269. Nozue, A.T. and S. Ono, *Effects of catecholamine and serotonin in central nervous system in newborn mice with special reference to neural crest cells; presumptive evidence of neural crest origin*. Anat Anz, 1991. **173**(3): p. 147-53.
270. Levens, D., *Development and cancer: common themes?* Lab Invest, 1990. **63**(4): p. 429-31.
271. Waddington, C.H., *Cancer and the theory of Organizers*. Nature, 1935. **135**(606): p. 606-608.
272. Fang, D., et al., *A tumorigenic subpopulation with stem cell properties in*

- melanomas*. *Cancer Res*, 2005. **65**(20): p. 9328-37.
273. Kulesa, P.M., et al., *Reprogramming metastatic melanoma cells to assume a neural crest cell-like phenotype in an embryonic microenvironment*. *Proc Natl Acad Sci U S A*, 2006. **103**(10): p. 3752-7.
274. Kasemeier-Kulesa, J.C., et al., *Reprogramming multipotent tumor cells with the embryonic neural crest microenvironment*. *Dev Dyn*, 2008. **237**(10): p. 2657-66.
275. Cardone, R.A., V. Casavola, and S.J. Reshkin, *The role of disturbed pH dynamics and the Na<sup>+</sup>/H<sup>+</sup> exchanger in metastasis*. *Nat Rev Cancer*, 2005. **5**(10): p. 786-95.
276. Heath, E.I. and L.B. Grochow, *Clinical potential of matrix metalloprotease inhibitors in cancer therapy*. *Drugs*, 2000. **59**(5): p. 1043-55.
277. Kelsh, R.N., B. Schmid, and J.S. Eisen, *Genetic analysis of melanophore development in zebrafish embryos*. *Dev Biol*, 2000. **225**(2): p. 277-93.
278. Stulberg, D.L., N. Clark, and D. Tovey, *Common hyperpigmentation disorders in adults: Part II. Melanoma, seborrheic keratoses, acanthosis nigricans, melasma, diabetic dermopathy, tinea versicolor, and postinflammatory hyperpigmentation*. *Am Fam Physician*, 2003. **68**(10): p. 1963-8.
279. Liu, L.Y., et al., *ET-1 inhibits B-16 murine melanoma cell migration by decreasing K<sup>+</sup> currents*. *Cell Motil Cytoskeleton*, 2004. **58**(2): p. 127-36.
280. Jin, M., D.M. Defoe, and R. Wondergem, *Hepatocyte growth factor/scatter factor stimulates Ca<sup>2+</sup>-activated membrane K<sup>+</sup> current and migration of MDCK II cells*. *J Membr Biol*, 2003. **191**(1): p. 77-86.
281. Cruse, G., et al., *Functional KCa3.1 K<sup>+</sup> channels are required for human lung mast cell migration*. *Thorax*, 2006. **61**(10): p. 880-5.
282. Kraft, R., et al., *BK channel openers inhibit migration of human glioma cells*. *Pflugers Arch*, 2003. **446**(2): p. 248-55.
283. Liu, L.Y., et al., *Delayed rectifier outward K<sup>+</sup> current mediates the migration of rat cerebellar granule cells stimulated by melatonin*. *J Neurochem*, 2007. **102**(2): p. 333-44.
284. Potier, M., et al., *Identification of SK3 channel as a new mediator of breast cancer cell migration*. *Mol Cancer Ther*, 2006. **5**(11): p. 2946-53.
285. Schwab, A., et al., *K<sup>+</sup> channel-dependent migration of fibroblasts and human melanoma cells*. *Cell Physiol Biochem*, 1999. **9**(3): p. 126-32.
286. Spitzner, M., et al., *Voltage-gated K<sup>+</sup> channels support proliferation of colonic carcinoma cells*. *FASEB J*, 2007. **21**(1): p. 35-44.

287. Wu, W.K., et al., *Involvement of voltage-gated K<sup>+</sup> and Na<sup>+</sup> channels in gastric epithelial cell migration*. Mol Cell Biochem, 2008. **308**(1-2): p. 219-26.
288. Bennett, E.S., B.A. Smith, and J.M. Harper, *Voltage-gated Na<sup>+</sup> channels confer invasive properties on human prostate cancer cells*. Pflugers Arch, 2004. **447**(6): p. 908-14.
289. Fraser, S.P., J.A. Grimes, and M.B. Djamgoz, *Effects of voltage-gated ion channel modulators on rat prostatic cancer cell proliferation: comparison of strongly and weakly metastatic cell lines*. Prostate, 2000. **44**(1): p. 61-76.
290. Lastraioli, E., et al., *herg1 gene and HERG1 protein are overexpressed in colorectal cancers and regulate cell invasion of tumor cells*. Cancer Res, 2004. **64**(2): p. 606-11.
291. Mu, D., et al., *Genomic amplification and oncogenic properties of the KCNK9 potassium channel gene*. Cancer Cell, 2003. **3**(3): p. 297-302.
292. Ouadid-Ahidouch, H. and A. Ahidouch, *K<sup>+</sup> channel expression in human breast cancer cells: involvement in cell cycle regulation and carcinogenesis*. J Membr Biol, 2008. **221**(1): p. 1-6.
293. Pardo, L.A., et al., *Oncogenic potential of EAG K(+) channels*. EMBO J, 1999. **18**(20): p. 5540-7.
294. Wissenbach, U., et al., *TRPV6 and prostate cancer: cancer growth beyond the prostate correlates with increased TRPV6 Ca<sup>2+</sup> channel expression*. Biochem Biophys Res Commun, 2004. **322**(4): p. 1359-63.
295. House, C.D., et al., *Voltage-gated Na<sup>+</sup> channel SCN5A is a key regulator of a gene transcriptional network that controls colon cancer invasion*. Cancer Res, 2010. **70**(17): p. 6957-67.
296. Aberg, P., et al., *Non-invasive and microinvasive electrical impedance spectra of skin cancer - a comparison between two techniques*. Skin Res Technol, 2005. **11**(4): p. 281-6.
297. Dumas, D. and J.F. Stoltz, *New tool to monitor membrane potential by FRET Voltage Sensitive Dye (FRET-VSD) using Spectral and Fluorescence Lifetime Imaging Microscopy (FLIM). Interest in cell engineering*. Clin Hemorheol Microcirc, 2005. **33**(3): p. 293-302.
298. Gupta, D., et al., *Bioelectrical impedance phase angle as a prognostic indicator in advanced pancreatic cancer*. Br J Nutr, 2004. **92**(6): p. 957-62.
299. Ouwerkerk, R., et al., *Elevated tissue sodium concentration in malignant breast lesions detected with non-invasive <sup>23</sup>Na MRI*. Breast Cancer Res Treat, 2007. **106**(2): p. 151-60.

300. Kim, C.F. and P.B. Dirks, *Cancer and Stem Cell Biology: How Tightly Intertwined?* Cell Stem Cell, 2008. **3**(2): p. 147-150.
301. Lindvall, C., et al., *Wnt signaling, stem cells, and the cellular origin of breast cancer.* Stem Cell Rev, 2007. **3**(2): p. 157-68.
302. Tan, B.T., et al., *The cancer stem cell hypothesis: a work in progress.* Lab Invest, 2006. **86**(12): p. 1203-7.
303. Tataria, M., S.V. Perryman, and K.G. Sylvester, *Stem cells: tissue regeneration and cancer.* Semin Pediatr Surg, 2006. **15**(4): p. 284-92.
304. Wicha, M.S., S. Liu, and G. Dontu, *Cancer stem cells: an old idea--a paradigm shift.* Cancer Res, 2006. **66**(4): p. 1883-90; discussion 1895-6.
305. Heukelbach, J., et al., *Selective mass treatment with ivermectin to control intestinal helminthiases and parasitic skin diseases in a severely affected population.* Bull World Health Organ, 2004. **82**(8): p. 563-71.
306. Levin, M., *A novel immunohistochemical method for evaluation of antibody specificity and detection of labile targets in biological tissue.* Journal of biochemical and biophysical methods, 2004. **58**(1): p. 85-96.
307. Finbow, M.E., M. Harrison, and P. Jones, *Ductin--a proton pump component, a gap junction channel and a neurotransmitter release channel.* Bioessays, 1995. **17**(3): p. 247-55.
308. Davies, D.L., et al., *Ethanol potentiation of glycine receptors expressed in Xenopus oocytes antagonized by increased atmospheric pressure.* Alcohol Clin Exp Res, 2003. **27**(5): p. 743-55.
309. Chakraborty, C., et al., *Zebrafish caspase-3: molecular cloning, characterization, crystallization and phylogenetic analysis.* Protein Pept Lett, 2006. **13**(6): p. 633-40.
310. Makino, S., et al., *Heat-shock protein 60 is required for blastema formation and maintenance during regeneration.* Proc Natl Acad Sci U S A, 2005. **102**(41): p. 14599-604.
311. Yu, S.Y., et al., *A pathway of signals regulating effector and initiator caspases in the developing Drosophila eye.* Development, 2002. **129**(13): p. 3269-78.
312. Stahelin, B.J., et al., *False positive staining in the TUNEL assay to detect apoptosis in liver and intestine is caused by endogenous nucleases and inhibited by diethyl pyrocarbonate.* Mol Pathol, 1998. **51**(4): p. 204-8.
313. Frankfurt, O.S., *Decreased stability of DNA in cells treated with alkylating agents.* Exp Cell Res, 1990. **191**(2): p. 181-5.
314. Pogge v Strandmann, E., S. Senkel, and G.U. Ryffel, *Ectopic*

- pigmentation in Xenopus in response to DCoH/PCD, the cofactor of HNF1 transcription factor/pterin-4alpha-carbinolamine dehydratase. Mech Dev, 2000. 91(1-2): p. 53-60.*
315. Rowlatt, C., *Some consequences of defining the neoplasm as focal self-perpetuating tissue disorganization*, in *New Frontiers in Cancer Causation*, O.H. Iversen, Editor. 1994, Taylor & Francis: Washington, DC. p. 45–58.
  316. Baker, S.G., et al., *Plausibility of stromal initiation of epithelial cancers without a mutation in the epithelium: a computer simulation of morphostats*. BMC Cancer, 2009. **9**: p. 89.
  317. Potter, J.D., *Morphogens, morphostats, microarchitecture and malignancy*. Nat Rev Cancer, 2007. **7**(6): p. 464-74.
  318. Potter, J.D., *Morphostats: a missing concept in cancer biology*. Cancer Epidemiol Biomarkers Prev, 2001. **10**(3): p. 161-70.
  319. Needham, J., *Chemical embryology*. 1963, New York,: Hafner Pub. Co. 3 v. (xxi, 2021 p.).
  320. Needham, J., *New Advances in the Chemistry and Biology of Organized Growth: (Section of Pathology)*. Proc R Soc Med, 1936. **29**(12): p. 1577-626.
  321. Waddington, C.H., *Cancer and the theory of Organisers*. Nature, 1935. **135**(606): p. 606-608.
  322. Sonnenschein, C. and A.M. Soto, *The society of cells : cancer control of cell proliferation*. 1999, Oxford New York: Springer. xiv, 154 p.
  323. Bissell, M.J. and W.C. Hines, *Why don't we get more cancer? A proposed role of the microenvironment in restraining cancer progression*. Nature medicine, 2011. **17**(3): p. 320-9.
  324. Roskelley, C.D. and M.J. Bissell, *The dominance of the microenvironment in breast and ovarian cancer*. Seminars in cancer biology, 2002. **12**(2): p. 97-104.
  325. Vaux, D.L., *Response to "The tissue organization field theory of cancer: a testable replacement for the somatic mutation theory"*. DOI: [10.1002/bies.201100025](https://doi.org/10.1002/bies.201100025). BioEssays : news and reviews in molecular, cellular and developmental biology, 2011. **33**(9): p. 660-1.
  326. Hanahan, D. and R.A. Weinberg, *Hallmarks of cancer: the next generation*. Cell, 2011. **144**(5): p. 646-74.
  327. Ingber, D.E., *Can cancer be reversed by engineering the tumor microenvironment?* Semin Cancer Biol, 2008. **18**(5): p. 356-64.

328. Del Rio-Tsonis, K. and P.A. Tsonis, *Amphibian tissue regeneration - a model for cancer regulation*. International Journal of Oncology, 1992. **1**: p. 161-164.
329. Fan, Y. and A. Bergmann, *Apoptosis-induced compensatory proliferation. The Cell is dead. Long live the Cell!* Trends Cell Biol, 2008. **18**(10): p. 467-73.
330. Bissell, M.J. and D. Radisky, *Putting tumours in context*. Nat Rev Cancer, 2001. **1**(1): p. 46-54.
331. Bizzarri, M., et al., *Beyond the oncogene paradigm: understanding complexity in cancerogenesis*. Acta Biotheor, 2008. **56**(3): p. 173-96.
332. Weaver, V.M. and P. Gilbert, *Watch thy neighbor: cancer is a communal affair*. J Cell Sci, 2004. **117**(Pt 8): p. 1287-90.
333. Bizzarri, M., et al., *Embryonic morphogenetic field induces phenotypic reversion in cancer cells. Review article*. Curr Pharm Biotechnol, 2011. **12**(2): p. 243-53.
334. Dinicola, S., et al., *A systems biology approach to cancer: fractals, attractors, and nonlinear dynamics*. OMICS, 2011. **15**(3): p. 93-104.
335. Huang, S., I. Ernberg, and S. Kauffman, *Cancer attractors: a systems view of tumors from a gene network dynamics and developmental perspective*. Semin Cell Dev Biol, 2009. **20**(7): p. 869-76.
336. Levin, M., *The wisdom of the body: future techniques and approaches to morphogenetic fields in regenerative medicine, developmental biology and cancer*. Regenerative medicine, 2011. **6**(6): p. 667-73.
337. Levin, M., *Molecular Bioelectricity In Developmental Biology: New Tools And Recent Discoveries*. BioEssays, 2011. **in press**.
338. McCaig, C.D., B. Song, and A.M. Rajnicek, *Electrical dimensions in cell science*. J Cell Sci, 2009. **122**(Pt 23): p. 4267-76.
339. McCaig, C.D., et al., *Controlling cell behavior electrically: current views and future potential*. Physiol Rev, 2005. **85**(3): p. 943-78.
340. Lund, E., *Bioelectric fields and growth*. 1947, Austin: Univ. of Texas Press.
341. Jaffe, L.F., *Control of development by ionic currents*, in *Membrane Transduction Mechanisms*, R.A. Cone, and John E. Dowling, eds., Editor. 1979, Raven Press: New York.
342. Borgens, R.B., *The role of natural and applied electric fields in neuronal regeneration and development*. Progress in Clinical & Biological Research, 1986. **210**: p. 239-50.

343. Burr, H.S., L.C. Strong, and G.M. Smith, *Bioelectric correlates of methylcolantherene-induced tumors in mice*. Yale J Biol. Med, 1938. **10**: p. 539–544.
344. Burr, H.S., *Biologic Organization and the Cancer Problem* \*. The Yale Journal of Biology and Medicine, 1940. **12**(3): p. 277-82.
345. Adams, D.S. and M. Levin, *General Principles For Measuring Resting Membrane Potential And Ion Concentration Using Fluorescent Bioelectricity Reporters*. Cold Spring Harbor Protocols, 2012. **in press**.
346. Adams, D.S. and M. Levin, *Endogenous voltage gradients as mediators of cell-cell communication: strategies for investigating bioelectrical signals during pattern formation*. Cell and tissue research, 2012.
347. Pu, J., et al., *EGF receptor signalling is essential for electric-field-directed migration of breast cancer cells*. J Cell Sci, 2007. **120**(Pt 19): p. 3395-403.
348. Pullar, C.E., et al., *Beta-adrenergic receptor agonists delay while antagonists accelerate epithelial wound healing: evidence of an endogenous adrenergic network within the corneal epithelium*. J Cell Physiol, 2007. **211**(1): p. 261-72.
349. Levin, M., *Bioelectric mechanisms in regeneration: Unique aspects and future perspectives*. Semin Cell Dev Biol, 2009. **20**(5): p. 543-56.
350. Sundelacruz, S., M. Levin, and D.L. Kaplan, *Role of membrane potential in the regulation of cell proliferation and differentiation*. Stem Cell Rev Rep, 2009. **5**(3): p. 231-46.
351. Adams, D.S., et al., *Early, H<sup>+</sup>-V-ATPase-dependent proton flux is necessary for consistent left-right patterning of non-mammalian vertebrates*. Development, 2006. **133**: p. 1657-1671.
352. Stojadinovic, A., et al., *Electrical impedance scanning for the early detection of breast cancer in young women: preliminary results of a multicenter prospective clinical trial*. J Clin Oncol, 2005. **23**(12): p. 2703-15.
353. Gupta, D., et al., *Bioelectrical impedance phase angle in clinical practice: implications for prognosis in advanced colorectal cancer*. Am J Clin Nutr, 2004. **80**(6): p. 1634-8.
354. Aberg, P., et al., *Skin cancer identification using multifrequency electrical impedance--a potential screening tool*. IEEE Trans Biomed Eng, 2004. **51**(12): p. 2097-102.
355. Burr, H.S., *Changes in the field properties of mice with transplanted tumors*. Yale Journal of Biology & Medicine, 1941. **13**: p. 783-788.

356. Rozengurt, E. and S. Mendoza, *Monovalent ion fluxes and the control of cell proliferation in cultured fibroblasts*. Ann N Y Acad Sci, 1980. **339**: p. 175-90.
357. Leffert, H.L. and K.S. Koch, *Ionic events at the membrane initiate rat liver regeneration*. Ann N Y Acad Sci, 1980. **339**: p. 201-15.
358. Jeter, J.R., Jr., et al., *Cell cycle-fluctuations in concentration of various elements in cytoplasm and in nucleus/chromatin of Physarum polycephalum*. Cytobios, 1982. **35**(137): p. 47-62.
359. Cameron, I.L., et al., *Intracellular concentration of sodium and other elements as related to mitogenesis and oncogenesis in vivo*. Cancer Res, 1980. **40**(5): p. 1493-500.
360. Cameron, I.L., T.B. Pool, and N.K. Smith, *An X-ray microanalysis survey of the concentration of elements in the cytoplasm of different mammalian cell types*. J Cell Physiol, 1979. **101**(3): p. 493-501.
361. Cameron, I.L. and N.K. Smith, *Energy dispersive x-ray microanalysis of the concentration of elements in relation to cell reproduction in normal and in cancer cells*. Scan Electron Microsc, 1980(Pt 2): p. 463-74.
362. Cameron, I.L., N.K. Smith, and T.B. Pool, *Element concentration changes in mitotically active and postmitotic enterocytes. An x-ray microanalysis study*. J Cell Biol, 1979. **80**(2): p. 444-50.
363. Smith, N.R., et al., *Differences in the intracellular concentration of elements in normal and cancerous liver cells as determined by X-ray microanalysis*. Cancer Res, 1978. **38**(7): p. 1952-9.
364. Sparks, R.L., et al., *Effects of amiloride on tumor growth and intracellular element content of tumor cells in vivo*. Cancer Res, 1983. **43**(1): p. 73-7.
365. Binggeli, R. and R.C. Weinstein, *Membrane potentials and sodium channels: hypotheses for growth regulation and cancer formation based on changes in sodium channels and gap junctions*. J Theor Biol, 1986. **123**(4): p. 377-401.
366. Arcangeli, A., et al., *A novel inward-rectifying K<sup>+</sup> current with a cell-cycle dependence governs the resting potential of mammalian neuroblastoma cells*. J Physiol, 1995. **489** ( Pt 2): p. 455-71.
367. O'Grady, S.M. and S.Y. Lee, *Molecular diversity and function of voltage-gated (Kv) potassium channels in epithelial cells*. Int J Biochem Cell Biol, 2005. **37**(8): p. 1578-94.
368. Pardo, L.A., *Voltage-gated potassium channels in cell proliferation*. Physiology (Bethesda), 2004. **19**: p. 285-92.
369. Wang, Z., *Roles of K<sup>+</sup> channels in regulating tumour cell proliferation and*

- apoptosis*. Pflugers Arch, 2004. **448**(3): p. 274-86.
370. Tseng, A.-S. and M. Levin, *Transducing bioelectric signals into epigenetic pathways during tadpole tail regeneration*. Anatomical Record, 2012. **in press**.
371. Carneiro, K., et al., *Histone Deacetylase activity is necessary for left-right patterning during vertebrate development*. BMC Dev Biol, 2011. **11**(1): p. 29.
372. Lange, C., et al., *The H(+) Vacuolar ATPase Maintains Neural Stem Cells in the Developing Mouse Cortex*. Stem Cells Dev, 2011.
373. Yasuda, T. and D.J. Adams, *Physiological roles of ion channels in adult neural stem cells and their progeny*. J Neurochem, 2010. **114**(4): p. 946-59.
374. Levin, M. and M. Mercola, *Gap junctions are involved in the early generation of left-right asymmetry*. Dev Biol, 1998. **203**(1): p. 90-105.
375. Onkal, R. and M.B. Djamgoz, *Molecular pharmacology of voltage-gated sodium channel expression in metastatic disease: clinical potential of neonatal Nav1.5 in breast cancer*. Eur J Pharmacol, 2009. **625**(1-3): p. 206-19.
376. Pei, L., et al., *Oncogenic potential of TASK3 (Kcnc9) depends on K+ channel function*. Proc Natl Acad Sci U S A, 2003. **100**(13): p. 7803-7.
377. Saito, T., et al., *Induction of cell transformation by mutated 16K vacuolar H+-atpase (ductin) is accompanied by down-regulation of gap junctional intercellular communication and translocation of connexin 43 in NIH3T3 cells*. Oncogene, 1998. **17**(13): p. 1673-80.
378. Gupta, N., et al., *SLC5A8 (SMCT1)-mediated transport of butyrate forms the basis for the tumor suppressive function of the transporter*. Life Sci, 2006. **78**(21): p. 2419-25.
379. Roepke, T.K., et al., *Targeted deletion of Kcne2 causes gastritis cystica profunda and gastric neoplasia*. PLoS One, 2010. **5**(7): p. e11451.
380. Temme, A., et al., *High incidence of spontaneous and chemically induced liver tumors in mice deficient for connexin32*. Current Biology, 1997. **7**(9): p. 713-6.
381. Conti, M., *Targeting K+ channels for cancer therapy*. J Exp Ther Oncol, 2004. **4**(2): p. 161-6.
382. Lin, H., et al., *Overexpression HERG K(+) channel gene mediates cell-growth signals on activation of oncoproteins SP1 and NF-kappaB and inactivation of tumor suppressor Nkx3.1*. J Cell Physiol, 2007.

383. Bianchi, L., et al., *herg encodes a K<sup>+</sup> current highly conserved in tumors of different histogenesis: a selective advantage for cancer cells?* Cancer Research, 1998. **58**(4): p. 815-22.
384. Wang, H., et al., *HERG K<sup>+</sup> channel, a regulator of tumor cell apoptosis and proliferation.* Cancer Res, 2002. **62**(17): p. 4843-8.
385. Kim, C.J., et al., *Altered expression of KCNK9 in colorectal cancers.* APMIS, 2004. **112**(9): p. 588-94.
386. Pei, L., et al., *Oncogenic potential of TASK3 (Kcnk9) depends on K<sup>+</sup> channel function.* Proc Natl Acad Sci U S A, 2003.
387. Farias, L.M., et al., *Ether a go-go potassium channels as human cervical cancer markers.* Cancer Res, 2004. **64**(19): p. 6996-7001.
388. Klezovitch, O., et al., *A causal role for ERG in neoplastic transformation of prostate epithelium.* Proc Natl Acad Sci U S A, 2008. **105**(6): p. 2105-10.
389. Meyer, R., et al., *Identification of ether a go-go and calcium-activated potassium channels in human melanoma cells.* J Membr Biol, 1999. **171**(2): p. 107-15.
390. Becchetti, A., *Ion channels and transporters in cancer. 1. Ion channels and cell proliferation in cancer.* American journal of physiology. Cell physiology, 2011. **301**(2): p. C255-65.
391. Prevarskaya, N., R. Skryma, and Y. Shuba, *Ion channels and the hallmarks of cancer.* Trends Mol Med, 2010. **16**(3): p. 107-21.
392. Perona, R. and R. Serrano, *Increased pH and tumorigenicity of fibroblasts expressing a yeast proton pump.* Nature, 1988. **334**(6181): p. 438-40.
393. Volkov, A., et al., *Circadian rhythms in biologically closed electrical circuits of plants.* Plant signaling & behavior, 2012. **7**(2): p. 282-4.
394. Habela, C.W., M.L. Olsen, and H. Sontheimer, *CIC3 is a critical regulator of the cell cycle in normal and malignant glial cells.* J Neurosci, 2008. **28**(37): p. 9205-17.
395. Jirsch, J., et al., *Inwardly rectifying K<sup>+</sup> channels and volume-regulated anion channels in multidrug-resistant small cell lung cancer cells.* Cancer Res, 1993. **53**(18): p. 4156-60.
396. Shuba, Y.M., et al., *Volume-regulated chloride conductance in the LNCaP human prostate cancer cell line.* Am J Physiol Cell Physiol, 2000. **279**(4): p. C1144-54.
397. Ousingsawat, J., et al., *Upregulation of colonic ion channels in APC (Min/+ ) mice.* Pflugers Arch, 2008. **456**(5): p. 847-55.

398. Brackenbury, W.J. and M.B. Djamgoz, *Activity-dependent regulation of voltage-gated Na<sup>+</sup> channel expression in Mat-LyLu rat prostate cancer cell line*. J Physiol, 2006. **573**(Pt 2): p. 343-56.
399. Onganer, P.U., M.J. Seckl, and M.B. Djamgoz, *Neuronal characteristics of small-cell lung cancer*. Br J Cancer, 2005. **93**(11): p. 1197-201.
400. Onganer, P.U. and M.B. Djamgoz, *Small-cell lung cancer (human): potentiation of endocytic membrane activity by voltage-gated Na<sup>+</sup> channel expression in vitro*. J Membr Biol, 2005. **204**(2): p. 67-75.
401. Fraser, S.P., et al., *Voltage-gated sodium channel expression and potentiation of human breast cancer metastasis*. Clin Cancer Res, 2005. **11**(15): p. 5381-9.
402. Diss, J.K., et al., *A potential novel marker for human prostate cancer: voltage-gated sodium channel expression in vivo*. Prostate Cancer Prostatic Dis, 2005. **8**(3): p. 266-73.
403. Arcangeli, A., et al., *Targeting ion channels in cancer: a novel frontier in antineoplastic therapy*. Current medicinal chemistry, 2009. **16**(1): p. 66-93.
404. Kometiani, P., L. Liu, and A. Askari, *Digitalis-induced signaling by Na<sup>+</sup>/K<sup>+</sup>-ATPase in human breast cancer cells*. Mol Pharmacol, 2005. **67**(3): p. 929-36.
405. Morokuma, J., et al., *Modulation of potassium channel function confers a hyperproliferative invasive phenotype on embryonic stem cells*. Proc Natl Acad Sci U S A, 2008. **105**(43): p. 16608-13.
406. Fukumoto, T., I.P. Kema, and M. Levin, *Serotonin signaling is a very early step in patterning of the left-right axis in chick and frog embryos*. Curr Biol, 2005. **15**(9): p. 794-803.
407. Chernet, B. and M. Levin, *Transmembrane potential is an instructive factor in cancerous transformation and normalization*. submitted, 2012.
408. Le, X., et al., *Heat shock-inducible Cre/Lox approaches to induce diverse types of tumors and hyperplasia in transgenic zebrafish*. Proc Natl Acad Sci U S A, 2007. **104**(22): p. 9410-5.
409. Dahmane, N., et al., *Activation of the transcription factor Gli1 and the Sonic hedgehog signalling pathway in skin tumours*. Nature, 1997. **389**(6653): p. 876-81.
410. Yang, S., et al., *Overexpression of a novel Xenopus rel mRNA gene induces tumors in early embryos*. J Biol Chem, 1998. **273**(22): p. 13746-52.
411. Wallingford, J.B., et al., *p53 activity is essential for normal development in*

- Xenopus*. *Curr Biol*, 1997. **7**(10): p. 747-57.
412. Lynagh, T. and J.W. Lynch, *An improved ivermectin-activated chloride channel receptor for inhibiting electrical activity in defined neuronal populations*. *The Journal of biological chemistry*, 2010. **285**(20): p. 14890-7.
413. Fakler, B., et al., *Heterooligomeric assembly of inward-rectifier K<sup>+</sup> channels from subunits of different subfamilies: Kir2.1 (IRK1) and Kir4.1 (BIR10)*. *Pflugers Arch*, 1996. **433**(1-2): p. 77-83.
414. Doherty, J.R., et al., *A flk-1 promoter/enhancer reporter transgenic Xenopus laevis generated using the Sleeping Beauty transposon system: an in vivo model for vascular studies*. *Developmental dynamics : an official publication of the American Association of Anatomists*, 2007. **236**(10): p. 2808-17.
415. Adams, D.S. and M. Levin, *Measuring resting membrane potential using the fluorescent voltage reporters DiBAC4(3) and CC2-DMPE*. *Cold Spring Harbor Protocols*, 2012. **in press**.
416. Chernet, B.T. and M. Levin, *A versatile protocol for mRNA electroporation of Xenopus laevis embryos*. *Cold Spring Harbor protocols*, 2012. **2012**(4): p. 447-52.
417. Moiseiwitsch, J.R., *The role of serotonin and neurotransmitters during craniofacial development*. *Critical reviews in oral biology and medicine : an official publication of the American Association of Oral Biologists*, 2000. **11**(2): p. 230-9.
418. Nguyen, L., et al., *Neurotransmitters as early signals for central nervous system development*. *Cell and Tissue Research*, 2001. **305**(2): p. 187-202.
419. Buznikov, G.A., H.W. Lambert, and J.J. Lauder, *Serotonin and serotonin-like substances as regulators of early embryogenesis and morphogenesis*. *Cell and Tissue Research*, 2001. **305**(2): p. 177-186.
420. Wimalasena, K., *Vesicular monoamine transporters: structure-function, pharmacology, and medicinal chemistry*. *Medicinal research reviews*, 2011. **31**(4): p. 483-519.
421. Barnes, N.M. and T. Sharp, *A review of central 5-HT receptors and their function*. *Neuropharmacology*, 1999. **38**(8): p. 1083-1152.
422. Monachon, M.A., et al., *Blockade of central 5-hydroxytryptamine receptors by methiothepin*. *Naunyn-Schmiedeberg's archives of pharmacology*, 1972. **274**(2): p. 192-7.
423. Pai, V.P. and N.D. Horseman, *Biphasic regulation of mammary epithelial resistance by serotonin through activation of multiple pathways*. *J Biol*

- Chem, 2008. **283**(45): p. 30901-10.
424. Stull, M.A., et al., *Mammary gland homeostasis employs serotonergic regulation of epithelial tight junctions*. Proc Natl Acad Sci U S A, 2007. **104**(42): p. 16708-13.
  425. Pai, V.P., et al., *Altered serotonin physiology in human breast cancers favors paradoxical growth and cell survival*. Breast cancer research : BCR, 2009. **11**(6): p. R81.
  426. Li, B., R.A. Cerione, and M. Antonyak, *Tissue transglutaminase and its role in human cancer progression*. Advances in enzymology and related areas of molecular biology, 2011. **78**: p. 247-93.
  427. Hirose, M., et al., *Transplantation of chemically induced gastric cancer in Wistar rats*. Gann, 1976. **67**(3): p. 365-9.
  428. Boroughs, L.K., et al., *A unique role for heat shock protein 70 and its binding partner tissue transglutaminase in cancer cell migration*. The Journal of biological chemistry, 2011. **286**(43): p. 37094-107.
  429. Binggeli, R. and R. Weinstein, *Membrane potentials and sodium channels: hypotheses for growth regulation and cancer formation based on changes in sodium channels and gap junctions*. Journal of Theoretical Biology, 1986. **123**: p. 377-401.
  430. Kasper, M., et al., *GLI transcription factors: mediators of oncogenic Hedgehog signalling*. Eur J Cancer, 2006. **42**(4): p. 437-45.
  431. Aw, S., et al., *H,K-ATPase protein localization and Kir4.1 function reveal concordance of three axes during early determination of left-right asymmetry*. Mech Dev, 2008. **125**: p. 353-372.
  432. Cone, C.D., *The role of the surface electrical transmembrane potential in normal and malignant mitogenesis*. Annals of the New York Academy of Sciences, 1974. **238**: p. 420-35.
  433. Levin, M., G.A. Buznikov, and J.M. Lauder, *Of minds and embryos: left-right asymmetry and the serotonergic controls of pre-neural morphogenesis*. Dev Neurosci, 2006. **28**(3): p. 171-85.
  434. Kannen, V., et al., *Fluoxetine induces preventive and complex effects against colon cancer development in epithelial and stromal areas in rats*. Toxicol Lett, 2011. **204**(2-3): p. 134-40.
  435. Meredith, E.J., et al., *The serotonin transporter (SLC6A4) is present in B-cell clones of diverse malignant origin: probing a potential antitumor target for psychotropics*. Faseb J, 2005.
  436. Dizeyi, N., et al., *Expression of serotonin receptors and role of serotonin in human prostate cancer tissue and cell lines*. Prostate, 2004. **59**(3): p.

328-36.

437. Vicaut, E., E. Laemmel, and O. Stucker, *Impact of serotonin on tumour growth*. Annals of Medicine, 2000. **32**(3): p. 187-94.
438. Manda, T., et al., *Important role of serotonin in the antitumor effects of recombinant human tumor necrosis factor-alpha in mice*. Cancer Research, 1988. **48**(15): p. 4250-5.
439. Brandes, L.J., et al., *Stimulation of malignant growth in rodents by antidepressant drugs at clinically relevant doses*. Cancer Res, 1992. **52**(13): p. 3796-800.
440. Antonyak, M.A., et al., *Cancer cell-derived microvesicles induce transformation by transferring tissue transglutaminase and fibronectin to recipient cells*. Proceedings of the National Academy of Sciences of the United States of America, 2011. **108**(12): p. 4852-7.
441. Dale, G.L., et al., *Stimulated platelets use serotonin to enhance their retention of procoagulant proteins on the cell surface*. Nature, 2002. **415**(6868): p. 175-9.
442. Walther, D.J., et al., *Serotonylation of small GTPases is a signal transduction pathway that triggers platelet alpha-granule release*. Cell, 2003. **115**(7): p. 851-62.
443. Paulmann, N., et al., *Intracellular serotonin modulates insulin secretion from pancreatic beta-cells by protein serotonylation*. PLoS Biol, 2009. **7**(10): p. e1000229.
444. Slominski, A., et al., *Functional activity of serotonergic and melatonergic systems expressed in the skin*. Journal of cellular physiology, 2003. **196**(1): p. 144-153.
445. Slominski, A., *Neuroendocrine activity of the melanocyte*. Experimental dermatology, 2009. **18**(9): p. 760-3.
446. Potenza, M.N. and M.R. Lerner, *Characterization of a serotonin receptor endogenous to frog melanophores*. Naunyn-Schmiedeberg's archives of pharmacology, 1994. **349**(1): p. 11-9.
447. English, K.B., et al., *Serotonin-like immunoreactivity in Merkel cells and their afferent neurons in touch domes from the hairy skin of rats*. The Anatomical record, 1992. **232**(1): p. 112-20.
448. Slominski, A., A. Pisarchik, and J. Wortsman, *Expression of genes coding melatonin and serotonin receptors in rodent skin*. Biochimica et biophysica acta, 2004. **1680**(2): p. 67-70.
449. Johansson, O., et al., *A serotonin-like immunoreactivity is present in human cutaneous melanocytes*. The Journal of investigative dermatology,

1998. **111**(6): p. 1010-4.
450. Brackenbury, W.J., M.B. Djamgoz, and L.L. Isom, *An emerging role for voltage-gated Na<sup>+</sup> channels in cellular migration: regulation of central nervous system development and potentiation of invasive cancers*. *Neuroscientist*, 2008. **14**(6): p. 571-83.
451. Gustafsson, B.I., et al., *Serotonin and fluoxetine modulate bone cell function in vitro*. *J Cell Biochem*, 2006. **98**(1): p. 139-51.
452. Lee, S.L., et al., *Serotonin stimulates mitogen-activated protein kinase activity through the formation of superoxide anion*. *Am J Physiol*, 1999. **277**(2 Pt 1): p. L282-91.
453. Fanburg, B. and S. Lee, *A new role for an old molecule: serotonin as a mitogen*. *American Journal of Physiology*, 1997. **272**(5 pt 1): p. L795-806.
454. Sachdeva, G., et al., *Bistable dynamics of cardiac cell models coupled by dynamic gap junctions linked to Cardiac Memory*. *Biological Cybernetics*, 2010. **102**(2): p. 109-121.
455. Gallaher, J., M. Bier, and J.S. van Heukelom, *First order phase transition and hysteresis in a cell's maintenance of the membrane potential-An essential role for the inward potassium rectifiers*. *Biosystems*, 2010. **101**(3): p. 149-155.
456. Xiong, W. and J.E. Ferrell, Jr., *A positive-feedback-based bistable 'memory module' that governs a cell fate decision*. *Nature*, 2003. **426**(6965): p. 460-5.
457. Ferrell, J.E. and W. Xiong, *Bistability in cell signaling: How to make continuous processes discontinuous, and reversible processes irreversible*. *Chaos*, 2001. **11**(1): p. 227-236.
458. Weissenberger, S., et al., *PACalpha--an optogenetic tool for in vivo manipulation of cellular cAMP levels, neurotransmitter release, and behavior in Caenorhabditis elegans*. *J Neurochem*, 2011. **116**(4): p. 616-25.
459. Volkov, A.G., et al., *Circadian rhythms in electrical circuits of Clivia miniata*. *Journal of plant physiology*, 2011. **168**(15): p. 1753-60.
460. Brink, P.R., et al., *Can gap junctions deliver?* *Biochimica et biophysica acta*, 2012. **1818**(8): p. 2076-81.
461. Volkov, A.G., et al., *Circadian variations in biologically closed electrochemical circuits in Aloe vera and Mimosa pudica*. *Bioelectrochemistry*, 2011. **81**(1): p. 39-45.
462. Williams, S.R., et al., *Membrane potential bistability is controlled by the hyperpolarization-activated current I(H) in rat cerebellar Purkinje neurons*

- in vitro*. The Journal of physiology, 2002. **539**(Pt 2): p. 469-83.
463. Rose, S.M. and H.M. Wallingford, *Transformation of renal tumors of frogs to normal tissues in regenerating limbs of salamanders*. Science, 1948. **107**: p. 457-.
464. Seilern-Aspang, F. and L. Kratochwill, *Relation between regeneration and tumor growth*, in *Regeneration in animals and related problems*. 1965, North-Holland Publishing Company: Amsterdam. p. 452-73.
465. Donaldson, D.J. and J.M. Mason, *Cancer-related aspects of regeneration research: a review*. Growth, 1975. **39**(4): p. 475-96.
466. Wolsky, A., *Regeneration and cancer*. Growth, 1978. **42**(4): p. 425-6.
467. Levin, M., *Molecular bioelectricity: how endogenous voltage potentials control cell behavior and instruct pattern regulation in vivo*. Mol Biol Cell, 2014. **25**(24): p. 3835-50.
468. Lobikin, M., et al., *Resting potential, oncogene-induced tumorigenesis, and metastasis: the bioelectric basis of cancer in vivo*. Physical biology, 2012. **9**(6): p. 065002.
469. Adams, D.S. and M. Levin, *Endogenous voltage gradients as mediators of cell-cell communication: strategies for investigating bioelectrical signals during pattern formation*. Cell and Tissue Research, 2013. **352**(1): p. 95-122.
470. Cang, C., K. Aranda, and D. Ren, *A non-inactivating high-voltage-activated two-pore Na(+) channel that supports ultra-long action potentials and membrane bistability*. Nat Commun, 2014. **5**: p. 5015.
471. Hinard, V., et al., *Initiation of human myoblast differentiation via dephosphorylation of Kir2.1 K+ channels at tyrosine 242*. Development, 2008. **135**(5): p. 859-67.
472. van Turnhout, M.C., S. Kranenbarg, and J.L. van Leeuwen, *Modeling optical behavior of birefringent biological tissues for evaluation of quantitative polarized light microscopy*. J Biomed Opt, 2009. **14**(5): p. 054018.
473. Mohun, T.J., et al., *The CArG promoter sequence is necessary for muscle-specific transcription of the cardiac actin gene in Xenopus embryos*. EMBO J, 1989. **8**(4): p. 1153-61.
474. Mohun, T.J., N. Garrett, and J.B. Gurdon, *Upstream sequences required for tissue-specific activation of the cardiac actin gene in Xenopus laevis embryos*. EMBO J, 1986. **5**(12): p. 3185-93.
475. Kroll, K.L. and E. Amaya, *Transgenic Xenopus embryos from sperm nuclear transplantations reveal FGF signaling requirements during*

- gastrulation*. Development, 1996. **122**(10): p. 3173-83.
476. Kintner, C.R. and J.P. Brockes, *Monoclonal antibodies identify blastemal cells derived from dedifferentiating limb regeneration*. Nature, 1984. **308**(5954): p. 67-9.
477. Blackiston, D.J. and M. Levin, *Aversive training methods in *Xenopus laevis*: general principles*. Cold Spring Harb Protoc, 2012. **2012**(5).
478. Levin, M., *Left-right asymmetry in embryonic development: a comprehensive review*. Mechanisms of development, 2005. **122**(1): p. 3-25.
479. Waugh, T.A., et al., *Fluoxetine prevents dystrophic changes in a zebrafish model of Duchenne muscular dystrophy*. Hum Mol Genet, 2014. **23**(17): p. 4651-62.
480. Chambers, S.M. and L. Studer, *Cell fate plug and play: direct reprogramming and induced pluripotency*. Cell, 2011. **145**(6): p. 827-30.
481. Weintraub, H., et al., *Activation of Muscle-Specific Genes in Pigment, Nerve, Fat, Liver, and Fibroblast Cell-Lines by Forced Expression of Myod*. Proceedings of the National Academy of Sciences of the United States of America, 1989. **86**(14): p. 5434-5438.
482. Mong, J., et al., *Transcription factor-induced lineage programming of noradrenaline and motor neurons from embryonic stem cells*. Stem Cells, 2014. **32**(3): p. 609-22.
483. Barth, L.G. and L.J. Barth, *Ionic regulation of embryonic induction and cell differentiation in *Rana pipiens**. Dev Biol, 1974. **39**(1): p. 1-22.
484. Lange, C., et al., *The H(+) vacuolar ATPase maintains neural stem cells in the developing mouse cortex*. Stem Cells Dev, 2011. **20**(5): p. 843-50.
485. Morrison, S.J. and J. Kimble, *Asymmetric and symmetric stem-cell divisions in development and cancer*. Nature, 2006. **441**(7097): p. 1068-74.
486. Chernet, B. and M. Levin, *Endogenous Voltage Potentials and the Microenvironment: Bioelectric Signals that Reveal, Induce and Normalize Cancer*. Journal of clinical & experimental oncology, 2013. **Suppl 1**.
487. Lin, G.F., Y. Chen, and J.M.W. Slack, *Transgenic Analysis of Signaling Pathways Required for *Xenopus Tadpole Spinal Cord and Muscle Regeneration**. Anatomical Record-Advances in Integrative Anatomy and Evolutionary Biology, 2012. **295**(10): p. 1532-1540.
488. Pai, V., Lemire, J. M., Pare, J-F., Lin, G., Chen, Y., and Levin, M., *Endogenous gradients of resting potential instructively pattern embryonic neural tissue via Notch signaling and regulation of proliferation*. Journal of

Neuroscience, 2015(In Press).

489. Blackiston, D., et al., *A second-generation device for automated training and quantitative behavior analyses of molecularly-tractable model organisms*. PLoS One, 2010. **5**(12): p. e14370.
490. You, M.H., et al., *Voltage-gated K<sup>+</sup> channels in adipogenic differentiation of bone marrow-derived human mesenchymal stem cells*. Acta pharmacologica Sinica, 2013. **34**(1): p. 129-36.
491. Lan, J.Y., et al., *Depolarization of Cellular Resting Membrane Potential Promotes Neonatal Cardiomyocyte Proliferation In Vitro*. Cell Mol Bioeng, 2014. **7**(3): p. 432-445.
492. Ding, F., et al., *Involvement of cationic channels in proliferation and migration of human mesenchymal stem cells*. Tissue Cell, 2012. **44**(6): p. 358-64.
493. Tseng, A. and M. Levin, *Cracking the bioelectric code: Probing endogenous ionic controls of pattern formation*. Communicative & Integrative Biology, 2013. **6**(1): p. 1-8.
494. Levin, M., *Molecular bioelectricity in developmental biology: new tools and recent discoveries: control of cell behavior and pattern formation by transmembrane potential gradients*. BioEssays, 2012. **34**(3): p. 205-17.
495. Levin, M., *Molecular bioelectricity: how endogenous voltage potentials control cell behavior and instruct pattern regulation in vivo*. Molecular biology of the cell, 2014. **25**(24): p. 3835-50.
496. Thompson, D.M., et al., *Electrical stimuli in the central nervous system microenvironment*. Annual review of biomedical engineering, 2014. **16**: p. 397-430.
497. Chernet, B. and M. Levin, *Bioelectric signaling in cancer*. Journal of Experimental and Clinical Oncology, 2014. **in press**.
498. Yang, M. and W.J. Brackenbury, *Membrane potential and cancer progression*. Frontiers in physiology, 2013. **4**: p. 185.
499. Arcangeli, A., *Ion channels and transporters in cancer. 3. Ion channels in the tumor cell-microenvironment cross talk*. American journal of physiology. Cell physiology, 2011. **301**(4): p. C762-71.
500. Than, B.L., et al., *The role of KCNQ1 in mouse and human gastrointestinal cancers*. Oncogene, 2013.
501. Brackenbury, W.J. and L.L. Isom, *Voltage-gated Na<sup>+</sup> channels: potential for beta subunits as therapeutic targets*. Expert opinion on therapeutic targets, 2008. **12**(9): p. 1191-203.

502. Stuhmer, W., et al., *Potassium channels as tumour markers*. FEBS Lett, 2006. **580**(12): p. 2850-2.
503. Felipe, A., et al., *Potassium channels: new targets in cancer therapy*. Cancer detection and prevention, 2006. **30**(4): p. 375-85.
504. Arcangeli, A., S. Pillozzi, and A. Becchetti, *Targeting ion channels in leukemias: a new challenge for treatment*. Current medicinal chemistry, 2012. **19**(5): p. 683-96.
505. Chernet, B.T. and M. Levin, *Transmembrane voltage potential is an essential cellular parameter for the detection and control of tumor development in a Xenopus model*. Disease models & mechanisms, 2013. **6**(3): p. 595-607.
506. Chernet, B.T. and M. Levin, *Transmembrane voltage potential of somatic cells controls oncogene-mediated tumorigenesis at long-range*. Oncotarget, 2014. **5**(10): p. 3287-306.
507. Alikhan, A., et al., *Vitiligo: a comprehensive overview Part I. Introduction, epidemiology, quality of life, diagnosis, differential diagnosis, associations, histopathology, etiology, and work-up*. J Am Acad Dermatol, 2011. **65**(3): p. 473-91.
508. Lin, J.Y. and D.E. Fisher, *Melanocyte biology and skin pigmentation*. Nature, 2007. **445**(7130): p. 843-850.
509. D'Anselmi, F., et al., *Microenvironment promotes tumor cell reprogramming in human breast cancer cell lines*. PloS one, 2013. **8**(12): p. e83770.
510. Kenny, P.A., G.Y. Lee, and M.J. Bissell, *Targeting the tumor microenvironment*. Frontiers in bioscience : a journal and virtual library, 2007. **12**: p. 3468-74.
511. Kenny, P.A. and M.J. Bissell, *Tumor reversion: correction of malignant behavior by microenvironmental cues*. International journal of cancer. Journal international du cancer, 2003. **107**(5): p. 688-95.
512. Maffini, M.V., et al., *The stroma as a crucial target in rat mammary gland carcinogenesis*. J Cell Sci, 2004. **117**(Pt 8): p. 1495-502.
513. Agnarsdottir, M., et al., *SOX10 expression in superficial spreading and nodular malignant melanomas*. Melanoma Res, 2010. **20**(6): p. 468-78.
514. Graf, S.A., et al., *SOX10 promotes melanoma cell invasion by regulating melanoma inhibitory activity*. J Invest Dermatol, 2014. **134**(8): p. 2212-20.
515. Shakhova, O., et al., *Sox10 promotes the formation and maintenance of giant congenital naevi and melanoma*. Nature cell biology, 2012. **14**(8): p. 882-90.

516. Casas, E., et al., *Snail2 is an essential mediator of Twist1-induced epithelial mesenchymal transition and metastasis*. *Cancer Res*, 2011. **71**(1): p. 245-54.
517. Dobroff, A.S., et al., *Silencing cAMP-response element-binding protein (CREB) identifies CYR61 as a tumor suppressor gene in melanoma*. *J Biol Chem*, 2009. **284**(38): p. 26194-206.
518. Rodriguez, C.I. and V. Setaluri, *Cyclic AMP (cAMP) signaling in melanocytes and melanoma*. *Arch Biochem Biophys*, 2014. **563**: p. 22-7.
519. Blackiston, D.J., et al., *A Novel Method for Inducing Nerve Growth via Modulation of Host Resting Potential: Gap Junction-Mediated and Serotonergic Signaling Mechanisms*. *Neurotherapeutics*, 2014.
520. Schmitt, A. and A.R. Nebreda, *Inhibition of Xenopus oocyte meiotic maturation by catalytically inactive protein kinase A*. *Proc Natl Acad Sci U S A*, 2002. **99**(7): p. 4361-6.
521. Bae, H.R. and A.S. Verkman, *Protein kinase A regulates chloride conductance in endocytic vesicles from proximal tubule*. *Nature*, 1990. **348**(6302): p. 637-9.
522. Hardie, D.G., *AMP-activated protein kinase: a cellular energy sensor with a key role in metabolic disorders and in cancer*. *Biochem Soc Trans*, 2011. **39**(1): p. 1-13.
523. Rehman, G., et al., *Role of AMP-activated protein kinase in cancer therapy*. *Arch Pharm (Weinheim)*, 2014. **347**(7): p. 457-68.
524. Kim, I. and Y.Y. He, *Targeting the AMP-Activated Protein Kinase for Cancer Prevention and Therapy*. *Front Oncol*, 2013. **3**: p. 175.
525. Mayr, B. and M. Montminy, *Transcriptional regulation by the phosphorylation-dependent factor CREB*. *Nat Rev Mol Cell Biol*, 2001. **2**(8): p. 599-609.
526. Lubelski, D., T.A. Ponzio, and H. Gainer, *Effects of A-CREB, a dominant negative inhibitor of CREB, on the expression of c-fos and other immediate early genes in the rat SON during hyperosmotic stimulation in vivo*. *Brain Res*, 2012. **1429**: p. 18-28.
527. Barco, A., J.M. Alarcon, and E.R. Kandel, *Expression of constitutively active CREB protein facilitates the late phase of long-term potentiation by enhancing synaptic capture*. *Cell*, 2002. **108**(5): p. 689-703.
528. Benito, E. and A. Barco, *CREB's control of intrinsic and synaptic plasticity: implications for CREB-dependent memory models*. *Trends Neurosci*, 2010. **33**(5): p. 230-40.
529. Blackiston, D., et al., *Transmembrane potential of GlyCl-expressing*

- instructor cells induces a neoplastic-like conversion of melanocytes via a serotonergic pathway*. Dis Model Mech, 2011. **4**(1): p. 67-85.
530. Besharse, J.C. and P.M. Iuvone, *Circadian clock in Xenopus eye controlling retinal serotonin N-acetyltransferase*. Nature, 1983. **305**(5930): p. 133-5.
531. Green, C.B., et al., *Ontogeny of circadian and light regulation of melatonin release in Xenopus laevis embryos*. Brain Res Dev Brain Res, 1999. **117**(1): p. 109-16.
532. Isoldi, M.C., I. Provencio, and A.M. Castrucci, *Light modulates the melanophore response to alpha-MSH in Xenopus laevis: an analysis of the signal transduction crosstalk mechanisms involved*. Gen Comp Endocrinol, 2010. **165**(1): p. 104-10.
533. Aoki, Y., et al., *Sox10 regulates the development of neural crest-derived melanocytes in Xenopus*. Dev Biol, 2003. **259**(1): p. 19-33.
534. Shi, J., et al., *Snail2 controls mesodermal BMP/Wnt induction of neural crest*. Development, 2011. **138**(15): p. 3135-45.
535. Eden, E., et al., *GOrilla: a tool for discovery and visualization of enriched GO terms in ranked gene lists*. BMC Bioinformatics, 2009. **10**: p. 48.
536. Stockholm, D., et al., *Bistable Cell Fate Specification as a Result of Stochastic Fluctuations and Collective Spatial Cell Behaviour*. PloS one, 2010. **5**(12).
537. Losick, R. and C. Desplan, *Stochasticity and cell fate*. Science, 2008. **320**(5872): p. 65-8.
538. Dietrich, J.E. and T. Hiiragi, *Stochastic patterning in the mouse pre-implantation embryo*. Development, 2007. **134**(23): p. 4219-4231.
539. Slominski, A., *Neuroendocrine activity of the melanocyte*. Exp Dermatol, 2009. **18**(9): p. 760-3.
540. Jenks, B.G., et al., *Plasticity in the melanotrope neuroendocrine interface of Xenopus laevis*. Neuroendocrinology, 2007. **85**(3): p. 177-85.
541. Lutz, B., et al., *Essential role of CREB family proteins during Xenopus embryogenesis*. Mech Dev, 1999. **88**(1): p. 55-66.
542. Holland, J.H., *Adaptation in natural and artificial systems: an introductory analysis with applications to biology, control, and artificial intelligence*. 1975, Ann Arbor, MI: Michigan Univ. Press.
543. Hou, L. and W.J. Pavan, *Transcriptional and signaling regulation in neural crest stem cell-derived melanocyte development: do all roads lead to Mitf?* Cell Res, 2008. **18**(12): p. 1163-76.

544. Kelsh, R.N., *Sorting out Sox10 functions in neural crest development*. Bioessays, 2006. **28**(8): p. 788-98.
545. Wegner, M., *Secrets to a healthy Sox life: lessons for melanocytes*. Pigment Cell Res, 2005. **18**(2): p. 74-85.
546. Bakos, R.M., et al., *Nestin and SOX9 and SOX10 transcription factors are coexpressed in melanoma*. Exp Dermatol, 2010. **19**(8): p. e89-94.
547. Krude, H., et al., *Severe early-onset obesity, adrenal insufficiency and red hair pigmentation caused by POMC mutations in humans*. Nat Genet, 1998. **19**(2): p. 155-7.
548. Hao, L., et al., *Positive expression of pro-opiomelanocortin (POMC) is a novel independent poor prognostic marker in surgically resected non-small cell lung cancer*. Tumour Biol, 2014.
549. Slominski, A., *POMC gene expression in mouse and hamster melanoma cells*. FEBS Lett, 1991. **291**(2): p. 165-8.
550. Tsai, H.E., et al., *Downregulation of hepatoma-derived growth factor contributes to retarded lung metastasis via inhibition of epithelial-mesenchymal transition by systemic POMC gene delivery in melanoma*. Mol Cancer Ther, 2013. **12**(6): p. 1016-25.
551. Farah, J.M., Jr., et al., *The effects of pro-opiomelanocortin peptides on cyclic AMP and tyrosinase in melanoma cells*. Peptides, 1986. **7**(3): p. 437-41.
552. Cui, R., et al., *Central role of p53 in the suntan response and pathologic hyperpigmentation*. Cell, 2007. **128**(5): p. 853-64.
553. Wu, G.S., et al., *Sequence polymorphisms of MC1R gene and their association with depression and antidepressant response*. Psychiatric genetics, 2011. **21**(1): p. 14-8.
554. Vaarala, M.H., et al., *The TMPRSS2 gene encoding transmembrane serine protease is overexpressed in a majority of prostate cancer patients: detection of mutated TMPRSS2 form in a case of aggressive disease*. Int J Cancer, 2001. **94**(5): p. 705-10.
555. Pedersen, L.M. and P.G. Sorensen, *Increased urinary albumin excretion rate in breast cancer patients*. Acta Oncol, 2000. **39**(2): p. 145-9.
556. Lis, C.G., et al., *Is serum albumin an independent predictor of survival in patients with breast cancer?* JPEN J Parenter Enteral Nutr, 2003. **27**(1): p. 10-5.
557. Gomez, P., M.E. Beltran, and M. Rabago, *Immunoelectrophoretic demonstration of albumin in breast cancer*. Arch Invest Med (Mex), 1983. **14**(3): p. 241-5.

558. Lo, J.A. and D.E. Fisher, *The melanoma revolution: from UV carcinogenesis to a new era in therapeutics*. Science, 2014. **346**(6212): p. 945-9.
559. Murase, D., et al., *The essential role of p53 in hyperpigmentation of the skin via regulation of paracrine melanogenic cytokine receptor signaling*. J Biol Chem, 2009. **284**(7): p. 4343-53.
560. Melnikova, V.O. and M. Bar-Eli, *Transcriptional control of the melanoma malignant phenotype*. Cancer Biol Ther, 2008. **7**(7): p. 997-1003.
561. Zhang, X., et al., *Genome-wide analysis of cAMP-response element binding protein occupancy, phosphorylation, and target gene activation in human tissues*. Proc Natl Acad Sci U S A, 2005. **102**(12): p. 4459-64.
562. Melnikova, V.O., et al., *CREB inhibits AP-2alpha expression to regulate the malignant phenotype of melanoma*. PLoS One, 2010. **5**(8): p. e12452.
563. Jean, D., et al., *CREB and its associated proteins act as survival factors for human melanoma cells*. J Biol Chem, 1998. **273**(38): p. 24884-90.
564. Aucoin, R., et al., *Dominant-negative CREB inhibits heparanase functionality and melanoma cell invasion*. J Cell Biochem, 2004. **93**(2): p. 215-23.
565. Kim, H.E. and S.G. Lee, *Induction of ATP synthase beta by H2O2 induces melanogenesis by activating PAH and cAMP/CREB/MITF signaling in melanoma cells*. Int J Biochem Cell Biol, 2013. **45**(7): p. 1217-22.
566. Jean, D. and M. Bar-Eli, *Regulation of tumor growth and metastasis of human melanoma by the CREB transcription factor family*. Molecular and cellular biochemistry, 2000. **212**(1-2): p. 19-28.
567. Dubnau, D. and R. Losick, *Bistability in bacteria*. Molecular Microbiology, 2006. **61**(3): p. 564-572.
568. Yang, Y., et al., *Hunger states switch a flip-flop memory circuit via a synaptic AMPK-dependent positive feedback loop*. Cell, 2011. **146**(6): p. 992-1003.
569. Tian, X.J., H. Zhang, and J. Xing, *Coupled reversible and irreversible bistable switches underlying TGFbeta-induced epithelial to mesenchymal transition*. Biophysical journal, 2013. **105**(4): p. 1079-89.
570. Johnston, R.J., et al., *MicroRNAs acting in a double-negative feedback loop to control a neuronal cell fate decision*. Proceedings of the National Academy of Sciences of the United States of America, 2005. **102**(35): p. 12449-12454.
571. Xiong, W. and J.E. Ferrell, *A positive-feedback-based bistable 'memory*

- module' that governs a cell fate decision. Nature, 2003. 426(6965): p. 460-465.*
572. Shiraishi, T., S. Matsuyama, and H. Kitano, *Large-Scale Analysis of Network Bistability for Human Cancers*. PLoS Comput Biol, 2010. **6**(7): p. e1000851.
  573. Ferrell, J.E., *Self-perpetuating states in signal transduction: positive feedback, double-negative feedback and bistability*. Current Opinion in Cell Biology, 2002. **14**(2): p. 140-148.
  574. Gardner, T.S., C.R. Cantor, and J.J. Collins, *Construction of a genetic toggle switch in Escherichia coli*. Nature, 2000. **403**(6767): p. 339-42.
  575. Kobayashi, H., et al., *Programmable cells: Interfacing natural and engineered gene networks*. Proceedings of the National Academy of Sciences of the United States of America, 2004. **101**(22): p. 8414-8419.
  576. Slusarczyk, A.L., A. Lin, and R. Weiss, *Foundations for the design and implementation of synthetic genetic circuits*. Nat Rev Genet, 2012. **13**(6): p. 406-20.
  577. Eldar, A. and M.B. Elowitz, *Functional roles for noise in genetic circuits*. Nature, 2010. **467**(7312): p. 167-173.
  578. Wernet, M.F., et al., *Stochastic spineless expression creates the retinal mosaic for colour vision*. Nature, 2006. **440**(7081): p. 174-180.
  579. Johnston, R.J., Jr. and C. Desplan, *Interchromosomal communication coordinates intrinsically stochastic expression between alleles*. Science, 2014. **343**(6171): p. 661-5.
  580. Johnston, R.J., Jr. and C. Desplan, *Stochastic mechanisms of cell fate specification that yield random or robust outcomes*. Annual review of cell and developmental biology, 2010. **26**: p. 689-719.
  581. Mombaerts, P., *Odorant receptor gene choice in olfactory sensory neurons: the one receptor–one neuron hypothesis revisited*. Current Opinion in Neurobiology, 2004. **14**(1): p. 31-36.
  582. Fukumoto, T., R. Blakely, and M. Levin, *Serotonin transporter function is an early step in left-right patterning in chick and frog embryos*. Dev Neurosci, 2005. **27**(6): p. 349-63.
  583. Wang, S., et al., *Chick Pcl2 regulates the left-right asymmetry by repressing Shh expression in Hensen's node*. Development, 2004. **131**(17): p. 4381-4391.
  584. Pagan-Westphal, S.M. and C.J. Tabin, *The transfer of left-right positional information during chick embryogenesis*. Cell, 1998. **93**(1): p. 25-35.

585. Lobo, D., et al., *A linear-encoding model explains the variability of the target morphology in regeneration*. *Journal of the Royal Society Interface*, 2014. **11**(92).
586. Francois, P. and V. Hakim, *Design of genetic networks with specified functions by evolution in silico*. *Proceedings of the National Academy of Sciences of the United States of America*, 2004. **101**(2): p. 580-585.
587. Bongard, J. and H. Lipson, *Automated reverse engineering of nonlinear dynamical systems*. *Proceedings of the National Academy of Sciences of the United States of America*, 2007. **104**(24): p. 9943-9948.
588. Yeung, M.K.S., J. Tegnér, and J.J. Collins, *Reverse engineering gene networks using singular value decomposition and robust regression*. *Proceedings of the National Academy of Sciences*, 2002. **99**(9): p. 6163-6168.
589. Tegner, J., et al., *Reverse engineering gene networks: integrating genetic perturbations with dynamical modeling*. *Proceedings of the National Academy of Sciences of the United States of America*, 2003. **100**(10): p. 5944-9.
590. Gardner, T.S., et al., *Inferring genetic networks and identifying compound mode of action via expression profiling*. *Science*, 2003. **301**(5629): p. 102-105.
591. Bonneau, R., et al., *A predictive model for transcriptional control of physiology in a free living cell*. *Cell*, 2007. **131**(7): p. 1354-1365.
592. Cantone, I., et al., *A Yeast Synthetic Network for In Vivo Assessment of Reverse-Engineering and Modeling Approaches*. *Cell*, 2009. **137**(1): p. 172-181.
593. Reinitz, J., E. Mjolsness, and D.H. Sharp, *Model for Cooperative Control of Positional Information in Drosophila by Bicoid and Maternal Hunchback*. *Journal of Experimental Zoology*, 1995. **271**(1): p. 47-56.
594. Jaeger, J., et al., *Dynamical analysis of regulatory interactions in the gap gene system of Drosophila melanogaster*. *Genetics*, 2004. **167**(4): p. 1721-1737.
595. Jaeger, J., et al., *Dynamic control of positional information in the early Drosophila embryo*. *Nature*, 2004. **430**(6997): p. 368-371.
596. Crombach, A., et al., *Efficient reverse-engineering of a developmental gene regulatory network*. *PLoS Computational Biology*, 2012. **8**(7): p. e1002589.
597. Lobo, D., W.S. Beane, and M. Levin, *Modeling planarian regeneration: a primer for reverse-engineering the worm*. *PLoS Computational Biology*, 2012. **8**(4): p. e1002481.

598. Amson, R., et al., *Reciprocal repression between P53 and TCTP*. Nature medicine, 2012. **18**(1): p. 91-9.
599. Bellono, N.W., et al., *UV light phototransduction activates transient receptor potential A1 ion channels in human melanocytes*. Proceedings of the National Academy of Sciences of the United States of America, 2013. **110**(6): p. 2383-8.
600. Bellono, N.W. and E. Oancea, *UV light phototransduction depolarizes human melanocytes*. Channels, 2013. **7**(4).
601. Hertz, D.L. and J. Rae, *Pharmacogenetics of cancer drugs*. Annual review of medicine, 2015. **66**: p. 65-81.
602. Pouget, J.G., et al., *Pharmacogenetics and outcome with antipsychotic drugs*. Dialogues in clinical neuroscience, 2014. **16**(4): p. 555-66.
603. Reynolds, G.P., *The pharmacogenetics of symptom response to antipsychotic drugs*. Psychiatry investigation, 2012. **9**(1): p. 1-7.
604. Lobo, D., T.J. Malone, and M. Levin, *Towards a bioinformatics of patterning: a computational approach to understanding regulative morphogenesis*. Biology Open, 2013. **2**(2): p. 156-169.
605. Lobo, D., T.J. Malone, and M. Levin, *Planform: an application and database of graph-encoded planarian regenerative experiments*. Bioinformatics, 2013. **29**(8): p. 1098-1100.
606. Lobo, D., et al., *A bioinformatics expert system linking functional data to anatomical outcomes in limb regeneration*. Regeneration, 2014. **1**(2): p. 37-56.
607. Lobo, D., et al., *Limbform: a functional ontology-based database of limb regeneration experiments*. Bioinformatics, 2014. **30**(24): p. 3598-600.
608. Sparkes, A., et al., *Towards Robot Scientists for autonomous scientific discovery*. Autom Exp, 2010. **2**: p. 1.
609. Qi, D., et al., *An ontology for description of drug discovery investigations*. J Integr Bioinform, 2010. **7**(3).
610. King, R.D., et al., *The automation of science*. Science, 2009. **324**(5923): p. 85-9.
611. Soldatova, L.N., et al., *An ontology for a Robot Scientist*. Bioinformatics, 2006. **22**(14): p. e464-71.
612. Nieuwkoop, P.D. and J. Faber, *Normal Tables of Xenopus Laevis:(Daudin) a Systematical and Chronological Survey of the Development from the Fertilized Egg Till the End of the Metamorphosis*. 1967: North-Holland.

613. Keren, A., A. Keren-Politansky, and E. Bengal, *A p38 MAPK-CREB pathway functions to pattern mesoderm in Xenopus*. *Dev Biol*, 2008. **322**(1): p. 86-94.
614. Barhanin, J., et al., *K(V)LQT1 and Isk (minK) proteins associate to form the I(Ks) cardiac potassium current*. *Nature*, 1996. **384**(6604): p. 78-80.
615. Harland, R.M., *In situ hybridization: an improved whole-mount method for Xenopus embryos*. *Methods in cell biology*, 1991. **36**: p. 685.
616. Untergasser, A., et al., *Primer3Plus, an enhanced web interface to Primer3*. *Nucleic Acids Res*, 2007. **35**(Web Server issue): p. W71-4.
617. Christen, B., et al., *Regeneration and reprogramming compared*. *BMC Biol*, 2010. **8**: p. 5.
618. Liang, X., et al., *Pyruvate carboxylase as a sensitive protein biomarker for exogenous steroid chemicals*. *Environ Pollut*, 2014. **189**: p. 184-93.
619. Legewie, S., N. Bluthgen, and H. Herzog, *Quantitative analysis of ultrasensitive responses*. *FEBS Journal*, 2005. **272**(16): p. 4071-4079.
620. Lobo, D. and M. Levin, *Inferring regulatory networks from experimental morphological phenotypes: a computational method reverse-engineers planarian regeneration*. *PLoS Comput Biol*, 2015: p. in press.
621. Jostins, L. and J. Jaeger, *Reverse engineering a gene network using an asynchronous parallel evolution strategy*. *BMC Syst Biol*, 2010. **4**: p. 17.
622. Bäck, T., *Evolutionary algorithms in theory and practice : evolution strategies, evolutionary programming, genetic algorithms*. 1995, Oxford ; New York: Oxford University Press. xii, 314.
623. Chantome, A., et al., *KCa2.3 channel-dependent hyperpolarization increases melanoma cell motility*. *Exp Cell Res*, 2009. **315**(20): p. 3620-30.
624. Lepple-Wienhues, A., et al., *K+ channels and the intracellular calcium signal in human melanoma cell proliferation*. *The Journal of membrane biology*, 1996. **151**(2): p. 149-57.
625. Nilius, B., G. Schwarz, and G. Droogmans, *Control of intracellular calcium by membrane potential in human melanoma cells*. *The American journal of physiology*, 1993. **265**(6 Pt 1): p. C1501-10.
626. Chantôme, A.I., et al., *Ion Channels as Promising Therapeutic Targets for Melanoma*, in *Breakthroughs in Melanoma Research*, D.Y. Tanaka, Editor. 2011, InTech.
627. Mathieu, V., et al., *The sodium pump alpha1 sub-unit: a disease progression-related target for metastatic melanoma treatment*. *J Cell Mol*

- Med, 2009. **13**(9B): p. 3960-72.
628. Pardo, L.A. and W. Stuhmer, *Eag1 as a cancer target*. Expert Opin Ther Targets, 2008. **12**(7): p. 837-43.
629. Afrasiabi, E., et al., *Expression and significance of HERG (KCNH2) potassium channels in the regulation of MDA-MB-435S melanoma cell proliferation and migration*. Cell Signal, 2010. **22**(1): p. 57-64.
630. Artym, V.V. and H.R. Petty, *Molecular proximity of Kv1.3 voltage-gated potassium channels and beta(1)-integrins on the plasma membrane of melanoma cells: effects of cell adherence and channel blockers*. J Gen Physiol, 2002. **120**(1): p. 29-37.
631. Yohem, K.H., et al., *Inhibition of tumor cell invasion by verapamil*. Pigment Cell Res, 1991. **4**(5-6): p. 225-33.
632. Pocsai, K., et al., *Melanoma cells exhibit strong intracellular TASK-3-specific immunopositivity in both tissue sections and cell culture*. Cell Mol Life Sci, 2006. **63**(19-20): p. 2364-76.
633. Rusznak, Z., et al., *Mitochondrial expression of the two-pore domain TASK-3 channels in malignantly transformed and non-malignant human cells*. Virchows Arch, 2008. **452**(4): p. 415-26.
634. Orfanelli, U., et al., *Identification of novel sense and antisense transcription at the TRPM2 locus in cancer*. Cell Res, 2008. **18**(11): p. 1128-40.
635. Chernet, B. and M. Levin, *Endogenous Voltage Potentials and the Microenvironment: Bioelectric Signals that Reveal, Induce and Normalize Cancer*. J Clin Exp Oncol, 2013. **Suppl 1**.
636. Sontheimer, H., *An unexpected role for ion channels in brain tumor metastasis*. Exp Biol Med (Maywood), 2008. **233**(7): p. 779-91.
637. Stuhmer, W. and L.A. Pardo, *K(+) channels as therapeutic targets in oncology*. Future Med Chem, 2010. **2**(5): p. 745-55.
638. Djamgoz, M.B. and R. Onkal, *Persistent current blockers of voltage-gated sodium channels: a clinical opportunity for controlling metastatic disease*. Recent Pat Anticancer Drug Discov, 2013. **8**(1): p. 66-84.
639. Seuwen, K. and J. Pouyssegur, *Serotonin as a growth factor*. Biochem Pharmacol, 1990. **39**(6): p. 985-90.
640. Siddiqui, E.J., et al., *The role of serotonin in tumour growth (review)*. Oncol Rep, 2005. **14**(6): p. 1593-7.
641. Sarrouilhe, D., et al., *Serotonin and cancer: what is the link?* Curr Mol Med, 2015. **15**(1): p. 62-77.

642. Julius, D., et al., *Ectopic expression of the serotonin 1c receptor and the triggering of malignant transformation*. Science, 1989. **244**(4908): p. 1057-62.
643. Julius, D., et al., *The 5HT<sub>2</sub> receptor defines a family of structurally distinct but functionally conserved serotonin receptors*. Proc Natl Acad Sci U S A, 1990. **87**(3): p. 928-32.
644. Launay, J.M., et al., *Ras involvement in signal transduction by the serotonin 5-HT<sub>2B</sub> receptor*. J Biol Chem, 1996. **271**(6): p. 3141-7.
645. Jungwirth, N., et al., *Serotonin used as prognostic marker of urological tumors*. World J Urol, 2008. **26**(5): p. 499-504.
646. Allen, D.H., A. Lepple-Wienhues, and M.D. Cahalan, *Ion channel phenotype of melanoma cell lines*. J Membr Biol, 1997. **155**(1): p. 27-34.
647. Bradding, P., et al., *Ion channel gene expression in human lung, skin, and cord blood-derived mast cells*. Journal of leukocyte biology, 2003. **73**(5): p. 614-20.
648. Tong, Y., et al., *Tyrosine decaging leads to substantial membrane trafficking during modulation of an inward rectifier potassium channel*. J Gen Physiol, 2001. **117**(2): p. 103-18.
649. Comes, N., et al., *The voltage-dependent K(+) channels Kv1.3 and Kv1.5 in human cancer*. Front Physiol, 2013. **4**: p. 283.
650. Shin, S.I., et al., *Tumorigenicity of virus-transformed cells in nude mice is correlated specifically with anchorage independent growth in vitro*. Proc Natl Acad Sci U S A, 1975. **72**(11): p. 4435-9.
651. Schwab, A., et al., *Potassium channels keep mobile cells on the go*. Physiology (Bethesda), 2008. **23**: p. 212-20.
652. Schwab, A., et al., *Migration of transformed renal epithelial cells is regulated by K<sup>+</sup> channel modulation of actin cytoskeleton and cell volume*. Pflugers Arch, 1999. **438**(3): p. 330-7.
653. Pardo, L.A. and W. Stuhmer, *The roles of K(+) channels in cancer*. Nat Rev Cancer, 2014. **14**(1): p. 39-48.
654. Huber, S.M., *Oncochannels*. Cell Calcium, 2013. **53**(4): p. 241-55.